THÈSE POUR OBTENIR LE GRADE DE DOCTEUR DE L'UNIVERSITÉ DE MONTPELLIER

En Biologie cellulaire

École doctorale Sciences Chimiques et Biologiques pour la Santé (CBS2)

Institut de Recherche en Infectiologie de Montpellier (IRIM)

Subversion of host cell pathways by *Coxiella burnetii* to favor replicative niche biogenesis

Présentée par Arthur BIENVENU

Le 24 Novembre 2023

Sous la direction de Matteo BONAZZI et Éric MARTINEZ

Devant le jury composé de

Maximiliano GUTIERREZ, Principal Group Leader, The Francis Crick Institute, Londres	Rapporteur
Nathalie SAUVONNET, Directrice de recherche, Institut Pasteur, Paris	Rapporteur
Frank LAFONT, Directeur de recherche, Institut Pasteur de Lille, Lille	Examinateur
Cécile GAUTHIER-ROUVIÈRE, Directrice de recherche, CRBM, Montpellier	Présidente du jury
Matteo BONAZZI, Directeur de recherche, IRIM, Montpellier	Directeur de thèse
Éric MARTINEZ, Chargé de recherche, IRIM, Montpellier	Directeur de thèse

UNIVERSITÉ DE MONTPELLIER

ACKNOWLEDGEMENTS

Tout d'abord, je remercie l'ensemble des chercheuses et chercheurs qui ont accepté et prendre du temps pour ma thèse, que ce soit lors des comités de suivi individuel mais aussi ceux qui font à présent partie de mon jury.

C'est en réalité grâce une succession de rencontres, d'évènements et de déconvenues que je suis en train de rédiger ces mots aujourd'hui.

Tout d'abord, parlons des déconvenues ; Comme mon équipe aime à me le rappeler, j'ai mis ma carrière de basketteur entre parenthèses pour me consacrer à mes études. Qui sait si j'avais été meilleur, je n'aurais certainement pas déchaussé les baskets pour m'installer sur les bancs de la fac. A cette époque ce projet sportif fut alors vécu comme un échec, une déconvenue. La vérité est cependant peut-être ailleurs, Grâce au soutien de ma famille, que l'on peut d'ailleurs considérer comme le fil rouge de cette histoire, cette déception se transforma rapidement en une succession de rencontres et d'évènements dans ma nouvelle vie d'étudiant.

Ma première rencontre, du moins celle qui a pris une place majeure dans ma vie, fut celle de ma (toute récente) femme, celle qui m'accompagne et me soutient dans cette aventure fastidieuse de la recherche scientifique.

Ensuite vient celle des amis, avec qui nous avons pour certains partagé l'ensemble de nos études supérieures jusqu'au doctorat. Enfin, sauf notre cher valentin évidemment, notre vilain petit canard.

Et puis, il y a la rencontre de certains professeurs qui font basculer un étudiant médiocre, ancien basketteur en un étudiant motivé et déterminé à aller le plus loin possible. Je n'en citerai que deux, car ils ont tous les deux été à la genèse de mon intérêt pour la recherche et m'ont tous les deux soutenu. Ils ont probablement vu en moi ce que je ne voyais peut-être pas moi-même à cette époque-là. C'est Stéphane Bodin a été le premier à me proposer de réaliser un stage, alors que j'étais totalement novice sur le sujet, et m'a donc introduit dans le milieu de la biologie.

Puis, Robert Zumbihl m'a guidé et a tout fait pour que je réalise mon premier stage dans mon équipe actuelle, même si le chef (Matteo) n'avait pas l'air d'être très intéressé par un basketteur aux notes moyennes.

J’ai finalement trouvé ma place dans cette équipe et pu de nouveau rencontrer des personnes qui m’ont accompagné et soutenu tout au long de cette aventure.

Alors Merci à toute l’équipe, particulièrement à Matteo pour sa confiance, et pour m’avoir laissé dès le début en totale autonomie.

Pour Rico et la Princesse de 93, je pense qu’il n’y a pas grand-chose que vous ne savez pas déjà. Alors juste, Merci.

Merci à tous les autres avec qui j’ai pu passer de long moments d’échange, notamment à Stephan avec qui l’état du trafic et de la météo remplissait nos discussions matinales.

Merci à toutes les personnes de l’institut avec qui j’ai travaillé ou passé d’agréables moments.

Maintenant, je pars pour de nouvelles aventures, de nouvelles rencontres, de nouveaux évènements, de nouvelles déconvenues, mais je n’oublierais pas ce qui m’a construit et permis d’avancer.

« Et surtout prenez bien soin de vous »

TABLE OF CONTENTS

THESIS SUMMARY 8

THESIS SUMMARY IN FRENCH 10

LIST OF FIGURES 13

LIST OF TABLES 15

LIST OF ABBREVIATIONS 16

INTRODUCTION 20

1. THE PATHOGENIC BACTERIUM *COXIELLA BURNETII* 20

1.1. Historical discovery & the Q fever disease *20*

1.1.1. Historical discovery. 20

1.1.2. The Q fever disease. 22

1.1.2.1. Infection & Symptoms. 22

1.1.2.2. Prevalence & diagnostic. 25

1.1.2.3. Treatment. 27

1.2. Microbiological specificities. *28*

2.1.1. Morphotype and Variants. 28

2.1.2. Genetics, strains and phase variation. 29

2.1.2. Dot/Icm Type 4B secretion system. 33

2.1.2.1 T4SS structure and composition 33

2.1.2.1 T4SS substrates 38

2. INTRACELLULAR LIFE CYCLE 40

2.1. Bacterial entry. *40*

2.1.1. Adhesion & Invasion. 40

2.1.1. Ezrin and CD44 participate in the internalization process of Coxiella burnetii into non-phagocytic cells. 41

2.2. Coxiella containing vacuole biogenesis. *60*

2.2.1. Host-cell vesicular trafficking and autophagy modulation. 60

2.2.1.1. Endocytosis. 60

2.2.1.2. Secretory pathways. 71

2.2.1.3. Autophagy 72

2.2.3. Host-cell lipid 78

2.2.3.1. Lipid biology and function. 78

2.2.3.2. Host-cell lipids and bacterial infections. 85

..... *91*

2.3. C. burnetii stealth strategies *92*

..... 93

AIM OF THE THESIS 111

RESULTS 112

1. THE MULTIFUNCTION *COXIELLA* EFFECTOR VICE STIMULATES MACROPINOCYTOSIS AND INTERFERES WITH THE ESCRT MACHINERY 112
2. VICE PROTEIN-PROTEIN INTERACTIONS. 169
3. MODIFICATION OF EXTRACELLULAR VESICLE PROTEIN PROFILE. 172
4. VICE MEMBRANE CURVATURE RECOGNITION. 174
5. VICE-INDUCED COMPARTMENT RAB PROFILE. 175
6. *C. BURNETII* CCV ULTRASTRUCTURE. 177

DISCUSSION & PERSPECTIVES 179

MATERIAL AND METHODS 189

BIBLIOGRAPHY 207

THESIS SUMMARY

Coxiella burnetii, the causal agent of the Q fever, is an obligate intracellular pathogen that replicates within host cells. This particular lifestyle is facilitated by the formation of *Coxiella*-containing vacuoles (CCVs). These specialized vacuoles provide a shielded environment for bacterial replication, enabling *C. burnetii* to evade host immune defenses and establish persistent infections. CCV development hinges on bacterial effector proteins translocated into host cells through the Dot/Icm Type 4 Secretion System (T4SS), which interact with host proteins to subvert membrane trafficking. Another pivotal, yet often overlooked facet of host-pathogen interactions, is the manipulation of lipid trafficking and metabolism within infected cells.Expanding on the earlier identification of CvpB as a *C. burnetii* Lipid-Interacting Effector (LIE) that manipulates PI(3)P metabolism, we have conducted further investigations into the lipid composition of CCVs. Previous work by the team, using lipid binding probes, revealed that 3 lipids; PI(3)P, PI(4)P and LBPA were actively enriched at the CCV by T4SS effectors. The thesis work have been focused on characterizing the effectors responsible of the active enrichment of LBPA , a phospholipid usually found in the membrane of multivesicular bodies. We have thus identified Vice (encoded by the gene *cbu2007*) as an additional LIE responsible for LPBA enrichment at the CCV. Vice interacts with phosphoinositides and late endosomal membranes, enriched in phosphatidylserine (PS) and lysobisphosphatidic acid (LBPA). CCVs generated by the *vice*::Tn mutant strains are negative for LBPA, showed a strong defect in size and an altered morphology as compared to *wt* CCVs. Strikingly, ectopic expression of Vice in eukaryotic cells leads to the formation of compartments closely resembling early CCVs in both morphology, protein and lipid composition. The biogenesis of these Vice-induced compartments (VICs) is driven by an intriguing dual role of Vice. Initially, the effector localizes at the plasma membrane of eukaryotic cells, triggering the internalization of large vacuoles through the induction of macropinocytosis. Subsequently, Vice stabilizes VICs by disrupting the ESCRT machinery, impeding the formation of intraluminal vesicles (ILVs). This mechanism may also affect the release of extracellular vesicles (EVs) as EVs released by Vice-expressing cells displayed a modified protein profile.

Taken together, our findings highlight Vice as a pivotal *C. burnetii* effector capable of exploiting two major cellular pathways to shape the bacterial replicative environment.

THESIS SUMMARY IN FRENCH

Coxiella burnetii, l'agent causatif de la zoonose fièvre Q, est un pathogène intracellulaire obligatoire qui génère des vacuoles parasitophores (CCVs) au sein des cellules hôtes afin de s'y multiplier. Ces vacuoles offrent un environnement protégé pour la réplication bactérienne, permettant à *C. burnetii* d'échapper aux défenses immunitaires de l'hôte et d'établir des infections persistantes. Le développement des CCVs repose sur des protéines effectrices bactériennes, transloquées dans les cellules hôtes par un système de sécrétion de type 4 Dot/Icm (T4SS), qui interagissent avec les protéines de l'hôte et perturbent le trafic membranaire. Un autre aspect essentiel mais souvent négligé des interactions hôte-pathogène lors des infections à *C. burnetii* est la manipulation du trafic et du métabolisme lipidique au sein des cellules infectées.

En nous appuyant sur l'identification préliminaire de CvpB en tant qu'effecteur de *C. burnetii* interagissant avec les lipides (LIE) qui module le métabolisme du PI(3)P, nous avons mené de nouvelles recherches sur la composition lipidique des CCVs. Des travaux effectués avant la thèse, utilisant des sondes lipidiques, ont révélé que trois lipides ; PI(3)P, PI(4)P et le LBPA étaient activement enrichis au niveau des CCVs par des effecteurs du T4SS. Mon travail de thèse s'est donc focalisé sur la caractérisation des effecteurs responsables de l'enrichissement actif des CCVs en LBPA, un phospholipide qui compose généralement la membrane des endosomes multivésiculaires. Nous avons ainsi identifié Vice (codé par le gène *cbu2007*) en tant que nouveau LIE responsable de l'enrichissement de LBPA au niveau des CCVs. Cet effecteur bactérien est capable d'interagir avec les phosphoinositides et les membranes endosomales tardives, riches en phosphatidylsérine (PS) et en acide lysobisphosphatidique (LBPA). En plus de l'absence de LBPA, les CCVs générées par les souches mutantes *vice*::Tn présentaient un défaut important de taille et de forme par rapport aux CCVs des souches sauvages.

De plus, l'expression ectopique de Vice dans des cellules eucaryotes conduit à la formation de compartiments ressemblant étroitement à des CCVs précoces tant au niveau de la structure que de la composition protéique et lipidique. La biogenèse de ces compartiments induits par Vice (VICs) est gouvernée par un double rôle de Vice. L'effecteur localise à la membrane plasmique des cellules eucaryotes, déclenchant l'internalisation de grandes

vacuoles par macropinocytose. Ensuite, Vice stabilise les VICs en perturbant la machinerie ESCRT, entravant ainsi la formation de vésicules intraluminales (ILVs). Ce mécanisme semble également affecter la sécrétion de vésicules extracellulaires (EVs), en effet, les EVs provenant de cellules exprimant Vice présentent un profil protéique modifié comparé aux cellules contrôle.

En résumé, nos découvertes mettent en évidence que Vice est un effecteur clé dans l'infection par *C. burnetii* capable d'exploiter deux voies cellulaires majeures afin de façonner l'environnement réplicatif de la bactérie.

LIST OF FIGURES

Figure 1: *C. burnetii* infectious cycle.

Figure 2: Morphological shift of *C. burnetii* during infection.

Figure 3: *C. burnetii* LPS phase variation, from NMI to NMII.

Figure 4: A visual representation of the VirB3-10 (T4ASS) and the Dot/Icm (T4BSS) secretion systems.

Figure 5: Model of *C. burnetii* T4SS depicted in both side view (left) and top (right) view orientations.

Figure 6: Conformational changes of the T4SS during the intracellular lifecycle of *C. burnetii*.

Figure 7: Importance of the invasin OmpA for *C. burnetii* entry.

Figure 8: Endocytosis and endosome maturation pathways.

Figure 9: Macropinocytosis process.

Figure 10: Intralumenal vesicle (ILVs) formation pathways.

Figure 11: ESCRT membrane repair and implication in HIV-1 egress.

Figure 12: CvpF participates in LC3B recruitment to CCV.

Figure 13: Phospholipid structure and Pi organelle signature.

Figure 14. PIs dynamic conversion during macropinocytosis.

Figure 15. LBPA structure and cellular localization.

Figure 16: *C. burnetii* effector CvpB is essential for PI(3)P enrichment at the CCV.

Figure 17: Overview of the modulation of cell lipids and trafficking pathways by *C. burnetii* effector proteins.

Figure 18: Modulation of host cell innate immunity pathways by *C. burnetii* effectors.

Figure 19: Vice may interact with AP2M1 Mu domain.

Figure 20: Vice expression leads modifies EVs protein profile.

Figure 21: Vice may recognize membrane curvature.

Figure 22: *C. burnetii* CCV ultrastructure.

Figure 23: Examples of cell undergoing methuosis.

Figure 24: Deformation of nucleus during *C. burnetii* infections and by VICs.

LIST OF TABLES

Table 1: Acute Q fever clinical symptoms overview.

Table 2: Current overview of the six genomic groups of *C. burnetii*.

Table 3: Results recap of Yeast Two Hybrid assay provided by the company Hybrigenics.

Table 4: Screen of RAB GTPases at the Vice-induced compartments.

Table 5: List of lipid-binding sensors and markers used in this study

Table 6: List of strains used in this study

Table 7: List of primers used in this study

Table 8: List of plasmids used in this study

LIST OF ABBREVIATIONS

ACCM-2 : Acidified citrate cysteine medium 2
ALIX : ALG-2 Interacting Protein X
AP2 : Adaptor protein 2
ApV : *A. phagocytophium*-occupied vacuole
BAF : Barrier-to-autointegration factor
BCL-2 : B-cell leukemia/lymphoma 2
BLAM : β-lactamase
Bp : Base pair
BSL-2/3 : Biosafety level 2/3
BZN : Benzethonium chloride
CCV : *C. burnetii* Containing Vacuole
CD(x) : Cluster of differentiation
CHMP4 : Charged Multivesicular Body Protein 4
CLIC : Clathrin-independent carrier
CLTC : Clathrin heavy chain
CME : Clathrin-coated pit-mediated endocytosis
COP : Coat protein complex
Cvp(x) : *C. burnetii* vacuolar protein X
DDR : DNA damage response
DHCR24 : 24-Dehydrocholesterol Reductase
DMEM : Dulbecco's Modified Eagle Medium
DNA : Deoxyribonucleic acid
dNTP : Nucleoside triphosphates containing deoxyribose
Dot/Icm : Defect in organelle trafficking/Intracellular multiplication
EFSA : European food safety authority
ELISA : Enzyme-linked immunosorbent assay
ER : Endoplasmic reticulum
ERK1/2 : Extracellular signal-regulated kinases
ESCRT : Endosomal Sorting Complexes Required for Transport
EVs : Extracellular vesicles
FBS : Fetal bovine serum
FCHO2 : FCH And Mu Domain Containing Endocytic Adaptor 2
FEME : fast endophilin-mediated endocytosis
FIB-SEM : Focused Ion Beam-Scanning Electron Microscopy
FISH : fluorescent in situ hybridization
GAG : Group Antigens (ag)
GAL3 : Galectin3
GAP : GTPase-activating protein
GEEC : Glycosylphosphatidylinositol-anchored protein enriched early endocytic compartment
GGs : Genomic groups
H-Ras : Harvey Rat sarcoma virus GTPASE
HA : Human influenza hemagglutinin
HIV : Human immunodeficiency virus
HSP70 : Heat shock protein 70

IFAT : Indirect fluorescent antibody test
ILV : Intralumenal vesicles
IM : Inner membrane
IP : Immunoprecipitation
IS : Insertion Sequence)
LAMP-1/2 : Lysosomal-associated membrane protein 1/2
LAP : LC3-associated phagocytosis
LB : Luria-Bertani broth
LBPA : Lysobisphosphatidic acid or Bis(monoacylglycerol)phosphate (BMP)
LC3 : Microtubule-associated protein 1A/1B-light chain 3
LCV : Large cell variant
LEM2 : LEM domain nuclear inner membrane protein Heh1/Lem2
LPS : Lipopolysaccharides
LRRK2 : Leucine-rich repeat kinase 2
mTORC1 : mechanistic target of rapamycin complex 1
MVB : Multivesicular bodies
NCBI : National Center for Biotechnology Information
NE : Nuclear envelope
NF-κB : nuclear factor-kappa B
NHE: Na+/H+ exchangers
Nluc: Nano-luciferase
NMI/NMII: Nine Mile I/II
ORP1L : Oxysterol binding protein related protein 1L
OSBP : Oxysterol-binding protein
PA : Phosphatidic acid
Pak1 : P21 (RAC1) Activated Kinase 1
PC : Phosphatidylcholines
PCR : Polymerase chain reaction
PDCD6 : Programmed Cell Death 6
PI : Phosphoinositides
PI(x)P : Phosphatidylinositol-X-phosphate
PI3K : Phosphoinositide 3-kinase
PS: Phosphatidylserine
PtdIns: Phosphatidylinositol
QFS : Q fever fatigue syndrome
RAB(x) : Ras-associated binding X
RNA : Ribonucleic acid
rRNA : Ribosomal ribonucleic acid
RTK : Receptor tyrosine kinases
SCID : Severe Combined ImmunoDeficiency
SCV : Small cell variant
SEM : scanning electron microscope
siRNA : small interfering RNA
SNP : single nucleotide polymorphism
SNX(x) : Sorting Nexin X
SQSTM-1 : Sequestosome-1
T(x)SS : Type X secretion system

T4CP : type IV coupling protein
TEM : Transmission electron microscopy
TFEB/3 : Transcription factor EB/ E3
THP-1 : Tohoku Hospital Pediatrics-1
TSG101 : Tumor susceptibility gene 101
U2OS : Human Bone Osteosarcoma Epithelial Cells
VIC : Vice-Induced compartment
Vice : Vacuole-inducing *Coxiella* effector (CBU2007)
VLP : Virus-like particle
VPS(x) : Vacuolar protein sorting X
WB : Western-Blot
WCL : Whole cell lysate
WHO : World health organization
wt : Wild-Type

INTRODUCTION

1. The pathogenic bacterium *Coxiella burnetii*

1.1. Historical discovery & the Q fever disease.

1.1.1. Historical discovery.

In August 1935, employees of the "Brisbane Abattoir" suffered from an unexplained fever. Dr Edward Holbrook Derrick was designed by the Bacteriological Institute of Brisbane to investigate the cause of the fever. His first clinical study revealed that the disease had some typhoid-like features and named the disease Q, for Query, fever (Derrick, 1937; Mackerras I. M., 1995). Derrick did not find any evidence of the nature of the germ responsible for the disease. Thinking it was probably a virus, he sent spleens from infected Guinea pigs to Macfarlane Burnet and Mavis Freeman. These were able to distinguish colonies of tiny rods by infecting mice instead of Guinea pigs (Burnet & Freeman, 1937; Maurin & Raoult, 1999).

Concurrently, in the state of Montana in the United States, Gordon E. Davis and Herald R. Cox identified an infectious agent in ticks collected near Nine Mile Creek. Based on the similarities of the symptoms and the notable cross-immunity the "Q" strain conferred to guinea pigs, they concluded that the isolated pathogen was possibly linked to the "Q" strain discovered a few years before in Australia (Davis & Cox, 1938).

A year later, Derrick deduced that the organism must belong to the *Rickettsia* species as they shared morphological similarities. Therefore, Derrick name the bacteria *Rickettsia burnetii* in honor of Burnet(Derrick, 1939). However, due to distinct phenotypic characters with rickettsial species, the name of *Coxiella burnetii* was given in 1948 in honor of both Herald R. Cox and Macfarlane Burnet to classify this pathogen into a separate genus (Philip, 1948). Many years after, in 1989, the sequencing of the 16S rRNA allowed to reclassify *C. burnetii* in the phylum Proteobacteria, class *γ-Proteobacteria*, order *Legionellales*, family *Coxiellaceae* (Weisburg et al., 1989).

Ever since, many Q fever outbreaks were reported. In the United States, three of them occurred in the 40s, in Chicago, Amarillo and Artesia in California where cases of Q fever were reported until 2016(Akamine et al., 2019; Shepard, 1947; Topping et al., 1947; Young, 1948).

Different outbreaks also occurred near the Mediterranean Sea during World War 2, notably among allied forces, and were associated with sleeping conditions of soldiers in hay contaminated by infected cattle and sheep (Robbins et al., 1946). More recently, in the 1980s-1990s, many European countries including France, Spain, Switzerland, Greece, Italy, the United Kingdom and Germany have reported cases of Q fever (Maurin & Raoult, 1999). Q fever has been classified as a worldwide zoonosis, as cases were reported in all continents, with the exception of New Zealand where no cases have ever been reported (Hilbink et al., 1993; Roest et al., 2011).

C. burnetii is a real threat for the economy and public health exemplified by the largest Q fever outbreak ever reported that occurred in the Netherlands between 2007 and 2011. During this period, up to 80% of spontaneous abortions in farm animals occurred and over 4000 human cases were reported (Roest et al., 2011). However, the Netherlands outbreak is not an isolated phenomenon as 1300 people fell ill in a much more restricted area in Poland in 1983 (Szymańska-Czerwińska et al., 2015).

As mentioned earlier, *C. burnetii* infections represent a biothreat during conflicts, as soldiers can be affected. More recently, over 30 American soldiers deployed in Afghanistan and Iraq were diagnosed positive for Q fever making them inoperative (Anderson et al., 2005; Aronson et al., 2006; Leung-Shea & Danaher, 2006).

The use of *C. burnetii* in military conflicts was envisioned during the cold war during which the bacterium was added to the biological weapons program (Madariaga et al., 2003). Due to its high infectivity through airborne transmission and strong resistance to environmental stresses, *C. burnetii* possesses characteristics of a usable biological weapon (Madariaga et al., 2003). Both United States and U.S.S.R included *C. burnetii* to their biological weapon research programs which consisted in human trials, weaponization and stockpiling of toxins or pathogens (Anderson et al., 2005; Madariaga et al., 2003; Noah et al., 2002). According to the World Health Organization, the aerosolization and release of 50 kg of *C. burnetii* over an urban area with 500 000 people would cause 125 000 cases of acute illness, 9000 cases of chronic Q fever and 150 deaths, thus the bacteria has been classified as a category B biothreat (Kagawa et al., 2003; Oyston & Davies, 2011).

1.1.2. The Q fever disease.

1.1.2.1. Infection & Symptoms.

C. burnetii infection in humans occur mainly by inhalation of contaminated aerosols. The infection may happen by direct contact with contaminated fluids from newborn animals, wool, or placenta (Maurin & Raoult, 1999). Consequently, farmers, veterinary and people in rural area are more susceptible to be infected (Pouquet et al., 2020). However, as *C. burnetii* is highly resistant to environmental stresses, wind can spread the microorganism far from farms and infections can occur without any evidence of direct contact with animals (Marrie & Raoult, 1997). As a striking example, a French study mentions that many Q fever cases were reported 40 km away from a sheep-rearing area during a very specific windy period of 1 month after the lambing season (Tissot-Dupont et al., 2004). Those airborne transmissions are supported by the very high infectivity of the bacteria; indeed, a challenge study indicate that the dose for 50% infection (ID50) in human subjects is 1.18 bacteria (Brooke et al., 2013).

Airborne transmission appears to be the main transmission mode for *C. burnetii* however, some studies report foodborne transmission for this bacterium. Transmission by infected raw milk was first suspected. Indeed, *C. burnetii* DNA could be found in raw milk in France or in the US but no live bacteria were detected (Kim et al., 2005; Pearson et al., 2014). It has also been demonstrated that contaminated milk could induce seropositivity in humans, but no clinical symptoms were ever reported in those cases (Angelakis & Raoult, 2010; Signs et al., 2012). Moreover, *C. burnetii* was detected in commercial eggs and mayonnaise in Japan and inoculation in mice demonstrated the infectivity of the isolated microbes (Tatsumi et al., 2006). However, it is currently considered by the World Organization for Animal Health that there is no significant evidence of transmission of *C. burnetii* by ingestion (Boarbi et al., 2015).
Ticks may play an important role as a reservoirs and vectors for the transmission of *C. burnetii* between animals (Celina & Cerný, 2022). A recent study reported the release of infectious bacteria during blood meals of infected ticks (Buysse et al., 2021). However, few clinical studies presented cases of tick-borne infections in humans (Duron, Sidi-Boumedine, et al., 2015).

Finally human-to-human transmission via blood transfusion, inhalation of aerosols during delivery of infected women, sexual transmission or trans-placental transmission, responsible for congenital infections, have been rarely mentioned (Boarbi et al., 2015). More recently, one case of contamination after injection of ovine cells (fetus and placenta) in the

context of cell therapy has been reported (Boarbi et al., 2015). However, human-to-human transmission remains rare and is not considered as a conventional transmission route.

The incubation period of Q fever is about 10 to 17 days and results in 40% of the cases presenting acute Q fever symptoms (Million et al., 2009). Acute Q fever onset is generally abrupt, symptoms are essentially high-grade fevers (up to 40°C),

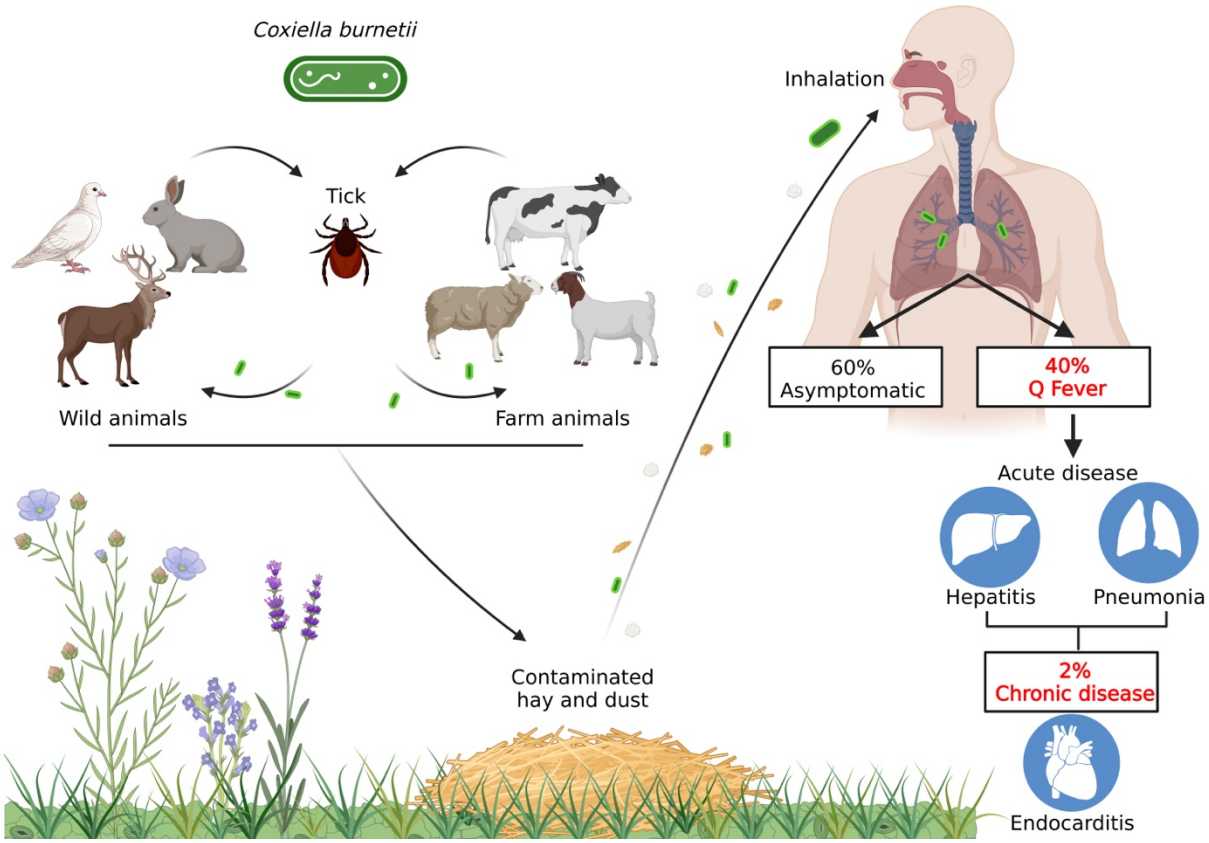


Figure 1: *C. burnetii* infectious cycle.

The zoonotic disease Q fever affects humans via the inhalation of contaminated hay and dust. Contaminated cattle and wild animals are the main reservoir that spread the bacteria in the environment during calving. In humans 60% of the infections are asymptomatic whereas 40% of infected people will develop an acute Q fever. For 2% of them, the disease can evolve into a chronic form that can be deadly.

headaches associated with photophobia, tiredness, and myalgias (Patil & Regunath, 2022). These symptoms can last for 1 to 3 weeks. Pneumonia associated with chest pain and nausea, is the main other symptom, with a high susceptibility for older adults (Keijmel et al., 2015). Hand rash is frequently found in kids. Younger individuals are also susceptible to acute hepatitis, which can be worsened by cholestatic jaundice or acalculous cholecystitis (Patil & Regunath, 2022).

Other atypical symptoms have been described and are listed in **table 1** (Hartzell et al., 2007; Parker et al., 2006).

Among infected people, 1 to 5 percent will develop a chronic infection (Million et al., 2009) that will result in symptomatic manifestations mostly during the first year after infection (Landais et al., 2007). Chronic Q fever patients may develop osteomyelitis, pericarditis, and hepatitis (Frankel et al., 2011) but in 75% of the cases they will suffer from endocarditis resulting from infections of vascular prostheses and aortic aneurysms (Kampschreur et al., 2014). Valvulopathy or previous valve surgery, aneurysm, vascular prostheses, renal insufficiency, older age, immunocompromised state, and cancer are some of the risk factors for the development of chronic infections (de Lange et al., 2019). A study made in the Netherlands with a cohort of known and suspected patients with chronic Q fever from the 2007 outbreak has evaluated the related mortality. In this study, over 60% of patients with proven chronic Q fever developed clinical complications and the overall mortality rate in these patients was 38% after a median follow-up of 3.6 years (van Roeden et al., 2019). However, antibiotic treatment (described below) of patient with chronic Q fever also affect and drastically reduce the mortality rate (Kampschreur et al., 2012).

It has also been shown that the second major symptom following Q fever is a chronic fatigue (QFS) syndrome, occurring in 15% of the cases (Strauss et al., 2012). In comparison to patients with prior acute Q-fever without the formation of QFS or chronic Q-fever in the first six months post infection, QFS patients report considerably higher levels of tiredness, more physical impairment, worse quality of life, and lower levels of social engagement (Reukers et al., 2022).

Finally, it remains unclear whether pregnancy increase the risk of obstetrical complications as contradictory results were reported in different studies (Million et al., 2014; Nielsen et al., 2014).

Common presentations	
Adults	"Flu-like" illness, with varying degrees of pneumonia, hepatitis high-grade fevers (up to 40°C), headaches associated with photophobia, tiredness, and myalgias.
Child	Cholestatic jaundice, acalculous cholecystitis and rash.
Less common presentations	
Neurological	Encephalitis , meningoencephalitis, encephalomyelitis , meningitis, cerebellitis Guillain-Barré syndrome, neuritis (including optic, brachial, and mononeuritis multiplex) Myelitis and peripheral neuropathy, polyradiculopathy, extrapyramidal neurological disease.
Gastrointestinal	Gastroenteritis, pancreatitis, splenic rupture, mesenteric panniculitis, acalculous cholecystitis.
Genital	Orchitis, epididymitis, priapism.
Cardiac	Myocarditis, pericarditis, myopericarditis.
Haematological	Haemolytic uraemic syndrome, haemophagocytosis, anaemia (haemolytic and transient hypoplastic). rhabdomyolysis, bone marrow necrosis.
Endocrine	Thyroiditis, inappropriate secretion of antidiuretic hormone.
Cutaneous	Maculopapular or purpuric rash, erythema nodosum.
Renal	Glomerulonephritis.
Other	Lymphadenopathy, severe respiratory distress syndrome.

Table 1: Acute Q fever clinical symptoms overview. (Adapted from *Parker et al. 2006* and *Patil et al.* 2022)

1.1.2.2. Prevalence & diagnostic.

Q fever is a zoonotic disease as it can infect animals provoking "*coxiellosis"* but most of the infections do not result in a symptomatic disease, making it challenging to diagnose. However, infected animals are believed to become the main reservoirs for *C. burnetii.* Among the reservoirs, cattle, sheep, and goats represent the main animal carriers (Eldin et al., 2017) but *C. burnetii* was also detected among wild mammals (González-Barrio & Ruiz-Fons, 2019), reptiles (Sander et al., 2021), and birds (Babudieri & Moscovici, 1952) indicating the existence of additional reservoirs in the wild. As mentioned earlier, arthropods, particularly several tick species, can carry *C. burnetii* (Abou Abdallah et al., 2022) and may also be a vector for human infections. However, in recent years in Europe, sheep and goat products were identified as the source of contamination for 90% of identified Q fever cases (EFSA Panel on Animal Health and Welfare 2010). Farm and slaughterhouse workers, laboratories staff as well as veterinarians are particularly exposed (Woldeyohannes et al., 2018). A recent study on the prevalence of *C. burnetii* in the Eastern Mediterranean region estimated that human seroprevalence was about 25.54%, while a prevalence of 28,3% was reported in Kenya (Ahmadinezhad et al., 2022; Knobel et al., 2013). However, this high human prevalence could be biased, as it has been showed that

in Africa, the human prevalence is highly variable and depends on the tested population (Vanderburg et al., 2014). Of note, the USA report around 150 cases of acute Q fever each year and the "Haut Conseil de la Santé publique" recorded 240 cases per year between 2000 and 2012 (Fièvre Q Recommandations de prise en charge, 2013). The latter report highlights that the number of reported cases may be highly underestimated as only hospitalized patients were considered. This may explain the large difference between the seroprevalence and the number of reported cases. In addition, acute Q fever diagnosis is complex as the symptoms lack specificity (c.f Table 1), and *C. burnetii* cannot be detected by routine bacterial identification assays.

The primary method for identifying *C. burnetii* infection is serology. In 90% of the cases, seroconversion is expected to be positive 3 weeks after the beginning of symptoms and is often discovered 6 weeks after the onset of symptoms. The methods for diagnosing Q fever are complement fixation, ELISA, indirect immunofluorescence antibody test (IFAT) and microagglutination, with the first three being commercially available (Fournier et al., 1998). Even if new ELISA tests are being developed(Ledda et al., 2020), IFAT remains the standard technique since it is the most precise and easiest to implement (Miller et al., 2018; Murphy & Field, 1970).

C. burnetii exhibits two phase variation, phase I and phase II, that correspond to differences in LPS structure, which will be discussed later in this manuscript. Differences in the LPS composition induces different adaptative responses that help to determine the temporality of the infection. Indeed, anti-phase I antibodies are generally present during chronic infections while anti-phase II antibodies are extensively found in acute Q fever. During infection, the antibody response varies as Anti-phase II IgM are the first detected antibodies followed by anti-phase II IgG, anti-phase I IgM, and finally then anti-phase I IgG antibodies are found in prolonged infections. Two to three weeks after the initiation of an acute illness, phase II IgG or IgM antibodies can be found; a meaningful diagnosis requires an IgG II titer of 1:200 and/or an IgM II titer of 1:50. After few months of infection and the establishment of a chronic infection, phase II antibodies titers decrease while phase I IgG titers increase (titer ≥ 800) (Dupuis et al., 1985; Eldin et al., 2017).

C. burnetii DNA and RNA can also be detected by Polymerase chain reaction (PCR) in different samples, such as blood, serum, or fresh tissues. Two specific repeated sequences are used, IS1111 and IS30a (IS for Insertion Sequence) (Klee et al., 2006). It has also been

demonstrated that lyophilization improves the sensitivity of *C. burnetii* PCR detection by concentrating bacterial genomic material. PCR diagnosis adds a significant value to the diagnosis of Q fever, essentially during acute stages of the disease in seronegative patients (Edouard & Raoult, 2016).

Culture of the bacteria and immunohistochemistry are sometimes used but present both major drawbacks. First, the culture of *C. burnetii* is quite fastidious as it requires specific growth conditions (Sanchez et al., 2018), this will be discussed later in the manuscript. Immunohistochemistry is used for *in situ* detection of *C. burnetii*, but the implemented antibodies have a low sensitivity (Lepidi et al., 2009).

To replace immunohistochemistry, fluorescent *in situ* hybridization (FISH) has been proposed to detect specific *C. burnetii* DNA or RNA *in situ* (Prudent et al., 2018). Detection of *C. burnetii* 16s rRNA by FISH has become a great complement to PCR, especially in the case of endocarditis (Aistleitner et al., 2018).

All these detection techniques are supported by clinical and radiological tools such as transthoracic and transoesophageal echocardiography that help to prevent early development of Q fever endocarditis (Melenotte, Epelboin, et al., 2019).

1.1.2.3. Treatment.

Animal vaccines are available (G. Zhang et al., 2007); however, human vaccines are not fully efficient nor safe. Since 1989, only one human vaccine, from inactivated phase I *C. burnetii* called Q-Vax, has been exclusively used in Australia (Gefenaite et al., 2011). However, its use has been constrained due to the serious side effects experienced by subjects already immune to *C. burnetii*. In order to receive the vaccine, each person must undergo pre-screening via a cutaneous test, which renders the worldwide distribution of Q-Vax logistically challenging. The Q-Vax vaccination is therefore recommended exclusively for those who are at risk, such as veterinarians, laboratory employees, farmers, or abattoir workers(Ruiz & Wolfe, 2014). Other attempts to developpe vaccines were performed but none were safer or more efficient (Boarbi et al., 2015). Today's new vaccine technologies and a better understanding of the immune response to *C. burnetii* infection will probably lead to the development of a non-reactive and efficient Q fever vaccine (Dold et al., 2023; Long, 2021).

Antibiotics are generally used to treat Q fever. The common treatment for acute Q fever is the administration of doxycycline for two weeks. This treatment can be extended to 18 months and be combined to hydroxychloroquine in the case of chronic Q fever, to prevent recurrence (Wiener-Well et al., 2010). Hydroxychloroquine enhances the efficiency of the bactericidal activity of doxycycline by increasing the pH of lysosomes and *C. burnetii* phagolysosomal-like replicative niche (discussed in chapter 2.2) (Maurin et al., 1992; Smith et al., 2019). Rifampin, macrolides, fluoroquinolones, and trimethoprim/sulfamethoxazole have all been suggested as alternatives to doxycycline and hydroxychloroquine but have never been demonstrated to be as efficient (Kersh, 2013). The emergence of *C. burnetii* strains resistant to doxycycline and hydroxychloroquine stresses the need for new vaccines and therapies (Rolain et al., 2005).

1.2. Microbiological specificities.

2.1.1. Morphotype and Variants.

C. burnetii is defined as a Gram-negative pleiomorphic obligate intracellular coccobacillus that measures 0.2 to 0.4 µm wide and 0.4 to 1 µm long. As mentioned earlier, the bacterium has two distinct morphological types: the small cell variant (SCV) and the large cell variant (LCV). The variant of the bacterium depends on the state of the developmental cycle of the bacteria. LCVs and SCVs differ in the structure of their bacterial cell wall, their gene expression, and their growth rates.

SCVs are small, non-replicating forms of the bacterium that are highly resistant to environmental stresses and metabolically inactive. SCVs can support harsh conditions such as nutrient limitation, desiccation, osmotic pressure, and elevated temperatures. Conversely, LCVs are the large form of the bacteria, which are metabolically active, replicative and are strictly intracellular.

The transition between the two morphological forms occurs into a membrane bound compartment called the CCV, for *Coxiella*-Containing Vacuole, during the infection (Discussed in part X). During the primo infection, the bacterial morphotype is SCV until 2 days of infection, then the shift to LCV occurs and the bacteria is replicating from day 2 to day 6 when it reaches

a stationary phase. At day 6 post infection, most of the bacteria turn back into an SCV form to infect other cells.

It has been shown that both forms have different protein composition but also different antigenic protein presentation leading to differential immune response (Figure 2).

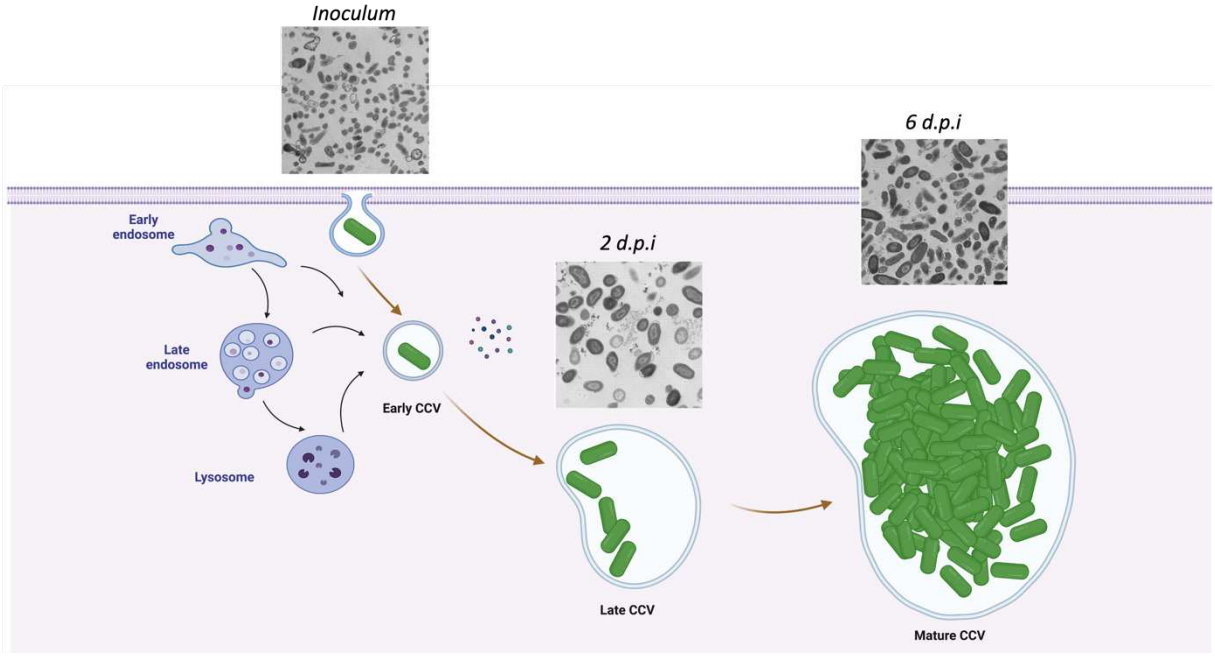


Figure 2: Morphological shift of *C. burnetii* during infection.

The non-replicating SCV form of *C. burnetii* enters the cell and resides in a membrane-bound compartment known as the *Coxiella*-containing vacuole (CCV). After the first two days of infection (lag phase), the non-replicative SCV switches into the replicative LCV form. Over the following four days, bacteria replicate exponentially until they reach a stationary phase at 6 days post-infection. A mixed population of LCVs and SCVs is then observed in mature CCVs.

2.1.2. Genetics, strains and phase variation.

The very first report on the genetic manipulation of *C. burnetii* took place in 1996 by Suhan et al., (1996) who transformed the organism using a vector containing *C. burnetii* autonomous replication sequence and an ampicillin-resistance gene. In 2009, a system utilizing a suicide plasmid for transposon mutagenesis was successfully engineered (Beare, Howe, et al., 2009). Since then, transposon mutagenesis has been employed to identify numerous genes that encode proteins with significant involvement in *C. burnetii* infection. The year 2009 marked

a pivotal milestone in *C. burnetii* research, as it witnessed the successful development of a complex culture medium called Acidified Citrate Cysteine Medium (ACCM) that enabled the axenic culture of the bacteria (Omsland et al., 2009).

The size of the chromosome in *C. burnetii* varies depending on the isolate, ranging from 1,989,565 to 2,214,254 base pairs (bp). Furthermore, most of *C. burnetii* strains possess a plasmid. Five distinct plasmid types have been identified: QpH1, QpRS, QpDV, QpDG, and a QpRS-like chromosomally integrated sequence (Jäger et al., 2002; Lautenschläger et al., 2000; Thiele et al., 1994; Valkova & Kazar, 1995; Willems et al., 1997). These plasmids vary in size, ranging from 32 to 54 kb, while also featuring a shared core region spanning 25 kb (Beare et al., 2006). This plasmid diversity underscores the genetic versatility of *C. burnetii* and its ability to adapt to different environmental conditions and hosts. It has also been shown that the QpH1 plasmid is also a virulence factor that is essential for the colonization of macrophages (Luo et al., 2021).

A recent study has revealed that, in addition to 505 genes encoded on the chromosome, six genes carried by the QpH1 plasmid are potentially essential for bacterial growth and survival in axenic media (Metters et al., 2023). However, it appears that there is no direct correlation between the virulence of *C. burnetii* and the size of its genome, as evidenced by the avirulent *C. burnetii* strain, Dugway 5J108-111, that has the biggest genome of any known strain, and the highly virulent Cb175 strain, which was identified in French Guiana that possess a significantly reduced genome size. (Beare et al., 2017; Melenotte, Million, et al., 2019)

Although *Coxiella burnetii* was first isolated from ticks in 1935, it was not until 2003 that the first genome sequencing of this bacterium was accomplished. The Nine Mile RSA493 isolate was specifically selected as the reference strain for genome sequencing (Seshadri et al., 2003). Currently, there are 83 sequences of *C. burnetii* documented in the NCBI database. These sequences belong to six distinct genomic groups (GGs), indicating substantial genetic variation among strains. This diversity is associated with different host species or geographical regions, as well as variations in virulence observed in animal models **(Table 2)** (Metters et al., 2019). GG I isolates are widely distributed globally and include commonly studied strains like NMI and NMII (Beare et al., 2006; D'Amato et al., 2016). GG II isolates are primarily found in Europe and were responsible of the 2007-2011 Q fever outbreak in the Netherlands (Tilburg et al., 2012). More recently, GG II has been further classified into three subgroups (GG IIa, GG IIb, and GG

IIc) based on variations in genome content and single nucleotide polymorphism (SNP) profiles (Hemsley et al., 2019; Tilburg et al., 2012). GG III isolates are specifically associated with cattle (Pearson et al., 2014), while GG IV isolates are linked to goats and do not grow in axenic media (Kersh et al., 2011; Pearson et al., 2014; Vincent, 2014). The Genomic Group IV has also been divided into three subgroups (GG IVa, GG IVb, and GG X) (Hemsley et al., 2019). GG V isolates are predominantly found in North America (D'Amato et al., 2016). Finally, GG VI, that contains the Dugway isolate, is associated with rodents but does not appear to cause disease in humans (Beare et al., 2017; Beare, Unsworth, Andoh, Voth, Omsland, Gilk, Williams, Sobral, John J. Kupko, et al., 2009). However, it has recently been proposed that some sub-lineages of GG II and GG IV might represent distinct groups themselves, but this has yet to be confirmed (Hemsley et al., 2021).

Genomic Group (GG)	Plasmid type	Geographical source of isolation	Host organisms
I	QpH1	Asia, Africa, Europe, North America, (South America)	Cow's milk, ticks, goats, sheep, acute Q fever patients
II	QpH1	Asia, Europe	Mainly goats and sheep, acute and chronic Q fever patients
III	QpH1	Europe, North America	Predominantly cattle; not usually associated with human disease
IV	QpRS/QpDV	Worldwide	Mainly goats and sheep, acute and chronic Q fever patients
V	Integrated	North America	Dogs, cats, chronic Q fever patients
VI	QpDG	North America	Rodents only; not associated with human disease

.Table 2: Current overview of the six genomic groups of *C. burnetii*. (Adapted from *Metters, et al. 2019)*

C. burnetii displays a phase variation altering the structure of its lipopolysaccharide (LPS), a key factor influencing its virulence and ability to cause acute or chronic disease. In phase II bacteria, a 26-kb deletion is observed in a specific genomic region housing genes involved in LPS biosynthesis (Baca et al., 1994; Hackstadt, 1990). Consequently, Phase I *C. burnetii* possesses a full-length LPS and is associated with the naturally occurring virulent strains observed in human and animal infections whereas, Phase II *C. burnetii* produces a truncated LPS and presents a loss in virulence (Beare et al., 2006, 2018; Hackstadt, 1990; Hoover et al., 2002). This phase variation resembles the smooth-to-rough transition observed in virulent and

avirulent forms of bacteria in the *Enterobacteriaceae* family (Abnave et al., 2017). This gene deletion is observed during serial passages of the bacterium in embryonated eggs and cell cultures and may occur during human infections as anti-phase II antibodies can be found in the serum of infected individuals.

The key difference between Phase I and Phase II LPS of *C. burnetii* lies in the LPS sugar composition and the absence of O-antigen. Phase I LPS contains L-virenose, dihydrohydroxystreptose, and galactosamineuronyl-α-(1,6)-glucosamine, whereas Phase II LPS lacks these components **(Figure 3)**. Immunodeficient mice infected with *C. burnetii* Nine Mile Phase II (NMII) are showing febrile reactions despite the absence of O-antigen in Phase II LPS, which allows the observation of clinical symptoms and the assessment of infection with this strain. (Abnave et al., 2017).

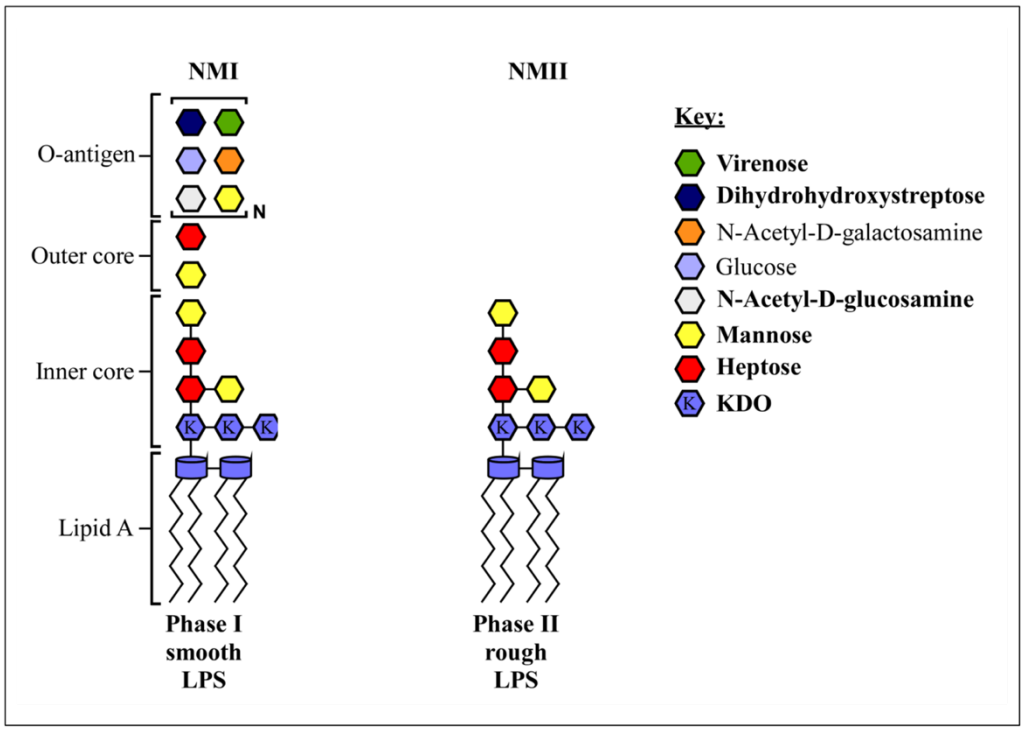


Figure 3 : *C. burnetii* LPS phase variation, from NMI to NMII. (Adapted from *Beare et al., 2018*)

All *C. burnetii* strains necessitate containment within biosafety level-3 (BSL-3) facilities. However, the NMII strain represent an interesting model that can be safely handled within biosafety level-2 (BSL-2) environments (with the exception of certain countries such as the UK), due to its non-reversible 26-kb deletion (Amano & Williams, 1984; Hackstadt, 1996).

Importantly, the loss of virulence in NMII does not affect its ability to replicate efficiently in myeloid and epithelial cell lines, making it a valuable model for studying *C. burnetii* infectious cycle (D. Howe et al., 2010).

2.1.2. Dot/Icm Type 4B secretion system.

2.1.2.1 T4SS structure and composition

The bioinformatic analysis of the *C. burnetii* genome revealed the presence of canonical components of a type I secretion system (T1SS), including a *tolC* homolog (Beare et al., 2009; Seshadri et al., 2003) The T1SS transports proteins directly from the bacterial cytoplasm into the surrounding environment in a one-step process (Delepelaire, 2004). In a study published in 2013, it was suggested that *C. burnetii* might use T1SS to secrete proteins directly into its CCV, although no additional studies were carried out on this subject (Stead et al., 2013). In addition to the T1SS, *C. burnetii* lacks some of the typical components of a type II secretion system (T2SS) (Cianciotto, 2005), but it does encode several genes involved in type IV pili (T4P) assembly, some of which show homology to counterparts found in type II secretion systems, suggesting a shared evolutionary origin and potential similar functions (Peabody et al., 2003).

To date, only the type 4 secretion system (T4SS) encoded by *C. burnetii* is considered functional and essential for its pathogenesis and intracellular development (Moffatt et al., 2015).

T4SSs are complex protein structures found in both Gram-negative and Gram-positive bacteria that are incorporated into bacterial cell wall which enable the transfer of proteins and nucleic acids to host cells. (Bhatty et al., 2013; Christie et al., 2014; Goessweiner-Mohr et al., 2013; Gonzalez-Rivera et al., 2016; Voth et al., 2012). These nanomachines play a crucial role in the virulence and pathogenesis of bacteria, as well as in antibiotic resistance (Vogel et al., 1998). Phylogenetically, T4SSs can be categorized into two main subtypes: type IVA (T4ASS) and type IVB (T4BSS) (Chandran Darbari & Waksman, 2015; Christie, 2016).

The T4ASS, initially discovered in the plant pathogen *Agrobacterium tumefaciens,* is composed of 8 to 12 different protein subunits and is found in many bacteria including *Brucella, Bartonella, Rickettsia*, and *Anaplasma* species (Chandran Darbari & Waksman, 2015) (Figure 4). The T4BSS exhibits greater complexity as it is composed of more than 20 proteins (Christie, 2016). The Defect in organelle trafficking/Intracellular multiplication (Dot/Icm) secretion system is a representative example of the type T4BSS and is present in intracellular bacterial pathogens such as *Legionella pneumophila, Rickettsiella grylli,* and *C. burnetii* (Nagai & Kubori, 2011) (**Figure 4**).

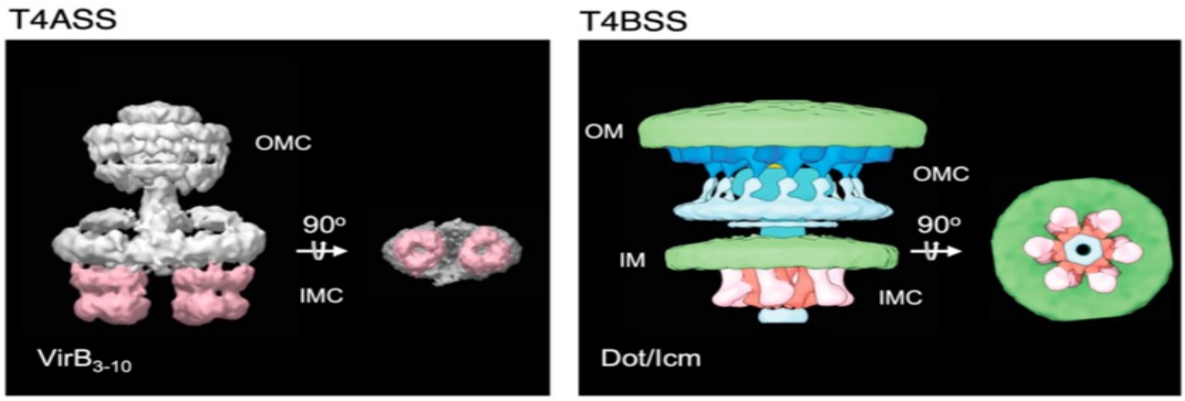


Figure 4: A visual representation of the VirB3-10 (T4ASS) and the Dot/Icm (T4BSS) secretion systems (Adapted from Grace & Christie, 2019)

The left panel provides a 3D representation of the VirB3-10 substructure, with side and bottom views. It highlights the VirB4 ATPase hexameric barrels positioned side by side, represented in pink color. In the right panel, a 3D surface rendering of the Dot/Icm T4SS is displayed from side and bottom perspectives. The bacterial membranes are depicted in green, while the entrance to the translocation channel is formed by the DotO and DotB hexameric ATPases, shown in shades of pink and purple, respectively.

The Dot/Icm Type 4B Secretion System was extensively studied in *L. pneumophila*, the causative agent of Legionnaires' disease. It is composed of 27 proteins, 22 structural proteins and 5 chaperones, classified as membrane and cytoplasmic components (Voth et al., 2012).These include one outer-membrane proteins (DotH) and three lipoproteins (DotC/D/K), the periplasmic protein (IcmX), multiple inner membrane proteins (DotA/E/F/G/I/J/M/P/U/V/F/T), inner membrane-associated ATPases (DotB/L/O) and soluble cytosolic proteins (DotN/Q/R/S/W and LvgA). We can also distinguish subcomplexes composed of these proteins, namely the outer membrane associated core complex and the type IV coupling protein (T4CP) subcomplex.

The outer membrane associated core complex is composed of DotC, DotD, DotF, DotG, and DotH proteins, while the Type IV coupling protein subcomplex comprises DotL, DotM, DotN, IcmS, IcmW, and LvgA proteins. Interestingly, the T4BSS of *C. burnetii* exhibits a high degree of similarity to that of *L. pneumophila*, and some of the *dot/icm* genes in *C. burnetii* can functionally compensate for their counterparts in *L. pneumophila* mutants. The close phylogenetic relationship between *C. burnetii* and *L. pneumophila* can explain the observed similarities (Vogel, 2004). However, there are notable discrepancies between the two systems. Notably, *L. pneumophila* and *C. burnetii* T4BSS contain 24 identical proteins, however the latter lacks the proteins DotJ, DotV, and IcmR.

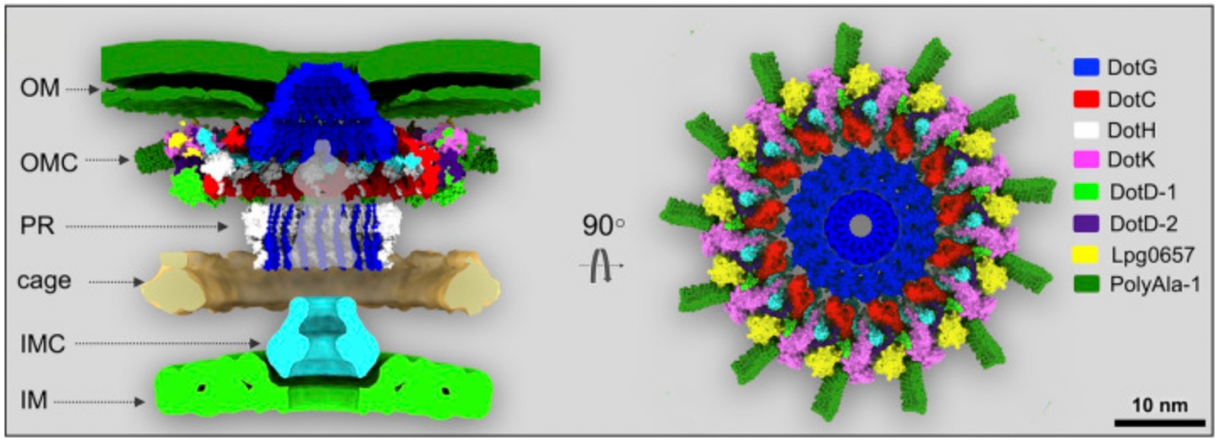


Figure 5: Model of *C. burnetii* T4SS depicted in both side view (left) and top (right) view orientations. (Adapted from *Park et.al 2022*)

OM: outer membrane. PG: peptidoglycan. OMC: outer membrane complex. PR: periplasmic ring. IMC: inner membrane complex.

A recent study determined the structure of *C. burnetii* T4SS (**Figure 5**) and showed that the absence of DotJ, DotV, and IcmR does not affect its ultrastructure (Park et al., 2022). They also showed that the structure of the T4SS changes during the intracellular cycle of *C. burnetii.* Indeed, during the first step of the infection, the T4SS is inactive and does not connect with the inner membrane of the bacterial cell wall, avoiding bacterial effector translocation. However, after acidification of the CCV, the T4SS changes its conformation and is then linked to the bacterial cytoplasm, thus allowing the translocation of bacterial proteins directly into the cytoplasm of the host cell (**Figure 6**). Furthermore, within the core complex, the cytoplasmic ATPase DotO has a crucial role in T4BSS assembly. Indeed, DotO allows the recruitment a

secondary cytoplasmic ATPase, DotB, indispensable for translocation of Dot/Icm substrates into the host cell cytoplasm. The formation of the DotO-DotB ATPase complex implies crucial structural modifications that promote the establishment of a channel, facilitating direct bacterial secretion.

Besides T4SS components the *C. burnetii* protein EirA (Essential for intracellular replication A) has been shown to play a crucial role in Dot/Icm effector translocation as mutantions in *eirA* lead to a significant impairment in *C. burnetii* replication. Interestingly, EirA itself is not translocated by the T4BSS and is localized within the bacterial cytoplasm or at the bacterial inner membrane. However, the absence of EirA blocks Dot/Icm effector translocation and *eirA*::Tn mutant CCVs are comparable to T4SS mutants CCVs. This suggests that EirA may have a functional role in regulating the assembly or expression levels of the T4BSS machinery (Kuba et al., 2020).

The Dot/Icm machinery transports bacterial proteins from the bacterial cytosol directly into the cytoplasm of the host cell. This process of delivery is well established and cytoplasmic chaperones such as LvgA, IcmS, and IcmW are in charge of recruiting effectors via their C-terminal Dot/Icm translocation signal known as the E-Block motif. Subsequently, these chaperones engage with inner membrane proteins and the T4CP subcomplex, positioning effectors to the bacterial inner membrane. This process enhances the delivery of Dot/Icm substrates to the secretion chamber, formed by three Dot proteins (G,F,H). Through this chamber, effectors are translocated through the periplasmic space and outer membrane, enabling direct bacterial secretion into the host cell cytoplasm (Chetrit et al., 2018; Durie et al., 2020; Sheedlo et al., 2021).

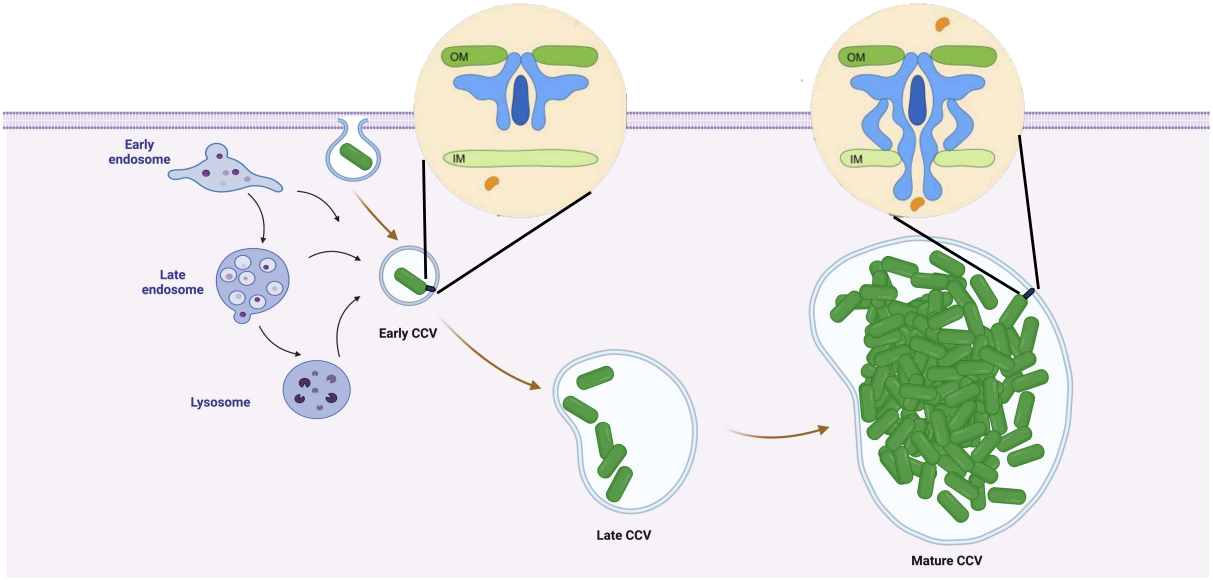


Figure 6: Conformational changes of the T4SS during the intracellular lifecycle of *C. burnetii.* (Adapted from *Park et al., 2022*)

C. burnetii undergoes dynamic developmental transitions within host cells, leading to the assembly Dot/Icm secretion system. This process occurs during the transition from the non-replicating SCV to the replicating LCV.

It is noteworthy that some Dot/Icm secretion system components, including IcmD, IcmX, DotA, DotC, DotD, and DotH, also possess a C-terminal translocation signal. However, only IcmX and DotA appear to be secreted in a Dot/Icm-dependent manner as they are found in axenic media during *C. burnetii* growth. Interestingly, during host cell infection, DotA localizes to the CCV membrane and to vesicles positive for CD63, a marker of multivesicular bodies (MVBs). The precise role of Dot/Icm translocated components remains unelucidated, but it can be postulated that DotA and IcmX are potentially participating in the transportation of effectors across the CCV membrane, as suggested by Luedtke et al. in 2017 (Luedtke et al., 2017). The role of Dot/Icm secretion system in *C. burnetii* intracellular lifecycle has been studied through the use of Dot/Icm gene mutants. Indeed, deletion of DotA and DotB, as well as transposon mutagenesis affecting various Dot/Icm genes, including DotA and IcmX, was restricting the formation of the CCV. This highlights the indispensable function of these genes and of the translocated proteins in intracellular bacterial replication (Beare et al., 2011; Carey et al., 2011; Martinez et al., 2014).

2.1.2.1 T4SS substrates

To date, there is no absolute rule to determine if a gene of *C. burnetii* encodes for a T4SS effector protein, however, it has been shown that most of the effector encoding genes share some features. Analysis of the amino acid sequence of validated effector proteins revealed that a high concentration of glutamic acid residues at their C-terminus is essential for their effective translocation. This specific arrangement of amino acids constitutes a secretion signal known as the E-block motif, which typically consists of 20 to 35 amino acid residues (L. Huang et al., 2011). The specific composition of the E-block domain allows the recognition of effectors by chaperones of the T4SS machinery. This sequence, in addition of being rich in glutamic acid, is characterized by a balanced distribution of small, polar, charged and hydrophobic amino acids (Lifshitz et al., 2013). Additionally, the expression of Dot/Icm genes and some of effector protein genes appears to be under the control of the PmrA/B two-component system. This system recognizes a specific regulatory element located in the predicted promoter region of these genes. The regulatory element consists of a tandem repeat sequence which is positioned approximately 100 base pairs upstream of the genes first ATG codon (Beare et al., 2014). A study has shown that the *C. burnetii* PmrA/B transcriptional activity depends on the presence of breakdown products deriving from the lysosomal activity in the CCV, including specific amino acids. This leads to an up-regulation of *dot*/*icm* and effector genes expression (Newton et al., 2020). These findings suggest that the PmrA/B system senses and responds to the environmental cues within the CCV, enabling the modulation of gene expression essential for the activity of the Dot/Icm secretion system.

Like other intracellular bacteria such as *Legionella* or *Chlamydia*, *C. burnetii* possesses effector proteins that contain domains or motifs, likely acquired through horizontal gene transfer during the co-evolution of the bacteria with host cells and that are commonly found in eucaryotes (De Felipe et al., 2005). The role of these motifs/domains might be essential to mimic host cell pathways to promote infection (Duron, Noël, et al., 2015). Effector proteins are de facto more susceptible to contain such characteristics due to their delivery on the host cell cytoplasm. To date, 56 genes in *Coxiella* genome have been described as containing putative eukaryotic like domains, notably Ankyrin repeat domains (Burette et al., 2020; Pan et al., 2008; Voth et al., 2009).

In a similar manner, the identification of effector proteins can be done through bioinformatics analysis of their homologies with other bacterial effectors that have already been identified (Meyer et al., 2013).

2. Intracellular life cycle

2.1. Bacterial entry.

2.1.1. Adhesion & Invasion.

C. burnetii exhibits a strong tropism towards monocytes/macrophages in humans (Fernandes et al., 2016; Sobotta et al., 2016). However, it can also invade and replicate within diverse cell types (Sobotta et al., 2017).

C. burnetii Phase I enters alveolar macrophages through actin-dependent phagocytosis, facilitated by the interaction between cellular lipid raft-associated $\alpha_v\beta_3$ integrins and an unknown bacterial ligand (Capo et al., 1999; Meconi et al., 1998). This interaction triggers the rearrangement of host cell actin cytoskeleton mediated by Rho family GTPases, including RhoA effectors mDia1 and ROCK, as well as cortactin, leading to membrane ruffling and internalization (Rosales et al., 2012; Salinas et al., 2015). As mentioned earlier, in addition to alveolar macrophages, *C. burnetii* is capable of invading non-phagocytic cells such as epithelial and endothelial cells. In these cells, the internalization process involves the interaction between *C. burnetii* invasin OmpA (Figure 7) and an unidentified host cell receptor, accompanied by actin cytoskeleton rearrangements (Martinez et al., 2014; Rosales et al., 2012). It is worth noting that, while $\alpha_v\beta_3$ integrin plays a significant role in the internalization process in alveolar macrophages, its expression is low in epithelial cells, suggesting the involvement of alternative receptors during *C. burnetii* invasion of epithelial cells.

C. burnetii phase variation also plays a major role in the attachment and internalization of the bacteria. Indeed, Phase I *C. burnetii*, which induces membrane protrusions, exhibits lower efficiency of internalization compared to phase II organisms in professional phagocytes (Capo et al., 1999) and fibroblast/epithelial cells (Moos & Hackstadt, 1987). The reduced internalization of phase I *C. burnetii* may be attributed to the differential engagement of host cell receptors by the phase variants. In addition to the integrin αvβ3, phase II bacteria additionally interact with the CR3 receptor (Capo et al., 1999). It is proposed that the membrane projections induced by phase I adherence restrict the involvement of the CR3 co-receptor, leading to lower internalization efficiency (Meconi et al., 1998). Moreover, the

presence of full-length LPS in phase I organisms can further impede CR3 binding due to masking of *C. burnetii* surface proteins (Shannon et al., 2005; Vishwanath & Hackstadt, 1988).

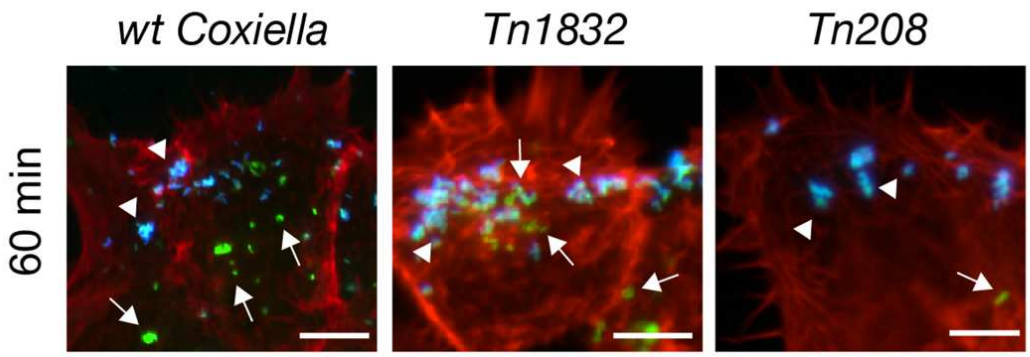


Figure 7: Importance of the invasin OmpA for *C. burnetii* entry.

A431 non-phagocytic epithelial cells were infected with wild-type (*wt*) *Coxiella*, the intergenic transposon mutant Tn1832, or the *ompA*::Tn mutant Tn208. After 60 minutes of infection, the cells were fixed and immunolabelled with anti-*Coxiella* antibodies to label extracellular (blue) and total (green) bacteria. The *ompA*::Tn mutant Tn208 was significantly less internalized than *wt Coxiella* or the Tn1832 mutant.

2.1.1. Ezrin and CD44 participate in the internalization process of Coxiella burnetii into non-phagocytic cells.

During my studies, I have been involved in a collaborative project that aimed at identifying the importance of CD44 and ezrin during *C. burnetii* entry. In particular, I investigated and analyzed the phosphorylation dynamics of ezrin at early time points of infection.

Check for updates

Received: 23 December 2021 | Revised: 11 July 2022 | Accepted: 15 July 2022

DOI: 10.1111/boc.202100096

Biology of the Cell

RESEARCH ARTICLE

Ezrin and CD44 participate in the internalization process of *Coxiella burnetii* into non-phagocytic cells

Jesús S. Distel[1] | **Rodolfo M. Ortiz Flores**[1,3] | **Arthur Bienvenu**[2] | **Milton O. Aguilera**[1,3] | **Matteo Bonazzi**[2] | **Walter Berón**[1]

[1]Instituto de Histología y Embriología, Facultad de Ciencias Médicas, Universidad Nacional de Cuyo - CONICET, Mendoza, Argentina

[2]Institut de Recherche en Infectiologie de Montpellier (IRIM) UMR 9004 CNRS, Université de Montpellier, Montpellier, France

[3]Cátedra de Microbiología, Parasitología e Inmunología, Facultad de Odontología, Universidad Nacional de Cuyo, Mendoza, Argentina

Correspondence
Walter Berón, Instituto de Histología y Embriología, Facultad de Ciencias Médicas, Universidad Nacional de Cuyo - CONICET, Mendoza, 5500, Argentina.
Email: wberon@fcm.uncu.edu.ar

Abstract

Ezrin protein is involved in the interaction of actin cytoskeleton with membrane receptors such as CD44. It regulates plasma membrane dynamics and intracellular signaling. *Coxiella burnetii*, the etiologic agent of Q fever, is internalized into host cell through a poorly characterized molecular mechanism. Here we analyzed the role of ezrin and CD44 in the *C. burnetii* internalization by HeLa cells. The knockdown of ezrin and CD44 inhibited the bacterial uptake. Interestingly, at early stages of *C. burnetii* internalization, ezrin was recruited to the cell membrane fraction and phosphorylated. Moreover, the overexpression of non-phosphorylatable and phosphomimetic ezrin mutants decreased and increased the bacterial entry, respectively. A decrease in the internalization of *C. burnetii* was observed by the overexpression of CD44 truncated forms containing the intracellular or the extracellular domains. Interestingly, the CD44 mutant was unable to interact with ERM proteins decreased the bacterial internalization. These findings demonstrate the participation of ezrin in the internalization process of *C. burnetii* in non-phagocytic cells. Additionally, we present evidence that CD44 receptor would be involved in that process.

KEYWORDS
Coxiella burnetii, CD44, Ezrin, phagocytosis

INTRODUCTION

Phagocytosis is the process by which cells recognize and ingest particles larger than 0.5 μm (Torres-Gomez et al., 2020). This complex mechanism begins with the recognition and engagement of the particle by cellular receptors. Receptor clustering induces actin cytoskeleton rearrangements and plasma membrane modifications that promote the internalization of the particle target (Jaqaman & Grinstein, 2012). Phagocytosis culminates with the formation of the nascent phagosome and its subsequent maturation, a process that comprises sequential fission and fusion events of the phagosome with endo/lysosomal compartments until the formation of the phagolysosome in which the ingested particle is degraded (Niedergang & Grinstein, 2018; Rosales & Uribe-Querol, 2017). Several bacterial pathogens have developed specific strategies to avoid intracellular killing and replicate inside the host cell (Thakur et al., 2019).

Coxiella burnetii, the causative agent of human Q fever, is an obligate intracellular bacterium found in a wide range of hosts, including livestock and humans (Angelakis & Raoult, 2010; Eldin et al., 2017). The primary route of human transmission is through inhalation of aerosols or dust contaminated with the bacterium (Angelakis & Raoult, 2010; Eldin et al., 2017). In the natural environment, *C. burnetii* exhibits tropism for monocytes/macrophages (Fernandes et al., 2016; Sobotta et al., 2016), however it can invade and replicate in a wide variety of cell lines (Baca & Paretsky, 1983; Sobotta et al., 2017). The adherence and internalization of *C. burnetii* into the host cell is a passive process

Abbreviations: CCV, *Coxiella* containing vacuole; ERM, Ezrin, Radixin, and Moesin; FERM, band 4.1/ezrin/radixin/moesin; PIP_2, phosphatidylinositol-(4,5)-bisphosphate.

© 2022 Société Française des Microscopies and Société de Biologie Cellulaire de France. Published by John Wiley & Sons Ltd.

that involves $\alpha_v\beta_3$ integrins (Capo et al., 1999; Gilk et al., 2013) and reorganizations of the actin cytoskeleton (Meconi et al., 1998; Rosales et al., 2012; Salinas et al., 2015). Recently, we have demonstrated that cortactin, Rho family GTPases and specifically RhoA effectors mDia1 and ROCK are involved in *C. burnetii* entry into the host cells (Rosales et al., 2012; Salinas et al., 2015). Within the nascent phagosome, the bacterium actively manipulates host factor to induce the biogenesis of the *Coxiella* Containing Vacuole (CCV) (Carey et al., 2011; Voth & Heinzen, 2007) along the endocytic and autophagic pathway.

The ERM protein family is composed of three members Ezrin, Radixin, and Moesin. Ezrin encodes a membrane-binding domain called FERM (band 4.1/ezrin/radixin/moesin) at the N-terminal region and the actin binding sites located at the C-terminus. Head-to-tail association/dissociation between N- and C-terminal domains (Gary & Bretscher, 1995; Li et al., 2007; Magendantz et al., 1995; Pearson et al., 2000) allows ezrin to cycle between a closed inactive conformation and an open active conformation. In its inactive state ezrin is mainly present in the cytosol and it has to be recruited to the plasma membrane to be activated. Ezrin activation is achieved by two sequential steps: the interaction of its FERM domain with phosphatidylinositol-(4,5)-bisphosphate (PIP_2) in the plasma membrane and the phosphorylation of a threonine residue located at position 567 by protein kinases, including ROCK (Chen et al., 2011; Fievet et al., 2004; Gautreau et al., 2000; Hébert et al., 2008; Matsui et al., 1998; Pelaseyed et al., 2017; Quang et al., 2000; Rey-Gallardo et al., 2018; Yonemura et al., 1999). This process stabilizes the open conformation of ezrin and enables ezrin-actin filaments interaction (Bosk et al., 2011; Gautreau et al., 2000).

ERMs are multifunctional proteins that coordinate the interaction of the actin cortex with the plasma membrane and transmit information from the external milieu to the cell, through their interaction with membrane receptors (García-Ortiz & Serrador, 2020). Recent works propose two different functions of ezrin in the phagocytic process. First, ezrin would function as a signaling molecule in phagocytic processes that are independent of the particle opsonization or immunoreceptor tyrosine-based activation motifs (ITAM) receptors. In this case, ezrin would activate the PIP_2-ERM-ITAM-Syk axis, participating to the ingestion of the particle (García-Ortiz & Serrador, 2020; Lau et al., 2011; Mu et al., 2018). On the other hand, ezrin could be the key regulator of membrane tension needed to allow the phagocytic process to develop correctly (García-Ortiz & Serrador, 2020; Roberts & Hallett, 2019; Tuckwell & Humphries, 2020). Several studies establish the participation of ERM proteins in the uptake of intracellular bacteria such as *Shigella flexneri* (Skoudy et al., 1999), *Escherichia coli* (Goosney et al., 2001), *Neisseria meningitidis* (Eugène et al., 2002), *Chlamydia trachomatis* (Swanson et al., 2007), *Brucella abortus* (Watanabe et al., 2009), *Staphylococcus aureus* (Li et al., 2018) by host cells.

CD44, the main receptor of hyaluronic acid, is a membrane glycoprotein widely distributed in different cell tissues (Aruffo et al., 1990). At the structural level, it presents an extracellular segment with binding sites for different ligands, a transmembrane domain that regulates its distribution in the plasma membrane and a cytoplasmic tail with binding sites for different cellular signaling proteins (Dzwonek & Wilczynski, 2015; Ponta et al., 2003). CD44 can be associated to the actin cytoskeleton through its interaction with ERM and ankyrin proteins (Thorne et al., 2003). The ERM binding site in CD44 is a small sequence of basic residues very close to the plasma membrane (Hao et al., 2009; Legg & Isacke, 1998; Sun et al., 2020).. CD44 can act as a fully functional phagocytic receptor for internalizing large particles (Vachon et al., 2006). Furthermore, CD44 can function as a co-receptor in the phagocytic process since it can induce the inside-out activation of $\alpha_M\beta_2$ integrins (Vachon et al., 2007). CD44 is implicated in the interaction with and internalization of different bacteria (Moffat et al., 1996) such as *Shigella* (Skoudy et al., 2000), *Mycobacterium tuberculosis* (Leemans et al., 2003) or *S. aureus* (Li et al., 2018) with the host cell.

This report describes the participation of ezrin and CD44 in the internalization process of *C. burnetii* into HeLa cells. We observed that the knockdown of ezrin using small interference RNA (siRNA) inhibited bacterial uptake. The overexpression of a non-phosphorylatable mutant of ezrin (T567A) produced a decrease in internalization level, while the phosphomimetic mutant (T567D) increased it. Furthermore, the phosphomimetic mutant T567D was capable of countering the inhibitory effect observed on the internalization of *C. burnetii* induced by the ROCK inhibitor Y-27632. Interestingly, an increase in the levels of phosphorylation of endogenous ERMs proteins was observed in early stages of infection. In agreement with these results, *C. burnetii* infection triggered the recruitment of ezrin at the plasma membrane of infected cells. Finally, the overexpression of truncated forms of the CD44 receptor or the silencing of CD44 in HeLa cells produced a significant decrease in *C. burnetii* uptake. In summary, our results indicate that ezrin and CD44 are involved in the internalization process of *C. burnetii* into non-phagocytic cells.

RESULTS

Depletion of ezrin affects the internalization of *C. burnetii*

ERM proteins regulate the interaction of actin microfilaments with the plasma membrane and receptors. They are involved in cellular membranes processes

1768322x, 2022, 9, Downloaded from https://onlinelibrary.wiley.com/doi/10.1111/boc.202100096 by Portail BibCNRS INSB, Wiley Online Library on [09/06/2023]. See the Terms and Conditions (https://onlinelibrary.wiley.com/terms-and-conditions) on Wiley Online Library for rules of use; OA articles are governed by the applicable Creative Commons License

such as endocytosis (Kvalvaag et al., 2018; Li et al., 2017), macropinocytosis (Chiasson-MacKenzie et al., 2018; D'Angelo et al., 2007) or phagocytosis (Marion et al., 2011; Murad et al., 2014).

To determine the role of ezrin in the internalization of *C. burnetii*, HeLa cells were co-transfected either with ezrin-targeting or scramble (non-targeting) siRNAs together with an EGFP expression vector to visualize transfected cells. Western Blot was used to assess the expression levels of endogenous ezrin for all conditions, using specific antibodies. Ezrin-targeting siRNA led to a six-fold decrease in the intracellular levels of ezrin as compared to cells transfected with control siRNA (Figure 1a,b). Cells were thus infected with *C. burnetii* for 6 h, fixed and processed for indirect immunofluorescence to estimate internalized bacteria by confocal microcopy (Figure 1). Ezrin depletion led to a significant decrease in bacterial internalization without affecting the number of total bacteria associated to host cells (Figure 1d,e). Similar results were observed in cells overexpressing a truncated non-functional mutant of ezrin (data not shown). These results suggest that ezrin is involved in the internalization of *C. burnetii* but not in the adhesion of the bacterium to the host cell.

Ezrin is recruited to the membrane of the host cell during *C. burnetii* infection

The ezrin activation process depends on two key steps: the recruitment of the protein to membranes and the phosphorylation of its residue threonine 567 to acquire its open conformation (Li et al., 2017; Shabardina et al., 2016; Tsai et al., 2018). Given that ezrin seems to regulate *C. burnetii* internalization, we speculated that infection might trigger ezrin recruitment to the host´s cell plasma membrane during infection. This was investigated by infecting HeLa cells for different periods of time and then determining ezrin localization by Western blot following cell fractionation. Indeed, endogenous ezrin was gradually recruited at the membrane fraction from 30 min of infection, peaked at 60 min, and then declined at 90 and 180 min of infection (Figure 2). These results suggest that ezrin is recruited to the cell membrane at early stage during *C. burnetii* internalization.

The phosphorylation state of ezrin is important for the uptake of *C. burnetii* by the host cell

Ezrin recruitment at the plasma membrane is dependent of its phosphorylation state. Therefore, we decided to study the role of ezrin phosphorylation in the uptake of *C. burnetii* using single amino acid substitution mutants at the threonine 567 (T567). For this purpose, HeLa cells were transfected with constructs that encode an inactive mutant form of ezrin unable to be phosphorylated (T567A) or an active pseudophosphorylated mutant that mimics a permanent phosphorylation state (T567D). Transfected cells were then infected with *C. burnetii* for 6 h, fixed, processed for immunofluorescence, and analyzed by confocal microscopy to quantify internalized and total bacteria (Figure 3a). The overexpression of the T567A mutant led to a decrease in the number of internalized bacteria, while the phosphomimetic mutant triggered a strong increase with respect to the control conditions (Figure 3b). Bacterial adhesion remained unaltered for all conditions tested (Figure 3c). These results indicate that phosphorylation of the residue T567 of ezrin is important for the uptake of *C. burnetii* into the host cell.

To determine whether *C. burnetii* induces ezrin phosphorylation, we analyzed the phosphorylation status of carboxy terminal threonine residue of endogenous ERMs proteins (567 of ezrin, 564 of radixin, and 558 of moesin) during infection. HeLa cells were infected with *C. burnetii* for different periods of time, lysed as previously indicated and analyzed by SDS-PAGE and Western blotting using a specific antibody. As shown in Figure 4, infection with *C. burnetii* induced phosphorylation of ERM proteins and maximum levels were observed between 60 and 90 min of infection. These results indicate that phosphorylation of ERM proteins occurs during early times of *C. burnetii* internalization.

Ezrin is a member of the ROCK pathway implicated in the internalization of *C. burnetii* to the host cell

We have previously demonstrated that Rho-associated kinase (ROCK) plays a key role in the internalization of *C. burnetii* in different cell lines (Salinas et al., 2015). The residue threonine 567 of ezrin is one of the ROCK substrates and the inhibition of this kinase causes an important decrease in ezrin phosphorylation levels (Chen et al., 2011; Hausrat et al., 2015; Hébert et al., 2008; Matsui et al., 1998; Quang et al., 2000). As we have shown that ezrin phosphorylation is crucial for *C. burnetii* internalization in epithelial cells (Figs. 3 and 4), we analyzed whether ROCK is involved in ezrin phosphorylation during infection using the pharmacological inhibitor of this kinase Y-27632. HeLa cells were transfected with plasmids encoding either mCherry alone, mCherry-ezrin-WT or the phosphomimetic mutant mCherry-ezrin-T567D. Cells were then treated for one hour with 10 μM Y-27632 (the lowest concentration used to produce a significant decrease in the internalization of *C. burnetii* [Salinas et al., 2015]) and infected for 6 h in the presence of the inhibitor. Cells overexpressing mCherry and not incubated with Y-27632 were used as control. Cells were fixed and processed as mentioned before to evaluate the num-

1768322x, 2022, 9, Downloaded from https://onlinelibrary.wiley.com/doi/10.1111/boc.202100096 by Portail BibCNRS INSB, Wiley Online Library on [09/06/2023]. See the Terms and Conditions (https://onlinelibrary.wiley.com/terms-and-conditions) on Wiley Online Library for rules of use; OA articles are governed by the applicable Creative Commons License

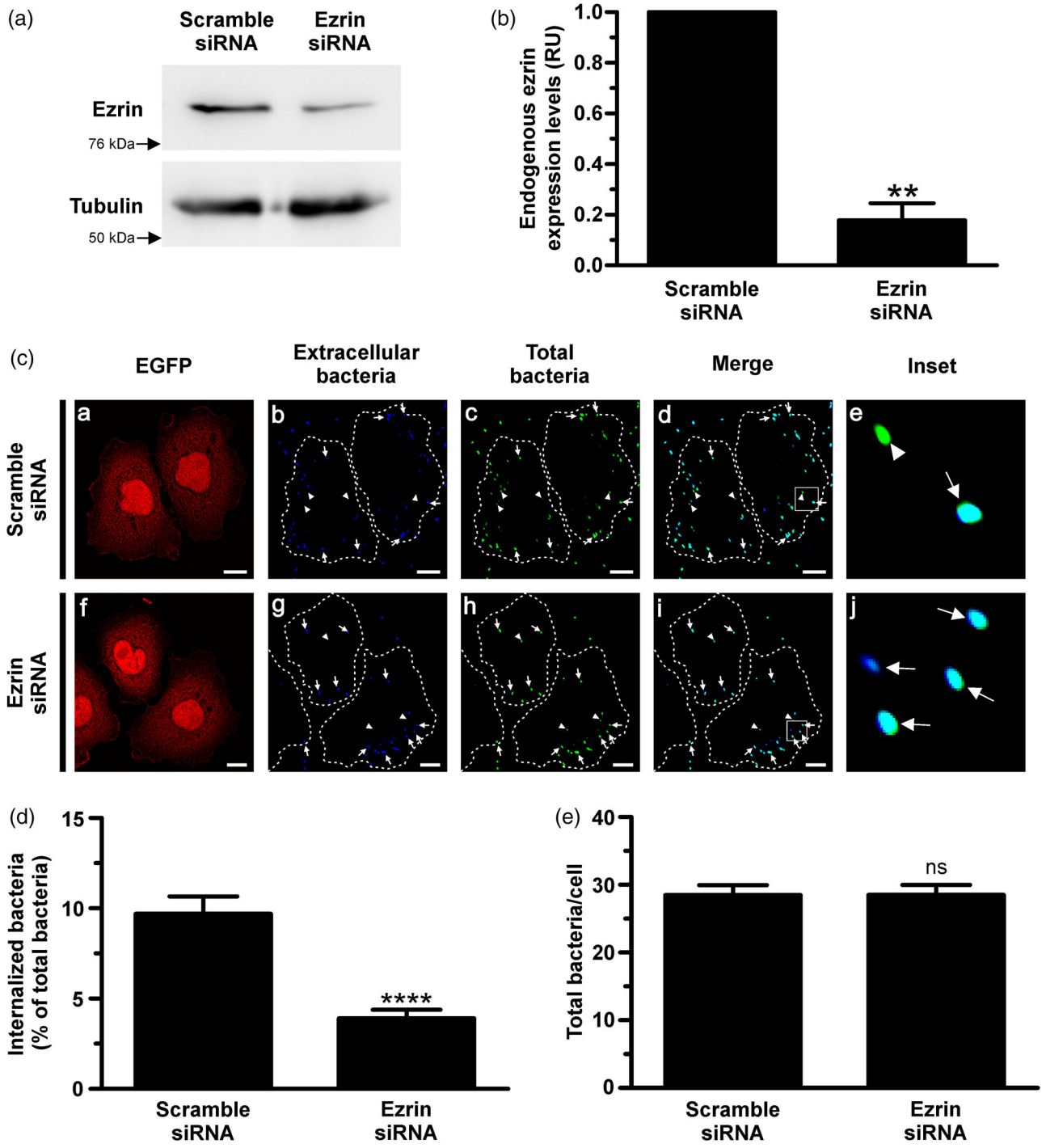


Figure 1 Knockdown of ezrin inhibits the internalization of *C. burnetii*. (A) Lysates of HeLa cells transfected with non-targeting (scramble) or ezrin-targeting siRNA were analyzed by Western blot using antibodies against ezrin. Anti-α-tubulin antibodies were used as loading control. (B) Protein band intensities were measured by the ImageJ software and normalized for the loading control. The level of ezrin expression in the scramble transfected cells was arbitrarily defined as 1. Results are expressed as means ± S.E.M. of three independent experiments. $^{**}p < 0.01$, compared to scramble siRNA (Two-tailed paired *t* test was used to determine statistical significance). (C) HeLa cells co-transfected with pEGFP (red pseudo color) in combination with either scramble (panels a-e) or ezrin-targeting (panels f-j) siRNAs were infected with *C. burnetii* for 6 h at 37°C, fixed and processed for immunofluorescence as described in section Materials and Methods. EGFP signal is shown in red pseudocolor. Extracellular *C. burnetii* are pseudocolored blue and green (double mark) while intracellular ones are pseudocolored only green (single mark). Cells were analyzed by confocal microscopy and representative micrographs of co-transfected cells are shown. Transfected cells boundaries were marked with dotted lines. In the insets, extracellular and intracellular *C. burnetii* are pointed with arrows and arrowheads, respectively. Scale bar: 10 μm. (D) Quantification of *C. burnetii* internalized by co-transfected HeLa cells and (E) total bacteria associated to host cells. An average of 30 cells and 900 bacteria were counted in each experiment. Results are expressed as means ± S.E.M. of three independent experiments. $^{****}p < 0.0001$, compared to scramble siRNA (two-tailed Wilcoxon matched-pairs signed rank test was used to determine statistical significance). ns: non-significant differences between groups ($p > 0.05$).

1768322x, 2022, 9, Downloaded from https://onlinelibrary.wiley.com/doi/10.1111/boc.202100096 by Portail BibCNRS INSB, Wiley Online Library on [09/06/2023]. See the Terms and Conditions (https://onlinelibrary.wiley.com/terms-and-conditions) on Wiley Online Library for rules of use; OA articles are governed by the applicable Creative Commons License

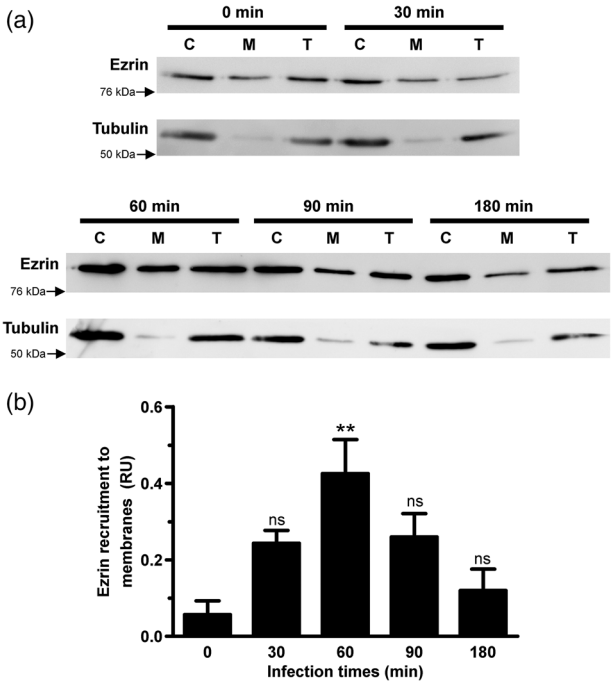


Figure 2 Ezrin is recruited to membrane of host cell infected with *C. burnetii*. HeLa cells were infected with *C. burnetii* for different lengths of time, lysed and centrifuged to obtain post-nuclear supernatant (T: total), membrane (M) and cytosolic (C) fractions as described in section Materials and Methods. (A) The obtained fractions were analyzed by SDS-PAGE and Western blot using specific antibodies against ezrin and α-tubulin (loading control). (B) The band intensities were quantified using the ImageJ software and the ratio between ezrin in the membrane fractions and α-tubulin total fractions was calculated and considerate as the ezrin recruitment to membranes. Results are expressed as means $\pm$ S.E.M. from at least four independent experiments. Mean values were compared with the 0 min of infection condition by one-way ANOVA and Dunnett's post hoc test ($^*p < 0.05$). ns: non-significant differences between groups ($p > 0.05$). RU: Relative Units.

ber of intracellular and total bacteria (Figure 5a). As shown in Figure 5b, treatment with Y-27632 produced a decrease in the internalization of *C. burnetii* in cells that overexpressed either mCherry alone or mCherry-ezrin-WT. However, there were no significant differences in cells overexpressing T567D mutant treated with the inhibitor compared to untreated cells. The number of total bacteria did not show significant changes in the different conditions used, indicating that adherence was not affected (Figure 5c), in agreement with our previous work (Salinas et al., 2015). These results would indicate that ezrin is part of the ROCK signaling pathway used by *C. burnetii* to promote its internalization in HeLa cells.

CD44 participates in the uptake of *C. burnetii* into the host cell

As previously mentioned, ezrin anchors actin filaments to plasma membrane domains enriched in PIP_2 (Jayasundar et al., 2012). A previous study shows that PIP_2 can induce the assembly of specific CD44-ezrin heterocomplexes (Chen et al., 2015). The authors indicate that such complexes may be involved in the assembly of receptor clusters dependent of actin cytoskeleton on the plasma membrane or at host-pathogen interaction sites (Chen et al., 2015; Grover et al., 2015). Because ezrin is recruited to the plasma membrane and phosphorylated during *C. burnetii* infection, we decided to analyze the role of the receptor CD44 in the internalization of the bacterium. To do this, HeLa cells were co-transfected with pcDNA3/HA-CD44 in combination either with scramble or CD44-targeting shRNA, lysed and analyzed by Western blot to assess the knockdown efficiency of CD44. As shown in Figure 6a,b, the CD44 shRNA effectively reduced the expression levels of the receptor. On the other hand, HeLa cells were co-transfected with the human CD44-targeting or the scramble (non-targeting) shRNA and the empty vector mCherry. The mCherry vector was used to visualize shRNA transfected cells. Cells were then infected with *C. burnetii* for 6 h at 37°C, fixed and processed as previously mentioned to analyze bacterial adherence and internalization by confocal microscopy (Figure 6c). The internalization levels of *C. burnetii* were significantly decreased in cells transfected with CD44 shRNA compared to the control (Figure 6d). The adherence of the bacteria to the host cell was not affected by the knockdown of the CD44 receptor (Figure 6e).

To further investigate the participation of CD44 in *C. burnetii* internalization we transfected HeLa cells with pFLAG-myc plasmids encoding either CD44 WT, a CD44 mutant unable to interact with ERM proteins following a point mutation of the binding site (CD44 KR), truncated forms of CD44 with deletions of the extracellular (CD44 ΔE) or the intracellular (CD44 ΔICD) domains. HeLa cells were transfected with the empty vector pFLAG-myc (control). Following transfection, cells were infected with *C. burnetii* during 6 h at 37°C, fixed and processed as mentioned in section Materials and Methods to evaluate the number of intracellular and total bacteria (Figure 7a). As shown in Figure 7, the overexpression of CD44 WT did not produce significant modifications in the internalization or the adherence of the bacterium to the host cell compared to control. Instead, all the mutant forms of CD44 induced an important decrease in the levels of internalization without affecting the number of total associated bacteria. Together these findings suggest that the receptor CD44 is important to the internalization of *C. burnetii* but would not be involved in the bacterial cell adherence.

DISCUSSION

C. burnetii is an obligate intracellular pathogen causative agent of Q fever. This bacterium displays a tropism for

1768322x, 2022, 9, Downloaded from https://onlinelibrary.wiley.com/doi/10.1111/boc.202100096 by Portail BibCNRS INSB, Wiley Online Library on [09/06/2023]. See the Terms and Conditions (https://onlinelibrary.wiley.com/terms-and-conditions) on Wiley Online Library for rules of use; OA articles are governed by the applicable Creative Commons License

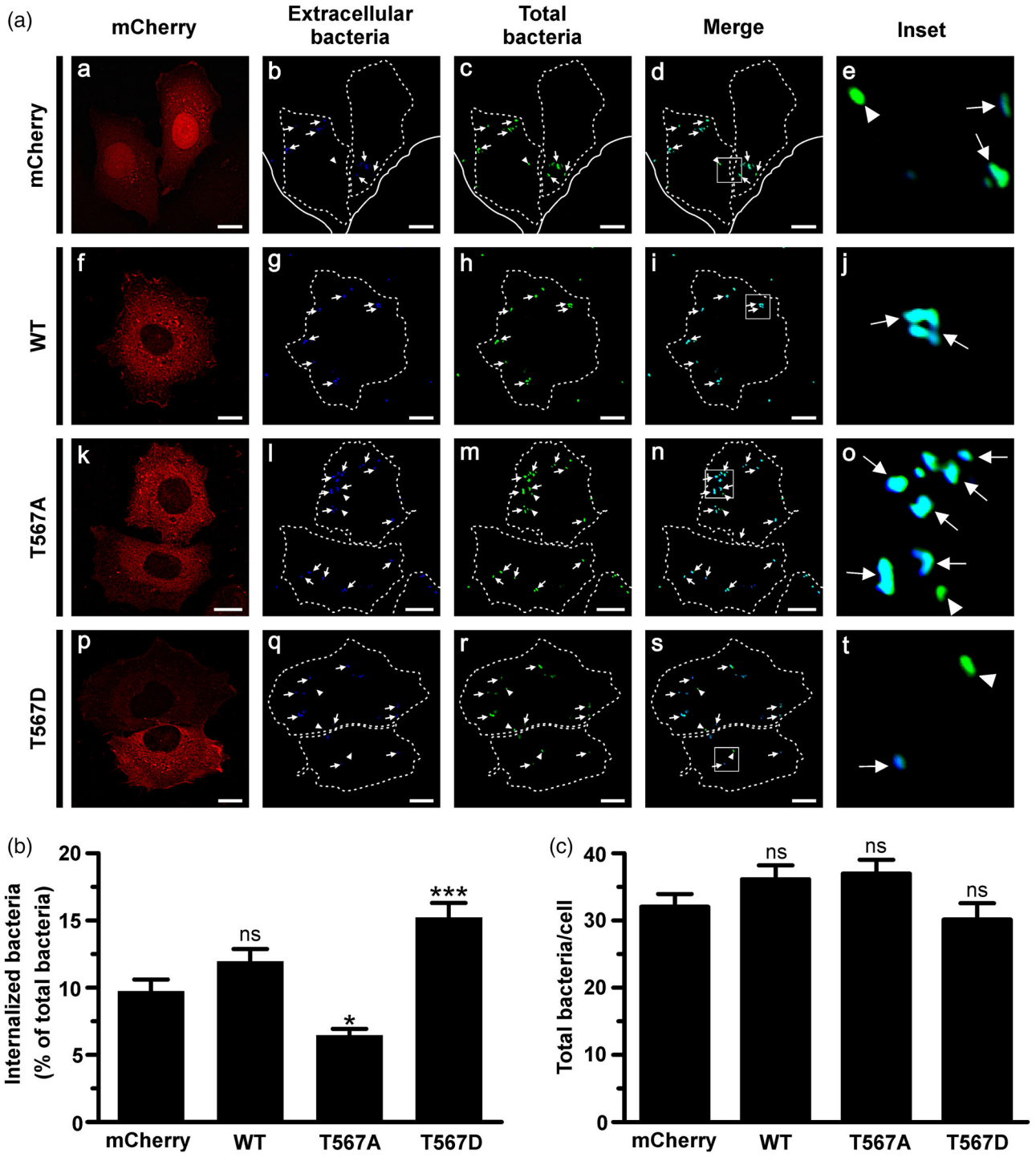


Figure 3 The phosphorylation state of ezrin regulates the uptake of *C. burnetii* by the host cell. (A) HeLa cells that overexpress mCherry (panels a–e), mCherry-ezrin-WT (panels f–j), mCherry-ezrin-T567A (panels k-o) or mCherry-ezrin-T567D (panels p–t) were infected for 6 h at 37°C with *C. burnetii*, fixed and processed for immunofluorescence as described in section Material and Methods. mCherry signal is shown in red color. Extracellular *C. burnetii* are pseudocolored blue and green (double mark) while intracellular ones are pseudocolored only green (single mark). Cells were analyzed by confocal microscopy and representative micrographs are presented in the panel. Transfected cells boundaries were marked with dotted lines and non-transfected with filled lines. In the insets, extracellular and intracellular *C. burnetii* are indicated with arrows and arrowheads, respectively. Scale bar: 10 μm. (B) Quantification of *C. burnetii* internalized and (C) total bacteria associated to host cells. An average of 30 cells and 900 bacteria were counted in each experiment. Results are expressed as means ± S.E.M. of three independent experiments. *$p < 0.05$, ***$p < 0.001$, compared to cell transfected with pmCherry (statistical differences were determined using Kruskal-Wallis test followed by Dunn's post hoc test for multiple comparisons). ns: non-significant differences between groups ($p > 0.05$).

1768322x, 2022, 9, Downloaded from https://onlinelibrary.wiley.com/doi/10.1111/boc.202100096 by Portail BibCNRS INSB, Wiley Online Library on [09/06/2023]. See the Terms and Conditions (https://onlinelibrary.wiley.com/terms-and-conditions) on Wiley Online Library for rules of use; OA articles are governed by the applicable Creative Commons License

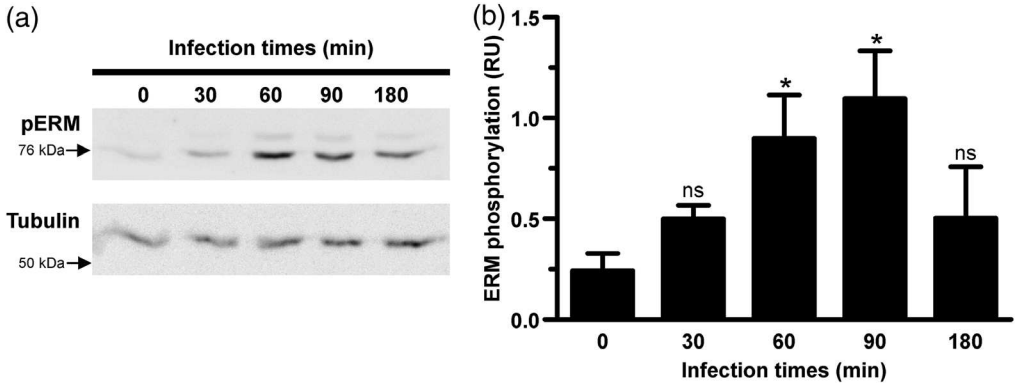


Figure 4 *C. burnetii* induces ERM protein phosphorylation early during internalization process. (A) Lysates of HeLa cells infected for different time periods with *C. burnetii* were analyzed by SDS-PAGE and subsequently Western Blot using specific antibodies for the detection of phosphorylated ERM proteins (pERM). The time 0 min (control) corresponds to HeLa cells exposed to *C. burnetii*, as indicated in section Materials and Methods, washed and lysed at time 0 min of infection. (B) The images obtained were analyzed with ImageJ software and protein band intensity ratio between pERM and α-tubulin was calculated. Results are expressed as average band intensity $\pm$ S.E.M. from at least three independent experiments. Statistical differences were determined using Kruskal-Wallis test followed by Dunn's post hoc test for multiple comparisons ($^*p < 0.05$). ns: non-significant differences between groups ($p > 0.05$). (RU): Relative Units.

monocytes and alveolar macrophages (Fernandes et al., 2016; Sobotta et al., 2016), however it has been shown that different types of epithelial cells are permissive to this microorganism (Baca & Paretsky, 1983; Sobotta et al., 2017). It would be considered that the intracellular trafficking of *C. burnetii* is much better known than the mechanisms implicated in its internalization which remain poorly characterized. *C. burnetii* internalization is independent of the bacterial secretion system (Beare et al., 2011; Carey et al., 2011) but requires the interaction between components of the bacterium surface and host cell factors (Capo et al., 1999; Dellacasagrande et al., 2000; Gilk et al., 2013; Martinez et al., 2014; Rosales et al., 2012; Salinas et al., 2015; van Schaik et al., 2013).

In our experimental model, ezrin knockdown in HeLa cells inhibits *C. burnetii* internalization. Our results are in agreement with what has been observed in previous studies carried out with other bacterial pathogens. For instance, the entry of *S. flexneri* into epithelial cells is blocked by overexpression of the dominant negative N-terminal domain of ezrin (Skoudy et al., 1999). Furthermore, it has been observed that the expression of that ezrin mutant in endothelial cells abolishes actin cytoskeleton reorganizations induced by *N. meningitidis* to promote its internalization (Eugène et al., 2002). In addition, the internalization of *C. trachomatis* into LLC-PK1 or HeLa cells is inhibited by overexpression of the N-terminal domain of ezrin or by depletion of endogenous ezrin using specific siRNA (Swanson et al., 2007). Moreover, it has been shown that ezrin knockdown decreases the uptake of *B. abortus* into giant trophoblasts (Watanabe et al., 2009). Interestingly, we observe that the overexpression of ezrin WT only slightly increased the uptake of *C. burnetii* by HeLa cells. Our results are consistent with several reports which have showed that cells transfected with plasmids encoding ezrin WT have similar behavior that those transfected with the empty vector (Gautreau et al., 2000; Zhang et al., 2020). This result suggests that the amount of ezrin expressed in HeLa cells is not a limiting factor for the bacterial internalization. Interestingly, a recent work has determined that HeLa cells have a very little amount of endogenous ezrin phosphorylated and that the overexpressed ezrin WT form is not phosphorylated (Kamiyama et al., 2018).

In the present study, we demonstrated the importance of the phosphorylation state of the residue threonine 567 of ezrin in the internalization process of *C. burnetii* by HeLa. We observed that while the non-phosphorylatable ezrin mutant (T567A) sufficiently decreases the levels of bacterium internalization, the phosphomimetic form (T567D) enhances the entry of the bacteria to the host cell. Moreover, we determined that *C. burnetii* induces phosphorylation of endogenous ERM proteins in HeLa cells during early stages of infection. Similar results were observed during *C. trachomatis* infection of HeLa cells induce ezrin phosphorylation at the early time points (before 2 h post-infection) (Swanson et al., 2007). Group A Streptococcal invasion into epithelial cells HEp-2 is dramatically blocked in the presence of the inhibitors of ezrin phosphorylation NSC668394 and disorazoles (Rox et al., 2017). A rapid and marked phosphorylation of ERM proteins of BMDMs during infection with *S. aureus* was observed (Li et al., 2018).

Several groups have identified specific substrates for Rho-kinase such as ezrin (Amano et al., 2010; Nishioka et al., 2012; Riento & Ridley, 2003). Chen et al. (2011) reported that the treatment of HepG2 cells with Y-27632 or ROCK siRNA produced a decrease in the levels of

1768322x, 2022, 9, Downloaded from https://onlinelibrary.wiley.com/doi/10.1111/boc.202100096 by Portail BibCNRS INSB, Wiley Online Library on [09/06/2023]. See the Terms and Conditions (https://onlinelibrary.wiley.com/terms-and-conditions) on Wiley Online Library for rules of use; OA articles are governed by the applicable Creative Commons License

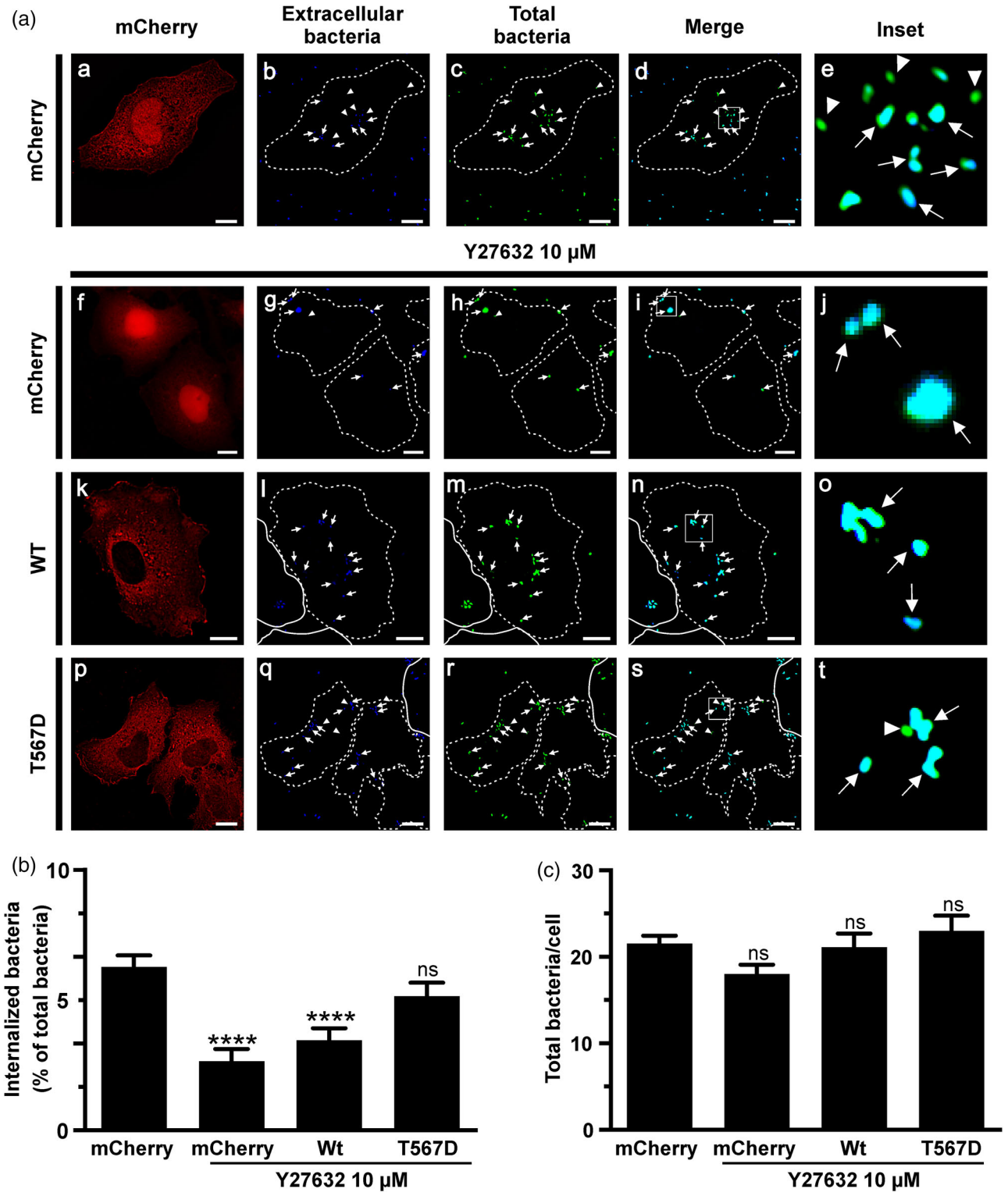


Figure 5 Ezrin phosphomimetic mutant abolishes the inhibitory effect of Y-27632 on the internalization of *C. burnetii*. (A) HeLa cells that overexpress mCherry (panels f–j), mCherry-ezrin-WT (panels k–o) or mCherry-ezrin-T567D (panels p–t) were treated for one hour with Y-27632, infected for 6 h at 37°C with *C. burnetii* and maintained during this time in the presence of the inhibitor as described in section Material and Methods. mCherry signal is shown in red color color. Extracellular *C. burnetii* are pseudocolored blue and green (double mark) while intracellular ones are pseudocolored only green (single mark). Untreated cells transfected with mCherry plasmid were used as controls (panels a–e). Cells were fixed, processed for immunofluorescence, analyzed by confocal microscopy and representative micrographs are presented in the panel. Transfected cells boundaries were marked with dotted lines and non-transfected with filled lines. In the Insets, extracellular and intracellular *C. burnetii* are indicated with arrows and arrowheads, respectively. Scale bar: 10 μm. (B) Quantification of *C. burnetii* internalized and (C) total bacteria associated to host cells. An average of 30 cells and 900 bacteria were counted in each experiment. Results are expressed as means ± S.E.M. of three independent experiments. ****$p < 0.0001$, compared to control cells (statistical differences were determined using Kruskal-Wallis test followed by Dunn's post hoc test for multiple comparisons). ns: non-significant differences between groups ($p > 0.05$).

1768322x, 2022, 9, Downloaded from https://onlinelibrary.wiley.com/doi/10.1111/boc.202100096 by Portail BibCNRS INSB, Wiley Online Library on [09/06/2023]. See the Terms and Conditions (https://onlinelibrary.wiley.com/terms-and-conditions) on Wiley Online Library for rules of use; OA articles are governed by the applicable Creative Commons License

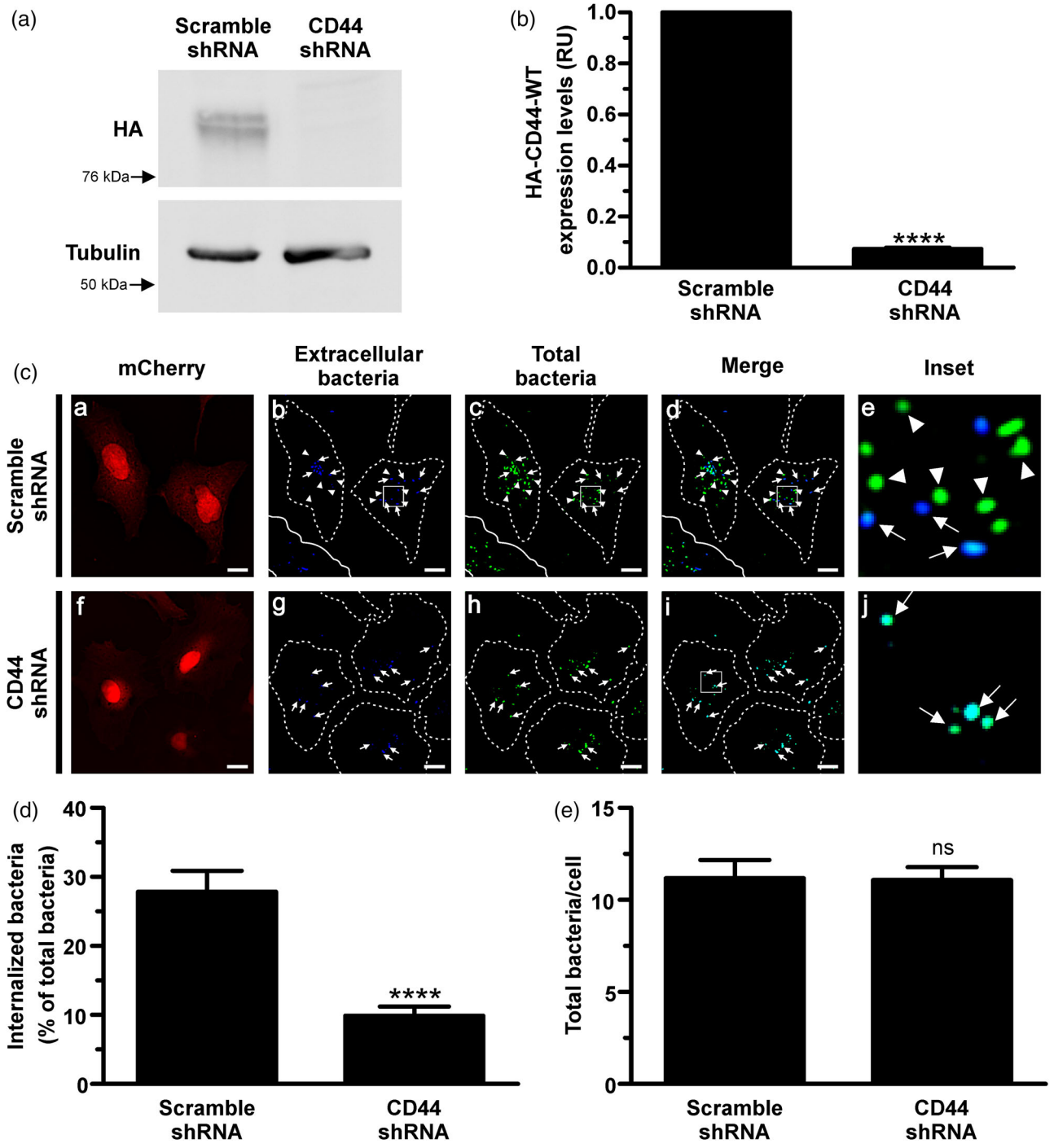


Figure 6 CD44 silencing diminishes the internalization of *C. burnetii*. (A) Lysates of HeLa cells co-transfected with pcDNA3/HA-CD44 and shRNA scramble or specific to CD44 were analyzed by SDS-PAGE and Western blot using specific antibodies against hemagglutinin (HA). Anti-α-tubulin antibodies were used as loading control. (B) Protein band intensities were measured by the ImageJ software and normalized with the loading control. The level of CD44 expression in the scramble transfected cells was arbitrarily defined as 1. (C) HeLa cells were co-transfected with mCherry plasmid and shRNA scramble or specific to CD44 (CD44 shRNA). Then cells were infected with *C. burnetii* for 6 h at 37°C, fixed and processed for immunofluorescence as described in section Materials and Methods. mCherry signal is shown in red color. Extracellular *C. burnetii* are pseudocolored blue and green (double mark) while intracellular ones are pseudocolored only green (single mark). Cells were analyzed by confocal microscopy and representative micrographs of cells are presented in the panel. Transfected cells boundaries were marked with dotted lines and non-transfected with filled lines. Insets extracellular *C. burnetii* are indicated with arrows and intracellular bacteria with arrowheads. Scale bar: 10 μm. (D) Quantification of *C. burnetii* internalized by transfected HeLa cells and (E) total bacteria associated to host cells. An average of 30 cells and 900 bacteria were counted in each experiment. Results are expressed as means ± S.E.M. of three independent experiments. ****$p < 0.0001$, compared to scramble shRNA (student two-tailed *t* test or two-tailed Wilcoxon matched-pairs signed rank test was used to determine statistical significance). ns: non-significant differences between groups ($p > 0.05$).

1768322x, 2022, 9, Downloaded from https://onlinelibrary.wiley.com/doi/10.1111/boc.202100096 by Portail BibCNRS INSB, Wiley Online Library on [09/06/2023]. See the Terms and Conditions (https://onlinelibrary.wiley.com/terms-and-conditions) on Wiley Online Library for rules of use; OA articles are governed by the applicable Creative Commons License

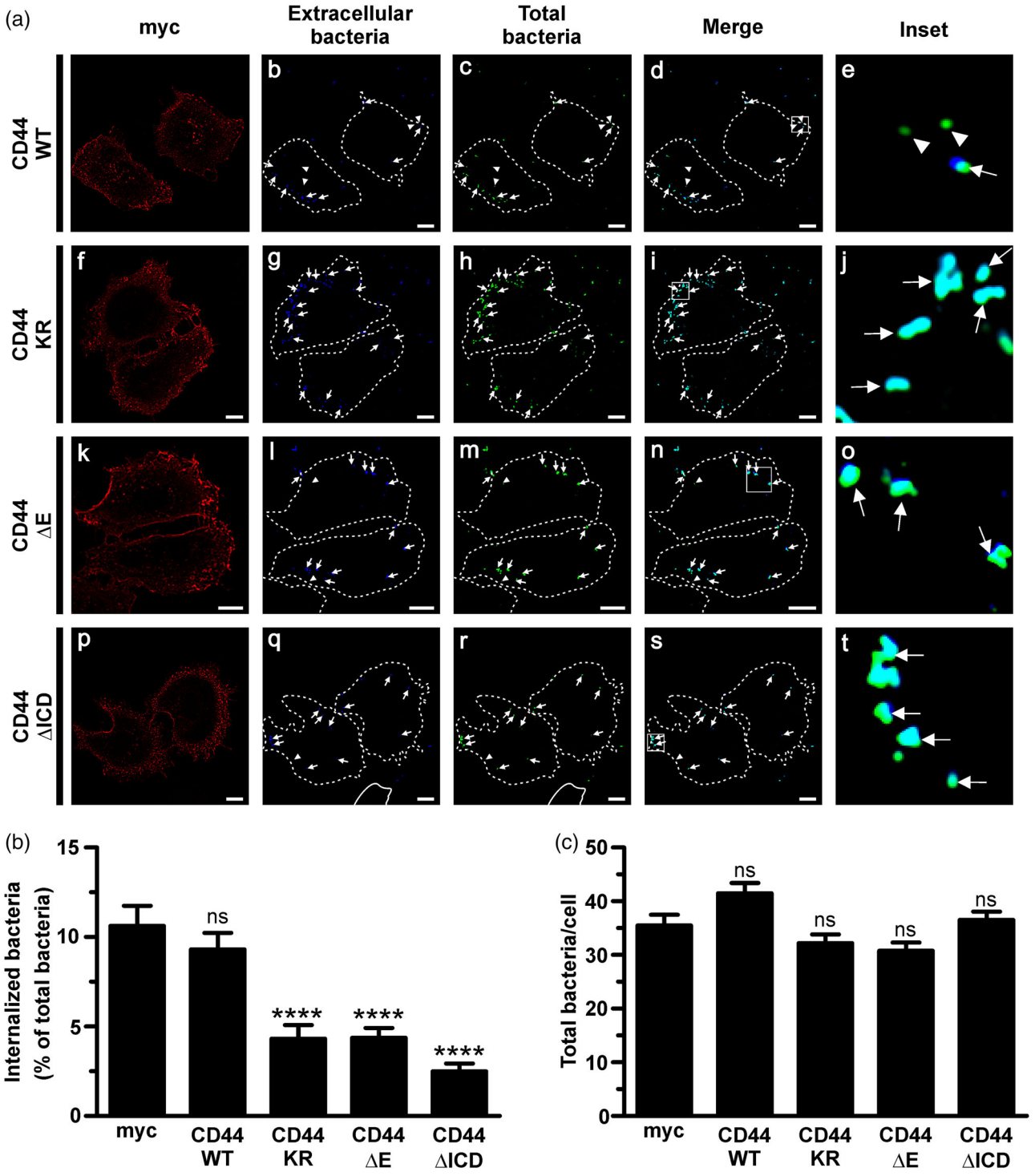


Figure 7 Overexpression of CD44 mutants decrease the uptake of *C. burnetii* into the host cell. (A) HeLa cells that overexpress FLAG-myc, myc-CD44-WT-FLAG, myc-CD44-KR-FLAG, myc-CD44-ΔE-FLAG, or myc-CD44-ΔICD-FLAG were infected for 6 h at 37°C with *C. burnetii*, fixed and processed for immunofluorescence as described in section Materials and Methods. mCherry signal is shown in red color. Extracellular *C. burnetii* are pseudocolored blue and green (double mark) while intracellular ones are pseudocolored only green (single mark). Cells were analyzed by confocal microscopy and representative micrographs are presented in the panel. Transfected cells boundaries were marked with dotted lines and non-transfected with filled lines. Insets extracellular *C. burnetii* are indicated with arrows and intracellular bacteria with arrowheads. Scale bar: 10 μm. (B) Quantification of *C. burnetii* internalized by transfected HeLa cells and (C) total bacteria associated to host cells. An average of 30 cells and 900 bacteria were counted in each experiment. Results are expressed as means ± S.E.M. of three independent experiments. ****$p < 0.0001$, compared to cell transfected with pFLAG-myc empty vector (Kruskal-Wallis test followed by Dunn's post hoc test for multiple comparisons). ns: non-significant differences between groups ($p > 0.05$).

1768322x, 2022, 9, Downloaded from https://onlinelibrary.wiley.com/doi/10.1111/boc.202100096 by Portail BibCNRS INSB, Wiley Online Library on [09/06/2023]. See the Terms and Conditions (https://onlinelibrary.wiley.com/terms-and-conditions) on Wiley Online Library for rules of use; OA articles are governed by the applicable Creative Commons License

ezrin phosphorylation (Chen et al., 2011). In a previous work, we demonstrated that ROCK is involved in the internalization of avirulent *C. burnetii* into phagocytic and non-phagocytic cells (Salinas et al., 2015). During the development of this work, we have demonstrated that the inhibitory effect of Y-27632 in the internalization is significantly reverting by the overexpression of the phosphomimetic mutant of ezrin (T567D) but not by the overexpression of the ezrin WT. These results would indicate that ezrin participates in the ROCK signaling pathway involved in the uptake of *C. burnetii*. Interestingly, in our system the fact that the T567D mutant did not completely restore the uptake levels of the bacteria in comparison to cells untreated with Y-27632 does not rule out that other substrates of ROCK could be involved in the internalization of *C. burnetii*. LIM kinases (LIMK) and non-muscular myosin type II (NMII) are two well know ROCK substrates (Amano et al., 2010; Nishioka et al., 2012; Riento & Ridley, 2003). When we studied LIMK and NMII, only the myosin affected the internalization of *C. burnetii* by HeLa cells (data not shown).

It is noteworthy that during the ezrin activation process, the protein migrates from the cytoplasm to the plasma membrane (Fievet et al., 2004; Gautreau et al., 2000; Yonemura et al., 1999). We have previously demonstrated that RhoA, the main regulator of ROCK, migrate to the membrane fraction after 30 min and peaked after 60 min of infection (Salinas et al., 2015). In the present study, we observe that endogenous ezrin is recruited to the membrane at 30 to 60 min of infection with *C. burnetii*. We have previously shown the kinetics of RhoA recruitment at the membrane during infection of HeLa cells infected with *C. burnetii* (Salinas et al., 2015) and, interestingly, it is similar to the ERM phosphorylation observed in this work.

The receptor CD44 participates in the internalization of different bacterial pathogens (Leemans et al., 2003; Li et al., 2018; Moffat et al., 1996; Skoudy et al., 2000). It has been described that $\alpha_v\beta_3$ integrins and complement receptor 3 (CR3) are involved in the internalization of *C. burnetii* by monocytes THP-1 (Capo et al., 1999; Gilk et al., 2013). However, epithelial cell lines such as HeLa cells lack CR3 (Tam et al., 2014) but express high levels of $\alpha_v\beta_3$ integrins (Oba et al., 2007; Orgovan et al., 2014; Xiong et al., 2009) and CD44 (Bruno et al., 2000; Figueroa et al., 2015; Liu et al., 2018; Picaud et al., 2014; Wang, 2013). We observe that knockdown of CD44 reduces the levels of internalization of *C. burnetii* without affecting bacterial adhesion to HeLa cells that could depend mainly on the $\alpha_v\beta_3$ integrins. Our results are consistent with a recent work which demonstrated that CD44 knockdown in macrophages produces lower levels of internalization of *S. aureus* without affecting its adhesion to the cell (Li et al., 2018) or inhibits phagocytosis of *P. aeruginosa* (Tian et al., 2019).

The overexpression of CD44 WT did not modify the internalization of *C. burnetii*. This could be due to the fact that HeLa cells present high levels of endogenous CD44 (Bruno et al., 2000; Figueroa et al., 2015; Liu et al., 2018; Picaud et al., 2014; Wang, 2013) and exogenous overexpression would have a redundant effect. Furthermore, the activity of CD44 could be limited by interaction with other receptors or signaling molecules. These hypotheses have yet to be tested. On the other hand, the effect generated by ΔE, ΔICD, and KR constructs allows us to describe the role of CD44 in the internalization of *C. burnetii*. In the case of the mutant that lack the extracellular domain (CD44 ΔE), the inhibitory effect could be due to competition with the endogenous receptor (Brown et al., 2005). It has been shown that the intracellular domain of CD44 acts as a dominant negative form interfering the association of the receptor with actin cytoskeleton and extracellular matrix proteins (Mellor et al., 2013). The mutant truncated in the intracellular region (CD44 ΔICD) could not trigger the corresponding signaling pathways or bind to host effectors. It has been shown that these domains participate in the interaction of the receptor with hyaluronic acid (Perschl et al., 1995) and its absence prevents the receptor endocytosis (Jiang et al., 2002). The result obtained with the construct CD44 KR, a mutant that is unable to interact with ERM proteins, is really interesting because it would establish the importance of the CD44 and ezrin relationship during internalization of *C. burnetii*. This interaction is necessary for the internalization of bacterial pathogens such as *S. aureus* (Li et al., 2018).

In conclusion, our results indicate that ezrin is involved in the uptake of *C. burnetii* by HeLa cells. Furthermore, the recruitment to the host cell membrane and the phosphorylation of ezrin are important to the internalization process of *C. burnetii*. We could speculate that ezrin is part of the RhoA/ROCK signaling pathway involved in the entry of *C. burnetii*. Moreover, we described CD44 as a possible novel receptor for the internalization of *C. burnetii*. The interaction of ezrin with CD44 during the entry of the bacteria remains to be determined.

MATERIALS AND METHODS

Materials

Dulbecco's Modified Eagle's Medium (DMEM), Fetal Bovine Serum (FBS), penicillin and streptomycin were obtained from Gibco BRL/Life Technologies (Buenos Aires, Argentina). Plasmid encoding mCherry-ezrin-WT was generated in the laboratory of the Dr. Matteo Bonazzi (Institut de Recherche en Infectiologie de Montpellier, Centre National de la Recherche Scientifique, Montpellier, France). Vectors encoding mutants

1768322x, 2022, 9, Downloaded from https://onlinelibrary.wiley.com/doi/10.1111/boc.202100096 by Portail BibCNRS INSB, Wiley Online Library on [09/06/2023]. See the Terms and Conditions (https://onlinelibrary.wiley.com/terms-and-conditions) on Wiley Online Library for rules of use; OA articles are governed by the applicable Creative Commons License

form of ezrin mCherry-ezrin-T567A and mCherry-ezrin-T567D were kindly provided by Dr. Lucas Pelkmans (Department of Molecular Life Sciences, University of Zurich, Zurich, Switzerland). Plasmids pFLAGmyc-CMV™-21 encoding the WT form of the rat receptor CD44 and its truncated mutants (CD44 KR, ΔE and ΔICD) doubly-tagged with both an N-terminal FLAG epitope and a C-terminal myc epitope were kindly provided by Dr. Peter Herrlich (Leibniz Institute for Age Research, Fritz Lipmann Institute, Jena, Germany). Vectors pcDNA3 encoding human CD44-WT tagged with human influenza hemagglutinin (HA) epitope was kindly provided by Dr. Miguel Quintanilla (Instituto de Investigaciones Biomédicas Alberto Sols, Consejo Superior de Investigaciones Científicas, Universidad Autónoma de Madrid, Madrid, Spain). Construct pSIREN-RetroQ encoding CD44 small hairpin RNA (shRNA) targeting all human CD44 isoforms and scramble control shRNA were kindly provided by Shinya Toyokuni (Department of Pathology and Biological Responses, Nagoya University Graduate School of Medicine, Nagoya, Japan). SiRNAs scramble and against ezrin were purchased from Bioneer (Alameda, USA). The mouse anti-ezrin monoclonal antibody (610602, 1:500) was purchased from BD Biosciences (California, USA). The rabbit anti-phospho-ezrin(Thr567)/radixin(Thr564)/moesin(Thr558) polyclonal antibody (#3141, 1:100) was purchased from Cell Signaling Technology (Leiden, The Netherlands). The mouse anti-HA monoclonal antibody (H-9658, 1:100) was obtained from Sigma-Aldrich (Buenos Aires, Argentina). The mouse anti-α-tubulin monoclonal antibody (T6074, 1:500) was purchased from Sigma-Aldrich (Buenos Aires, Argentina). The rabbit anti-myc polyclonal antibody (PA1-981, 1:100) was purchased from Invitrogen (Buenos Aires, Argentina). The guinea pig anti-*C. burnetii* antiserum (1:1000) was kindly provided by Dr. Robert Heinzen (Rocky Mountain Laboratories, NIAID, NIH, Hamilton, MT, USA). Secondary antibodies (1:500) were purchased from Jackson ImmunoResearch Laboratories, Inc. (West Grove, PA, USA). The inhibitor Y27632 were from Merck-Calbiochem® (Buenos Aires, Argentina).

Cell culture

HeLa cells (ATCC) (Asociación Banco Argentino de Células, Buenos Aires, Argentina) were routinely tested for mycoplasma by PCR. Cells were grown in DMEM supplemented with 10% heat-inactivated FBS, 2.2 g/l sodium bicarbonate, 2 mM glutamine, 100 IU/ml penicillin and 100 μg/ml streptomycin, pH 7, at 37°C under a 5% CO_2 atmosphere. Vero cells used for propagation of phase II *C. burnetii* were maintained in the same culture conditions described for HeLa cells.

Cell transfection

HeLa cells (5×10^5) seeded in 24-well on sterile glass coverslips placed in 24-well plates were transfected with 2 μg/ml of the different constructs used in this work. To knockdown ezrin, cells were co-transfected with pEGFP and ezrin siRNA or scramble siRNA at concentration of 100 nM (Bioneer, Alameda, USA). Cell transfection was carried out using Lipofectamine® 2000 (Invitrogen, Buenos Aires, Argentina) diluted in OptiMEM (Thermo Fisher Scientific, Argentina). Briefly, HeLa cells were incubated with Lipofectamine® 2000 and the specific plasmids or siRNA during 2 h. Then, cells were washed and incubated for 18–24 h in DMEM supplemented with 10% heat-inactivated FBS, 2.2 g/l sodium bicarbonate, 2 mM glutamine, pH 7 at 37°C under a 5% CO_2 atmosphere.

Cells transfected with the different CD44 myc-tagged constructs were detected by indirect immunofluorescence using anti-myc antibody.

Propagation of phase II *C. burnetii*

Clone 4 phase II Nine Mile strain of *C. burnetii* which are infective for cells in culture but not for mammals, were provided by Ted Hackstadt (Rocky Mountain Laboratories, NIAID, NIH, Hamilton, MT, USA) and handled in a biosafety level II facility. Vero cells were seeded at low confluence in T75 flasks at 37°C under a 5% CO_2 atmosphere in DMEM supplemented with 5% FBS, 2.2 g/l sodium bicarbonate, 2 mM glutamine, pH 7. Cultures were infected with *C. burnetii* phase II suspensions for 6 days at 37°C under a 5% CO_2 atmosphere. In order to prepare cell lysates, cells were frozen at –70°C, then thawed at 37°C, scraped and passed 20 times through a 27-gauge needle connected to a syringe. Cell lysates were centrifuged at 800 x *g* for 10 min at 4°C. Supernatants were centrifuged at 24,000 x *g* for 30 min at 4°C, and pellets containing *C. burnetii* were resuspended in phosphate-buffered saline (PBS; 10 mM sodium phosphate, 0.9% NaCl), aliquoted and frozen at –-70°C.

Infection of HeLa with *C. burnetii*

HeLa cells (5×10^5) were seeded in 24-well on sterile glass coverslips placed in 24-well plates. For infection, a 5 μl aliquot of *C. burnetii* suspension mixed with DMEM supplemented with 5% FBS, 2.2 g/l sodium bicarbonate, 2 mM glutamine, pH 7 was added per well (Multiplicity of infection: 30–60). Cells were centrifuged at 400 x *g* for 10 min at 4°C to allow an efficient contact between cells and bacteria. Cells were then washed to remove unbound bacteria, incubated for different lengths of time

1768322x, 2022, 9, Downloaded from https://onlinelibrary.wiley.com/doi/10.1111/boc.202100096 by Portail BibCNRS INSB, Wiley Online Library on [09/06/2023]. See the Terms and Conditions (https://onlinelibrary.wiley.com/terms-and-conditions) on Wiley Online Library for rules of use; OA articles are governed by the applicable Creative Commons License

at 37°C under a 5% CO_2 atmosphere with DMEM supplemented with 5% FBS and processed for the different assays carried out.

Immunofluorescence. Detection of intracellular *C. burnetii* by double immunofluorescence staining technique

HeLa cells on sterile glass coverslips placed in 24-well plates were fixed with 2% paraformaldehyde in PBS for 10 min at 37°C, washed with PBS and blocked with 50 mM NH_4Cl in PBS. After washing, cells were incubated with a guinea pig antiserum against *C. burnetii* (1:1000) and a goat anti-guinea pig secondary antiserum conjugated to Alexa Fluor 647 diluted 1:500 in PBS containing 0.5% BSA (Bovine Serum Albumin) (non-permeabilizing conditions). In this condition, only extracellular bacteria were stained (blue pseudo color). After washing, cells were incubated with the same guinea pig antiserum against *C. burnetii* (1:1000) and a goat anti-guinea pig secondary antiserum conjugated to Alexa Fluor 488 or Alexa Fluor 594 diluted 1:500 in PBS containing 0.5% BSA and 0.05% saponin (permeabilizing conditions). Under these conditions, the blue-labeled extracellular bacteria were stained in green pseudo color (double mark), thus the extracellular one acquired both colors, while the intracellular ones were only stained in green pseudo color (simple mark). After washing, coverslips were mounted with Mowiol (Sigma-Aldrich, Buenos Aires, Argentina) and examined under confocal fluorescence microscope.

Infected cells transfected with CD44 myc-tagged constructs and processed by immunofluorescence as described above were incubated with an anti-myc antibody followed by an appropriate fluorophore conjugated secondary antibodies to detect infected cell overexpressing the different CD44 constructs.

Fluorescence microscopy

Cells were analyzed by confocal fluorescence microscopy using an FV1000 Olympus Confocal Microscope and the FV10-ASW 1.7 software (Olympus, Japan [https://www.olympus-lifescience.com/en/support/downloads]). Projections of confocal planes along the Z axis were generated using ImageJ software (NIH, USA [http://rsb.info.nih.gov/ij]). The number of adhered extracellular (double label) and internalized (single label) bacteria were manually quantified from the confocal projections. The sum of these two values was considered as the number of total bacteria per cells. The percentage of internalization was calculated as the number of bacteria internalized with respect to the total bacteria in each cell analyzed (Internalized *C. burnetii* * 100 / Total *C. burnetii*). Panel images were deconvolved using the plugin Parallel Spectral Deconvolution from ImageJ software (NIH, USA [http://rsb.info.nih.gov/ij]).

Subcellular fractionation

HeLa cells were cultured in T-25 flasks and infected as described above for different lengths of time. Cells were washed with cold PBS and homogenization buffer (HB) (250 mM sucrose, 3 mM imidazole, pH 7.4), and scraped in HB containing protease inhibitors and 0.5 mM Ethylenediaminetetraacetic acid (EDTA). Scraped cells were homogenized using a Dounce type homogenizer with a Teflon pestle. The homogenate was centrifuged at 13,000 x *g* for 15 s at 4°C. The supernatant (post-nuclear supernatant) was centrifuged at 100,000 x *g* for 30 min at 4°C. The supernatant and the pellet obtained represented the cytosolic (C) and membrane (M) fractions, respectively. Equal volumes of the different fractions were transferred to clean tubes, mixed with Laemmli buffer, boiled for 5 min and analyzed by SDS-PAGE and Western blot.

Detection of ERM phosphorylation

HeLa cells were cultured in 6-wells plates and infected as described earlier for different lengths of time. After infection, cells were washed with PBS, scraped into ice-cold lysis buffer (50 mM Tris-HCl, pH 7.2, 1% Triton X-100, 0.5% deoxycholate, 0.1% SDS, 50 mM NaCl, 10 mM $MgCl_2$, 2 mM Na_3VO_4, 10 mM NaF, 0.5 mg/ml DTT, 2 mM EDTA) supplemented with a protease inhibitor cocktail and kept on ice for 15 min. Lysates were clarified by centrifugation at 12,500 x *g* for 15 min at 4°C. Clarified lysates were transferred to clean tubes, mixed with Laemmli buffer and boiled for 5 min. Samples were analyzed by SDS-PAGE and Western blot.

Western blots

Samples were resolved by SDS-PAGE and the proteins transferred to nitrocellulose membranes using standard procedures. Membranes were blocked for 2 h at 4°C in Tween-Tris-buffered saline (TTBS; 0.1% Tween 20, 100 mM Tris/HCl, 0.9% NaCl) supplemented with 5% BSA, then incubated overnight at 4°C with the appropriate primary antibodies. Anti-α-tubulin antibody was used as loading controls. Membranes were washed three times with TTBS and then incubated for 2 h at room temperature with appropriate HRP-conjugated secondary antibodies. After washing with TTBS, membranes were incubated with the Enhanced

1768322x, 2022, 9, Downloaded from https://onlinelibrary.wiley.com/doi/10.1111/boc.202100096 by Portail BibCNRS INSB, Wiley Online Library on [09/06/2023]. See the Terms and Conditions (https://onlinelibrary.wiley.com/terms-and-conditions) on Wiley Online Library for rules of use; OA articles are governed by the applicable Creative Commons License

Chemiluminescence (ECL) reagent (General Electric, # RPN2232) and analyzed with a Fujifilm LAS-4000 equipment. Band densitometry was performed with the ImageJ software (NIH, USA [http://rsb.info.nih.gov/ij]).

Statistical analysis

All data analysis was performed using GraphPad Prism 5.0 (San Diego, CA, USA [https://www.graphpad.com]). Differences between conditions were tested by one-way analysis of variance (ANOVA) and Dunnett's post hoc tests or Kruskal-Wallis test followed by Dunn's post hoc test for multiple comparisons and Student's *t* single group test or two-tailed Wilcoxon matched-pairs signed rank test for two groups analyses. Differences were considered significant at $p < 0.05$.

ACKNOWLEDGMENTS

The authors wish to thank Lucas Pelkmans (Department of Molecular Life Sciences, University of Zurich, Zurich, Switzerland) for providing the plasmids encoding ezrin mutants. We would also like to thank Peter Herrlich (Leibniz Institute for Age Research, Fritz Lipmann Institute, Jena, Germany), Miguel Quintanilla (Instituto de Investigaciones Biomédicas Alberto Sols, Consejo Superior de Investigaciones Científicas, Universidad Autónoma de Madrid, Madrid, Spain) and Shinya Toyokuni (Department of Pathology and Biological Responses, Nagoya University Graduate School of Medicine, Nagoya, Japan) for kindly providing the constructs that encoding CD44 WT and mutants, human CD44 WT and shRNA targeting CD44, respectively. We are grateful to Robert Heinzen (Rocky Mountain Laboratories, NIAID, NIH, Hamilton, MT, USA) for providing the rabbit polyclonal anti-*Coxiella* antibody and Ted Hackstadt (Rocky Mountain Laboratories, NIAID, NIH, Hamilton, MT, USA) for providing *C. burnetii*. The authors wish to thank Luis Mayorga for critical reading of this manuscript. The authors are also grateful to Alejandra Medero and Tirso Sartor for their help with tissue culture and biochemical techniques. D.J.S. is a recipient of postdoctoral fellowship from the CONICET (Consejo Nacional de Investigaciones Científicas y Técnicas) and a travel grant from Boehringer Ingelheim Fonds Foundation for Basic Research in Medicine (Mainz, Germany). This work was supported by grants from ANPCyT (Agencia Nacional de Promoción Científica y Tecnológica) (PICT-2012-2425) and SIIP (Secretaría de Investigación, Internacionales y Posgrado) (2019-2020), Universidad Nacional de Cuyo, to WB. The funders had no role in study design, data collection and analysis, decision to publish, or preparation of the manuscript.

CONFLICT OF INTEREST

No competing interests declared.

DATA AVAILABILITY STATEMENT

The data that support the findings of this study are available from the corresponding author upon reasonable request.

ORCID

Walter Berón https://orcid.org/0000-0001-9654-5467

REFERENCES

Angelakis, E. & Raoult, D. (2010) Q fever. *Veterinary Microbiology*, 140, 297–309.

Aruffo, A., Stamenkovic, I., Melnick, M., Underhill, C.B. & Seed, B. (1990) CD44 is the principal cell surface receptor for hyaluronate. *Cell*, 61, 1303–1313.

Baca, O.G. & Paretsky, D. (1983) Q fever and Coxiella burnetii: a model for host-parasite interactions. *Microbiological Reviews*, 47, 127–49.

Beare, P. A., Gilk, S. D., Larson, C. L., Hill, J., Stead, C. M., Omsland, A., Cockrell, D. C., Howe, D., Voth, D. E., & Heinzen, R. A. (2011) Dot/Icm Type IVB secretion system requirements for coxiella burnetii growth in human macrophages. *MBio*, 2. https://doi.org/10.1128/mbio.00175-11

Bosk, S., Braunger, J.A., Gerke, V. & Steinem, C. (2011) Activation of F-actin binding capacity of ezrin: synergism of PIP_2 interaction and phosphorylation. *Biophysical Journal*, 100, 1708–1717.

Bruno, S., Fabbi, M., Tiso, M., Santamaria, B., Ghiotto, F., Saverino, D., Tenca, C., Zarcone, D., Ferrini, S., Ciccone, E., Grossi, C.E. (2000) Cell activation via CD44 occurs in advanced stages of squamous cell carcinogenesis. *Carcinogenesis*, 21, 893–900.

Capo, C., Lindberg, F.P., Meconi, S., Zaffran, Y., Tardei, G., Brown, E.J., Raoult, D. & Mege, J.L. (1999) Subversion of monocyte functions by *Coxiella burnetii*: impairment of the cross-talk between alphavbeta3 integrin and CR3. *Journal of Immunology*, 163, 6078–85.

Carey, K.L., Newton, H.J., Lührmann, A. & Roy, C.R. (2011) The *Coxiella burnetii* Dot/Icm system delivers a unique repertoire of Type IV effectors into host cells and is required for intracellular replication. *PLoS Pathogens*, 7, e1002056.

Chen, Y., Wang, D., Guo, Z., Zhao, J., Wu, B., Deng, H., et al. (2011) Rho kinase phosphorylation promotes ezrin-mediated metastasis in hepatocellular carcinoma. *Cancer Research*, 71, 1721–1729.

Chen, X., Khajeh, J.A., Ju, J.H., Gupta, Y.K., Stanley, C.B., Do, C., Heller, W.T., Aggarwal, A.K., Callaway, D.J.E. & Bu, Z. (2015) Phosphatidylinositol 4,5-bisphosphate clusters the cell adhesion molecule CD44 and assembles a specific CD44-Ezrin heterocomplex, as revealed by small angle neutron scattering. *Journal of Biological Chemistry*, 290, 6639–6652.

Chiasson-MacKenzie, C., Morris, Z.S., Liu, C.-H., Bradford, W.B., Koorman, T. & McClatchey, A.I. (2018) Merlin/ERM proteins regulate growth factor-induced macropinocytosis and receptor recycling by organizing the plasma membrane: cytoskeleton interface. *Genes & Development*, 32, 1201–1214.

D'Angelo, R., Aresta, S., Blangy, A., Del Maestro, L., Louvard, D. & Arpin, M. (2007) Interaction of ezrin with the novel guanine nucleotide exchange factor PLEKHG6 promotes RhoG-dependent apical cytoskeleton rearrangements in epithelial cells. *Molecular Biology of the Cell*, 18, 4780–4793.

Dellacasagrande, J., Ghigo, E., Capo, C., Raoult, D., & Mege, J.-L. (2000) Coxiella burnetii survives in monocytes from patients with Q fever endocarditis: involvement of tumor necrosis factor. *Infection and Immunity*, 68, 160–164.

Dzwonek, J. & Wilczynski, G.M. (2015) CD44: molecular interactions, signaling and functions in the nervous system. *Frontiers in Cellular Neuroscience*, 9, 175.

Eldin, C., Mélenotte, C., Mediannikov, O., Ghigo, E., Million, M., Edouard, S., Mege, J.L., Maurin, M. & Raoult, D. (2017) From Q fever to *Coxiella burnetii* infection: a paradigm change. *Clinical Microbiology Reviews*, 30, 115–190.

1768322x, 2022, 9, Downloaded from https://onlinelibrary.wiley.com/doi/10.1111/boc.202100096 by Portail BibCNRS INSB, Wiley Online Library on [09/06/2023]. See the Terms and Conditions (https://onlinelibrary.wiley.com/terms-and-conditions) on Wiley Online Library for rules of use; OA articles are governed by the applicable Creative Commons License

Eugène, E., Hoffmann, I., Pujol, C., Couraud, P.-O., Bourdoulous, S. & Nassif, X. (2002) Microvilli-like structures are associated with the internalization of virulent capsulated *Neisseria meningitidis* into vascular endothelial cells. *Journal of Cell Science*, 115, 1231–41.

Fernandes, T.D., Cunha, L.D., Ribeiro, J.M., Massis, L.M., Lima-Junior, D.S., Newton, H.J. & Zamboni, D.S. (2016) Murine alveolar macrophages are highly susceptible to replication of *Coxiella burnetii* phase II in vitro. *Infection and Immunity*, 84, 2439–2448.

Fievet, B.T., Gautreau, A., Roy, C., Del Maestro, L., Mangeat, P., Louvard, D. & Arpin, M. (2004) Phosphoinositide binding and phosphorylation act sequentially in the activation mechanism of ezrin. *Journal of Cell Biology*, 164, 653–9.

Figueroa, C.M., Morales-Cruz, M., Suárezm, B.N., Fernández, J.C., Molina, A.M., Quiñones, C.M., Griebenow, K. (2015) Induction of cancer cell death by hyaluronic acid-mediated uptake of cytochrome C. *Journal of Nanomedicine & Nanotechnology*, 6. https://doi.org/10.4172/2157-7439.1000316

García-Ortiz, A. & Serrador, J.M. (2020) ERM proteins at the crossroad of leukocyte polarization, migration and intercellular adhesion. *International Journal of Molecular Sciences*, 21, 1502.

Gary, R. & Bretscher, A. (1995) Ezrin self-association involves binding of an N-terminal domain to a normally masked C-terminal domain that includes the F-actin binding site. *Molecular Biology of the Cell*, 6, 1061–1075.

Gautreau, A., Louvard, D. & Arpin, M. (2000) Morphogenic effects of ezrin require a phosphorylation-induced transition from oligomers to monomers at the plasma membrane. *Journal of Cell Biology*, 150, 193–203.

Gilk, S.D., Cockrell, D.C., Luterbach, C., Hansen, B., Knodler, L.A., Ibarra, J.A., Steele-Mortimer, O. & Heinzen, R.A. (2013) Bacterial colonization of host cells in the absence of cholesterol. *PLoS Pathogens*, 9, e1003107.

Goosney, D.L., DeVinney, R. & Finlay, B.B. (2001) Recruitment of cytoskeletal and signaling proteins to enteropathogenic and enterohemorrhagic Escherichia coli pedestals. *Infection and Immunity*, 69, 3315–3322.

Grover, J.R., Veatch, S.L. & Ono, A. (2015) Basic motifs target PSGL-1, CD43, and CD44 to plasma membrane sites where HIV-1 assembles. *Journal of Virology*, 89, 454–467.

Hao, J.J., Liu, Y., Kruhlak, M., Debell, K.E., Rellahan, B.L. & Shaw, S. (2009) Phospholipase C - mediated hydrolysis of PIP2 releases ERM proteins from lymphocyte membrane. *Journal of Cell Biology*, 184, 451–462.

Hausrat, T.J., Muhia, M., Gerrow, K., Thomas, P., Hirdes, W., Tsukita, S., et al. (2015) Radixin regulates synaptic GABAA receptor density and is essential for reversal learning and short-term memory. *Nature Communication*, 6, 6872.

Hébert, M., Potin, S., Sebbagh, M., Bertoglio, J., Bréard, J. & Hamelin, J. (2008) Rho-ROCK-dependent ezrin-radixin-moesin phosphorylation regulates fas-mediated apoptosis in Jurkat cells. *Journal of Immunology*, 181, 5963–5973.

Jaqaman, K. & Grinstein, S. (2012) Regulation from within: the cytoskeleton in transmembrane signaling. *Trends in Cell Biology*, 22, 515–526.

Jayasundar, J.J., Ju, J.H., He, L., Liu, D., Meilleur, F., Zhao, J., Callaway, D.J.E. & Bu, Z. (2012) Open conformation of ezrin bound to phosphatidylinositol 4,5-bisphosphate and to F-actin revealed by neutron scattering. *Journal of Biological Chemistry*, 287, 37119–37133.

Jiang, H., Peterson, R. S., Wang, W., Bartnik, E., Knudson, C. B., & Knudson, W. (2002) A requirement for the CD44 cytoplasmic domain for hyaluronan binding, pericellular matrix assembly, and receptor-mediated endocytosis in COS-7 cells. *Journal of Biological Chemistry*, 277, 10531–10538.

Kamiyama, H., Izumida, M., Umemura, Y., Hayashi, H., Matsuyama, T., & Kubo, Y. (2018) Role of ezrin phosphorylation in HIV-1 replication. *Frontiers in Microbiology*, 9. https://doi.org/10.3389/fmicb.2018.01912

Kvalvaag, A.S., Schink, K.O., Brech, A., Sandvig, K. & Pust, S. (2018) ERM proteins: the missing actin linkers in clathrin-mediated endocytosis. *bioRxiv*, 307272.

Lau, C., Castellanos, P., Ranev, D., Wang, X. & Chow, C.-W. (2011) HRV signaling in airway epithelial cells is regulated by ITAM-mediated recruitment and activation of Syk. *Protein & Peptide Letters*, 18, 518–529.

Leemans, J.C., Florquin, S., Heikens, M., Pals, S.T., Van der Neut, R., Van der Poll, T., van der Neut, R. & Van der Poll, T. (2003) CD44 is a macrophage binding site for *Mycobacterium tuberculosis* that mediates macrophage recruitment and protective immunity against tuberculosis. *Journal of Clinical Investigation*, 111, 681–689.

Legg, J.W. & Isacke, C.M. (1998) Identification and functional analysis of the ezrin-binding site in the hyaluronan receptor, CD44. *Current Biology*, 8, 705–8.

Li, Q., Nance, M.R., Kulikauskas, R., Nyberg, K., Fehon, R., Karplus, P.A., Bretscher, A. & Tesmer, J.J.G. (2007) Self-masking in an intact ERM-merlin protein: an active role for the central alpha-helical domain. *Journal of Molecular Biology*, 365, 1446–1459.

Li, W., Jin, W.W., Tsuji, K., Chen, Y., Nomura, N., Su, L., Yui, N., Arthur, J., Cotecchia, S., Păunescu, T.G., et al. (2017) Ezrin directly interacts with AQP2 and promotes its endocytosis. *Journal of Cell Science*, 130, 2914–2925.

Li, C., Wu, Y., Riehle, A., Orian-Rousseau, V., Zhang, Y., Gulbins, E. & Grassmé, H. (2018) Regulation of *Staphylococcus aureus* infection of macrophages by CD44, reactive oxygen species, and acid sphingomyelinase. *Antioxidants Redox Signal*. 28, 916–934.

Liu, T., Yan, Z., Liu, Y., Choy, E., Hornicek, F. J., Mankin, H., & Duan, Z. (2018) CRISPR-Cas9-mediated silencing of CD44 in human highly metastatic osteosarcoma cells. *Cellular Physiology and Biochemistry*, 46, 1218–1230.

Magendantz, M., Henry, M.D., Lander, A. & Solomon, F. (1995) Interdomain interactions of radixin in vitro. *Journal of Biological Chemistry*, 270, 25324–25327.

Marion, S., Hoffmann, E., Holzer, D., Le Clainche, C., Martin, M., Sachse, M., Ganeva, I., Mangeat, P. & Griffiths, G. (2011) Ezrin promotes actin assembly at the phagosome membrane and regulates phago-lysosomal fusion. *Traffic (Copenhagen, Denmark)*, 12, 421–437.

Martinez, E., Cantet, F., Fava, L., Norville, I., & Bonazzi, M. (2014) Identification of OmpA, a coxiella burnetii protein involved in host cell invasion, by multi-phenotypic high-content screening. *PLoS Pathogens*, 10, e1004013. https://doi.org/10.1371/journal.ppat.1004013

Matsui, T., Maeda, M., Doi, Y., Yonemura, S., Amano, M., Kaibuchi, K., Tsukita, S. & Tsukita, S. (1998) Rho-kinase phosphorylates COOH-terminal threonines of ezrin/radixin/moesin (ERM) proteins and regulates their head-to-tail association. *Journal of Cell Biology*, 140, 647–657.

Meconi, S., Jacomo, V., Boquet, P., Raoult, D., Mege, J.L. & Capo, C. (1998) Coxiella burnetii induces reorganization of the actin cytoskeleton in human monocytes. *Infection and Immunity*, 66, 5527–5533.

Mellor, L., Knudson, C. B., Hida, D., Askew, E. B., & Knudson, W. (2013) Intracellular domain fragment of CD44 alters CD44 function in chondrocytes. *Journal of Biological Chemistry*, 288, 25838–25850.

Moffat, F.L., Han, T., Li, Z.M., Peck, M.D., Falk, R.E., Spalding, P.B., Jy, W., Ahn, Y.S., Chu, A.J. & Bourguignon, L.Y.W. (1996) Involvement of CD44 and the cytoskeletal linker protein ankyrin in human neutrophil bacterial phagocytosis. *Journal of Cellular Physiology*, 168, 638–647.

Mu, L., Tu, Z., Miao, L., Ruan, H., Kang, N., Hei, Y., et al. (2018) A phosphatidylinositol 4,5-bisphosphate redistribution-based sensing mechanism initiates a phagocytosis programing. *Nature Communication*, 9, 1–16.

1768322x, 2022, 9, Downloaded from https://onlinelibrary.wiley.com/doi/10.1111/boc.202100096 by Portail BibCNRS INSB, Wiley Online Library on [09/06/2023]. See the Terms and Conditions (https://onlinelibrary.wiley.com/terms-and-conditions) on Wiley Online Library for rules of use; OA articles are governed by the applicable Creative Commons License

Murad, N., Kokkinaki, M., Gunawardena, N., Gunawan, M.S., Hathout, Y., Janczura, K.J., Theos, A.C. & Golestaneh, N. (2014) miR-184 regulates ezrin, LAMP-1 expression, affects phagocytosis in human retinal pigment epithelium and is downregulated in age-related macular degeneration. *FEBS Journal*, 281, 5251–5264.

Niedergang, F. & Grinstein, S. (2018) How to build a phagosome: new concepts for an old process. *Current Opinion in Cell Biology*, 50, 57–63.

Oba, M., Fukushima, S., Kanayama, N., Aoyagi, K., Nishiyama, N., Koyama, H., & Kataoka, K. (2007) Cyclic RGD peptide-conjugated polyplex micelles as a targetable gene delivery system directed to cells possessing $\alpha v\beta 3$ and $\alpha v\beta 5$ integrins. *Bioconjugate Chemistry*, 18, 1415–1423.

Orgovan, N., Peter, B., Bősze, S., Ramsden, J. J., Szabó, B., & Horvath, R. (2014) Dependence of cancer cell adhesion kinetics on integrin ligand surface density measured by a high-throughput label-free resonant waveguide grating biosensor. *Scientific Reports*, 4. https://doi.org/10.1038/srep04034

Pearson, M.A., Reczek, D., Bretscher, A. & Karplus, P.A. (2000) Structure of the ERM protein moesin reveals the FERM domain fold masked by an extended actin binding tail domain. *Cell*, 101, 259–70.

Pelaseyed, T., Viswanatha, R., Sauvanet, C., Filter, J.J., Goldberg, M.L. & Bretscher, A. (2017) Ezrin activation by LOK phosphorylation involves a PIP(2)-dependent wedge mechanism. *Elife*, 6, e22759.

Perschl, A., Lesley, J., English, N., Trowbridge, I., & Hyman, R. (1995) Role of CD44 cytoplasmic domain in hyaluronan binding. *European Journal of Immunology*, 25, 495–501.

Picaud, L., Thibault, B., Mery, E., Ouali, M., Martinez, A., Delord, J.-P., Couderc, B., & Ferron, G. (2014) Evaluation of the effects of hyaluronic acid-carboxymethyl cellulose barrier on ovarian tumor progression. *Journal of Ovarian Research*, 7. https://doi.org/10.1186/1757-2215-7-40

Ponta, H., Sherman, L. & Herrlich, P.A. (2003) CD44: From adhesion molecules to signalling regulators. *Nature Reviews Molecular Cell Biology*, 4, 33–45.

Quang, C.T., Gautreau, A., Arpin, M. & Treisman, R. (2000) Ezrin function is required for ROCK-mediated fibroblast transformation by the Net and Dbl oncogenes. *EMBO Journal*, 19, 4565–4576.

Rey-Gallardo, A., Tomlins, H., Joachim, J., Rahman, I., Kitscha, P., Frudd, K., Parsons, M. & Ivetic, A. (2018) Sequential binding of ezrin and moesin to L-selectin regulates monocyte protrusive behaviour during transendothelial migration. *Journal of Cell Science*, 131, jcs215541.

Roberts, R. & Hallett, M. (2019) Neutrophil cell shape change: mechanism and signalling during cell spreading and phagocytosis. *International Journal of Molecular Sciences*, 20, 1383.

Rosales, C. & Uribe-Querol, E. (2017) Phagocytosis: a fundamental process in immunity. *BioMed Research International*, 2017, 1–18.

Rosales, E.M., Aguilera, M.O., Salinas, R.P., Carminati, S.A., Colombo, M.I., Martinez-Quiles, N. & Berón, W. (2012) Cortactin is involved in the entry of *Coxiella burnetii* into non-phagocytic cells. *Plos One* 7, e39348.

Salinas, R.P., Ortiz Flores, R.M., Distel, J.S., Aguilera, M.O., Colombo, M.I. & Berón, W. (2015) *Coxiella burnetii* phagocytosis is regulated by GTPases of the Rho family and the RhoA effectors mDia1 and ROCK. *Plos One*, 10, e0145211.

Shabardina, V., Kramer, C., Gerdes, B., Braunger, J., Cordes, A., Schäfer, J., Mey, I., Grill, D., Gerke, V. & Steinem, C. (2016) Mode of Ezrin-membrane interaction as a function of PIP2 binding and pseudophosphorylation. *Biophysical Journal*, 110, 2710–2719.

Skoudy, A., Nhieu, G.T., Mantis, N., Arpin, M., Mounier, J., Gounon, P. & Sansonetti, P. (1999) A functional role for ezrin during *Shigella flexneri* entry into epithelial cells. *Journal of Cell Science*, 112, 2059–68.

Skoudy, A., Mounier, J., Aruffo, A., Ohayon, H., Gounon, P., Sansonetti, P. & Tran Van Nhieu, G. (2000) CD44 binds to the Shigella IpaB protein and participates in bacterial invasion of epithelial cells. *Cellular Microbiology*, 2, 19–33.

Sobotta, K., Hillarius, K., Mager, M., Kerner, K., Heydel, C. & Menge, C. (2016) *Coxiella burnetii* infects primary bovine macrophages and limits their host cell response. *Infection and Immunity*, 84, 1722–1734.

Sobotta, K., Bonkowski, K., Liebler-Tenorio, E., Germon, P., Rainard, P., Hambruch, N., Pfarrer, C., Jacobsen, I.D. & Menge, C. (2017) Permissiveness of bovine epithelial cells from lung, intestine, placenta and udder for infection with *Coxiella burnetii*. *Veterinary Research*, 48, 1–15.

Sun, F., Schroer, C.F.E., Palacios, C.R., Xu, L., Luo, S.Z. & Marrink, S.J. (2020) Molecular mechanism for bidirectional regulation of CD44 for lipid raft affiliation by palmitoylations and PIP2. *Plos Computational Biology*, 16, 1–20.

Swanson, K.A., Crane, D.D. & Caldwell, H.D. (2007) *Chlamydia trachomatis* species-specific induction of ezrin tyrosine phosphorylation functions in pathogen entry. *Infection and Immunity*, 75, 5669–77.

Tam, J. C. H., Bidgood, S. R., McEwan, W. A., & James, L. C. (2014) Intracellular sensing of complement C3 activates cell autonomous immunity. *Science*, 345. https://doi.org/10.1126/science.1256070

Thakur, A., Mikkelsen, H. & Jungersen, G. (2019) Intracellular pathogens: host immunity and microbial persistence strategies. *Journal of Immunology Research*, 2019, 1–24.

Thorne, R.F., Legg, J.W., Isacke, C.M., Hyman, R. & Trowbridge, I.S. (2003) The role of the CD44 transmembrane and cytoplasmic domains in co-ordinating adhesive and signalling events. *Journal of Cell Science*, 117, 373–380.

Tian, Z., Cheng, S., Xia, B., Jin, Y., Bai, F., Cheng, Z., Jin, S., Liu, X. & Wu, W. (2019) *Pseudomonas aeruginosa* ExsA regulates a metalloprotease, ImpA, that inhibits phagocytosis of macrophages. *Infection and Immunity*, 87, 1–17.

Torres-Gomez, A., Cabañas, C. & Lafuente, E.M. (2020) Phagocytic integrins: activation and signaling. *Frontiers in Immunology*, 11, 1–10.

Tsai, F.-C., Bertin, A., Bousquet, H., Manzi, J., Senju, Y., Tsai, M.-C., Picas, L., Miserey-Lenkei, S., Lappalainen, P., Lemichez, E., Coudrier, E. & Bassereau, P. (2018) Ezrin enrichment on curved membranes requires a specific conformation or interaction with a curvature-sensitive partner. *Elife*, 7, 1–27.

Tuckwell, D.S. & Humphries, M.J. (2020) *Molecular and cellular biology of phagocytosis*. In: Hallett, M. B. (Eds.) Cham: Springer International Publishing.

Vachon, E., Martin, R., Plumb, J., Kwok, V., Vandivier, R.W., Glogauer, M., Kapus, A., Wang, X., Chow, C., Grinstein, S. & Downey, G.P. (2006) CD44 is a phagocytic receptor. *Blood*, 107, 4149–4159.

Vachon, E., Martin, R., Kwok, V., Cherepanov, V., Chow, C.-W., Doerschuk, C.M., Plumb, J., Grinstein, S. & Downey, G.P. (2007) CD44-mediated phagocytosis induces inside-out activation of complement receptor-3 in murine macrophages. *Blood*, 110, 4492–4502.

van Schaik, E. J., Chen, C., Mertens, K., Weber, M. M., & Samuel, J. E. (2013) Molecular pathogenesis of the obligate intracellular bacterium Coxiella burnetii. *Nature Reviews Microbiology*, 11, 561–573.

Voth, D.E. & Heinzen, R.A. (2007) Lounging in a lysosome: The intracellular lifestyle of Coxiella burnetii. *Cellular Microbiology*, 9, 829–840.

Wang, K., Zeng, J., Luo, L., Yang, J., Chen, J., Li, B., & Shen, K. (2013) Identification of a cancer stem cell-like side population in the HeLa human cervical carcinoma cell line. *Oncology Letters*, 6, 1673–1680.

Watanabe, K., Tachibana, M., Kim, S. & Watarai, M. (2009) Participation of ezrin in bacterial uptake by trophoblast giant cells. *Reproductive Biology and Endocrinology [Electronic Resource]: RB&E*, 7, 95.

Xiong, L., Yu, M., Cheng, M., Zhang, M., Zhang, X., Xu, C., & Li, F. (2009) A photostable fluorescent probe for targeted imaging of

1768322x, 2022, 9, Downloaded from https://onlinelibrary.wiley.com/doi/10.1111/boc.202100096 by Portail BibCNRS INSB, Wiley Online Library on [09/06/2023]. See the Terms and Conditions (https://onlinelibrary.wiley.com/terms-and-conditions) on Wiley Online Library for rules of use; OA articles are governed by the applicable Creative Commons License

tumour cells possessing integrin αvβ3**. *Molecular BioSystems*, 5, 241. https://doi.org/10.1039/b820576k

Yonemura, S., Tsukita, S. & Tsukita, S. (1999) Direct involvement of ezrin/radixin/moesin (ERM)-binding membrane proteins in the organization of microvilli in collaboration with activated ERM proteins. *Journal of Cell Biology*, 145, 1497–1509.

Zhang, X., Flores, L. R., Keeling, M. C., Sliogeryte, K., & Gavara, N. (2020) Ezrin phosphorylation at T567 modulates cell migration, mechanical properties, and cytoskeletal organization. *International Journal of Molecular Sciences*, 21, 435. https://doi.org/10.3390/ijms21020435

How to cite this article: Distel, J.S., Ortiz Flores, R.M., Bienvenu, A., Aguilera, M.O., Bonazzi, M. & Berón, M. (2022) Ezrin and CD44 participate in the internalization process of *Coxiella burnetii* into non-phagocytic cells. *Biology of the Cell*, 114, 237–253. https://doi.org/10.1111/boc.202100096

1768322x, 2022, 9, Downloaded from https://onlinelibrary.wiley.com/doi/10.1111/boc.202100096 by Portail BibCNRS INSB, Wiley Online Library on [09/06/2023]. See the Terms and Conditions (https://onlinelibrary.wiley.com/terms-and-conditions) on Wiley Online Library for rules of use; OA articles are governed by the applicable Creative Commons License

2.2. *Coxiella* containing vacuole biogenesis.

2.2.1. Host-cell vesicular trafficking and autophagy modulation.

2.2.1.1. Endocytosis.

Endocytosis is a cellular process that involves the generation of internal membranes from the lipid bilayer of the plasma membrane. Through endocytosis, plasma membrane lipids, proteins, and extracellular fluid are internalized and incorporated into the cell. It can be viewed as the structural opposite of exocytosis, which involves the fusion of internal membranes with the plasma membrane. Exocytosis allows the release of cellular material into the extracellular medium and as well as the transport of lipids and proteins to the plasma membrane (Doherty & McMahon, 2009). Six major endocytic mechanisms have been described and can be divided in two major groups: dynamin-dependent and dynamin-independent endocytosis (Rennick et al., 2021). At sites of membrane invagination, dynamins assemble into a helical ring structure and promote GTPase activity. This GTPase activity facilitates the internalization of encapsulated cargo (Heymann & Hinshaw, 2009). The three major dynamin-dependent route are clathrin-coated pit-mediated endocytosis (CME), fast endophilin-mediated endocytosis (FEME) a clathrin-independent pathway for rapid ligand-driven endocytosis of specific membrane proteins, and Caveolin mediated endocytosis. Conversely, clathrin-independent carrier (CLIC)/glycosylphosphatidylinositol-anchored protein enriched early endocytic compartment (GEEC) endocytosis, macropinocytosis and phagocytosis are all dynamin-independent pathways (**figure 8)** (Rennick et al., 2021).

In this thesis study, we focused on macropinocytosis. As mentioned earlier, macropinocytosis is a type of endocytic pathway that allows cells to internalize extracellular fluid and its content, including solutes and macromolecules, into large vesicles called macropinosomes (Bloomfield & Kay, 2016; Egami & Araki, 2009). It is a non-selective process, that can take in any soluble macromolecule present in the cell's environment. Macropinocytosis is initiated by actin-driven protrusions of the plasma membrane, which form cup-shaped structures known as ruffles. These membrane ruffles fold back and enclose

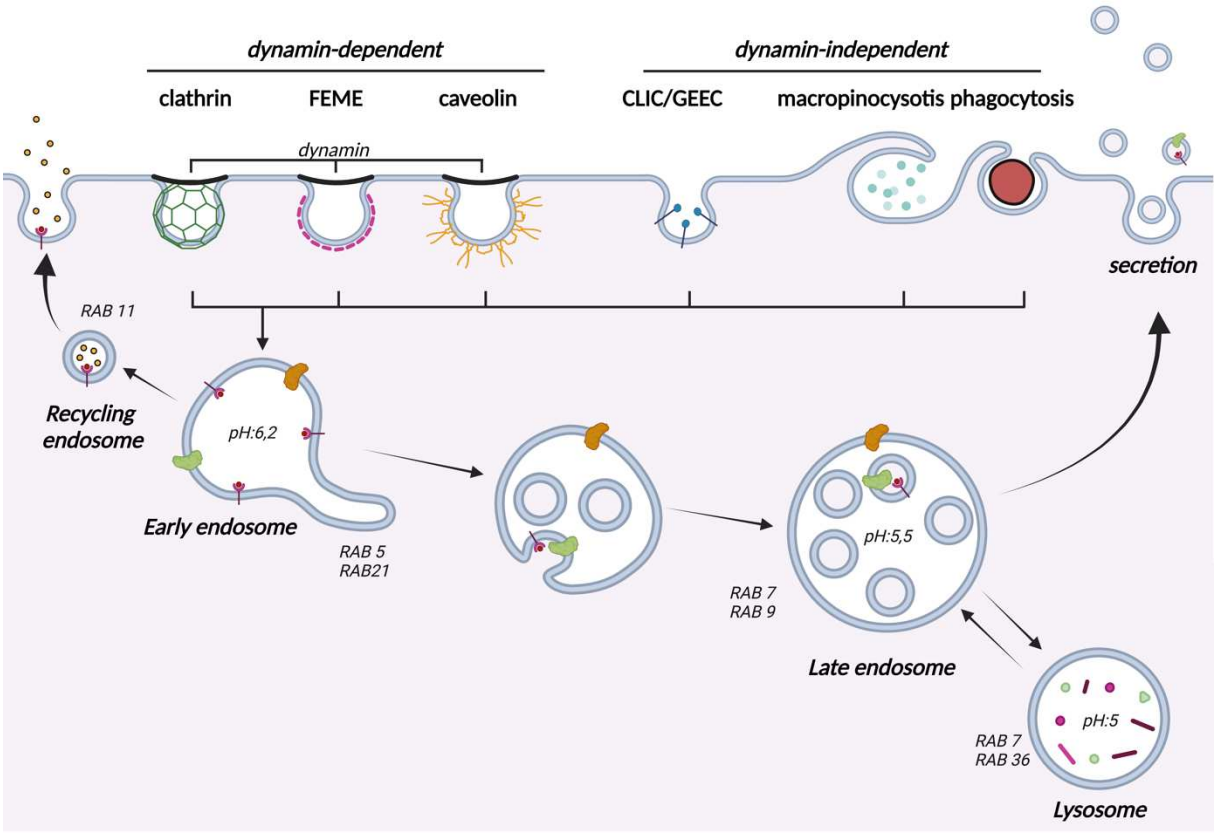


Figure 8: Endocytosis and endosome maturation pathways. (Adapted from *Rennick et al., 2021*)

Endocytosis can either be dynamin dependent or independent. Clathrin-mediated endocytosis (CME) is initiated by the adaptor complex AP2, which recruits clathrin to specific receptor domains on the cytoplasmic side of the membrane, leading to the formation of clathrin-coated pits. On the other hand, clathrin-independent endocytosis known as fast endophilin-mediated endocytosis (FEME) is triggered by ligand-receptor interactions and regulated by the recruitment of endophilin A2 and actin polymerization. Both CME and FEME require the protein dynamin for membrane scission and involve interactions between the intracellular domains of cell surface receptors and cytoplasmic machinery.

The formation of caveolae, another type of endocytic pathway that relies on dynamin, is dependent on the recruitment of caveolin and cavin proteins. EHD2 plays a role in stabilizing the neck of caveolae to regulate their endocytosis. CLIC/GEEC endocytosis, in contrast, is a constitutive process that occurs independently of receptor-ligand interactions and does not require clathrin or dynamin. In CLIC/GEEC endocytosis, extracellular galectin proteins cluster with glycoproteins and glycolipids to drive carrier formation and cargo incorporation. Macropinocytosis, which involves the uptake of large volumes of fluid, is typically a stimulated pathway. It is regulated by actin dynamics and involves different proteins and lipids. The fission of macropinosomes from the cell surface is also influenced by C-terminal-binding protein 1 (CTBP1). Phagocytosis occurs when a binding event at the cell surface triggers actin polymerization, leading to the formation of a vesicle that tightly engulfs the bound material.

After internalization, the various endocytic pathways converge to early endosomes, where sorting takes place. From there, materials may be either sent back to the cell surface via recycling endosomes or

directed towards late endosomes and lysosomes for further processing and degradation. Every compartment possesses a specific pH and a RAB composition that can be referred as the compartment signature.

portions of extracellular fluid, eventually pinching off from the plasma membrane to form irregularly shaped vesicles of various sizes. The process of macropinocytosis closely resembles that of phagocytosis, another type of endocytic pathway initiated by actin-driven protrusions of the plasma membrane in myeloid cells. However, a key distinction of macropinocytosis is its ability to be induced in the absence of cargo. In contrast, phagocytosis requires solid particles such as bacteria, and receptor-mediated endocytosis is triggered by the binding of macromolecules to specific cell surface receptors (Mayor et al., 2014; Mercer & Helenius, 2009).

Macropinocytosis uptake includes diverse macromolecules and even cell-derived particles such as exosomes, apoptotic bodies, cellular debris and can be studied by the monitoring of high molecular weight dextran uptake (Palm & Thompson, 2017). Once formed, macropinosomes associate with Rab5 and can have two intracellular fates: they can either directly recycle back to the cell surface for cargo release or associate with RAB7 and traffic to the lysosome for degradation of their content (Developed latter in the paragraph).

Due to its non-selective nature, macropinocytosis plays a crucial role in allowing macrophages and immature dendritic cells to survey their surroundings and sample soluble antigens for presentation to T cells. This process enables immune cells to capture a wide range of potential antigens, contributing to the immune surveillance and the initiation of immune responses (Sallusto et al., 1995). The initiation of macropinocytosis has been shown to be dependent on extra-cellular calcium, which is detected through calcium-sensing receptors (Canton et al., 2016).

Macropinocytosis can also be exploited by certain viruses and bacteria as an entry pathway to invade host cells. These pathogens take advantage of the large vesicles formed during macropinocytosis to enter cells, thus facilitating their infection and propagation within the host (Lin et al., 2020). This cellular process can also be initiated via the activation of receptor tyrosine kinases (RTKs) by growth factors, leading to the activation of signaling pathways involving Ras, Rac, Cdc42, and PI3K.

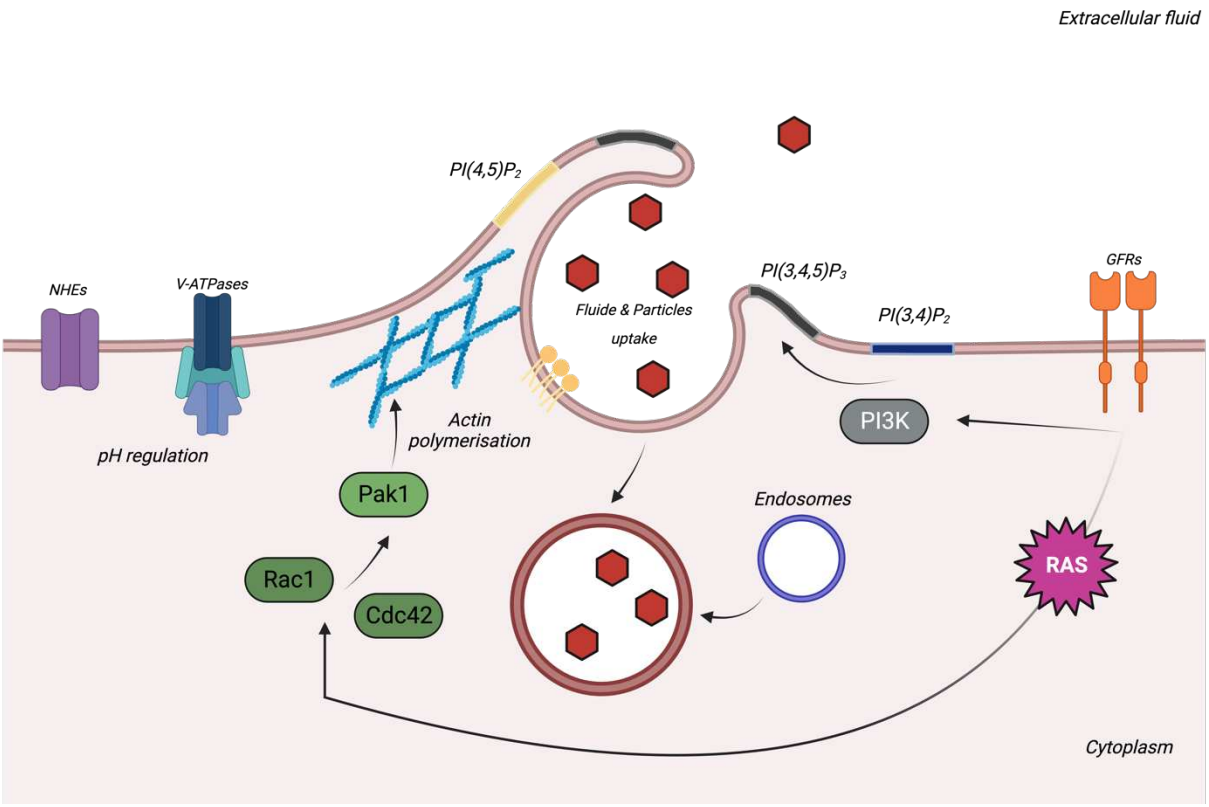


Figure 9: The macropinocytosis process. (Adapted from *Recouvreux et.al, 2017*)

Extracellular protein uptake via macropinocytosis involves a series of molecular events. Activation of Ras, whether through growth factor stimulation or oncogenic mutation, triggers an increase in membrane ruffling and initiates macropinocytosis. This process is facilitated by the activation of Rac1 and Cdc42, which in turn stimulate p21-activated kinase 1 (Pak1) to induce actin polymerization, resulting in the formation of macropinosomes. The activation of Rac1 and Cdc42 is sensitive to changes in submembranous pH, and the maintenance of pH homeostasis relies on the activity of Na+/H+ exchangers (NHEs) and vacuolar H+-ATPase (V-ATPases). Additionally, the conversion of membrane phosphoinositides by PI3-kinase (PI3K) is necessary for the occurrence of macropinocytosis.

These signaling proteins regulate membrane ruffling, actin polymerization and vesicle formation during macropinocytosis but this endocytic pathway is also dependent on the phospholipid composition of the plasma membrane (discussed in chapter 2.2.3.1) (Recouvreux & Commisso, 2017). Additionally, macropinocytosis is closely associated with pH homeostasis, as alterations in intracellular and submembranous pH can affect this process (**Figure 9**). Inhibition of Na+/H+ exchangers and vacuolar H+-ATPases can block macropinocytosis by

disrupting pH regulation. Of note, drugs such as 5-(*N*-ethyl-*N*-isopropyl)amiloride (EIPA) can target these exchangers and specifically inhibit macropinocytosis (Koivusalo et al., 2010).

Despite their different mode of action, all endocytic mechanisms lead to the formation of vesicles that will mature into early endosomes. The early endosome acts as a crucial sorting station by segregating membrane components that need to be reused from those destined for lysosomal degradation. Indeed, housekeeping receptors and other membrane proteins undergo recycling either directly to the plasma membrane or indirectly through the recycling endosome while certain molecules are directed towards the lysosomes for degradation (Scott & Gruenberg, 2011). Significant modifications in protein and lipid composition occur during the early to late endosomes maturation, which are accompanied with changes in the internal environment of the endosomes. Notably, phosphoinositides (PI) and membrane-anchored RAB GTPase proteins are very specific to vesicular compartments and organelles, representing a molecular signature of the nature of these compartments. Of note, early endosomes are mainly enriched in RAB5 and RAB21 while late endosomes are enriched in RAB7 and RAB9 or RAB36 for lysosomes (**Figure 8)** (Wandinger-Ness & Zerial, 2014).

In the process of endosome maturation, V-ATPase, a multi-subunit proton pump, plays a crucial role in acidifying early and late endosomes as well as lysosomes, reducing their pH to approximately 6.2 and 5.5/5.0, respectively. This acidification process is essential for regulating various functions within the endo-lysosomal system, such as the dissociation of receptor-ligand interactions, activation of lysosomal enzymes, and proper transport processes(Huotari & Helenius, 2011).

Molecules and proteins, such as activated signaling receptors, that are targeted to late endosomes and lysosomes undergo selective sorting into luminal invaginations within the endosomes. These invaginations are then released as separate intralumenal vesicles (ILVs) containing the cargo. These multivesicular regions detach or mature from early endosomes, turning into multivesicular bodies (MVBs, also known as multivesicular endosomes) (Gruenberg, 2020).

These multivesicular bodies act as a transitional step in the fate of endosomes, has they can either fuse with lysosome as mentioned earlier or get re-routed to the plasma membrane. This re-routing is dependent on a direct contact between the MVB and the endoplasmic

reticulum where it acquires the RAB GTPase RAB27a which triggers its trafficking to the plasma membrane (Verweij et al., 2022).

At the plasma membrane, MVBs deliver their lumen content into the extracellular milieu. The release from the plasma membrane and the mobilization, docking, and fusion of secretory MVBs with the cell surface involve essential components such as the cytoskeleton (actin and microtubules), molecular motors (kinesins and myosins), but also small GTPases as mentioned earlier and the fusion machinery with SNAREs and tethering factors (Raposo & Stoorvogel, 2013). ILVs released in the extracellular milieu are called exosomes. They are part of the large family of extracellular vesicles (EVs), their typical size ranges between 30 and 150 nm (which can vary depending on the cell type) and they possess typical markers such as components of the Endosomal Sorting Complexes Required for Transport (ESCRT) machinery (ex: TSG101, ALIX), tetraspanins (ex: CD63, CD9, CD81) and are enriched in specific lipids such as LBPA or cholesterol for instance. (Dimik et al., 2022; Skotland et al., 2019; Vacca et al., 2016).The formation of ILVs can have multiple origins and is either dependent on the ESCRT machinery or not. If not, ILVs are formed in tetraspanin-enriched microdomains or in a lipid-dependent manner (Figure 10)(Bissig et al., 2013; Gruenberg, 2020).

The ESCRT protein family consists of multiple complexes, including ESCRT-0, -I, -II, and -III, which sequentially associate with the membrane of multivesicular bodies.

It is proposed that ESCRT-0 plays a crucial role in initiating the process by binding to both phosphatidylinositol 3-phosphate (PI(3)P) on the membrane of early endosomes and ubiquitin molecules that are conjugated to cargos. This complex then recruits ESCRT-I, which further recruits ESCRT-II, serving as a nucleator for the assembly of ESCRT-III filaments. This sequential recruitment of ESCRT complexes facilitates the formation of filamentous structures composed of ESCRT-III and the ATPase activity of vacuolar sorting-associated protein 4 (VPS4), enabling membrane detachment. This process can be spontaneous; however, it is mainly helped by the intervention of the ALG-2-interacting protein X (ALIX). Indeed, ALIX binds to the lysobisphosphatidic acid (LBPA), a phospholipid only found at the membrane of MVBs (Discussed in chapter 2.2.3.1) (Kobayashi et al., 1998), allowing ALIX to promote the formation of filamentous structures formed by ESCRT-III (Figure 10) (Gruenberg, 2020).

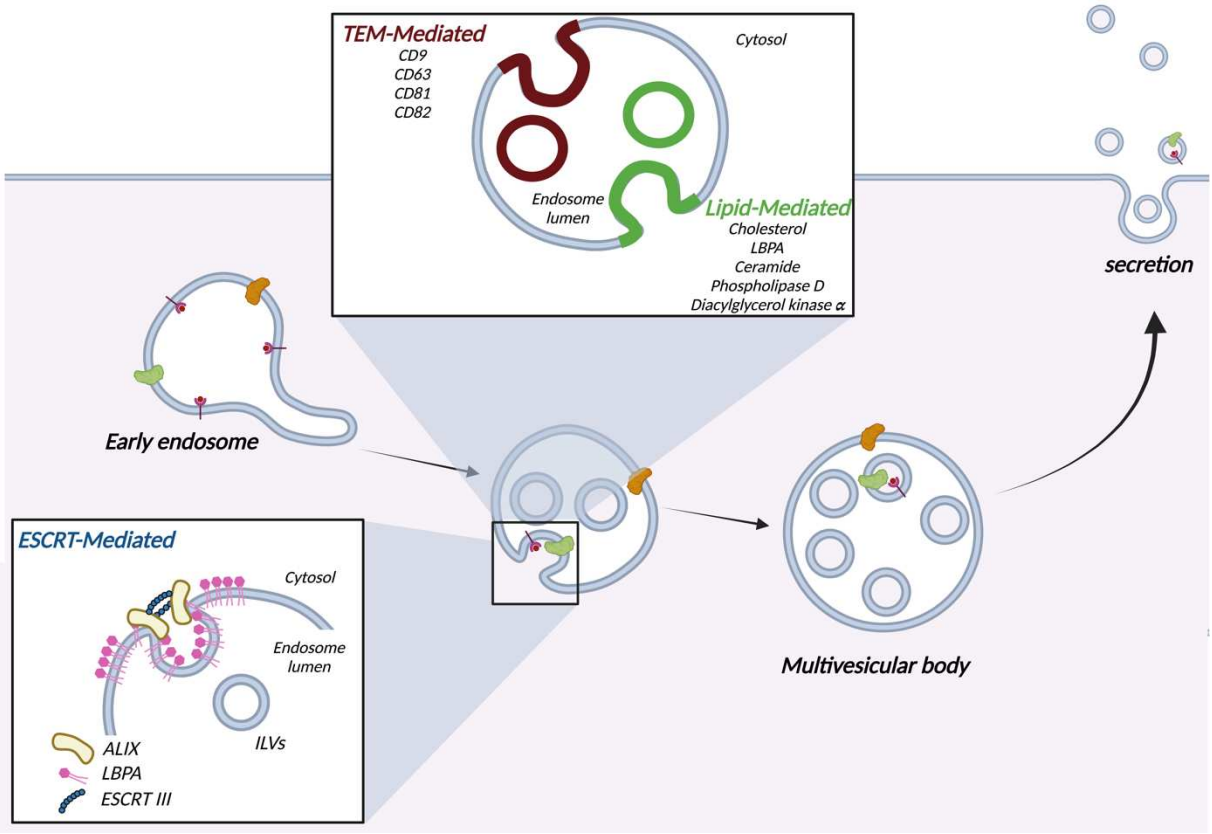


Figure 10: Intralumenal vesicle (ILVs) formation pathways. (Adapted from *Bissig et al., 2013*; *Ventimiglia & Alonso, 2016*)

ILVs are formed through intraluminal budding of specific membrane nanodomains in the multivesicular body. This process can be mediated by the ESCRT machinery (Blue), Tetraspanin microdomains (Brown), or specific lipids domain enriched in cholesterol, ceramide or LBPA (Green).

Cellular membranes are prone to damage, and cells have developed mechanisms to repair these membrane ruptures to ensure cell survival. Various studies have shed light on the role of the ESCRT machinery in repairing damage in different cellular membranes, including the plasma membrane, nuclear envelope, and the endolysosomal network. The ESCRT machinery plays crucial roles in maintaining membrane integrity and promoting membrane repair processes thanks to its unequal ability to exclude damaged membranes from their corresponding compartment (Figure 11) (Fernandez et al., 2022; Hurley, 2015; Skowyra et al., 2018).

Besides its regular role in host cell pathways, the ESCRT machinery can also be be hijacked by the human immunodeficiency virus 1 (HIV-1) during infection to promote viral particle release (Hudait et al., 2023). The p6 domain at the C-terminus of the viral protein Gag interacts with Tsg101, which is a component of the ESCRT-I complex, allowing the interaction of the p6 domain with the V-domain of Alix. A study has demonstrated that mutations in the TSG101- and ALIX-binding sites within p6 only result in a delay in virus release, suggesting that the involvement of ESCRTs may not be essential or that they may be recruited through other sites. Other experiments utilizing various techniques have provided evidence that ESCRT-I, ESCRT-II, ESCRT-III, ALIX, and VPS4 are indeed involved in the process of HIV-1 release, highlighting the importance of the ESCRT machinery in the viral egress (**Figure 11**) (Freed, 2015; Meusser et al., 2020).

In addition to HIV-1, the ESCRT machinery can be hijacked by many other pathogens during infection. Intracellular parasites or bacteria such as *Salmonella* actively recruit this machinery to develop their intracellular vacuole, and conversely, *Mycobacteria* needs to impair the ESCRT function to avoid lysosome clearance (Rivera-Cuevas & Carruthers, 2023).

Intracellular bacteria, including *C. burnetii*, exploit the endocytic pathway to establish their intracellular niche. While some intracellular bacteria such as *Legionella* or *Brucella* implement strategies to evade from lysosomal degradation (Pizarro-Cerdá et al., 1998; Roy & Kagan, 2013), *C. burnetii* requires an acidic environment for efficient replication. The CCV acquires the endocytic markers RAB5 and RAB7 in a Dot/Icm-independent manner during its maturation along the endocytic pathway. This heterotypic fusion with early and late endosomes appears to be essential for CCV formation and bacterial replication. Indeed, the depletion of RAB5 and RAB7 using small interfering RNA (siRNA) has shown that these regulators are key to CCV biogenesis (V. Howe et al., 2003; McDonough et al., 2013; Van Schaik et al., 2013). In a similar manner, two major components of phagolysosomal membranes, Lysosome associated membrane protein-1 (LAMP-1) and LAMP-2(Baca et al., 1994; Eskelinen, 2006) are enriched at the CCV membrane and are essential for its complete development (Schulze-Luehrmann et al., 2016). Interestingly, LAMP-1 is now widely used as the typical marker of CCV membrane.

The CCV follows the endocytic pathway and fuses with lysosomes, thus triggering the activation of *C. burnetii* T4SS and the secretion of bacterial effectors that actively manipulate the vesicular trafficking to promote the CCV expansion.

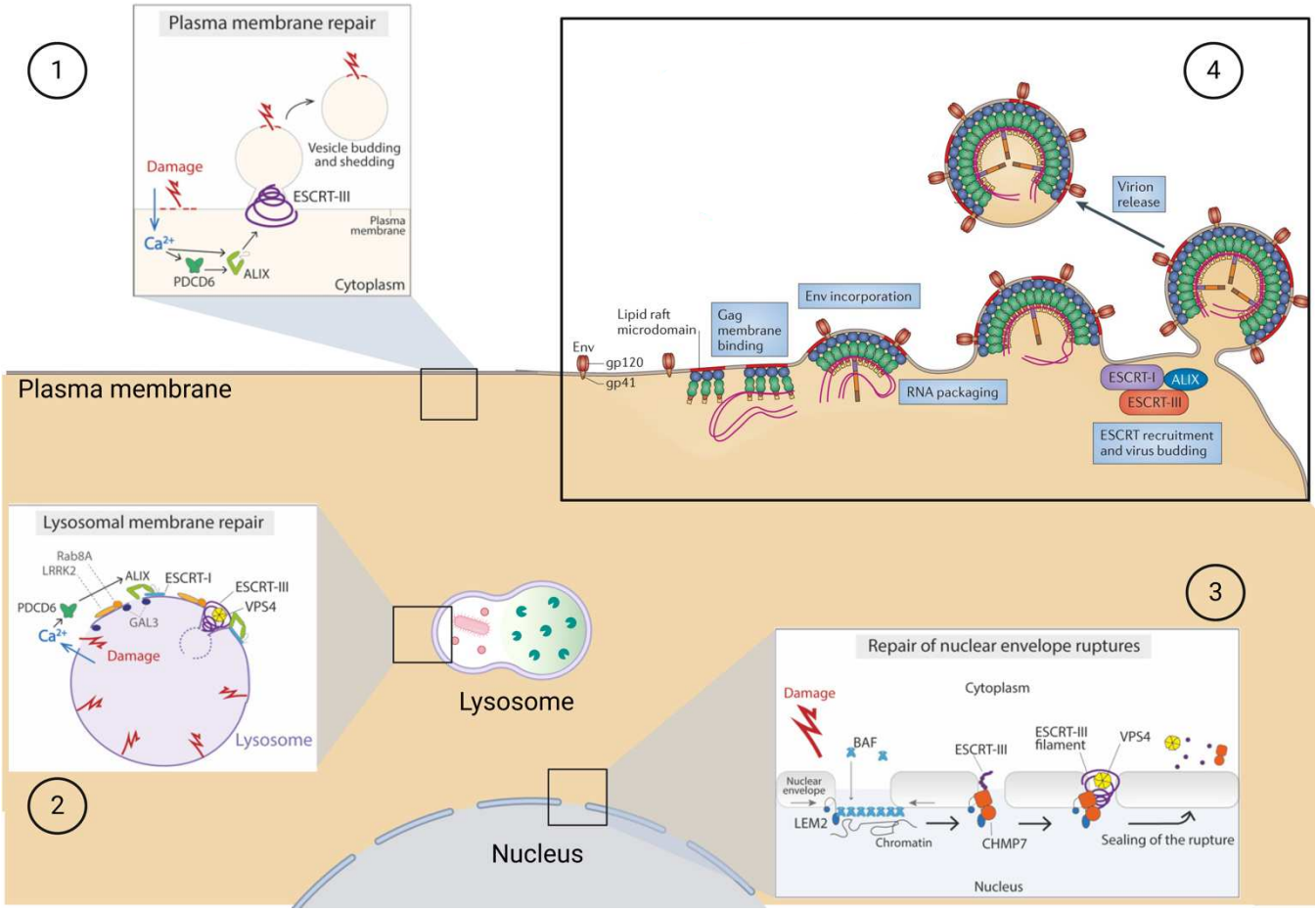


Figure 11: ESCRT membrane repair and implication in HIV-1 egress. (adapted from *Fernandez et al., 2022*; *Freed, 2015*)

The ESCRT machinery participates in three distinct membrane repair processes: plasma membrane repair, nuclear envelope (NE) repair, and lysosome repair. In plasma membrane repair (1), the entry of calcium through the damaged membrane triggers the rapid recruitment of ESCRTs, facilitated by PDCD6 and ALIX. ESCRTs are believed to promote the budding and shedding of small membrane domains containing the site of damage. In NE repair (2), when the nuclear envelope ruptures, cytosolic BAF coats the exposed chromatin and interacts with LEM2. This interaction facilitates the recruitment of nuclear membrane and the recruitment of CHMP7. Subsequently, CHMP7 promotes the nucleation and polymerization of ESCRT-III, which, together with VPS4, constricts the rupture and promotes sealing. In lysosome repair (3), after damage to the lysosome, calcium efflux triggers the

recruitment of ESCRT-I and ESCRT-III through factors such as PDCD6, ALIX, GAL3, and LRRK2. The membrane-remodeling activity of ESCRT-III filament spirals is thought to facilitate the shedding of damaged membranes into the lysosome's lumen for recycling. During HIV-1 infection, Gag interacts with the plasma membrane through lipid raft microdomains and phosphatidylinositol-(4,5)-bisphosphate. It recruits ESCRT-I through direct association with its p6 domain and the ESCRT-I subunit TSG101. Gag also binds ALIX through the YPXL motif in p6. ESCRT-III and VPS4 are subsequently recruited, leading to membrane scission and particle release.

Of note, *C. burnetii* vacuolar protein A (CvpA) and the Co-regulated *icm* gene 57 (Cig57) can modulate CME pathway by hijacking clathrin-coated vesicles to the CCV. Thanks to several endocytic sorting motifs, CvpA interacts directly with clathrin but also with the adaptor protein-2 (AP-2) subunit while Cig57 interacts with the endocytic adaptor FCH and mu domain-containing endocytic adaptor 2 (FCHO2). Inhibition of clathrin expression via SiRNA or mutations in *cvpA* and *cig57* genes affect *C. burnetii* replication and CCV formation, suggesting that manipulation of CME supports CCV development. Clathrin has also been implicated in facilitating the fusion of autophagosomes with the CCV, indicating its involvement in different vesicular pathways during *C. burnetii* infections(C. L. Larson et al., 2013; Latomanski et al., 2016).

CvpA belongs to the effector family of the Cvp (*Coxiella* vacuolar protein), together with CvpB/Cig2, CvpC/Cig50, CvpD, and CvpE. Similarly to CvpA, these four other Cvps play an important role in intracellular bacterial replication and CCV development in the THP-1 myeloid cell line (C. Chen et al., 2010; C. Larson et al., 2015; Lifshitz et al., 2014). CvpB, CvpD and CvpE are involved in CCV homotypic fusion, the function of CvpB will be further developed in the current chapter (C. Larson et al., 2015). CvpC shows partial localization with the transferrin receptor, indicating a potential targeting of recycling endosomes, although it does not interfere with transferrin uptake (C. Larson et al., 2015).

C. burnetii small noncoding RNA *CbsR12,* which is itself essential for replication, downregulates the amount of the full-length transcript of CvpD, suggesting a regulatory mechanism that may vary throughout infection (Wachter et al., 2019). Even if the direct link between the modulation of endocytic trafficking and these Cvps is not made, we can speculate that they may have a role in CCV biogenesis due to their localization at the CCV. A further

characterization is then needed to fully understand the role of CvpC, CvpD, and CvpE during *C. burnetii* infection.

The *C. burnetii* effector CirA promotes CCV biogenesis by stimulating the GTPase activity of RhoA as a GTPase-activating protein (GAP). CirA is thought to induce cytoskeletal rearrangements and redirect host vesicles to the CCV. Recent studies have identified specific motifs within CirA that further support the notion that this effector manipulates endocytic trafficking by facilitating vesicular fusion events. It has been shown that RAB7 GTP-activating protein TBC1D5 interacts with *C. burnetii* serine/threonine kinase (CstK), another *C. burnetii* effector. TBC1D5 is actively recruited at CCVs during *C. burnetii* infections, and TBC1D5-targeting siRNAs significantly affect CCVs development(Martinez et al., 2020; Weber et al., 2016). Vimentin, an intermediate filament that plays a crucial role in vesicular trafficking (Margiotta & Bucci, 2016) has been shown to interact with the effector AnkF, an effector important for optimal intracellular replication of *C. burnetii* (Pechstein et al., 2020). Other validated effectors have been shown to be implicated in CCV biogenesis but their mode of action is still uncharacterized (Crabill et al., 2018; C. L. Larson et al., 2023). We can speculate that some of them may interfere with the endocytic trafficking during the infection.

Overall, multiple *C. burnetii* effectors play a role in the manipulation of the endocytic pathways, facilitating CCV formation, and promoting intracellular replication.

An interesting study demonstrated that CCVs undergo transient damage during *C. burnetii* infections, and that the bacterium actively manipulates both the endocytic and autophagy pathways (discussed in chapter 2.2.1.3) to repair CCV membranes (Pareja et al., 2017). The galectin protein family is characterized by a carbohydrate (glycan) binding capacity. They are expressed by a diverse range of cells and have an affinity for glycans containing galactose. Galectins can be found within the nucleus and cytoplasm in cells, or they can be released into the extracellular environment. Due to their specific ability to recognize glycans they play a major role in membrane reparation. Indeed, glycans are exposed in the cytosol after the rupture of organelles membranes. In this context, galectin-3 for instance, bind to glycans at rupture site and will recruits other proteins such as ALIX to initiate reparation. (Jia et al., 2020; Liu & Stowell, 2023; Paz et al., 2010).

During its intracellular cycle, both galectin-3 and the ESCRT machinery are transiently recruited to damaged membrane sites at the CCVs, and their function is essential for *C. burnetii* intracellular replication (Pareja et al., 2017; Radulovic et al., 2018). More precisely, it has been shown that at the CCV, galectin-3 is recruited to damaged membrane sites at the same time as CHMP4b (ESCRT III). However, the whole ESCRT machinery might be important as, in the same study, the depletion of TSG101 (ESCRT I) impeded bacterial replication.

Additionally, *C. burnetii* has been observed to delay CCV maturation and lysosomal fusion during infection, possibly to enhance the acquisition of peptides and amino acids (Voth & Heinzen, 2007) and regulate CCV pH to prevent bacterial lysis (Mulye et al., 2017; Samanta et al., 2019). In mouse embryonic fibroblasts, the proteins LAMP-1 and LAMP-2 have been implicated in reducing CCV fusion and delaying vacuole maturation, although the specific bacterial factors involved in this process have yet to be identified (Schulze-Luehrmann et al., 2016).

2.2.1.2. Secretory pathways.

The secretory pathway orchestrates the synthesis and the delivery of proteins and lipids cargos from the rough endoplasmic reticulum (ER) to the Golgi apparatus, followed by a fusion to the plasma membrane for exocytosis or to targeted specific cellular compartments. COP (Coat protein complex) proteins are essential in this trafficking process. Indeed, COPII proteins mediate the delivering of cargos from the ER to the Golgi by harnessing Sar1-GTPase activity, while COPI proteins support cargo recycling from the Golgi to the ER, regulated through the activity of Arf GTPases. (Duden, 2003).

Within the Golgi apparatus, glycosylated proteins and lipids are packaged into transport vesicles for delivery. The retrograde pathway is another essential mechanism involved in the trafficking of proteins and lipids, allowing their recycling from endosomes back to the Golgi and the ER. This pathway ensures the adequate localization of proteins and lipid homeostasis in the cell (Gomez-Navarro & Miller, 2016).

Studies have revealed that *C. burnetii* exploits both the secretory and retrograde pathways to facilitate CCV formation and intracellular replication. In later stages of infection, CCVs display the RAB GTPase RAB1B, that regulates transport from the ER to the Golgi,

indicating a redirection of the early secretory pathway (Campoy et al., 2011). Disruption of the secretory pathway through siRNA-mediated depletion of RAB1B or the use of brefeldin A, a chemical agent that interferes with secretion, impacts CCV biogenesis, emphasizing the crucial role of the secretory pathway *C. burnetii* infection (Campoy et al., 2011).

Thus far, there is five *C. burnetii* effectors, namely CBU0635, CvpC, CBU1825, CBUA0019, and ElpA (ER-localizing protein A), that have been identified as potential modulators of the host secretory pathway. Thanks to the secreted embryonic alkaline phosphatase reporter assay, it has been shown that overexpression of these effectors in mammalian cell significantly reduces the release of host proteins (Carey et al., 2011; Graham et al., 2015; Weber et al., 2013). Aside from manipulating the secretory pathway, retrograde transport has emerged as another essential element in the intracellular replication of C. burnetii. Notably, the depletion of critical retrograde pathway components, including Vacuolar Protein Sorting 29 and 35 (VPS29 and VPS35) from the retromer subunits and Sorting Nexins 2, 3, 5, and 6 (SNX2, SNX3, SNX5, SNX6), results in a significant reduction of bacterial intracellular replication (McDonough et al., 2013). However, the precise mechanisms by which the pathogen modulates this pathway remain unclear.

2.2.1.3. Autophagy.

Autophagy is a highly conserved process that plays a crucial role in maintaining cellular homeostasis and responding to various stresses (Cooper, 2018). This process can be either selective or non-selective and leads to the degradation and the recycling of cellular components in lysosomes. It is activated in response to stressors such as starvation or can be stimulated by rapamycin, through the involvement of regulatory signaling complexes (Füllgrabe et al., 2016; Yun & Lee, 2018). Autophagy is also important for the degradation of intracellular pathogens and maintaining the balance of bodily systems, making it essential for normal cellular function (M. S. Lee, 2018; Y. A. Lee et al., 2018; Mizushima, 2007; Yang & Klionsky, 2010).

During macroautophagy (hereafter named autophagy), large portions of cytoplasm, including long-lived proteins, aggregated proteins, damaged organelles, and intracellular pathogens, are sequestered into a double-membrane structure called the autophagosome. The autophagosome fuses with lysosomes to form an autolysosome, in which the enclosed contents

undergo degradation, and macromolecules are recycled for reuse (Khandia et al., 2019). This process is mediated by LC3 family proteins (three isoforms of LC3 are known, A-B-C) that are essential for autophagosome maturation. LC3 can be found as a cytosolic form (LC3-I) or it can be recruited to autophagosomal membranes (LC3-II) when conjugated with phosphatidylethanolamine (Tanida et al., 2008).

In the battle against microbial pathogens, cells employ two pathways related to autophagy to facilitate the degradation of microbes in lysosomes: LC3-associated phagocytosis (LAP) and xenophagy. When certain pathogen recognition receptors (PRRs) are activated by microbes, the LAP pathway utilizes autophagy proteins in a non-canonical manner after phagocytosis, enhancing the maturation of the phagosome. Some pathogens, to avoid destruction within phagolysosomes, manage to escape into the cytosol, while others inflict damages to the phagosome and release microbial effectors into the cytosol, disrupting the trafficking to lysosomes. When confronted with compromised phagosomes, host cells employ xenophagy, a form of canonical autophagy that selectively captures invading microbes within a double-membrane compartment, guiding them towards lysosomes for degradation (Upadhyay & Philips, 2019).

Multiple studies conducted with *Listeria monocytogenes, Shigella flexneri, Salmonella typhimurium,* or *Mycobacterium tuberculosis*, have demonstrated the role of autophagy in targeting bacteria in the cytoplasm (Ogawa et al., 2005; Yoshikawa et al., 2009) or inside the phagosome (Aylan et al., 2023; Birmingham et al., 2006). These pathogens have evolved different mechanisms in order to escape from autophagy such as secreting effector proteins that target autophagic pathways. However, *S. aureus* or other T4SS equipped bacteria such as *Legionella* or *Brucella,* exploit autophagy to favor their replication or egress. *C. burnetii* appears unique among pathogens as autophagy favors the biogenesis of its replicative compartment and bacterial replication (Wu & Li, 2019; Xiong et al., 2019).

As mentioned earlier, the CCV undergoes fusion with early and late endosomes, lysosomes but also with autophagosomes during its maturation process (Heinzen et al., 1996; Voth & Heinzen, 2007). These fusion events lead to the incorporation of various endocytic markers discussed earlier but also some autophagy-related proteins onto the CCV, including

LC3, Beclin-1, Rab24 and p62/sequestosome 1 (SQSTM-1) (Berón et al., 2002; Gutierrez et al., 2005; Vázquez & Colombo, 2010; Winchell et al., 2014).

C. burnetii quickly engages with autophagy following internalization, and the maturation of the CCV into an acidic compartment is crucial for bacterial metabolism and CCV complete biogenesis (Hackstadt & Williams, 1981; Newton et al., 2013).Inhibition of autophagy, such as by targeting the protein syntaxin-17 (STX17), disrupts proper homotypic fusion of the CCV, leading to a multi-vacuolar phenotype (Berón et al., 2002; Latomanski & Newton, 2018; McDonough et al., 2013; Newton et al., 2014). Conversely, induction of autophagy increases CCV size (Gutierrez et al., 2005; C. L. Larson et al., 2019; Latomanski & Newton, 2018). However, the precise role of *C. burnetii* in modulating autophagy is still investigated, and it is likely that the interaction is more complex than simple induction or inhibition (Thomas et al., 2020).

Although *C. burnetii* increases the levels of LC3 and p62 during infection, this does not appear to significantly impact the autophagic flux (C. L. Larson et al., 2019; Latomanski & Newton, 2018; Newton et al., 2014; Winchell et al., 2014, 2018).

C. burnetii employs multiple strategies to interact with autophagic signaling pathways. One mechanism involves the T4SS-dependent inhibition of mTORC1, which promotes CCV biogenesis (C. L. Larson et al., 2019). mTORC1 is inhibited during nutrient starvation, leading to the translocation of transcription factors TFEB and TFE3 to the nucleus, which induces lysosomal biogenesis and autophagy (Rabanal-Ruiz et al., 2017). However, *C. burnetii* inhibits mTORC1 independently of cellular nutrient levels, resulting in an increased lysosomal fusion without impacting the autophagic flux (C. L. Larson et al., 2019). In infected cells, activation of TFEB and TFE3 is observed, and these proteins play a role in CCV development, but not in bacterial replication (C. L. Larson et al., 2019; Padmanabhan et al., 2020). Interestingly, overexpression of TFEB leads to decreased CCV size and bacterial growth, likely due to excessive CCV acidification, indicating that excessive activation of TFEB can be detrimental to *C. burnetii* (Samanta et al., 2019).

Another mechanism by which *C. burnetii* regulates autophagy is through the modulation of Beclin-1 and BCL-2 (Vázquez & Colombo, 2010). Beclin-1 is a key promoter of autophagy and interacts with the anti-apoptotic protein BCL-2 (Liang et al., 1998, 1999). The interaction between Beclin-1 and BCL-2 is important for the regulation of autophagy and apoptosis, as BCL-2 negatively regulates Beclin-1, and mutations in Beclin-1 that disrupt its binding to BCL-2 result

in excessive autophagy and cell death (Pattingre et al., 2005). Beclin-1 and BCL-2 are independently recruited to the CCV, and their overexpression has distinct effects: Beclin-1 overexpression promotes the development of large vacuoles and increases bacterial replication, while BCL-2 overexpression leads to the formation of multiple small CCVs without affecting replication (Vázquez & Colombo, 2010). However, the interaction between BCL-2 and Beclin-1 is necessary for the benefits of Beclin-1 on CCV development and bacterial replication, as well as for apoptosis inhibition (Vázquez & Colombo, 2010). These findings highlight the importance of proper expression and interaction between Beclin-1 and BCL-2 during *C. burnetii* infection and demonstrate how *C. burnetii* modulates both autophagy and apoptosis signaling pathways.

The modulation of autophagy and the fusion of autophagosomes with CCVs are directly affected by secreted effectors. As mentioned earlier, CvpA plays a crucial role in vacuole biogenesis by modulating clathrin-mediated vesicle trafficking. It localizes to the CCV, plasma membrane, as well as sorting and recycling endosomes. By recruiting clathrin to the CCV, CvpA disrupts the endocytic signaling and reduces transferrin uptake. Notably, the enrichment of clathrin heavy chain at the CCV by CvpA promotes autophagy dependent CCV expansion (C. L. Larson et al., 2013; Latomanski & Newton, 2018).

CvpB (or Cig2) is essential for homotypic fusion of CCVs and fusion with autophagosomes, but not lysosomes. Mutations in *cvpB* result in a multi-vacuolar phenotype and CCVs generated by *cvpB*::Tn mutants lack several autophagy markers (Kohler et al., 2016; C. Larson et al., 2015; Martinez et al., 2014, 2016; Newton et al., 2014). In a similar manner as CvpA, CvpB also plays a role in the localization of clathrin heavy chain (CLTC) at the CCV (Latomanski & Newton, 2018). While CvpB is not required for bacterial replication in HeLa cells, it is necessary for *C. burnetii* replication in the THP-1 myeloid cell line and contributes to bacterial virulence in *G. mellonella*. During infection, CvpB interaction with host cell lipids is essential for vacuole fusion and LC3B recruitment at the CCV, this will be discussed in the next chapter “Host-cell lipids and bacterial infections” (Martinez et al., 2016).

The effector protein CvpF also plays a significant role in manipulating autophagy and promoting the formation of CCVs. By diverting RAB26-dependent autophagy, CvpF enhances CCV biogenesis and contributes to the virulence of the bacterium. CCVs generated by *cvpF*::Tn mutants also lack the autophagosomal marker LC3B, indicating its involvement in autophagy manipulation (Figure 12). Ectopic expression of CvpF leads to increased levels of both LC3B-II

and p62, suggesting its role in autolysosome formation. However, the actions of CvpF may be counteracted by other *C. burnetii* effectors during infection, impacting p62 degradation or transcriptional expression. Overall, CvpF contributes to autophagy modulation and CCV formation, while other effectors may influence p62 stability during *C. burnetii* infection (Siadous et al., 2020).

Additionally, Cig57 is another effector involved in CCV localization of CLTC and LC3B. It is required for CLTC and LC3B recruitment to the CCV and contains endocytic sorting motifs important for replication and CCV development. Cig57 interacts with the endocytosis accessory protein FCHO2, which promotes bacterial replication and CLTC recruitment but is not recruited to the CCV or required for LC3B recruitment (Latomanski et al., 2016; Latomanski & Newton, 2018).

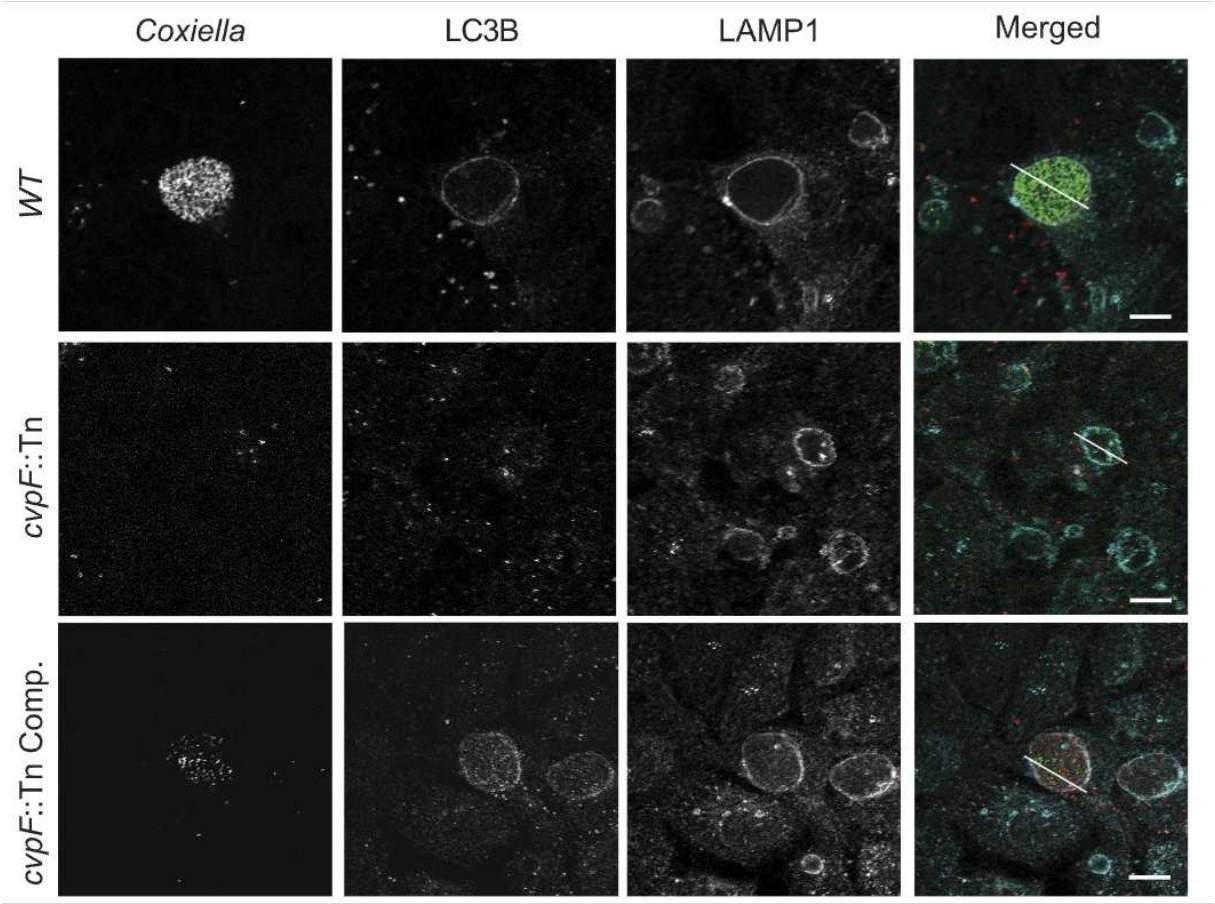


Figure 12: CvpF participates in LC3B recruitment to CCV. (Adapted from Siadous et.al, 2021)

U2OS cells infected with *wt C. burnetii* (top panels), *cvpF*::Tn (middle panels), or the complemented *cvpF*::Tn strain (*cvpF*::Tn Comp., bottom panels) for 6 days. Cells were then fixed and LC3B localization at the CCV was observed using anti-LAMP1 (cyan) and anti-LC3B (red). Bacteria are shown in white. Scale bar = 10 µm.

Recently, the effector protein CinF has been shown to play a crucial role in inhibiting NF-κB activation and suppressing host immunity. CinF promotes CCV biogenesis by manipulating autophagy and the recruitment of LC3B (Crabill et al., 2018). Furthermore, CinF inhibits NF-κB signaling by inhibiting the degradation of IκBα, a critical component of the NF-κB pathway. CinF shares significant similarity with a fructose-1,6-bisphosphate aldolase/phosphatase found in various bacteria. However, unlike its counterpart in *Sulfolobus tokodaii*, CinF lacks FBP phosphatase activity. Instead, it acts as a protein phosphatase that specifically dephosphorylates and stabilizes IκBα. The impact of CinF on LC3 recruitment is likely mediated through its effect on NF-κB activation, as a reciprocal crosstalk between NF-κB and the autophagy pathway has already been described (Verzella et al., 2020; Y. Zhang et al., 2022).

Finally, the presence of *C. burnetii* plasmid QpH1 has been associated with increased LC3-II accumulation on CCVs, larger CCVs, and higher bacterial loads in host cells. However, expression of *cpeB* in the QpH1-cured *C. burnetii* strain restored LC3-II accumulation on CCVs but does not restore their size. In a severe combined immune deficiency (SCID) mouse model, infections with the QpH1-cured *C. burnetii* strain resulted in significantly lower bacterial burdens in the spleen and liver compared to the wild-type strain. Further investigations revealed that CpeB targets RAB11a to promote LC3-II accumulation. In Rab11a conditional knockout mice, intratracheal inoculation of *C. burnetii* led to lower bacterial burdens and milder lung lesions. These findings suggest that CpeB enhances *C. burnetii* virulence by inducing LC3-II accumulation through a pathway involving RAB11a (Fu et al., 2022).

Overall, Cvp family effectors, CinF, Cig57, CpeB and probably many other undescribed effectors play crucial roles in *C. burnetii's* interactions with autophagy, vesicle trafficking, and vacuole biogenesis, contributing to the establishment of the CCV and optimal bacterial replication.

2.2.3. Host-cell lipid

2.2.3.1. Lipid biology and function.

Lipids play a vital role in eukaryotic cells, serving as energy sources, structural components of membranes, and signaling molecules (Van Meer et al., 2008). Cell membranes consist of lipids and proteins, creating a protective barrier that shields the cell and its organelles from the surrounding environment. Lipids are separated into three main categories: glycerophospholipids, sphingolipids, and sterols (Harayama & Riezman, 2018). Glycerophospholipids, the predominant lipids in membranes, are composed of a glycerol core connected to fatty acids and a modified phosphate head group. Eukaryotic membranes contain several types of glycerophospholipids, including phosphatidic acid (PA), phosphatidylcholine, and phosphatidylethanolamine (Harayama & Riezman, 2018). Sphingolipids, the second major lipid class in membranes, are composed of a sphingoid base, a hydrophobic acyl chain, and a phosphate head group. These lipids encompass simple sphingolipids such as ceramides and complex glycosphingolipids such as sphingomyelins, which are involved in the regulation of endocytosis and receptor-mediated ligand uptake and can be used by bacterial toxins as ligand receptors (Slotte, 2013). Sterols, such as cholesterol in mammalian cells, have a distinct structure consisting of four fused hydrocarbon rings and a hydroxyl group. Cholesterol, the primary sterol in mammalian cells, plays a critical role in membrane structure and function, influencing membrane rigidity and participating in the formation of specialized microdomains called lipid rafts when interacting with sphingolipids (Ikonen, 2008; Van Meer et al., 2008). Lipid rafts serve as signaling platforms engaged in diverse cellular functions, such as endocytosis, signal transduction, protein sorting or intracellular membrane trafficking. (Levental et al., 2020).

The endoplasmic reticulum (ER) serves as the primary site for lipid biosynthesis, where most lipids are produced by specific enzymes (Jacquemyn et al., 2017). However, lipid synthesis can also take place in other organelles, such as late endosomes and lysosomes for Lysobisphosphatidic Acid (LBPA), mitochondria for cardiolipin, and the Golgi apparatus for sphingolipids (Gaspard & McMaster, 2015; Kobayashi et al., 1998; Somerharju, 1979; Van Meer et al., 2008). The ER plays a crucial role in regulating lipid levels within cell membranes by distributing newly synthesized lipids to organelles and the plasma membrane (PM). This

distribution occurs through the secretory pathway via vesicle budding and fusion processes and via ER contact sites facilitated by lipid transfer proteins (Funato et al., 2020; Jain & Holthuis, 2017).

Among the glycerophospholipids, the Phosphoinositides (PI), which are phosphorylated derivatives of phosphatidylinositol (PtdIns), play a critical role in determining the identity of compartmental membranes and serve as spatiotemporal cues for directing membrane dynamics (Posor et al., 2022). For instance, PtdIns 3-phosphate (PI(3)P) acts as a marker lipid that recruits specific cytosolic proteins to early endosomes, defining their identity (Di Paolo & De Camilli, 2006; Gillooly et al., 2000). Like many other lipids, PtdIns are synthesized in the endoplasmic reticulum (ER) and are transported to other organelles through lipid exchange proteins at membrane contact sites and vesicular or tubular carriers along the secretory pathway and endolysosomal system (Balla, 2013). Phosphorylation and dephosphorylation of the inositol ring by phosphoinositide kinases and phosphatases generate seven distinct phosphoinositides (Figure 13.a).

Despite constituting less than 1% of the total cellular phospholipid pool, phosphoinositides exhibit a highly localized subcellular distribution due to tight regulation of their synthesis and turnover (Posor et al., 2022).Their presence directly affects the localization and activity of cytosolic effector proteins and membrane-integral proteins, such as receptors, ion channels, or transporters, that interact with these lipids and elicit specific physiological responses, such as signaling cascades or membrane remodeling through protein complex assembly. Phosphoinositide-binding domains in effector proteins typically exhibit low affinity for their target lipid, necessitating multivalent coincident recognition of additional factors like small GTP-binding proteins and other lipids, as well as avidity effects facilitated by multiple lipid-binding sites or domains on effector proteins for their proper function (Balla, 2013; Behnia & Munro, 2005; Di Paolo & De Camilli, 2006). Together, with the RAB proteins, they represent the signature and the identity of membrane compartments.

As mentioned earlier, phosphatidylinositol 3-phosphate (PI(3)P) is highly enriched in phagosomes, early endosomes and autophagosomes. To a lesser extent, (PI(3)P) is present in the membranes of the Golgi apparatus, the endoplasmic reticulum (ER) and even platelet plasma membrane (Mujalli et al., 2023; Sarkes & Rameh, 2010). It is also found at late endosomes where it serve as a precursor to phosphatidylinositol 3,5-bisphosphate (PI(3,5)P2)

that is highly enriched in late endosomes, MVBs and particularly in lysosomes (Posor et al., 2022; Viaud & Payrastre, 2015). PI(3,5)P2 is a key factor in regulating membrane dynamics by controlling vacuole membrane fission and fusion processes. Similarly to PI(3)P, PI(3,5)P2 play an important role in membrane trafficking and protein sorting. PI(3,5)P2, in particular, is suggested to be essential for cargo selection within multivesicular bodies (MVBs) as VpS4 is known to bind this phospholipid (N. Jin et al., 2016).

Two of the most abundant phosphoinositides in mammalian cells are phosphatidylinositol 4-phosphate (PI(4)P) and phosphatidylinositol 4,5-bisphosphate (PI(4,5)P2) (Dickson & Hille, 2019). PI(4)P is highly enriched at the Golgi apparatus and at the plasma membrane (PM) and plays important roles in vesicular trafficking, lipid metabolism, and mitochondrial fission (Lorente-Rodríguez & Barlowe, 2011; Nagashima et al., 2020; Yamaji & Hanada, 2015). On the other hand, PI(4,5)P2 is predominantly found at the PM, but reports mentioned its presence in the membranes of the ER, Golgi apparatus, endosomes, and the nucleus but in all to a lesser extend (X. Tan et al., 2015; Watt et al., 2002). It has two main functions at the PM, as a key lipid in the process of exocytic vesicle fusion and in endocytosis and actin rearrangements (Martin, 2012; Sun et al., 2013).

PI(5)P represents only 0.5% of the PI pool present in the cells and does not seem to have a specific localization as it can be found either at the plasma membrane or at the nuclear membrane (Poli et al., 2019). Its function is not really clear, however it seems to play an important role in signaling, notably in T cell biology (Nunès & Guittard, 2013). It is also important to note that PI(5)P levels are highly increased during *Shigella* and *Salmonella* infections, suggesting a putative importance in pathogenesis(Mason et al., 2007; Niebuhr et al., 2002). Lastly, when membrane receptors are activated during the beginning of phagocytosis or in particular cancer settings, PI(3,4,5)P3, which is initially only present at the plasma membrane in very small amounts, experiences a significant rise in local concentration. (Gozzelino et al., 2020; Salamon & Backer, 2013) (**Figure 13.b**).

To preserve organellar membrane identity, traffic between compartments needs to be coupled to the interconversion of phosphoinositide species by functional units comprising phosphoinositide phosphatases and kinases that act in concert (Posor et al., 2022). This dynamic conversion in between PIs also allows cellular events at the plasma membrane such as the macropinocytosis previously described (**Figure 14**).

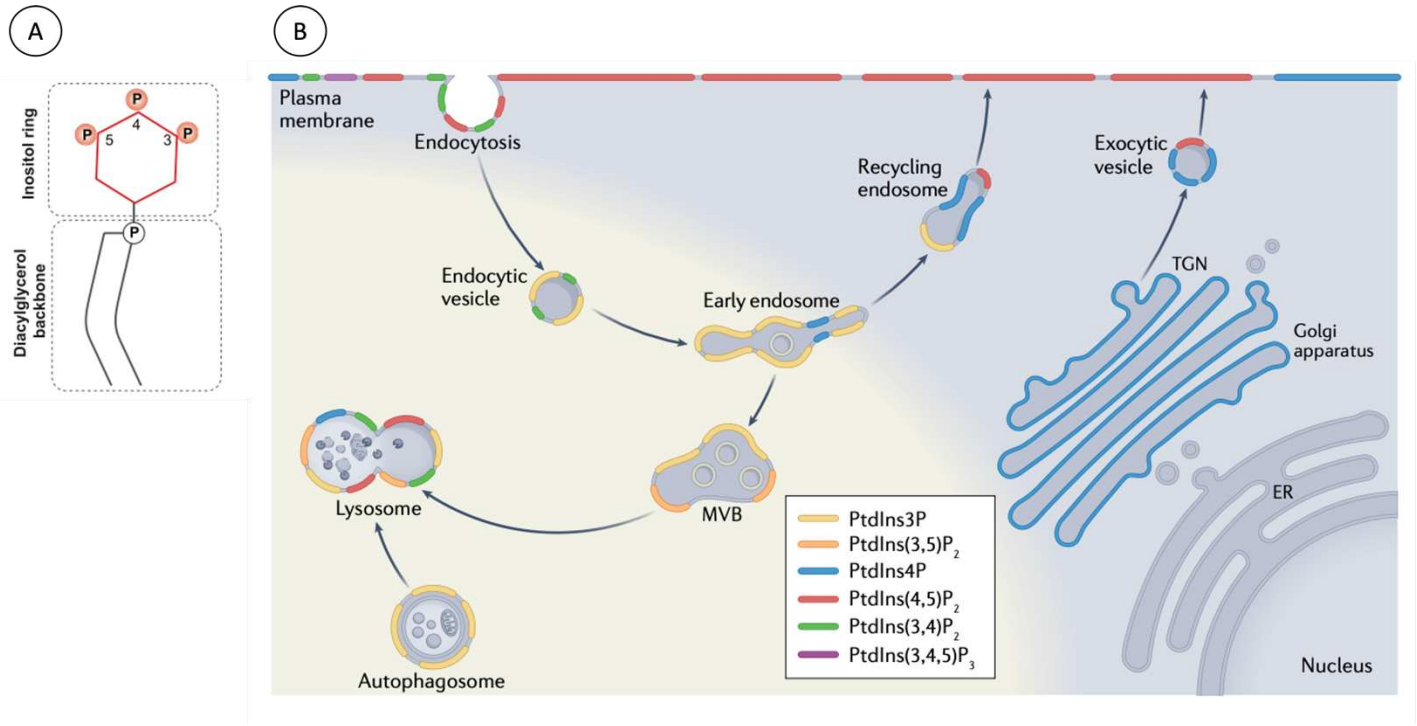


Figure 13: Phospholipid structure and Pi organelle signature. (Adapted from *Goud et al., 2016; Posor et al., 2022*)

(A) The phosphatidylinositol (PI) phospholipid structure consists of an inositol ring that can be phosphorylated at three different positions. It is connected to a diacylglycerol backbone through a phosphodiester linker. Different isoforms of PI are localized to specific cellular compartments. (B) PI(4,5)P2 (PtdIns(4,5)P2) is highly enriched at the plasma membrane, while PI(4)P (PtdIns4P) is characteristic of the Golgi apparatus and trans-Golgi network. Early endosomes are marked by PI(3)P (PtdIns3P), while late endosomes contain PI(3,5)P2 (PtdIns(3,5)P2). Lysosomes exhibit a diverse range of phosphoinositides. During endocytosis, nascent carriers form PI(3,4)P2 (PtdIns(3,4)P2), which is subsequently converted to PtdIns3P in endocytic vesicles.

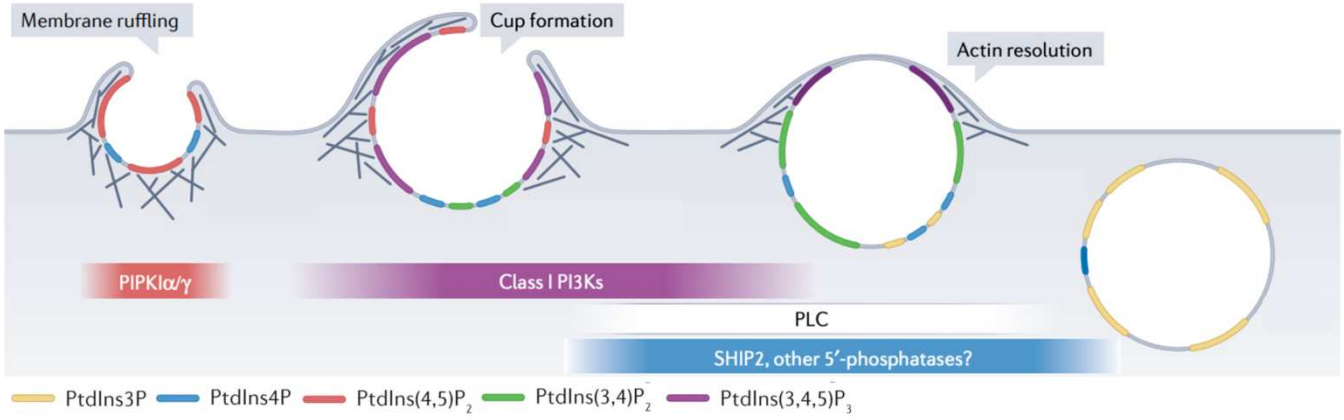


Figure 14. PIs dynamic conversion during macropinocytosis (Adapted from Posor et al., 2022).

Macropinocytosis is driven by membrane remodeling through the formation of branched F-actin. The initial membrane ruffling is mediated by the production of PI(4,5)P2 (PtdIns(4,5)P2) by PIPKIα/γ, which promotes actin polymerization. During cup formation, generation of PI(3,4,5)P3 (PtdIns(3,4,5)P3) by is led by the activity of class I phosphatidylinositol 3-kinases (PI3Ks). The remodeling and resolution of the subcortical actin cytoskeleton require the depletion of PI(4,5)P2 by phospholipase C (PLC) and 5-phosphatases from the base of the cup. These phosphoinositide conversions is facilitated by the recruitment of both PI3P phosphate (PtdIns3P) and PI(4P) (PtdIns4P) and is essential for actin remodeling.

For my thesis work I have been focusing my work on the role of LBPA during *C. burnetii* infections. LBPA is an unconventional phospholipid due to its unique characteristics and distinctive distribution within cells. It exhibits a rare sn-1-glycerophosphate-sn-1'glycerol (sn-1:sn-1') stereo-configuration, which sets it apart from conventional phospholipids (**Figure 15.1**) (H. H. Tan et al., 2012). LBPA is not found in any lower eukaryotes except for a potential presence in *Dictyostelium*, while it is ubiquitously present in mammalian cells and tissues of high eukaryotes (Nolta et al., 1994). Prokaryotes and possibly plants contain a related lipid known as acyl-PG (Holmback et al., 2001; Kito et al., 1975). The study of LBPA have been accelerated in the late 90's with the development of an anti-LBPA antibody (Kobayashi et al., 1998). Then, immunofluorescence and immunogold labeling techniques have revealed that LBPA is exclusively localized in multivesicular regions of late endosomes and is highly abundant in intralumenal membranes, supporting its original association with lysosomes (**Figure 15.2**) (Brankatschk et al., 2011; Kobayashi et al., 2002). LBPA restricted distribution in late endocytic compartments can account for 15-20% of total phospholipids (Bergelson et al., 1974; Somerharju, 1979). This distinct distribution contrasts with phosphoinositides, which are mostly not limited to specific membranes within the endocytic and secretory organelles (Schink et al., 2016).

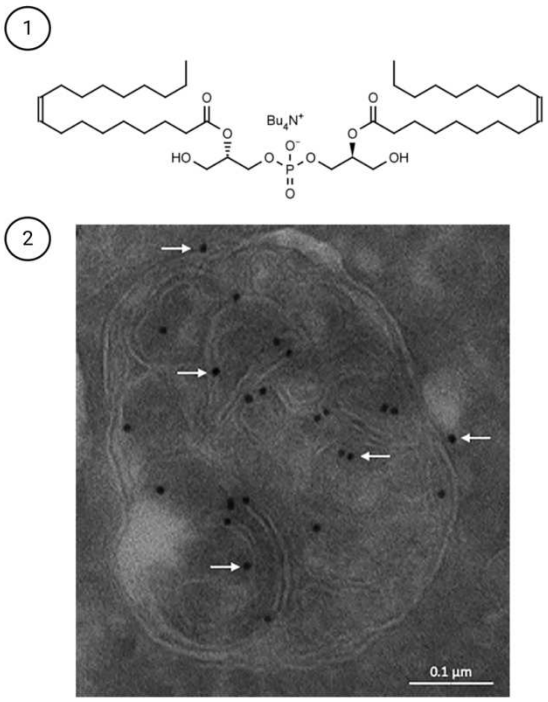


Figure 15. LBPA structure and cellular localization (adapted from Gruenberg, 2020; Echelon-inc.com)

(**1**) Structural representation of (S,S) Bisoleoyl-lysobisphosphatidic acid is the naturally occurring, biologically active isomer of LPBA. (**2**) Immunogold labeling of cryosections provides visualization of LBPA distribution within late endosomes. HeLa cells that have been labeled with the anti-LBPA monoclonal antibody (clone 6C4), detected with 10 nm protein A-gold particles coupled to secondary antibodies. The gold particles, indicated by arrows, highlight the presence of LBPA within the late endosome, revealing its localization in this cellular compartment. (Scale bar : 0.1µm)

The unconventional stereo-configuration and subcellular distribution of LBPA raise questions regarding its metabolism. Unlike other phospholipids synthesized in the early secretory pathway, LBPA is believed to be synthesized within late endocytic compartments from a precursor phospholipid (Gruenberg, 2020). Studies suggest that LBPA may be synthesized from phosphatidyl glycerol (PG) through a complex series of enzymatic reactions, with sn-3-PG potentially converted into sn-1:sn-1'-LBPA (Amidon et al., 1995, 1996). While PG may serve as an LBPA precursor, the precise biosynthetic pathway remains unclear (Hullin-Matsuda et al., 2007). Notably, PG is synthesized and confined to mitochondria, similar to cardiolipin, which is derived from PG (Mayr, 2015; Van Meer & De Kroon, 2011). This raises the

intriguing possibility that mitochondrial PG could become available as an LBPA precursor in late endocytic compartments through mitophagy (Mijaljica et al., 2007). The enzymes responsible for LBPA biosynthesis or conversion from PG are expected to be present in the endosome lumen, potentially contributing to the restricted distribution of LBPA to late endocytic compartments. Newly synthesized LBPA must be asymmetrically inserted into the exoplasmic leaflet of late endosomal membranes, including ILVs and limiting membranes. Additionally, it seems that LBPA binds endocytosed function-blocking anti-LBPA antibodies, indicating an exoplasmic localization (Gruenberg, 2020). It is also suggested that LBPA-rich membranes may also serve as antigens for antibodies associated with the antiphospholipid syndrome (Alessandri et al., 2005).

Translocation of LBPA across the bilayer to the cytoplasmic leaflet is necessary as it interacts with the cytosolic ESCRT-protein ALIX. Although the identity of an LBPA flippase remains unknown, it is speculated that LBPA, like other negatively charged phospholipids, may undergo rapid flipping across the membrane when the charge is neutralized at low pH (Van Meer et al., 2008). The proximity of LBPA headgroups due to self-assembly or clustering may lead to partial protonation of nearby LBPA phosphate groups, facilitating transbilayer redistribution (Gruenberg, 2020). This phenomenon could drive membrane shape changes, as evidenced by the capacity of LBPA to deform the bilayer in a pH-dependent manner (Farge & Devaux, 1992; Matos et al., 2013). It is worth noting that even a very small fraction of redistributed phospholipids (<0.1%) can induce significant shape changes (Farge & Devaux, 1992). Despite its presence in both leaflets of the bilayer and its abundance in ILVs and limiting membranes, LBPA is specifically localized to multivesicular regions within late endosomes. This suggests that LBPA preferentially incorporates into forming ILVs and potentially plays a direct role in ILV biogenesis, preventing its redistribution to other membranes and ensuring lumenal content replenishment (Matsuo et al., 2004).

LBPA is predominantly observed as the dioleoyl isoform in various cell types (50-80% of LBPA), while rat liver and brain exhibit a more complex acyl chain composition, including long polyunsaturated acyl chains (Moreau et al., 2019). The acyl chains are primarily present on positions 2 and 2' of the LBPA glycerol backbone but can migrate to positions 3 and 3' as they are unstable (Chevallier et al., 2000; Kobayashi et al., 2002). The extent of acyl chain remodeling

in vivo and its association with changes in intralumenal membrane organization remain to be fully elucidated. The position and composition of acyl chains likely determine the shape, functions, and endosomal dynamics of LBPA-enriched membranes (Goursot et al., 2010). LBPA's unique structure and organization, particularly its presence in LBPA-rich membrane domains, contribute to its antigenicity (Galve-de Rochemonteix et al., 2000; Kobayashi et al., 1998).

In addition to its distinctive properties, LBPA-enriched membranes play a critical role in regulating the fate of other lipids, particularly sphingolipids and cholesterol, which are functionally interconnected in various cellular processes and implicated in sphingolipid and cholesterol storage disorders (Breiden & Sandhoff, 2019; Liscum, 2000; Simons & Gruenberg, 2000).

2.2.3.2. Host-cell lipids and bacterial infections.

Pathogenic intracellular bacteria have evolved strategies to manipulate human host lipids for various functions related to disease initiation and progression. These functions include bacterial entry into host cells, formation of intracellular compartments, metabolic requirements for bacterial survival and replication which lead to disease progression. However, the specific mechanisms used by intracellular bacterial pathogens to manipulate host lipids can vary, depending on the bacterial species and the pathogenic mechanisms employed. Intracellular bacteria can be categorized into those that persist within vacuolar compartments inside host cells and those that survive and replicate within the host cell cytosol. These distinctions suggest that the utilization of host cell lipids varies among different bacterial species and within vacuolar and cytosolic groups (Allen & Martinez, 2020).

For instance, it is known that PI(4)P is enriched at the phagosome containing the bacterial pathogen *Legionella pneumophila*. There, it plays a crucial role in anchoring specific virulence factors of the bacterium. It may also be involved in signaling processes related to the formation of the Legionella-containing vacuole (LCV), which provides an intracellular environment favorable for the growth and survival of the bacteria. It has been described that *Legionella* secretes an effector called MavQ that can catalyze the formation of PtdIns3P using PtdIns as a substrate. Following the synthesis of PI(3)P, findings indicate that MavQ collaborates

with two other effectors, LepB and SidF, to sequentially synthesize PI(4)P on the surface of the LCV by respectively phosphorylating PI(3)P into PI(3,4)P followed by the removal of 3-phosphate (Li et al., 2021).

On the other hand, as mentioned earlier, it has been described that during cytosolic bacterial invasion, cellular PI(5)P levels increase as a result of the catalytic activity of bacterial effectors such as IpgD from *Shigella flexneri* (Niebuhr et al., 2002) or SigD/SopB from *Salmonella sp* (Mason et al., 2007). This suggests that PI(5)P may have a role in membrane and cytoskeleton events that facilitate pathogen invasion.

An essential lipid needed for both *C. burnetii* internalization and CCV biogenesis is cholesterol. Indeed, a study showed that *C. burnetii* could not be internalized effectively in DHCR24(-/-) cells as they are unable to produce endogenous cholesterol, highlighting its importance (Gilk et al., 2013). Similar effects on CCV biogenesis and intracellular replication are shown when cholesterol metabolism is inhibited (D. Howe & Heinzen, 2006). The CCV membrane is enriched in sterols, notably cholesterol and lipid raft-associated proteins flotillin-1 and 2 are found at its surface, where they form structured microdomains that may attract crucial proteins involved in CCV formation (D. Howe & Heinzen, 2006).

Remarkably, *C. burnetii* has the capacity to increase the cholesterol content within host cells by upregulating genes associated with cholesterol biosynthesis and probably by facilitating the uptake of exogenous cholesterol (Gilk et al., 2013). Intriguingly, *C. burnetii* does not appear to synthesize cholesterol autonomously but rather actively manipulate host cell cholesterol metabolism. In *C. burnetii* genome, there are two eukaryotic-like sterol reductases, namely CBU1158 (a potential Δ7 sterol reductase) and CBU1206 (a potential Δ24 sterol reductase). Nevertheless, only CBU1206 enzymatic activity has been experimentally confirmed, implying that *C. burnetii*, potentially through CBU1206, may affect the final stages of cholesterol biosynthesis in mammalian cells, thanks to its Δ24 sterol reductases that play a role in the concluding reduction step during ergosterol synthesis (Beare et al., 2009; Seshadri et al., 2003).

The presence of cholesterol within CCVs may come from their fusion with multivesicular bodies that are themselves enriched in cholesterol (Gilk et al., 2013). Additionally, *C. burnetii* can hijack both intrinsic and extrinsic cholesterol trafficking pathways, contributing to its enrichment within CCVs. Studies have demonstrated the importance of lipid droplets, which are key cellular components for lipid storage, notably for cholesterol, in *C. burnetii* intracellular growth. This suggests that *C. burnetii* employs diverse mechanisms to recruit cholesterol to CCVs (Mulye et al., 2018).

Conversely, elevated cholesterol levels, have been described to perturbs CCV biogenesis as they are smaller and bacterial growth is affected, this probably due to an abnormal acidification of CCVs. This underscores the essential requirement for tightly regulated cholesterol homeostasis in *C. burnetii* (Mulye et al., 2017).

Studies have identified the oxysterol-binding protein (OSBP)-related protein 1, long (ORP1L) as a key host protein involved in the tight cholesterol regulation at the CCV. Within eukaryotic cells, ORP1L serves as a mediator for the transport of cholesterol from late endosomes and lysosomes to the endoplasmic reticulum. This process occurs at specific membrane contact sites that are established via the interaction between ORP1L and proteins located in the ER membrane (Zhao & Ridgway, 2017).

Similarly, in the context of *C. burnetii* infections, ORP1L have been described to be recruited at the CCV and appeared to be essential to create contact site between the CCV and the ER. Interestingly, ORP1L function during infection seems to be dependent of the T4SS activity (Justis et al., 2017). Considering the role of ORP1L in regulating cholesterol dynamics, it was proposed that *C. burnetii* might manipulate and regulate cholesterol trafficking within CCVs by hijacking ORP1L . This hypothesis was recently verified as it has been observed that the absence of ORP1L led to significantly attenuated expansion of the CCV. CCVs in ORP1-null cells exhibited higher sterol content compared to wild-type cells, supporting the hypothesis that ORP1 promotes cholesterol efflux from the CCV. *C. burnetii* growth in HeLa cells was not affected by the absence of ORP1L, but both CCV expansion and bacterial growth were inhibited in ORP1-deficient murine alveolar macrophage cells (Schuler et al., 2023). These findings demonstrate that ORP1L plays a role in promoting CCV development during *C. burnetii* infection. While ORP1L's effect on *C. burnetii* growth varies in different cell models, it suggests

that compensatory cholesterol transport mechanisms may be sufficient to sustain bacterial growth in the absence of ORP1 in some cell types.

To date, the identity and consequently the mechanisms of *C. burnetii* effectors that hijack and manipulate ORP1L remain however unknown.

Beside cholesterol, phosphoinositides are widely targeted by intravacuolar bacteria. Because of their unique signaling capacity, bacteria use phosphoinositides notably to enable the formation of their replicative compartments.

Similarly, to what has been described with *Legionella*, the modulation of host phosphoinositides is achieved through the secretion of effector proteins that directly bind PIs and/or modify their metabolism. *C. burnetii*, also uses this strategy to hijack PI metabolism. The effector protein CvpB (*Coxiella* vacuolar protein B, also known as Cig2) plays a crucial role in manipulating PI(3)P metabolism to promote the optimal development of the CCV (Beare et al., 2014; Kohler et al., 2016; Martinez et al., 2016).

CvpB localizes to CCVs and early endosomes by interacting with PI(3)P and PS. It has been described to disrupt the recruitment of the PI 5-kinase PIKfyve, thereby preventing the phosphorylation of PI(3)P to PI(3,5)P2. Its mechanism appears to be critical during *C. burnetii* infection. Homotypic fusion of CCVs is promoted by the accumulation of PI(3)P and CvpB stabilize the autophagosomal machinery through its interaction with PI(3)P. Furthermore, CvpB stimulates the expansion and clustering of early endosomes, which results in the formation of spacious PI(3)P-positive compartments that fuse with CCVs increasing the vacuole size. (**Figure 16**) (Martinez et al., 2016).

Mutation in *cvpB* results in a multivacuolar phenotype, which can be rescued by gene complementation, highlighting the central role of CvpB in CCV homotypic fusion (Martinez et al., 2016). The importance of PI metabolism manipulation for CCV biogenesis and virulence has been demonstrated in infection models using *Galleria mellonella* (an insect model) and SCID mice. In these models, *cvpB*::Tn mutants showed less colonization capacity and host survival was increased, which demonstrate the importance of phosphoinositides manipulation for *C. burnetii* pathogenicity (Martinez et al., 2016; van Schaik et al., 2017).

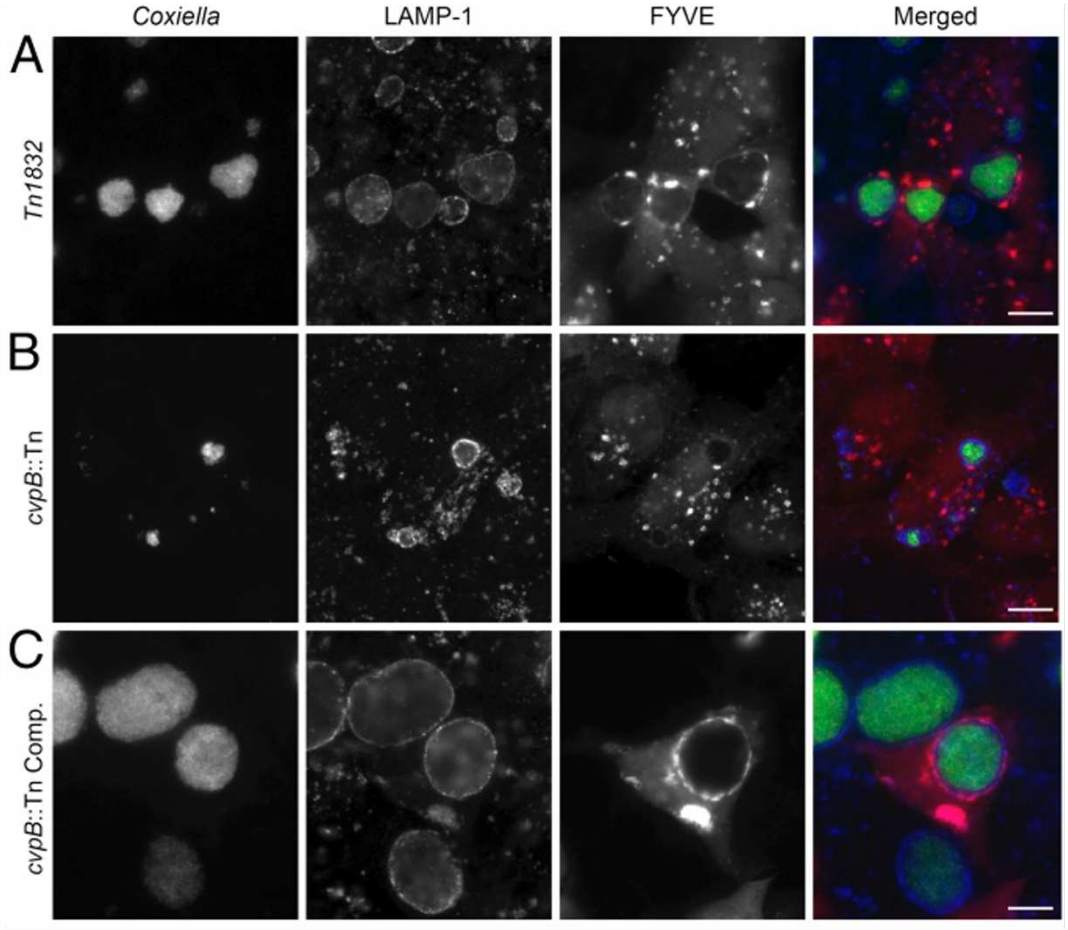


Figure 16: *C. burnetii* effector CvpB is essential for PI(3)P enrichment at the CCV.(*Martinez et.al, 2016*)

U2OS cells stably expressing the PI(3)P probe mCherry-2xFYVE (red) were infected with *wt C. burnetii* (A) the *cvpB*::Tn mutant (B) or the complemented strain (C) for 3 days. Immunofluorescence analysis shows that PI(3)P (red) co-localizes with the lysosomal marker LAMP1 (blue) at the CCVs while *C. burnetii* colonies are shown in green. This co-localization is observed in the *wt* strain and the complemented strain but is significantly reduced in the *cvpB*::Tn mutant, indicating that CvpB is necessary for the recruitment of PI(3)P at the CCV membrane. Scale bars : 10 µm.

Only one *C. burnetii* T4BSS effector has been shown to manipulate PI metabolism for CCV biogenesis. We have highlighted in this thesis study that some other effectors must be implicated in the recruitment and enrichment of other PIs to the CCV.

As mentioned earlier, we have focused this thesis work on LBPA, and more precisely on the role and the subversion of LBPA during *C. burnetii* infections. Indeed, LBPA has already been shown to be subverted during intracellular bacterial infection. For instance, *A. phagocytophilum* exploits MVB related machineries to perform each major stage of its intracellular infection cycle from intravacuolar proliferation and morphotype conversion to infectious progeny release. Just like CCV, the *A. phagocytophilum*-occupied vacuole (ApV) is an acidified organelle that accumulates MVBs markers, ESCRT components ALIX, ILVs, and especially LBPA (Huang et al., 2012; Read et al., 2022a). ApV and MVBs have many similarities, notably their lipid and protein composition, they both escape from lysosomal fusion and they are rerouted to the plasma membrane. In this sense we can correlate the release of ILVs from MVBs and the egress of *A. phagocytophilum* via their fusion with the plasma membrane. (Van Niel et al., 2018). However, it is proposed that LBPA recruitment is not due to a fusion with surrounding MVBs as TEM observations show intact MVBs proximal to but not fusing with ApVs. On the other hand, unlike *A. phagocytophilum, Chlamydia trachomatis* is known to hijack Rab39a to divert LBPA and sphingomyelin from MVBs as well as using other pathways to sequester and recruit many other phospholipids and cholesterol (Elwell & Engel, 2012; Tudela et al., 2015).

Recently, it has been shown that *Brucella*-containing vacuoles are also enriched in LBPA and, similarly to *Anaplasma,* require MVBs to promote egress (Spera et al., 2023).

In this study we have also looked at the recruitment of LBPA concomitant with other MVBs markers during *C. burnetii* infections but unlike *Brucella* and *Anaplasma* we have not observed any link with bacterial egress.

The following cartoon (Figure 17) summarizes all lipid and trafficking manipulation by C. burnetii effectors during infections.

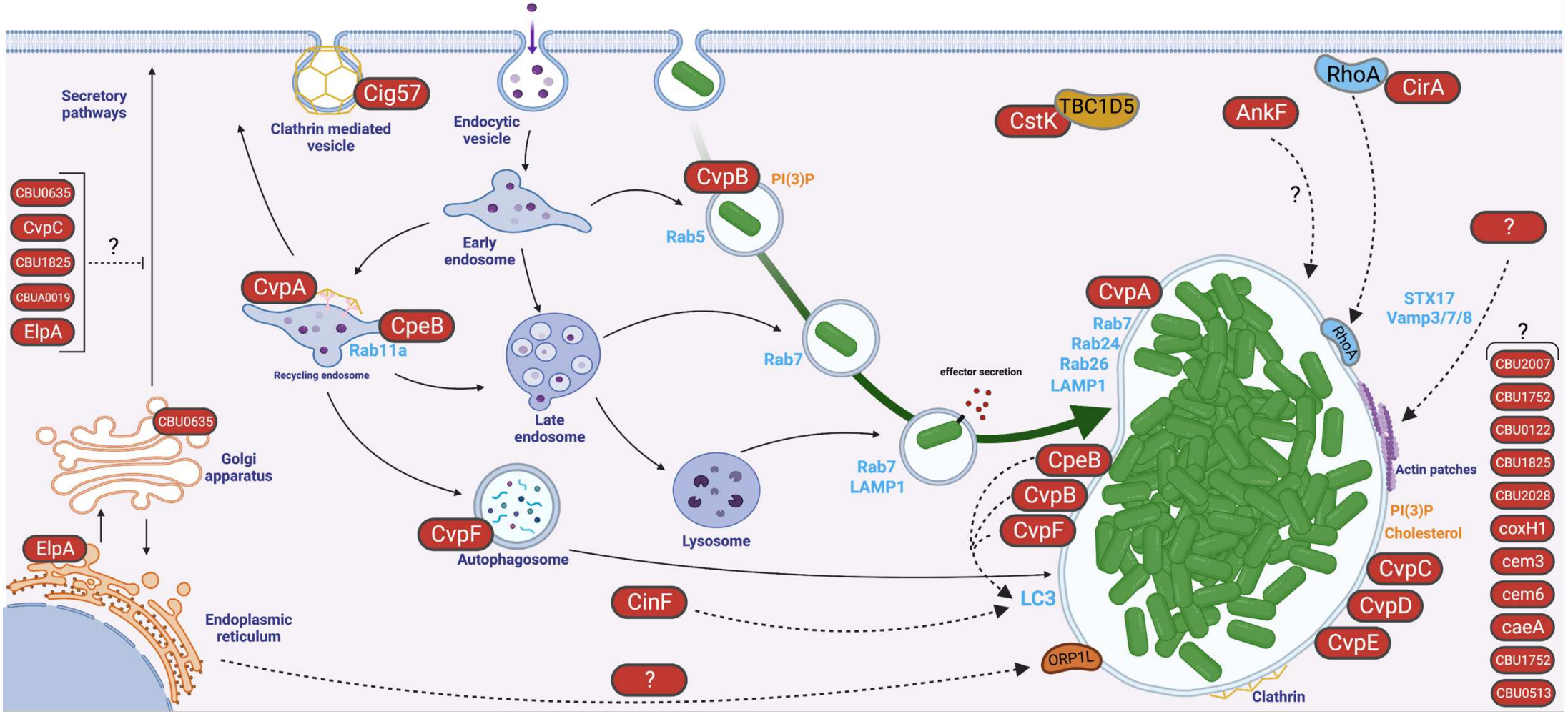


Figure 17. Overview of the modulation of host cell lipids and trafficking pathways by *C. burnetii* effector proteins.

Red pellet represent *C. burnetii* (green) effectors. Doted lines represent modulation of host cell components to the the CCV while full lines represent canonical host cell pathways. "?" associated with effectors means that these proteins have been described to play a role in a pathway essential for the bacteria, but the mechanism is not known yet.

2.3. *C. burnetii* stealth strategies

During my thesis internship, I have authored a review describing the stealth strategies of T4SS-equipped bacteria, including *C. burnetii* (Bienvenu et al., 2021).

C. burnetii modulation of host cell innate immunity pathways by effectors have been summarized in Figure 18.

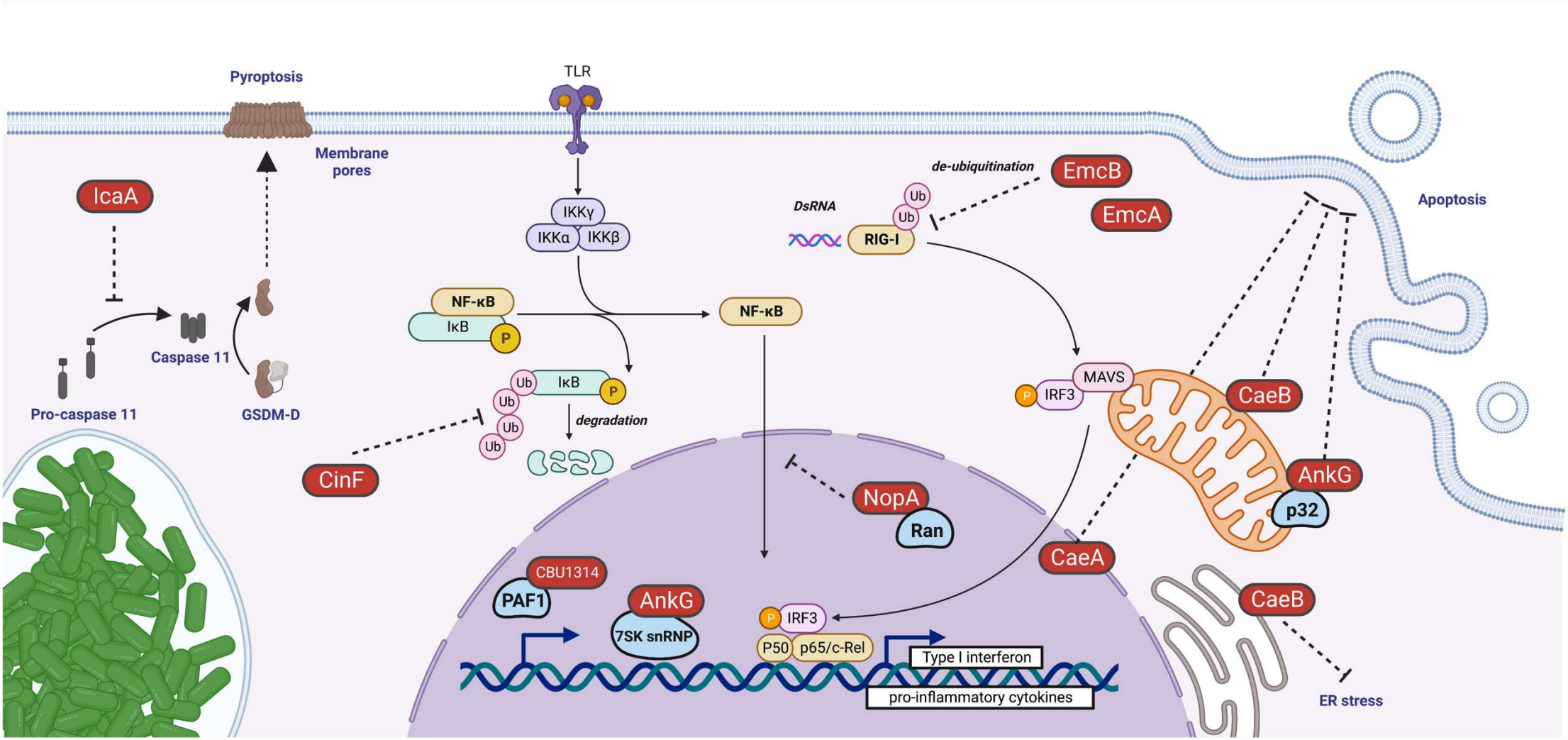


Figure 18. Modulation of host cell innate immunity pathways by *C.burnetii* effectors.
Red pellet represent *C. burnetii* (green) effectors. Doted lines represent modulation of host cell components to the the CCV while full lines represent canonical host cell pathways.

toxins

MDPI

Review

Undercover Agents of Infection: The Stealth Strategies of T4SS-Equipped Bacterial Pathogens

Arthur Bienvenu, Eric Martinez * and Matteo Bonazzi *

Institut de Recherche en Infectiologie de Montpellier (IRIM), Université de Montpellier, CNRS, CEDEX 5, 34293 Montpellier, France; arthur.bienvenu@irim.cnrs.fr

* Correspondence: eric.martinez@irim.cnrs.fr (E.M.); matteo.bonazzi@irim.cnrs.fr (M.B.)

Abstract: Intracellular bacterial pathogens establish their replicative niches within membrane-encompassed compartments, called vacuoles. A subset of these bacteria uses a nanochannel called the type 4 secretion system (T4SS) to inject effector proteins that subvert the host cell machinery and drive the biogenesis of these compartments. These bacteria have also developed sophisticated ways of altering the innate immune sensing and response of their host cells, which allow them to cause long-lasting infections and chronic diseases. This review covers the mechanisms employed by intravacuolar pathogens to escape innate immune sensing and how Type 4-secreted bacterial effectors manipulate host cell mechanisms to allow the persistence of bacteria.

Keywords: stealth bacterial pathogens; type 4 secretion system; innate immunity; inflammation; host-pathogen interactions

Key Contribution: Bacterial pathogens have developed elaborated means to escape the immune response of their host and establish their replicative niche. Some bacteria use a type 4 secretion system to translocate effector proteins in the host cell cytoplasm. These effectors can then modulate and attenuate different pathways, such as inflammation, apoptosis or autophagy, to favor bacterial persistence.

check for updates

Citation: Bienvenu, A.; Martinez, E.; Bonazzi, M. Undercover Agents of Infection: The Stealth Strategies of T4SS-Equipped Bacterial Pathogens. *Toxins* **2021**, *13*, 713. https://doi.org/10.3390/toxins13100713

Received: 29 July 2021
Accepted: 6 October 2021
Published: 9 October 2021

Publisher's Note: MDPI stays neutral with regard to jurisdictional claims in published maps and institutional affiliations.

Copyright: © 2021 by the authors. Licensee MDPI, Basel, Switzerland. This article is an open access article distributed under the terms and conditions of the Creative Commons Attribution (CC BY) license (https://creativecommons.org/licenses/by/4.0/).

1. Introduction

Gram-negative bacteria use complex nanomachines, called secretion systems, to translocate effector proteins, molecules and DNA in order to modulate the microbial response to the environment. Nine secretion systems have been identified to date: five span the inner and outer bacterial membrane, while the remaining four are embedded in the outer membrane [1]. Initially described in the context of bacterial conjugation and horizontal gene transfer, type 4 secretion systems (T4SS) are large protein complexes that span through the inner and outer membranes of several Gram-negative and Gram-positive bacteria [2]. These highly versatile nanomachines are characterised by an internal channel that mediates the translocation of proteins, toxins and genetic material. Cytoplasmic ATPases typically energise translocation. Depending on their function, T4SS can be divided into three functional groups [3]. T4SSs belonging to the first group mediate the conjugative transfer of DNA and transposon among bacteria, or from bacteria to plants, fungi and mammalian cells. Notably, DNA exchange has been associated with genome plasticity, the acquisition of eukaryotic domains and the acquisition of antibiotic resistance traits [3]. T4SSs belonging to the second group mediate the release and uptake of DNA directly from the extracellular milieu. Finally, the third group of T4SS mediates the translocation of proteins. These are primarily found in pathogenic bacteria and are essential virulence factors that coordinate host/pathogen interactions. Interestingly, T4SSs are not exclusive, and some bacteria, including *Helicobacter pylori*, encode both a DNA exchange system and a protein delivery system [4]. Genes encoding T4SSs are usually arranged in operons or clusters of operons [2]. The type 4a secretion system (T4SSa, also known as VirB/D4

secretion system) was initially discovered in the plant pathogen *Agrobacterium tumefaciens* and is usually composed of 12 genes [5]. Bacterial pathogens, including *Orientia tsutsugamushi*, *Brucella* spp., *Bartonella* spp., *Anaplasma* spp. and *Ehrlichia* spp., possess a T4SSa [6]. *Bartonella* species, except *B. bacilliformis*, can also express additional T4SSs, such as the Vbh/TraG and Trw secretion systems, that play a role in bacterial conjugation and erythrocyte invasion, respectively [7]. The T4SSb (also known as the Dot/Icm secretion system) is composed of 23 to 25 genes, and it is only found in *Legionella* and *Coxiella* species [8].

Notably, many bacterial pathogens equipped with a type 4 secretion system (T4SS) have evolved to colonise host cells from the safe haven of replicative vacuoles. These membrane-bound compartments derive from the initial internalisation vacuole that hosts the pathogen and are de facto intracellular compartments of eukaryotic composition, which only exist in the context of infection. Life in a membrane-enclosed compartment presents several advantages, including access to nutrients and escape from cytosolic immune surveillance. On the other hand, without bacterial intervention, internalisation vacuoles fuse with lysosomes, which in most cases is fatal for the pathogen itself. Thus, these pathogens rely on their T4SS to translocate effector proteins through the membrane of the replicative vacuole, directly into the host cytoplasm, where they subvert membrane trafficking to deviate their replicative niche off the tracks of the endocytic pathway [9]. Each replicative niche is remarkably specific to its pathogen and is characterised by a unique protein and lipid signature and morphology. Furthermore, the "fate" of these compartments may differ depending on the pathogen's lifestyle: some remain intact and host non-replicative bacteria for an extended time, whereas others rupture to release bacteria and facilitate the infection of bystander cells. Importantly, infected cells are not entirely blind to these pathogens, which are readily recognised by cell surface and endosomal Toll-like receptors (TLRs) that transduce signals leading to the activation of the antimicrobial response [10]. Later, during the intracellular cycle, cytosolic receptors sense pathogen-derived ligands, which may include the effector proteins themselves [11]. Furthermore, infected cells can destabilise the membrane of the bacterial replicative niche, thereby exposing microbes to immune surveillance [12]. Finally, innate immunity can also be alerted by recognition of the hybrid membranes of replicative vacuoles as foreign bodies [13]. Thus, several T4SS pathogens have evolved stealth strategies to remain undetected within infected cells and avoid triggering inflammation.

This review illustrates the diverse strategies developed by stealth pathogens equipped with a T4SS to elude innate immune recognition and/or silence the multiple signalling pathways coordinating the inflammatory response.

2. Escape from Host Sensing

In immune cells, the surveillance and detection of invading bacterial pathogens are ensured by pattern-recognition receptors (PRR), such as surface and endosomal TLRs and cytosolic Nucleotide oligomerization domain (NOD)-like receptors (NLRs) [14]. The NLR family of proteins comprises 22 members, who are critical in triggering and modulating the inflammatory response of immune cells. TLRs are transmembrane proteins that localise either at the cell surface or at the membranes of intracellular compartments, such as the endoplasmic reticulum (ER), endosomes, lysosomes, or endolysosomes. The human genome encodes 10 proteins of the TLR family. They recognise distinct or overlapping pathogens associated molecular patterns (PAMPs), such as lipids, lipoproteins, proteins, and nucleic acid [15]. Each TLR comprises an ectodomain with leucine-rich repeats (LRRs) that mediate PAMPs recognition, a transmembrane domain, and a cytoplasmic Toll/Interleukin-1 (IL-1) receptor (TIR) domain that initiates downstream signalling. Some stealth bacteria adapted their microbe-associated molecular patterns (MAMPs) to escape recognition by cell sensors. For example, the *Bartonella* lipid A is poorly recognised by TLR4 as its structure is characterised by a short glycosyl backbone (di-aminoglucose), a pentaacylation, and a very long fatty acid side chain [16]. This lipid A impedes a broad inflammatory response [17].

Furthermore, *B. quintana* Lipopolysaccharide (LPS) is a potent antagonist of TLR4 signalling (Figure 1) [18,19].

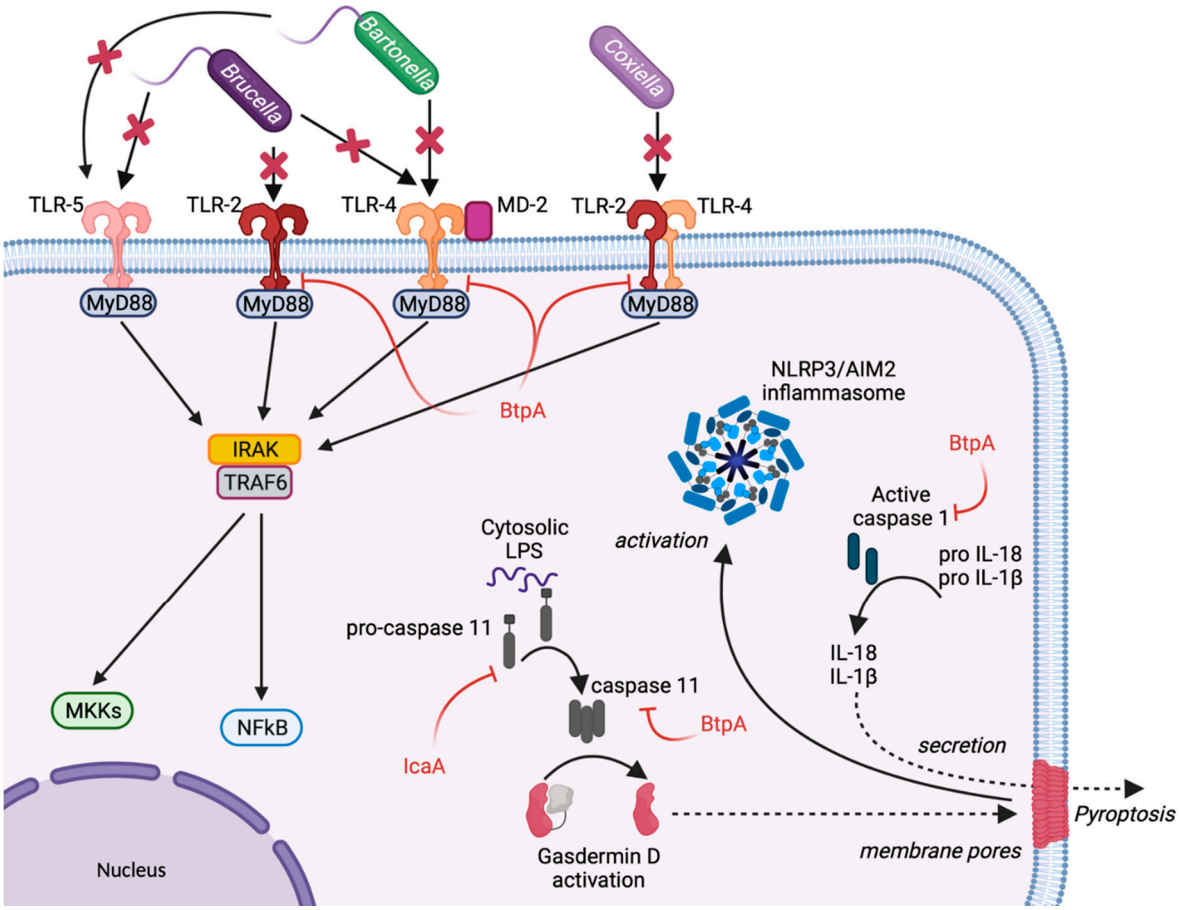


Figure 1. Pathogen evasion of host cell sensing. Pathogen recognition is essential to initiate an inflammatory response. Due to their specific LPS structure, *Brucella* spp., *Bartonella* spp. and *C. burnetii* are poorly recognised by TLRs. Furthermore, *Brucella melitensis* and *Bartonella bacilliformis* flagellin are weak activators of TLR5. By competing with the interaction of TLRs with MyD88, the *Brucella* effector protein BtpA is the only bacterial protein currently known to directly inhibit the TLR signalling pathway. BtpA also induces caspases 1, 4 and 11 degradation, impairing interleukin secretion. The *C. burnetii* effector protein IcaA actively modulates the inflammatory response by inhibiting the activation of caspase 11.

Brucella LPS exhibits low toxicity, and its atypical structure was postulated to delay the host immune response, favouring the establishment of chronic disease [20]. *Brucella* Lipid A is a 2,3-diaminoglucose disaccharide substituted with C16, C18, C28 and other very long acyl chains [21]. This peculiar structure is a poor agonist of TLR4/myeloid differentiation-2 (MD-2), and a paradigm has emerged proposing *Brucella* LPS as a crucial virulence factor that hampers recognition by PRRs and plays essential roles during infection (Figure 1) [16]. One study showed that *Brucella* LPS does not induce inflammatory responses in macrophages and dendritic cells (DCs), two of the most important immune system sentinels. This was attributed to its poor recognition by TLR4/MD-2, which is widely considered the major receptor complex for LPS binding and signalling [22].

As previously mentioned, the activation of TLR4 and TLR2 is dependent on strong affinity and direct interaction with bacterial LPS. In macrophages challenged with avirulent *Coxiella burnetii* LPS, TLR-4 and TLR-2 co-immunoprecipitate, indicating that the avirulent strain can be recognised by these receptors. However, this association was absent in cells challenged by the LPS of virulent *C. burnetii* (Figure 1). The disruption makes TLRs unable to signal during the recognition of the LPS of pathogenic *C. burnetii* [23]. The re-organization of the macrophage cytoskeleton induced the disruption of TLR-2 and TLR-4

by *C. burnetii* LPS. Interestingly, blocking the actin cytoskeleton re-organization relieved the disruption of the association TLR-2/TLR-4 by pathogenic *C. burnetii* and rescued the p38α-mitogen-activated protein kinase (MAPK) activation by *C. burnetii* [23].

Bacterial flagellin is another major MAMP that can be sensed by TLR5 and NLR family CARD domain containing 4 (NLRC4), leading to a robust pro-inflammatory response. While flagellin from *Brucella melitensis* is weakly detected by TLR5 and might play an essential role in immune escape [24], *Bartonella bacilliformis* synthesises flagellin molecules that escape TLR5 recognition entirely (Figure 1). This is due to the presence of aspartic acid and serine amino acids in the 89–96 region of *N*-terminal D1 domain of flagellin, which is usually recognised by TLR5. These changes in amino acids prevent TLR sensing while preserving bacterial motility [25].

Besides eluding TLR recognition, *Brucella* uses additional evasion strategies by suppressing innate immune signalling. The *B. abortus* Btp1 effector protein and its *B. melitensis* homolog TcpB (now both referred to as BtpA) encode a TIR domain that competes with myeloid differentiation response gene 88 (MyD88) for binding with TIR domain-containing adaptor protein (TIRAP, Figure 1), which ultimately facilitates the ubiquitination and degradation of MyD88 adaptor-like (Mal) and inhibits both TLR4 and TLR2 signalling [26,27]. TcpB seems to be important in the bacterial immune escape, as the *B. melitensis tcpB* mutant displays a markedly retarded systemic spread in a mouse model of infection. The weakened phenotype of *tcpB* mutants for immune-competent mice suggests that *Brucella* can evade innate immunity by using multiple strategies [28]. Finally, the *Brucella* effector BtpB inhibits TLR signalling and contributes to the control of dendritic cell activation [29]. Recently, BtpA and BtpB have been shown to modulate energy metabolism through NAD+ hydrolysis, which could in part explain the down-modulation of innate immune signalling in *Brucella*-infected cells [30].

3. Inhibition of Inflammasome

Upon detection of PAMPs, several NLRs (such as NLR family Pyrin Domain containing 1 (NLRP1), NLR family Pyrin Domain containing 3 (NRLP3) or Pyrin) oligomerise with the apoptosis-associated speck-like protein containing a CARD (ASC) to activate inflammatory Caspase-1 [11]. The major Caspase-1 substrates are Gasdermin-D (GSDMD), pro-IL-1β, and pro-IL-18. Cleaved GSDMD targets and permeabilizes the plasma membrane, thus triggering ion imbalance and necrotic cell death, which is termed "pyroptosis" [31]. During this process, cleaved IL-1β and IL-18 are also secreted and stimulate inflammatory responses in neighbouring cells. Cytosolic LPS can be sensed directly by Caspase-11 (in mouse cells) and Caspase-4 and -5 (in human cells), which leads to GSDMD cleavage and pyroptosis [32]. These caspases belong to the non-canonical inflammasome pathway as they cannot directly process the inflammatory cytokines IL-1β and IL-18 [33].

Brucella effector BtpA interacts with Caspase-4 and induces the ubiquitination of inflammatory caspases-1, 4, and 11, leading to their degradation [34]. BtpA expression leads to a reduction of IL-1β secretion, induced by the non-canonical inflammasome in *Brucella*-infected macrophages (Figure 1). BtpA also attenuates pyroptosis and proinflammatory cytokine secretion in macrophages infected with *Salmonella enterica* [34].

C. burnetii does not stimulate inflammasome activation in primary mouse macrophages, as Caspase-1 is not activated during infection [35]. The secretion of the effector protein IcaA inhibits the non-canonical caspase-11-mediated activation of the NLRP3 inflammasome (Figure 1). However, the molecular targets of this effector protein remain unknown [35]. Other *C. burnetii* mechanisms may be involved in the inhibition of inflammation as several *Coxiella* transposon mutants displayed a cytotoxic phenotype during infection [36].

4. Inhibition of Transcription and Translation

The recognition of danger-associated molecular patterns (DAMPs) by infected cells triggers an important transcriptional reprogramming, which is essential to mount a specific proinflammatory response. The three primary inflammation signal-transducing pathways

are the signal transducers and activators of transcription (STATs), the interferon regulatory factors (IRFs), and the nuclear factor κB (NFκB) [37]. To counter this, stealth pathogens effectively subvert the host transcriptional response, either by epigenetic silencing or by perturbing the nuclear accumulation of the main transcriptional regulators.

Controlling DNA methylation and histones after -translational modifications are efficient strategies to control the transcriptional landscape of infected cells. Thus, over the past decade, epigenetic silencing of host defences has emerged as a common strategy of several bacterial pathogens. DNA methylation interferes with the recruitment of transcription factors and leads to transcriptional repression [38]. Global changes in the methylation state of intergenic DNA regions have been described in cells infected by *Helicobacter pylori* [39] or *Anaplasma phagocytophilum* [40] (Figure 2). In the latter case, this is required for optimal intracellular replication. However, whether DNA methylation is actively triggered by bacterial effectors or reflects the cellular response to infection remains to be defined.

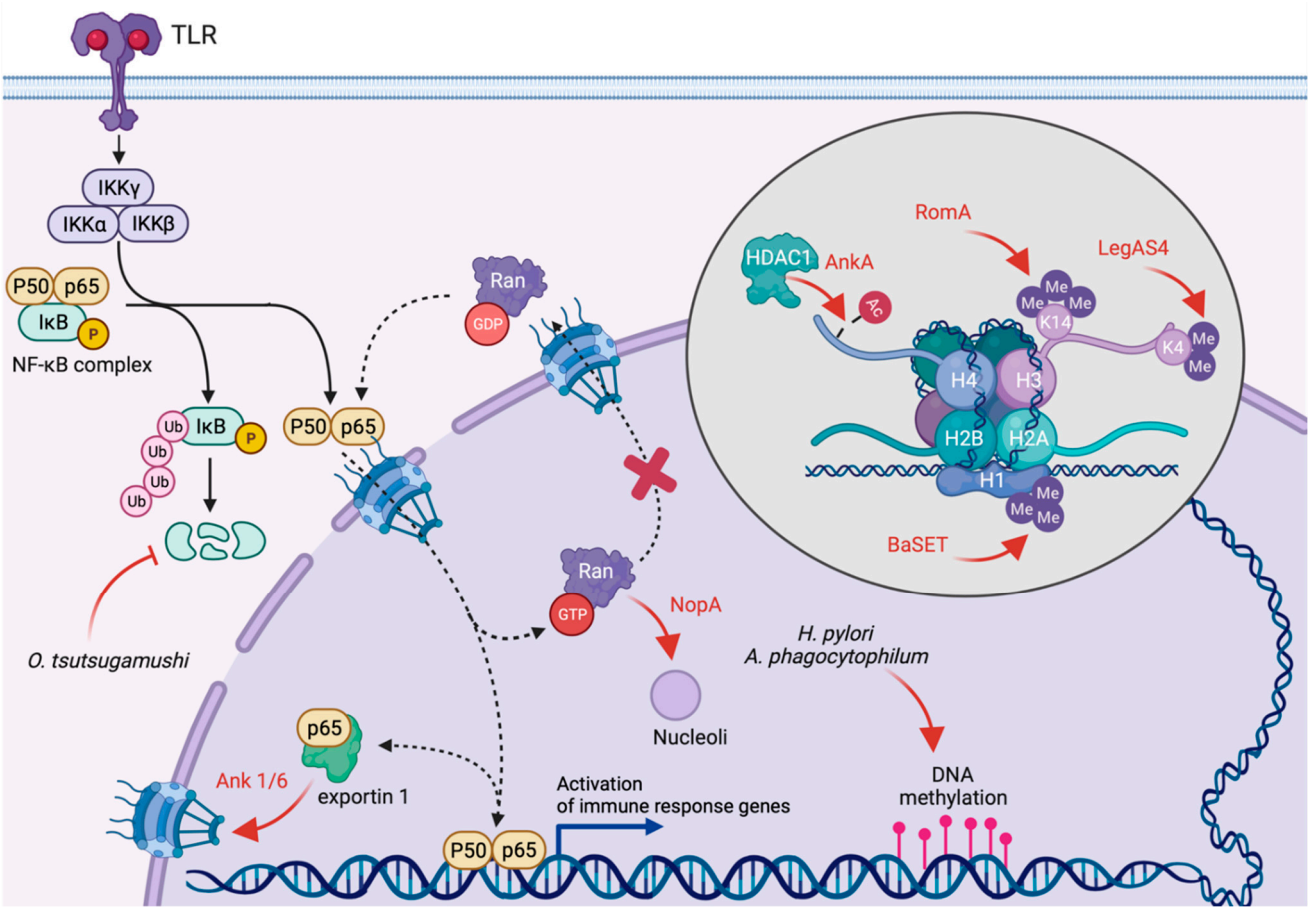


Figure 2. Modulation of the host transcriptional landscape by bacterial pathogens. T4SS-equipped bacterial pathogens manipulate the host transcriptional response to infection by subverting the NF-kB signalling pathway or remodelling the host epigenome. Unidentified *O. tsutsugamushi* effector proteins stabilise IkB, thereby preventing NF-kB translocation to the nucleus. Furthermore, this microbe also translocates the ankyrin repeat effector proteins Ank1 and Ank6, promoting the nuclear export of p65. On the contrary, the *C. burnetii* effector protein NopA sequesters Ran at nucleoli, thereby perturbing nucleocytoplasmic traffic preventing the nuclear import of p65 and IRF3 transcription factors. Infections by *H. pylori* and *A. phagocytophilum* trigger an increase in DNA methylation, silencing transcription, whereas other bacteria specifically target histones after translational modifications. The *L. pneumophila* effector RomA/LegAS4 targets histone H3 methylation. RomA promotes trimethylation at lysine 14, whereas LegAS4 promotes the dimethylation of lysine 4. The *B. anthracis* effector BaSET promotes trimethylation of histone H1, whereas the *A. phagocytophilum* effector AnkA subverts HDAC1 function, promoting histone de-acetylation.

Histone modifications include acetylation, methylation and phosphorylation. Collectively, they regulate the accessibility of DNA to transcription factors, thus regulating gene expression [41]. Enzymatically active bacterial effectors can modulate epigenetic histone marks directly. Examples include an emerging class of bacterial effectors encoding a eukaryotic-like suppression of variegation, enhancer of zeste and trithorax (SET) domain with methyltransferase activity. *Legionella pneumophila* translocates the effector protein RomA/LegAS4 [42,43], which localises to the nucleus of cells infected with the Paris strain, an endemic *Legionella* strain predominant in France [44], but displays a marked nucleolar localisation when cells are infected with *L. pneumophila* Lp02, a virulent thymine auxotroph derived from the serogroup 1 Philadelphia-1 strain [45]. Interestingly, despite their high homology, RomA catalyses the tri-methylation of histone H3 at lysine 14 (Figure 2), which results in the repression of host innate immune genes, such as Tumor Necrosis Factor (TNF), IL-6, TLR5 and NLRP3 [42]. On the contrary, LegAS4 catalyses a di-methylation of histone H3 at lysine 4, leading to increased transcription of rDNA genes [43] (Figure 2). Similar to RomA, the *Bacillus anthracis* protein BaSET encodes a SET domain and localises to the nucleus of infected cells and specifically tri-methylates histone H1 [46] (Figure 2). The ectopic expression of BaSET represses the activity of NF-kB response elements, including the pro-inflammatory cytokines IL-6 and IL-8 [46]. Furthermore, BaSET is important for virulence as assessed using a murine bacteremia model [46]. However, whether BaSET is a T4SS substrate remains to be defined. Of note, SET domain proteins have been identified in other bacterial pathogens, including *Chlamydia* spp. [47] and *Burkholderia thailandensis* [43], which encode type 3 and type 6 secretion systems, respectively.

Other bacterial effector proteins indirectly manipulate histone marks. Among T4SS-equipped pathogens, the best example is the *A. phagocytophilum* effector protein AnkA, which translocates into the nucleus of infected cells and directly interacts with the histone deacetylase HDAC1 [48] (Figure 2). The removal of acetyl groups from histones mediated by HDACs favours a closed conformation of chromatin, thereby terminating transcription. Importantly, AnkA also binds host DNA at ATC-rich intergenic regions upstream of genes involved in the antimicrobial immune response [49], targeting HDAC1 activity towards the specific silencing of host defence genes [50]. Interestingly, *A. phagocytophilum* infections also increase the expression of HDAC through an unknown mechanism [50].

The mammalian NF-κB complex consists of five proteins that function by forming homo- or heterodimers. Among these, the transcription factor p65 is retained in the cytosol by the interaction with members of the NF-κB inhibitor (IκB) family, which hides its nuclear localisation signal (NLS). Exposure to PAMPs or TNFα activates a signalling cascade that leads to the phosphorylation and proteasomal degradation of IκB proteins. This exposes the NLS on p65, which translocates into the nucleus and coordinates the expression of antimicrobial and pro-inflammatory genes, such as Interleukin-1α (IL-1α), Interleukin-1β (IL-1β), Interleukin-6 (IL-6), etc (Figure 2). Several bacterial pathogens interfere directly with this signalling cascade at different levels, thereby activating or inhibiting the NF-κB pathway [51].

Emerging evidence indicates that T4SS-equipped microbes translocate effector proteins that manipulate the NF-κB pathway indirectly, by subverting the host nucleocytoplasmic transport. The *Orientia tsutsugamushi* ankyrin repeat-containing effectors Ank1 and Ank6 are transported to the nucleus of infected cells in an importin β1-dependent manner [52]. There, they interact with and rely on the function of exportin 1 to promote p65 nuclear export [52] (Figure 2). The cytoplasmic accumulation of p65 should be sufficient to reduce NF-κB-dependent transcriptional activation. Interestingly, however, preventing nuclear export in *O. tsutsugamushi*-infected cells does not restore NF-κB-dependent transcription [52], suggesting the existence of redundant strategies to dampen the innate immune response to *Orientia* infections. Indeed, it has recently been reported that *O. tsutsugamushi* also stabilises the intracellular levels of the IκB family member p105, thereby fostering p65 cytoplasmic retention (Figure 2). While the molecular mechanisms regulating this phenomenon remain to be defined, p105 stabilisation depends on the bacterial load and protein

synthesis, suggesting the implication of effector proteins [53]. Similar to *Orientia*, *C. burnetii* also perturbs nucleocytoplasmic traffic to dampen the NF-κB-dependent transcriptional response to infection. The effector protein NopA (for nucleolar protein A) localises at the nucleoli of infected cells, interacts with the eukaryotic small GTPase Ran, and sequesters it within the nucleus [54] (Figure 2). As nucleocytoplasmic transport depends on a protein concentration gradient of Ran between the cytoplasm and the nucleus [55], NopA activity effectively perturbs the nuclear import of proteins, including the transcription factors p65 and interferon regulatory transcription factor 3 (IRF3) (Figure 2). Consequently, cytokines expression is strongly attenuated in cells infected by wild-type *Coxiella*, whereas this effect is completely lost in cells infected either with *nopA* or T4SS-defective *dotA* mutants [54]. Notably, despite their subcellular localisation, neither Ank1, Ank6, nor NopA encode canonical nuclear localisation signals (NLS), suggesting that bacterial effector proteins have evolved alternative strategies to target subcellular compartments.

Parallel to the NF-κB pathway, and besides its role in cell development and differentiation, the Janus Kinase (JAK)-Signal Transducer and Activator of Transcription (STAT) signalling pathway is central to the host cell's response to viral and bacterial infections. Signal transducer and activator of transcription 3 (STAT3) is a key regulator of the switch between pro- and anti-inflammatory signalling in cells [56]. In its inactive form, STAT3 is found as a monomer in the cytoplasm. Cellular stressors, including cytokines, activate surface receptors and transduce the signal to cytoplasmic Janus kinases (JAKs), which phosphorylate STAT3, triggering its dimerisation and nuclear translocation. Notably, STAT3 can also be phosphorylated by non-receptor tyrosine kinases, including MAP kinases, Src and c-Abl. The *Bartonella henselae* effector protein BepD possesses several EPIYA-related motifs that can be phosphorylated by host Src-family tyrosine kinases. Importantly, this leads to the recruitment of STAT3 and facilitates its activation by c-Abl-dependent phosphorylation, thereby bypassing the canonical JAK pathway. BepD-mediated activation of the STAT3 pathway leads to impairment of pro-inflammatory TNFα secretion and stimulation of the anti-inflammatory cytokine Interleukine-10 (IL-10) [57].

5. Modulation of the Unfolded Protein Response

The unfolded protein response (UPR) also plays a relevant role in the interplay between pathogens and inflammation. UPR is triggered by stress conditions at the level of the ER in response to the accumulation of unfolded or misfolded proteins in the ER lumen due to an increase of protein secretion or a direct disruption of ER protein folding [58]. UPR includes multiple signal transduction pathways that regulate gene transcription, protein modifications, and mRNA translation to restore cellular homeostasis. Rapid modifications of the transcriptional profile of cells exposed to pathogens can trigger UPR. Three main pathways have been identified and depend on three ER transmembrane protein sensors: inositol-requiring enzyme-1α (IRE1α), protein kinase RNA-like endoplasmic reticulum kinase (PERK), and activating transcription factor 6α (ATF6α) [59]. The failure of the UPR to restore cellular homeostasis results in apoptosis. Notably, some intravacuolar pathogens, including *Brucella* spp. and *L. pneumophila*, escape the endocytic maturation pathway by favouring interactions between the membranes of their replicative niches with those of the ER, which can be sensed as an ER stress. UPR induction may be triggered explicitly by effector proteins and may be required for intracellular replication, as shown for the *Brucella* effector proteins VceC and TcpB [60,61]. During *L. pneumophila* infections, the IRE1α pathway is activated by TLRs upon extracellular pathogen sensing. However, *L. pneumophila* silences the downstream UPR pathways by two different mechanisms involving the effector proteins Lgt1 and Lgt2, which inhibit the splicing of XBP1u to XBP1s, thereby blocking the IRE1 pathway and unidentified effector proteins that inhibit the translation of ATF6-upregulated genes, leading to an inhibition of the cell response [62,63]. Interestingly, infections by *C. burnetii* also activate the UPR, as indicated by an increase in the intracellular levels of CCAAT/enhancer binding proteins (C/EBPs) homologous protein (CHOP). As for *Brucella* infections, UPR activation is required for optimal *Coxiella*-containing vacuole (CCV)

expansion. However, unidentified *C. burnetii* effectors actively prevent CHOP nuclear translocation and downstream apoptosis [64]. Furthermore, the intracellular localisation of the *C. burnetii* effector CaeB has been recently re-assessed, and it has been shown that the effector localises at the ER upon ectopic expression. CaeB specifically modulates IRE1 signalling in cells exposed to tunicamycin, which ultimately leads to the inhibition of apoptosis [65]. This is in line with previous observations on the anti-apoptotic properties of CaeB in cells exposed to staurosporine, which is mediated by an inhibition of mitochondrial outer membrane permeabilisation (MOMP) [66]. Finally, another aspect of the UPR pathway is the stress response leading to the ER-associated degradation (ERAD) of misfolded proteins. Ank4, an effector protein of *O. tsutsugamushi*, has been shown to interact with HLA-B-associated transcript 3 (Bat3) to impair ERAD mechanism during the early stages of infection. Bat3 is an essential protein of ERAD that acts as a chaperone to mediate the translocation of misfolded proteins to the cytosol, where they can be ubiquitinated prior to degradation by the proteasome [67]. *O. tsutsugamushi* temporarily blocks ERAD until ERAD-derived amino acids are needed to support its growth [68].

6. Subversion of Autophagy

Macroautophagy (hereafter referred to as autophagy) is a eukaryotic process for the engulfment and degradation of cytosolic material, including misfolded proteins, damaged organelles and macromolecules [69]. While basal autophagy is crucial to maintain cellular homeostasis by providing energy substrates to the cell, it plays an important role in the innate immune response against intracellular pathogens. Intravacuolar pathogens developed strategies to either avoid degradation by the autophagic machinery or divert autophagy elements to generate their replicative niche. *L. pneumophila* uses effector proteins to inhibit autophagy and avoid destruction in lytic autolysosomes. The bacterium secretes the cysteine protease RavZ that specifically and irreversibly cleaves the autophagy adapter protein LC3B from autophagosomes, allowing the *Legionella*-containing vacuoles (LCVs) to escape degradation by the autophagy machinery (Figure 3) [70]. Interestingly, LCVs generated by Δ*ravZ* mutants still lack the autophagy marker LC3B, strongly suggesting that the bacterium secretes additional effectors capable of diverting the autophagy machinery away from the *Legionella* replicative niche. *L. pneumophila* also secretes Lpg1137, a serine protease that triggers the degradation of Syntaxin 17 (Stx17), a SNARE involved in vesicle trafficking and autophagy [71]. Additionally, some *Legionella* strains exert additional control over the autophagy machinery via host sphingosine-1-phosphate lipid levels (Figure 3). This lipid mediates the balance between sphingolipid-induced autophagy and cell death. *L. pneumophila* secretes the effector LpSPL (Sphingosine-1 phosphate lyase) to downregulate host sphingolipid levels, which causes a delay in the autophagic response to *L. pneumophila* infections [72]. *A. phagocytophilum* and *Ehrlichia chaffeensis* hijack the autophagosome initiation machinery to develop inside vacuoles with autophagosomal properties. *A. phagocytophilum* secretes the effector protein Ats-1, which interacts with Beclin-1 and ATG14L to induce autophagosome formation [73]. *E. chaffeensis* secrete Etf-1, which stimulates autophagy by activating class III phosphatidylinositol 3-kinase and Rab5 [74], and Etf-2, which binds to active Rab5 and delays endosomal maturation (Figure 3) [75]. For these two intracellular bacteria, the diversion of autophagy seems devoted to the acquisition of nutrients and membranes, as their respective vacuoles do not fuse with lysosomes and avoid being acidified. *C. burnetii* appears unique in the group of intravacuolar pathogens as the biogenesis of its vacuole relies on the autophagy machinery and fusion with lysosomes [76,77]. *C. burnetii* secretes several effector proteins to manipulate autophagy and promote CCV biogenesis and expansion. *Coxiella* vacuolar protein B (CvpB) localises to CCVs, where it stabilises the host lipid phosphatidylinositol 3-phosphate (PI(3)P) to stimulate autophagy and the homotypic fusion of CCVs [78–80]. Recently, effector protein CvpF was shown to stimulate Rab26-dependent autophagy to expand *Coxiella*-containing vacuoles [81]. Finally, the effector protein Cig57 interacts with the clathrin accessory protein FCHO2 [82] and stimulates the clathrin-dependent recruitment of autophagy markers to CCVs (Figure 3) [83]. In the

case of *Brucella*, the autophagy initiation machinery intervenes at the end of the bacterial cell cycle to facilitate egress of the bacterium [84]. Interestingly, the autophagy adapter LC3B is upregulated during *Brucella* infections of human peripheral blood mononuclear cells (PBMCs). *Brucella*-induced autophagy leads to a defect in monocyte polarisation, as these cells fail to differentiate into M1 (pro-inflammatory) or M2 (anti-inflammatory) macrophages [85], suggesting that autophagy upregulation could favour the bacterial escape from a controlled immune response.

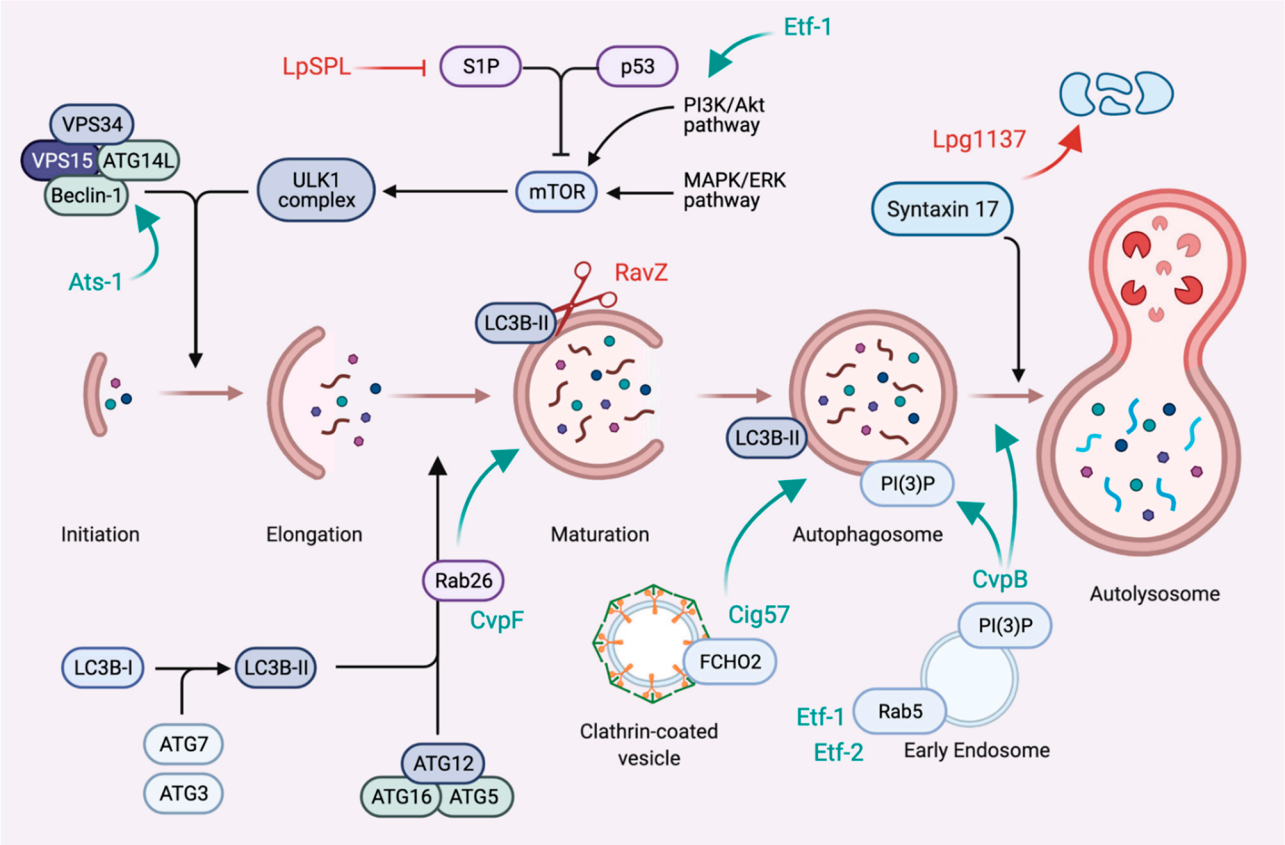


Figure 3. Subversion of autophagy by stealth bacterial pathogens. Stealth pathogens equipped with a T4SS translocate effector proteins to either activate or inhibit autophagy and establish infections. *L. pneumophila* inhibits autophagy, thus allowing LCVs to escape the degradative pathway. LpSPL downregulates host sphingolipid levels to perturb autophagy initiation; RavZ irreversibly cleaves the autophagy adapter protein LC3B from autophagosomes to inhibit autophagosomes maturation, and Lpg1137 degrades Syntaxin 17 to inhibit the fusion of autophagosomes with lysosomes. *C. burnetii* promotes autophagy, probably to reroute membranes and nutrients to CCVs. The effector protein CvpF enhances the Rab26-mediated recruitment of LC3B to autophagosomes; Cig57 stimulates the clathrin-dependent recruitment of autophagy markers to CCVs and CvpB manipulates PI(3)P metabolism to enhance autophagosomes fusion with CCVs, thereby favouring their homotypic fusion. *E. chaffeensis* also stimulates autophagy by secreting the effectors Etf-1 and Etf-2, which activate class III phosphatidylinositol 3-kinase and Rab5. Finally, the *A. phagocytophilum* effector protein Ats-1 interacts with Beclin-1 and ATG14L to stimulate autophagosome formation.

7. Inhibition of Apoptosis

Programmed cell death is common to all multicellular organisms. It is essential to dispose of unwanted cells, either during development or disease. Apoptosis can be activated by the extrinsic pathway upon sensing environmental stress by cell surface-exposed death receptors or by the intrinsic pathway, which detects intracellular stress (DNA damage, starvation, hypoxia, etc.) (Figure 4) [86]. Both pathways lead to the activation of caspases to coordinate intracellular proteolytic events. The intrinsic pathway also promotes mitochondrial outer membrane permeabilisation (MOMP), followed by cytochrome C release, which initiates the apoptosome assembly. Several intravacuolar pathogens promote

the lysis of infected cells to propagate infections; however, host cell death by apoptosis is important to control intracellular bacteria replication and survival. Thus, stealth pathogens translocate effector proteins to prevent untimely cell death and preserve their replicative niche during chronic infections. The inhibition of apoptosis by *C. burnetii* is particularly well detailed and stands as a remarkable example of how important host/pathogen interaction hubs can be multilayered and regulated by redundant mechanisms. Indeed, *C. burnetii* infections trigger an anti-apoptotic transcriptional program [87] and the activation of pro-survival kinases, including Akt, Erk1/2, and cAMP-dependent protein kinase (PKA) [88,89]. Activated PKA phosphorylates the pro-apoptotic protein Bad, which is sequestered at CCVs during infections. While this process relies on a functional T4SS, the effector protein/s involved remain unidentified [88]. *C. burnetii* possesses at least 3 effector proteins capable of inhibiting apoptosis. AnkG inhibits apoptosis by interacting with the proapoptotic mammalian protein p32 (Figure 4) [90]. Ectopically expressed AnkG associates with mitochondria but traffics to the nucleus after staurosporine-induced apoptosis. AnkG lacks typical NLS; however, binding to p32 and importin-α1 is required for nuclear translocation, suggesting that the effector protein might piggyback on host proteins [91,92]. How AnkG prevents apoptosis remains to be defined. Besides AnkG, *Coxiella* anti-apoptotic effectors A and B (CaeA and CaeB, respectively) block both intrinsic and extrinsic apoptosis (Figure 4). As already discussed above, CaeB localises at the ER, targets the ER stress sensors IRE1 [65] and prevents MOMP [66]. Ectopically expressed CaeA localises at the nucleus and prevents the activation of executioner caspase 7 [93]. Although the molecular mechanisms regulating CaeA function remain to be described, its antiapoptotic effect depends on the number of EK repetitions embedded in its protein sequence, which is variable among *Coxiella* isolates [93]. While the secretion of this protein still needs to be confirmed, the *Brucella abortus* protein BspJ also localises at nuclei upon ectopic expression and is important for the intracellular survival of the bacterium. Preliminary experiments indicate that BspJ could interact with NME/NM23 nucleoside diphosphate kinase 2 (NME2) and creatine kinase B (CKB) to inhibit macrophage apoptosis [94]. *Ehrlichia* and *Anaplasma* target mitochondria to prevent apoptosis during infections. The *Ehrlichia* type IV effector ECH0825 is highly upregulated during exponential growth in human monocytes and localises to the mitochondria upon T4SS-mediated translocation (Figure 4). ECH0825 upregulates mitochondrial manganese superoxide dismutase (MnSOD) to decrease reactive oxygen species (ROS) and dampen ROS-mediated cellular damages and apoptosis [95]. The *Anaplasma* effector protein Ats-1 has a dual role in apoptosis and autophagy. The protein translocates to the mitochondria, where it is cleaved by host proteases and inhibits cytochrome c release and poly ADP-ribose polymerase (PARP) cleavage [96]. Finally, the *Bartonella* BepA effector binds the C2 catalytic domain of host adenylyl cyclase (AC) and stabilises its interaction with G protein-coupled receptor (GPCR) subunit Gαs. The latter stimulates the activity of AC, leading to an increase in cellular cAMP levels, which protect endothelial cells from apoptosis [97,98].

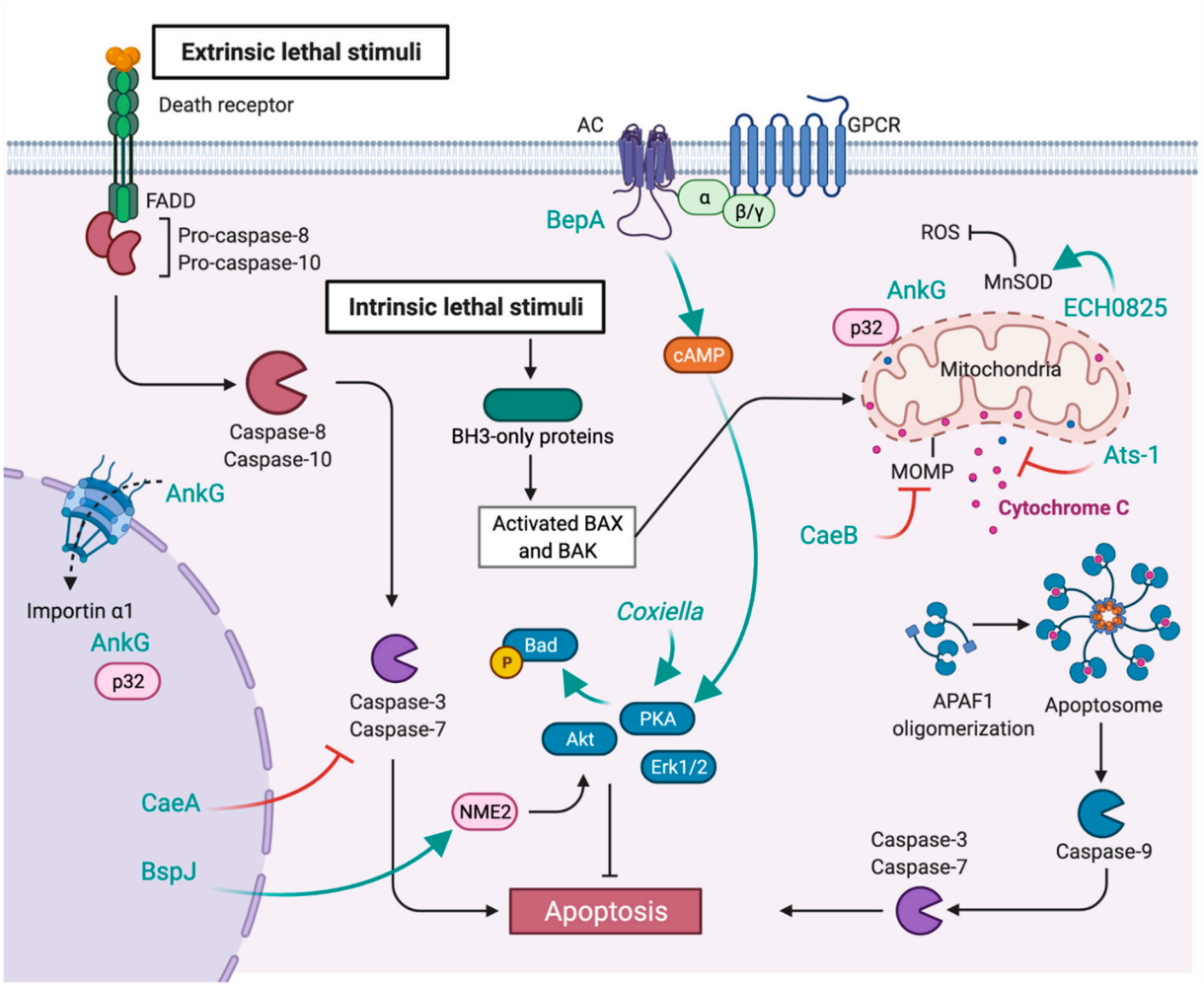


Figure 4. Subversion of apoptosis by stealth bacterial pathogens. Stealth pathogens inhibit apoptosis of infected cells to establish persistent infections. Unidentified *C. burnetii* effectors stimulate the activity of the anti-apoptotic factors PKA, Akt and Erk1/2. The effector protein AnkG localises at mitochondria but can translocate to the nucleus where it interacts with the proapoptotic factor p32. The effector proteins CaeA and B inhibit extrinsic and intrinsic apoptosis by preventing the activation of caspase 7 and by inhibiting mitochondrial outer membrane permeabilisation, respectively. The *Brucella* effector BspJ could interact with NME2 and CKB (not shown) to inhibit macrophage apoptosis. The *Ehrlichia* effector ECH0825 localises to the mitochondria, where it upregulates MnSOD, thereby decreasing ROS-mediated apoptosis. The *Anaplasma* effector protein Ats-1 translocates to mitochondria, where it inhibits cytochrome c release. Finally, the *Bartonella* BepA effector binds the adenylyl cyclase (AC), thereby stabilising its interaction with the G-protein-coupled receptor (GPCR) subunit, Gαs. This leads to an increase in cellular cAMP levels, protecting endothelial cells from apoptosis.

8. Concluding Remarks

Infections by pathogens are typically characterised by two possible outcomes: pathogens are either cleared by an efficient innate immune response, pre-existing immunity and, of course, medical treatment; or pathogens overcome host defences, eventually killing their hosts. Either way, infections typically manifest with detectable symptoms that allow a rapid response. However, a number of pathogens, including viruses, fungi and bacteria, have adapted to their hosts in such a way that they evade innate immune recognition and/or suppress the downstream signalling pathways that lead to the mounting of an antimicrobial response. These microorganisms are thus called stealth pathogens and can be the cause of long-lasting chronic infections that often remain undiagnosed. Notably, many stealth bacteria are equipped with a T4SS and replicate within membrane-bound compartments whose biogenesis relies on the subversion of host cell membrane trafficking

by bacterial effector proteins. Interestingly, however, despite their shared lifestyle and secretion system, stealth bacteria target an extremely diverse variety of host pathways involved in mounting an inflammatory response. In some cases, multiple effector proteins target the same pathway, suggesting the existence of fail-safe mechanisms. Understanding how stealth pathogens manipulate the host immune response is of utmost importance to counter latent chronic infections, both by developing specialised diagnostic tools to improve detection, and by specifically boosting adaptive immunity to clear these pathogens. On the other hand, understanding the mode of action of stealth pathogen effector proteins may provide us with innovative tools to modulate the immune system in the context of non-infectious chronic diseases.

Author Contributions: Conceptualization, E.M. and M.B.; writing—original draft preparation, A.B., E.M. and M.B.; writing—review and editing, A.B., E.M. and M.B. All authors have read and agreed to the published version of the manuscript.

Funding: This research was funded by Agence Nationale de la Recherche (ANR; ANR-17-CE15-0021, project QPiD; ANR-21-CE15-0015, project ST-Health).

Institutional Review Board Statement: Not applicable.

Informed Consent Statement: Not applicable.

Data Availability Statement: Not applicable.

Acknowledgments: Figures were created with BioRender.com. We apologize to all colleagues whose work was not discussed in this review.

Conflicts of Interest: The authors declare no conflict of interest.

References

1. Green, E.R.; Mecsas, J. Bacterial Secretion Systems: An Overview. *Microbiol. Spectr.* **2016**, *4*. [CrossRef] [PubMed]
2. Wallden, K.; Rivera-Calzada, A.; Waksman, G. Microreview: Type IV Secretion Systems: Versatility and Diversity in Function. *Cell. Microbiol.* **2010**, *12*, 1203–1212. [CrossRef]
3. Costa, T.R.D.; Felisberto-Rodrigues, C.; Meir, A.; Prevost, M.S.; Redzej, A.; Trokter, M.; Waksman, G. Secretion Systems in Gram-Negative Bacteria: Structural and Mechanistic Insights. *Nat. Rev. Microbiol.* **2015**, *13*, 343–359. [CrossRef] [PubMed]
4. Fischer, W.; Tegtmeyer, N.; Stingl, K.; Backert, S. Four Chromosomal Type IV Secretion Systems in *Helicobacter pylori*: Composition, Structure and Function. *Front. Microbiol.* **2020**, *11*, 1592. [CrossRef]
5. Li, Y.G.; Christie, P.J. *Agrobacterium* Biology, from Basic Science to Biotechnology. *Curr. Top Microbiol.* **2018**, *418*, 233–260. [CrossRef]
6. Gonzalez-Rivera, C.; Bhatty, M.; Christie, P.J. Mechanism and Function of Type IV Secretion during Infection of the Human Host. *Microbiol. Spectr.* **2016**, *4*. [CrossRef] [PubMed]
7. Wagner, A.; Dehio, C. Role of Distinct Type-IV-secretion Systems and Secreted Effector Sets in Host Adaptation by Pathogenic *Bartonella* Species. *Cell. Microbiol.* **2019**, *21*, e13004. [CrossRef]
8. Kubori, T.; Nagai, H. The Type IVB Secretion System: An Enigmatic Chimera. *Curr. Opin. Microbiol.* **2016**, *29*, 22–29. [CrossRef] [PubMed]
9. Martinez, E.; Siadous, F.A.; Bonazzi, M. Tiny Architects: Biogenesis of Intracellular Replicative Niches by Bacterial Pathogens. *FEMS Microbiol. Rev.* **2018**, *42*, 425–447. [CrossRef]
10. Fitzgerald, K.A.; Kagan, J.C. Toll-like Receptors and the Control of Immunity. *Cell* **2020**, *180*, 1044–1066. [CrossRef]
11. Broz, P.; Dixit, V.M. Inflammasomes: Mechanism of Assembly, Regulation and Signalling. *Nat. Rev. Immunol.* **2016**, *16*, 407–420. [CrossRef] [PubMed]
12. Santos, J.C.; Broz, P. Sensing of Invading Pathogens by GBPs: At the Crossroads between Cell-autonomous and Innate Immunity. *J. Leukoc. Biol.* **2018**, *104*, 729–735. [CrossRef] [PubMed]
13. Coers, J. Self and Non-Self Discrimination of Intracellular Membranes by the Innate Immune System. *PLoS Pathog.* **2013**, *9*, e1003538. [CrossRef] [PubMed]
14. Kumar, S.; Ingle, H.; Prasad, D.V.R.; Kumar, H. Recognition of Bacterial Infection by Innate Immune Sensors. *Crit. Rev. Microbiol.* **2012**, *39*, 229–246. [CrossRef]
15. Amarante-Mendes, G.P.; Adjemian, S.; Branco, L.M.; Zanetti, L.C.; Weinlich, R.; Bortoluci, K.R. Pattern Recognition Receptors and the Host Cell Death Molecular Machinery. *Front. Immunol.* **2018**, *9*, 2379. [CrossRef]
16. Ben-Tekaya, H.; Gorvel, J.-P.; Dehio, C. *Bartonella* and *Brucella*—Weapons and Strategies for Stealth Attack. *Csh. Perspect. Med.* **2013**, *3*, a010231. [CrossRef] [PubMed]
17. Miller, S.I.; Ernst, R.K.; Bader, M.W. LPS, TLR4 and Infectious Disease Diversity. *Nat. Rev. Microbiol.* **2005**, *3*, 36–46. [CrossRef]

18. Popa, C.; Abdollahi-Roodsaz, S.; Joosten, L.A.B.; Takahashi, N.; Sprong, T.; Matera, G.; Liberto, M.C.; Foca, A.; van Deuren, M.; Kullberg, B.J.; et al. *Bartonella quintana* Lipopolysaccharide Is a Natural Antagonist of Toll-Like Receptor 4. *Infect. Immun.* **2007**, *75*, 4831–4837. [CrossRef]
19. Malgorzata-Miller, G.; Heinbockel, L.; Brandenburg, K.; van der Meer, J.W.M.; Netea, M.G.; Joosten, L.A.B. *Bartonella quintana* Lipopolysaccharide (LPS): Structure and Characteristics of a Potent TLR4 Antagonist for in-Vitro and in-Vivo Applications. *Sci. Rep.* **2016**, *6*, 34221. [CrossRef]
20. Smith, J.A. *Brucella* Lipopolysaccharide and Pathogenicity: The Core of the Matter. *Virulence* **2018**, *9*, 379–382. [CrossRef]
21. Conde-Álvarez, R.; Arce-Gorvel, V.; Iriarte, M.; Manček-Keber, M.; Barquero-Calvo, E.; Palacios-Chaves, L.; Chacón-Díaz, C.; Chaves-Olarte, E.; Martirosyan, A.; von Bargen, K.; et al. The Lipopolysaccharide Core of *Brucella abortus* Acts as a Shield Against Innate Immunity Recognition. *PLoS Pathog.* **2012**, *8*, e1002675. [CrossRef]
22. Park, B.S.; Song, D.H.; Kim, H.M.; Choi, B.-S.; Lee, H.; Lee, J.-O. The Structural Basis of Lipopolysaccharide Recognition by the TLR4–MD-2 Complex. *Nature* **2009**, *458*, 1191–1195. [CrossRef] [PubMed]
23. Conti, F.; Boucherit, N.; Baldassarre, V.; Trouplin, V.; Toman, R.; Mottola, G.; Mege, J.-L.; Ghigo, E. *Coxiella burnetii* Lipopolysaccharide Blocks P38α-MAPK Activation through the Disruption of TLR-2 and TLR-4 Association. *Front. Cell. Infect. Microbiol.* **2015**, *4*, 182. [CrossRef] [PubMed]
24. Terwagne, M.; Ferooz, J.; Rolán, H.G.; Sun, Y.; Atluri, V.; Xavier, M.N.; Franchi, L.; Núñez, G.; Legrand, T.; Flavell, R.A.; et al. Innate Immune Recognition of Flagellin Limits Systemic Persistence of *Brucella*. *Cell. Microbiol.* **2013**, *15*, 942–960. [CrossRef]
25. Andersen-Nissen, E.; Smith, K.D.; Strobe, K.L.; Barrett, S.L.R.; Cookson, B.T.; Logan, S.M.; Aderem, A. Evasion of Toll-like Receptor 5 by Flagellated Bacteria. *Proc. Natl. Acad. Sci. USA* **2005**, *102*, 9247–9252. [CrossRef]
26. Snyder, G.A.; Deredge, D.; Waldhuber, A.; Fresquez, T.; Wilkins, D.Z.; Smith, P.T.; Durr, S.; Cirl, C.; Jiang, J.; Jennings, W.; et al. Crystal Structures of the Toll/Interleukin-1 Receptor (TIR) Domains from the *Brucella* Protein TcpB and Host Adaptor TIRAP Reveal Mechanisms of Molecular Mimicry. *J. Biol. Chem.* **2014**, *289*, 669–679. [CrossRef]
27. Sengupta, D.; Koblansky, A.; Gaines, J.; Brown, T.; West, A.P.; Zhang, D.; Nishikawa, T.; Park, S.-G.; Roop, R.M.; Ghosh, S. Subversion of Innate Immune Responses by *Brucella* through the Targeted Degradation of the TLR Signaling Adapter, MAL. *J. Immunol.* **2010**, *184*, 956–964. [CrossRef]
28. Radhakrishnan, G.K.; Yu, Q.; Harms, J.S.; Splitter, G.A. *Brucella* TIR Domain-Containing Protein Mimics Properties of the Toll-like Receptor Adaptor Protein TIRAP. *J. Biol. Chem.* **2009**, *284*, 9892–9898. [CrossRef] [PubMed]
29. Salcedo, S.P.; Marchesini, M.I.; Degos, C.; Terwagne, M.; Bargen, K.V.; Lepidi, H.; Herrmann, C.K.; Lacerda, T.L.S.; Imbert, P.R.C.; Pierre, P.; et al. BtpB, a Novel *Brucella* TIR-Containing Effector Protein with Immune Modulatory Functions. *Front. Cell. Infect. Microbiol.* **2013**, *3*, 28. [CrossRef]
30. Coronas-Serna, J.M.; Louche, A.; Rodríguez-Escudero, M.; Roussin, M.; Imbert, P.R.C.; Rodríguez-Escudero, I.; Terradot, L.; Molina, M.; Gorvel, J.-P.; Cid, V.J.; et al. The TIR-Domain Containing Effectors BtpA and BtpB from *Brucella abortus* Impact NAD Metabolism. *PLoS Pathog.* **2020**, *16*, e1007979. [CrossRef] [PubMed]
31. Krakauer, T. Inflammasomes, Autophagy, and Cell Death: The Trinity of Innate Host Defense against Intracellular Bacteria. *Mediat. Inflamm.* **2019**, *2019*, 2471215. [CrossRef] [PubMed]
32. Ding, J.; Shao, F. SnapShot: The Noncanonical Inflammasome. *Cell* **2017**, *168*, 544. [CrossRef]
33. Broz, P. Recognition of Intracellular Bacteria by Inflammasomes. *Microbiol. Spectr.* **2019**, *7*. [CrossRef]
34. Jakka, P.; Namani, S.; Murugan, S.; Rai, N.; Radhakrishnan, G. The *Brucella* Effector Protein TcpB Induces Degradation of Inflammatory Caspases and Thereby Subverts Non-Canonical Inflammasome Activation in Macrophages. *J. Biol. Chem.* **2017**, *292*, 20613–20627. [CrossRef]
35. Cunha, L.D.; Ribeiro, J.M.; Fernandes, T.D.; Massis, L.M.; Khoo, C.A.; Moffatt, J.H.; Newton, H.J.; Roy, C.R.; Zamboni, D.S. Inhibition of Inflammasome Activation by *Coxiella burnetii* Type IV Secretion System Effector IcaA. *Nat. Commun.* **2015**, *6*, 10205. [CrossRef]
36. Martinez, E.; Cantet, F.; Fava, L.; Norville, I.; Bonazzi, M. Identification of OmpA, a *Coxiella burnetii* Protein Involved in Host Cell Invasion, by Multi-Phenotypic High-Content Screening. *PLoS Pathog.* **2014**, *10*, e1004013. [CrossRef] [PubMed]
37. Platanitis, E.; Decker, T. Regulatory Networks Involving STATs, IRFs, and NFκB in Inflammation. *Front. Immunol.* **2018**, *9*, 2542. [CrossRef] [PubMed]
38. Zhu, H.; Wang, G.; Qian, J. Transcription Factors as Readers and Effectors of DNA Methylation. *Nat. Rev. Genet.* **2016**, *17*, 551–565. [CrossRef] [PubMed]
39. Maekita, T.; Nakazawa, K.; Mihara, M.; Nakajima, T.; Yanaoka, K.; Iguchi, M.; Arii, K.; Kaneda, A.; Tsukamoto, T.; Tatematsu, M.; et al. High Levels of Aberrant DNA Methylation in *Helicobacter pylori*–Infected Gastric Mucosae and Its Possible Association with Gastric Cancer Risk. *Clin. Cancer Res.* **2006**, *12*, 989–995. [CrossRef]
40. Sinclair, S.H.G.; Yegnasubramanian, S.; Dumler, J.S. Global DNA Methylation Changes and Differential Gene Expression in *Anaplasma phagocytophilum*-Infected Human Neutrophils. *Clin. Epigenet.* **2015**, *7*, 77. [CrossRef] [PubMed]
41. Grabiec, A.M.; Potempa, J. Epigenetic Regulation in Bacterial Infections: Targeting Histone Deacetylases. *Crit. Rev. Microbiol.* **2017**, *44*, 336–350. [CrossRef]
42. Rolando, M.; Sanulli, S.; Rusniok, C.; Gomez-Valero, L.; Bertholet, C.; Sahr, T.; Margueron, R.; Buchrieser, C. *Legionella pneumophila* Effector RomA Uniquely Modifies Host Chromatin to Repress Gene Expression and Promote Intracellular Bacterial Replication. *Cell Host Microbe* **2013**, *13*, 395–405. [CrossRef]

43. Li, T.; Lu, Q.; Wang, G.; Xu, H.; Huang, H.; Cai, T.; Kan, B.; Ge, J.; Shao, F. SET-domain Bacterial Effectors Target Heterochromatin Protein 1 to Activate Host RDNA Transcription. *EMBO Rep.* **2013**, *14*, 733–740. [CrossRef]
44. Cazalet, C.; Rusniok, C.; Brüggemann, H.; Zidane, N.; Magnier, A.; Ma, L.; Tichit, M.; Jarraud, S.; Bouchier, C.; Vandenesch, F.; et al. Evidence in the *Legionella pneumophila* Genome for Exploitation of Host Cell Functions and High Genome Plasticity. *Nat. Genet.* **2004**, *36*, 1165–1173. [CrossRef]
45. Joshi, A.D.; Swanson, M.S. Comparative Analysis of *Legionella pneumophila* and *Legionella micdadei* Virulence Traits. *Infect. Immun.* **1999**, *67*, 4134–4142. [CrossRef]
46. Mujtaba, S.; Winer, B.Y.; Jaganathan, A.; Patel, J.; Sgobba, M.; Schuch, R.; Gupta, Y.K.; Haider, S.; Wang, R.; Fischetti, V.A. Anthrax SET Protein a potential virulence determinant that epigenetically represses NF-kB activation in infected macrophages. *J. Biol. Chem.* **2013**, *288*, 23458–23472. [CrossRef] [PubMed]
47. Pennini, M.E.; Perrinet, S.; Dautry-Varsat, A.; Subtil, A. Histone Methylation by NUE, a Novel Nuclear Effector of the Intracellular Pathogen *Chlamydia trachomatis*. *PLoS Pathog.* **2010**, *6*, e1000995. [CrossRef]
48. Rennoll-Bankert, K.E.; Garcia-Garcia, J.C.; Sinclair, S.H.; Dumler, J.S. Chromatin-bound Bacterial Effector Ankyrin A Recruits Histone Deacetylase 1 and Modifies Host Gene Expression. *Cell. Microbiol.* **2015**, *17*, 1640–1652. [CrossRef] [PubMed]
49. Garcia-Garcia, J.C.; Rennoll-Bankert, K.E.; Pelly, S.; Milstone, A.M.; Dumler, J.S. Silencing of Host Cell CYBB Gene Expression by the Nuclear Effector AnkA of the Intracellular Pathogen *Anaplasma phagocytophilum*. *Infect. Immun.* **2009**, *77*, 2385–2391. [CrossRef]
50. Garcia-Garcia, J.C.; Barat, N.C.; Trembley, S.J.; Dumler, J.S. Epigenetic Silencing of Host Cell Defense Genes Enhances Intracellular Survival of the Rickettsial Pathogen *Anaplasma phagocytophilum*. *PLoS Pathog.* **2009**, *5*, e1000488. [CrossRef] [PubMed]
51. Dorrington, M.G.; Fraser, I.D.C. NF-KB Signaling in Macrophages: Dynamics, Crosstalk, and Signal Integration. *Front. Immunol.* **2019**, *10*, 705. [CrossRef]
52. Evans, S.M.; Rodino, K.G.; Adcox, H.E.; Carlyon, J.A. *Orientia tsutsugamushi* Uses Two Ank Effectors to Modulate NF-KB P65 Nuclear Transport and Inhibit NF-KB Transcriptional Activation. *PLoS Pathog.* **2018**, *14*, e1007023. [CrossRef] [PubMed]
53. Wangsanut, T.; Brann, K.R.; Adcox, H.E.; Carlyon, J.A. *Orientia tsutsugamushi* Modulates Cellular Levels of NF-kB Inhibitor P105. *PLoS Neglect. Trop. Dis.* **2021**, *15*, e0009339. [CrossRef]
54. Burette, M.; Allombert, J.; Lambou, K.; Maarifi, G.; Nisole, S.; Case, E.D.R.; Blanchet, F.P.; Hassen-Khodja, C.; Cabantous, S.; Samuel, J.; et al. Modulation of Innate Immune Signaling by a *Coxiella burnetii* Eukaryotic-like Effector Protein. *Proc. Natl. Acad. Sci. USA* **2020**, *117*, 13708–13718. [CrossRef] [PubMed]
55. Stewart, M. Molecular Mechanism of the Nuclear Protein Import Cycle. *Nat. Rev. Mol. Cell Biol.* **2007**, *8*, 195–208. [CrossRef]
56. Hillmer, E.J.; Zhang, H.; Li, H.S.; Watowich, S.S. STAT3 Signaling in Immunity. *Cytokine Growth Factor Rev.* **2016**, *31*, 1–15. [CrossRef] [PubMed]
57. Sorg, I.; Schmutz, C.; Lu, Y.-Y.; Fromm, K.; Siewert, L.K.; Bögli, A.; Strack, K.; Harms, A.; Dehio, C. A *Bartonella* Effector Acts as Signaling Hub for Intrinsic STAT3 Activation to Trigger Anti-Inflammatory Responses. *Cell Host Microbe* **2020**, *27*, 476–485.e7. [CrossRef]
58. Hetz, C. The Unfolded Protein Response: Controlling Cell Fate Decisions under ER Stress and Beyond. *Nat. Rev. Mol. Cell Biol.* **2012**, *13*, 89–102. [CrossRef]
59. Hetz, C.; Zhang, K.; Kaufman, R.J. Mechanisms, Regulation and Functions of the Unfolded Protein Response. *Nat. Rev. Mol. Cell Biol.* **2020**, *21*, 421–438. [CrossRef]
60. De Jong, M.F.; Starr, T.; Winter, M.G.; den Hartigh, A.B.; Child, R.; Knodler, L.A.; van Dijl, J.M.; Celli, J.; Tsolis, R.M. Sensing of Bacterial Type IV Secretion via the Unfolded Protein Response. *Mbio* **2013**, *4*, e00418-12. [CrossRef]
61. Smith, J.A.; Khan, M.; Magnani, D.D.; Harms, J.S.; Durward, M.; Radhakrishnan, G.K.; Liu, Y.-P.; Splitter, G.A. *Brucella* Induces an Unfolded Protein Response via TcpB That Supports Intracellular Replication in Macrophages. *PLoS Pathog.* **2013**, *9*, e1003785. [CrossRef]
62. Hempstead, A.D.; Isberg, R.R. Inhibition of Host Cell Translation Elongation by *Legionella pneumophila* Blocks the Host Cell Unfolded Protein Response. *Proc. Natl. Acad. Sci. USA* **2015**, *112*, E6790–E6797. [CrossRef] [PubMed]
63. Treacy-Abarca, S.; Mukherjee, S. *Legionella* Suppresses the Host Unfolded Protein Response via Multiple Mechanisms. *Nat. Commun.* **2015**, *6*, 7887. [CrossRef]
64. Brann, K.R.; Fullerton, M.S.; Voth, D.E. *Coxiella burnetii* Requires Host Eukaryotic Initiation Factor 2α Activity for Efficient Intracellular Replication. *Infect. Immun.* **2020**, *88*, e00096-20. [CrossRef] [PubMed]
65. Friedrich, A.; Beare, P.A.; Schulze-Luehrmann, J.; Cordsmeier, A.; Pazen, T.; Sonnewald, S.; Lührmann, A. The *Coxiella burnetii* Effector Protein CaeB Modulates Endoplasmatic Reticulum (ER) Stress Signalling and Is Required for Efficient Replication in *Galleria mellonella*. *Cell. Microbiol.* **2021**, *23*, e13305. [CrossRef] [PubMed]
66. Klingenbeck, L.; Eckart, R.A.; Berens, C.; Lührmann, A. The *Coxiella burnetii* Type IV Secretion System Substrate CaeB Inhibits Intrinsic Apoptosis at the Mitochondrial Level. *Cell. Microbiol.* **2013**, *15*, 675–687. [CrossRef]
67. Lee, J.; Ye, Y. Bag6/Bat3/Scythe: A Novel Chaperone Activity with Diverse Regulatory Functions in Protein Biogenesis and Degradation. *Bioessays* **2013**, *35*, 377–385. [CrossRef]
68. Rodino, K.G.; VieBrock, L.; Evans, S.M.; Ge, H.; Richards, A.L.; Carlyon, J.A. *Orientia tsutsugamushi* Modulates Endoplasmic Reticulum-Associated Degradation to Benefit Its Growth. *Infect. Immun.* **2018**, *86*, e00596-17. [CrossRef]
69. Yin, Z.; Pascual, C.; Klionsky, D.J. Autophagy: Machinery and Regulation. *Microb. Cell* **2016**, *3*, 588. [CrossRef]

70. Choy, A.; Dancourt, J.; Mugo, B.; O'Connor, T.J.; Isberg, R.R.; Melia, T.J.; Roy, C.R. The *Legionella* Effector RavZ Inhibits Host Autophagy Through Irreversible Atg8 Deconjugation. *Science* **2012**, *338*, 1072–1076. [CrossRef] [PubMed]
71. Arasaki, K.; Mikami, Y.; Shames, S.R.; Inoue, H.; Wakana, Y.; Tagaya, M. *Legionella* Effector Lpg1137 Shuts down ER-Mitochondria Communication through Cleavage of Syntaxin 17. *Nat. Commun.* **2017**, *8*, 15406. [CrossRef] [PubMed]
72. Rolando, M.; Escoll, P.; Nora, T.; Botti, J.; Boitez, V.; Bedia, C.; Daniels, C.; Abraham, G.; Stogios, P.J.; Skarina, T.; et al. *Legionella pneumophila* S1P-Lyase Targets Host Sphingolipid Metabolism and Restrains Autophagy. *Proc. Natl. Acad. Sci. USA* **2016**, *113*, 1901–1906. [CrossRef] [PubMed]
73. Niu, H.; Xiong, Q.; Yamamoto, A.; Hayashi-Nishino, M.; Rikihisa, Y. Autophagosomes Induced by a Bacterial Beclin 1 Binding Protein Facilitate Obligatory Intracellular Infection. *Proc. Natl. Acad. Sci. USA* **2012**, *109*, 20800–20807. [CrossRef]
74. Lin, M.; Liu, H.; Xiong, Q.; Niu, H.; Cheng, Z.; Yamamoto, A.; Rikihisa, Y. *Ehrlichia* Secretes Etf-1 to Induce Autophagy and Capture Nutrients for Its Growth through RAB5 and Class III Phosphatidylinositol 3-Kinase. *Autophagy* **2016**, *12*, 2145–2166. [CrossRef]
75. Yan, Q.; Lin, M.; Huang, W.; Teymournejad, O.; Johnson, J.M.; Hays, F.A.; Liang, Z.; Li, G.; Rikihisa, Y. *Ehrlichia* Type IV Secretion System Effector Etf-2 Binds to Active RAB5 and Delays Endosome Maturation. *Proc. Natl. Acad. Sci. USA* **2018**, *115*, 201806904. [CrossRef] [PubMed]
76. Gutierrez, M.G.; Vázquez, C.L.; Munafó, D.B.; Zoppino, F.C.M.; Berón, W.; Rabinovitch, M.; Colombo, M.I. Autophagy Induction Favours the Generation and Maturation of the *Coxiella*-replicative Vacuoles. *Cell. Microbiol.* **2005**, *7*, 981–993. [CrossRef]
77. Newton, P.; Thomas, D.R.; Reed, S.C.O.; Lau, N.; Xu, B.; Ong, S.Y.; Pasricha, S.; Madhamshettiwar, P.B.; Edgington-Mitchell, L.E.; Simpson, K.J.; et al. Lysosomal Degradation Products Induce *Coxiella burnetii* Virulence. *Proc. Natl. Acad. Sci. USA* **2020**, *117*, 6801–6810. [CrossRef]
78. Newton, H.J.; Kohler, L.J.; McDonough, J.A.; Temoche-Diaz, M.; Crabill, E.; Hartland, E.L.; Roy, C.R. A Screen of *Coxiella burnetii* Mutants Reveals Important Roles for Dot/Icm Effectors and Host Autophagy in Vacuole Biogenesis. *PLoS Pathog.* **2014**, *10*, e1004286. [CrossRef]
79. Kohler, L.J.; Reed, S.R.; Sarraf, S.A.; Arteaga, D.D.; Newton, H.J.; Roy, C.R. Effector Protein Cig2 Decreases Host Tolerance of Infection by Directing Constitutive Fusion of Autophagosomes with the *Coxiella*-Containing Vacuole. *Mbio* **2016**, *7*, e01127-16. [CrossRef]
80. Martinez, E.; Allombert, J.; Cantet, F.; Lakhani, A.; Yandrapalli, N.; Neyret, A.; Norville, I.H.; Favard, C.; Muriaux, D.; Bonazzi, M. *Coxiella burnetii* Effector CvpB Modulates Phosphoinositide Metabolism for Optimal Vacuole Development. *Proc. Natl. Acad. Sci. USA* **2016**, *113*, E3260–E3269. [CrossRef] [PubMed]
81. Siadous, F.A.; Cantet, F.; Schaik, E.V.; Burette, M.; Allombert, J.; Lakhani, A.; Bonaventure, B.; Goujon, C.; Samuel, J.; Bonazzi, M.; et al. *Coxiella* Effector Protein CvpF Subverts RAB26-Dependent Autophagy to Promote Vacuole Biogenesis and Virulence. *Autophagy* **2020**, *17*, 706–722. [CrossRef]
82. Latomanski, E.A.; Newton, P.; Khoo, C.A.; Newton, H.J. The Effector Cig57 Hijacks FCHO-Mediated Vesicular Trafficking to Facilitate Intracellular Replication of *Coxiella burnetii*. *PLoS Pathog.* **2016**, *12*, e1006101. [CrossRef]
83. Latomanski, E.A.; Newton, H.J. Interaction between Autophagic Vesicles and the *Coxiella*-Containing Vacuole Requires CLTC (Clathrin Heavy Chain). *Autophagy* **2018**, *14*, 1710–1725. [CrossRef] [PubMed]
84. Starr, T.; Child, R.; Wehrly, T.D.; Hansen, B.; Hwang, S.; López-Otin, C.; Virgin, H.W.; Celli, J. Selective Subversion of Autophagy Complexes Facilitates Completion of the *Brucella* Intracellular Cycle. *Cell Host Microbe* **2012**, *11*, 33–45. [CrossRef] [PubMed]
85. Wang, Y.; Li, Y.; Li, H.; Song, H.; Zhai, N.; Lou, L.; Wang, F.; Zhang, K.; Bao, W.; Jin, X.; et al. *Brucella* Dysregulates Monocytes and Inhibits Macrophage Polarization through LC3-Dependent Autophagy. *Front. Immunol.* **2017**, *8*, 691. [CrossRef] [PubMed]
86. Bertheloot, D.; Latz, E.; Franklin, B.S. Necroptosis, Pyroptosis and Apoptosis: An Intricate Game of Cell Death. *Cell. Mol. Immunol.* **2021**, *18*, 1106–1121. [CrossRef] [PubMed]
87. Voth, D.E.; Howe, D.; Heinzen, R.A. *Coxiella burnetii* Inhibits Apoptosis in Human THP-1 Cells and Monkey Primary Alveolar Macrophages. *Infect. Immun.* **2007**, *75*, 4263–4271. [CrossRef]
88. MacDonald, L.J.; Graham, J.G.; Kurten, R.C.; Voth, D.E. *Coxiella burnetii* Exploits Host CAMP-dependent Protein Kinase Signalling to Promote Macrophage Survival. *Cell. Microbiol.* **2014**, *16*, 146–159. [CrossRef]
89. Voth, D.E.; Heinzen, R.A. Sustained Activation of Akt and Erk1/2 Is Required for *Coxiella burnetii* Antiapoptotic Activity. *Infect. Immun.* **2009**, *77*, 205–213. [CrossRef]
90. Lührmann, A.; Nogueira, C.V.; Carey, K.L.; Roy, C.R. Inhibition of Pathogen-Induced Apoptosis by a *Coxiella burnetii* Type IV Effector Protein. *Proc. Natl. Acad. Sci. USA* **2010**, *107*, 18997–19001. [CrossRef]
91. Eckart, R.A.; Bisle, S.; Schulze-Luehrmann, J.; Wittmann, I.; Jantsch, J.; Schmid, B.; Berens, C.; Lührmann, A. Antiapoptotic Activity of *Coxiella burnetii* Effector Protein AnkG Is Controlled by P32-Dependent Trafficking. *Infect. Immun.* **2014**, *82*, 2763–2771. [CrossRef]
92. Schäfer, W.; Eckart, R.A.; Schmid, B.; Cagköylü, H.; Hof, K.; Muller, Y.A.; Amin, B.; Lührmann, A. Nuclear Trafficking of the Anti-apoptotic *Coxiella burnetii* Effector Protein AnkG Requires Binding to P32 and Importin-α1. *Cell. Microbiol.* **2016**, *19*, e12634. [CrossRef] [PubMed]
93. Bisle, S.; Klingenbeck, L.; Borges, V.; Sobotta, K.; Schulze-Luehrmann, J.; Menge, C.; Heydel, C.; Gomes, J.P.; Lührmann, A. The Inhibition of the Apoptosis Pathway by the *Coxiella burnetii* Effector Protein CaeA Requires the EK Repetition Motif, but Is Independent of Survivin. *Virulence* **2016**, *7*, 400–412. [CrossRef]

94. Ma, Z.; Li, R.; Hu, R.; Deng, X.; Xu, Y.; Zheng, W.; Yi, J.; Wang, Y.; Chen, C. *Brucella abortus* BspJ Is a Nucleomodulin That Inhibits Macrophage Apoptosis and Promotes Intracellular Survival of *Brucella*. *Front. Microbiol.* **2020**, *11*, 599205. [CrossRef]
95. Liu, H.; Bao, W.; Lin, M.; Niu, H.; Rikihisa, Y. *Ehrlichia* Type IV Secretion Effector ECH0825 Is Translocated to Mitochondria and Curbs ROS and Apoptosis by Upregulating Host MnSOD. *Cell. Microbiol.* **2012**, *14*, 1037–1050. [CrossRef]
96. Niu, H.; Kozjak-Pavlovic, V.; Rudel, T.; Rikihisa, Y. Ats-1 Is Imported into Host Cell Mitochondria and Interferes with Apoptosis Induction. *PLoS Pathog.* **2010**, *6*, e1000774. [CrossRef]
97. Schmid, M.C.; Scheidegger, F.; Dehio, M.; Balmelle-Devaux, N.; Schulein, R.; Guye, P.; Chennakesava, C.S.; Biedermann, B.; Dehio, C. A Translocated Bacterial Protein Protects Vascular Endothelial Cells from Apoptosis. *PLoS Pathog.* **2006**, *2*, e115. [CrossRef] [PubMed]
98. Pulliainen, A.T.; Pieles, K.; Brand, C.S.; Hauert, B.; Böhm, A.; Quebatte, M.; Wepf, A.; Gstaiger, M.; Aebersold, R.; Dessauer, C.W.; et al. Bacterial Effector Binds Host Cell Adenylyl Cyclase to Potentiate Gαs-Dependent CAMP Production. *Proc. Natl. Acad. Sci. USA* **2012**, *109*, 9581–9586. [CrossRef] [PubMed]

AIM OF THE THESIS

Coxiella burnetii human infections can cause severe clinical symptoms, and currently, no vaccines are available against this pathogen, only a long and complex antibiotic treatment is delivered to patients. With the development of axenic medium, it is now possible to grow *C. burnetii in vitro* and use genomic tools to understand essential pathogenic mechanisms and identify potential therapeutic targets.

In our research group, a library of *C. burnetii* transposon mutants has been developed, enabling us to explore the roles of various bacterial proteins in entry, immune response modulation, and CCV development. Many of these proteins are Dot/Icm effector substrates secreted into the host cell's cytosol during infection. One such effector, called CvpB, was reported as crucial in CCV biogenesis by manipulating host cell PI(3)P metabolism, leading to the accumulation of the phosphoinositide at CCVs. Notably, *cvpB* transposon mutants showed reduced bacterial virulence in animal models. This was the first time that an effector of *C. burnetii* was identified to directly manipulate host cell lipids, and more importantly, it was the first time that a direct link between CCV biogenesis and virulence was described.

Based on these results, the team explored the role of host lipids in the biogenesis of *Coxiella*-containing vacuoles. First, a catalogue of lipid binding probes was used to determine the lipid profile of CCVs. This screen demonstrated that, besides PI(3)P, PS and PI(3,5)P_2, PI(4)P and Lysobisphosphatidic acid (LBPA) also accumulate at CCVs. The use of the Dot/Icm-defective *dotA*::Tn mutant also allowed to demonstrate that the accumulation of PI(3)P, PI(4)P and LBPA at CCVs depends on the translocation of effector proteins.

During my PhD project, I aimed to uncover the *C. burnetii* effector proteins responsible for LBPA recruitment at the CCV and characterize the mechanisms of these effectors and explore their role during infection.

RESULTS

During my thesis work we identified CBU_2007 (hereafter named Vice) as a T4SS substrate responsible for the recruitment of LBPA at the CCV during infections. The following manuscript discusses the work that has been carried out on the CCV lipid profiling of the CCV before my arrival in the team and the characterization of the role of Vice during infections, which was my major PhD project.

Other preliminary data that I have generated are discussed later in this chapter.

1. The multifunction *Coxiella* effector Vice stimulates macropinocytosis and interferes with the ESCRT machinery

Supplemental videos are available via this link : https://filesender.renater.fr/?s=download&token=bff19d16-96a6-4071-84cc-9f3de50f52ca

If the link does not work anymore, feel free to ask us directly to send it back.

The multifunction *Coxiella* effector Vice stimulates macropinocytosis and interferes with the ESCRT machinery

Authors

Arthur Bienvenu[a,1], Melanie Burette[a,1], Manon Gourdelier[a], Jitendriya Swain[a], Chantal Cazevieille[b], Franck Cantet[a], Tatiana Clemente[c], Arif Sadi[c], Claire Dupont[a], Nicolas Bonetto[a], Benoit Bordignon[d], Delphine Muriaux[a], Stacey Gilk[c], Eric Martinez[a,*], Matteo Bonazzi[a,*].

[a] *IRIM, CNRS, Université de Montpellier, Montpellier, France.*
[b] *INM, Université de Montpellier, INSERM, Montpellier, France.*
[c] *Department of Pathology and Microbiology, University of Nebraska Medical Center, United States.*
[d] *MRI, BioCampus Montpellier, CNRS, INSERM, Université de Montpellier, Montpellier, France.*

[1] These authors contributed equally to this work

For correspondence: matteo.bonazzi@irim.cnrs.fr; eric.martinez@irim.cnrs.fr

Keywords

Coxiella burnetii, effector protein, macropinocytosis, ESCRT machinery

Abstract

Intracellular bacterial pathogens divert multiple cellular pathways to establish their niche and persist inside their host. *Coxiella burnetii*, the causative agent of Q fever, secretes bacterial effector proteins via its Type 4 secretion system to generate a *Coxiella*-containing vacuole (CCV). Manipulation of lipid and protein trafficking by these effectors is essential for bacterial replication and virulence. Here, we have characterized the lipid composition of CCVs and discovered that the effector Vice interacts with phosphoinositides and membranes enriched in phosphatidylserine (PS) and lysobisphosphatidic acid (LBPA). Remarkably, eukaryotic cells ectopically expressing Vice present compartments that resemble early CCVs in both morphology and composition. We discovered that the biogenesis of these compartments relies on the double function of Vice. The effector protein initially localizes at the plasma membrane of eukaryotic cells where it triggers the internalization of large vacuoles by macropinocytosis. Then, Vice stabilizes these compartments by perturbing the ESCRT machinery and inhibiting the formation of intraluminal vesicles (ILVs). Collectively, our results reveal that Vice is an essential *C. burnetii* effector protein capable of hijacking two major cellular pathways to shape the bacterial replicative niche.

Significance statement

Coxiella burnetii is a unique bacterial pathogen that secretes more than a hundred effector proteins to manipulate cellular processes and establish a replicative niche, the *Coxiella*-containing vacuole (CCV). Our study identified host cell lipids that are actively recruited by the bacterium to the CCV. Using a library of effector mutants, we identified the protein Vice (for Vacuole-inducing *Coxiella* effector) as the first bacterial effector capable of interacting with lysobisphosphatydic acid-enriched membranes and accumulating this lipid to CCVs. We show that Vice is also capable of stimulating macropinocytosis and inhibiting the ESCRT machinery. Together, our data show how a single bacterial effector can manipulate different cellular processes to favor the biogenesis of a bacterial pathogen's niche.

Introduction

Intracellular bacterial pathogens have evolved a variety of strategies to survive and replicate inside infected cells. While intra-cytosolic bacteria actively escape phagosomes and establish their replicative niche in the cytoplasm, intravacuolar bacteria remain confined within host-derived compartments and escape degradation by subverting membrane trafficking to generate pathogen-specific replicative niches(1).

The obligate intracellular bacterium *Coxiella burnetii* is a highly infectious pathogen responsible for the re-emerging zoonosis Q fever, a debilitating flu-like disease with severe health and economic burdens(2). Upon internalization by host cells, *C. burnetii* remains confined within membrane-bound compartments that follow the degradative endocytic pathway. Once in an acidic and degradative environment, the bacterium activates its Type 4b Secretion System (T4SS) to translocate over 140 effector proteins into the host cell cytoplasm(3). These effector proteins subvert multiple host cell functions to ensure the biogenesis of *Coxiella*-containing vacuoles (CCVs). A remarkable feature of CCV biogenesis is the rapid expansion of these compartments that precedes bacterial replication. Thus, at the early stages of infection, CCVs appear as large, spacious intracellular compartments harboring few bacteria. Later during infection, bacterial replication ensues and CCVs are rapidly filled with bacteria. While the role of host proteins subverted by *C. burnetii* during infections is well investigated, lipids are emerging as important players in *C. burnetii* intracellular replication and in CCV biogenesis. For example, CvpB (or Cig2) is a *C. burnetii* lipid-interacting effector (LIE) that triggers an increase of phosphatidylinositol 3-phosphate (PI(3)P) at CCVs and favors the homotypic fusion of CCVs(4). Notably, the characterization of CvpB revealed an unexpected lipid composition of CCVs and demonstrated how defective CCV biogenesis severely impacts *C. burnetii* virulence(5).

Lipids constitute an essential component of the “membrane code”(6), regulating signal transduction, cytoskeleton architecture and membrane trafficking. Specific lipid-modifying enzymes control lipid spatial and temporal distribution allowing precise and local modulation of essential processes including endocytosis and phagocytosis, membrane traffic and autophagy(7).

Phosphatidylinositol can be phosphorylated on three carbons to give rise to 7 different phospholipids essential to orchestrate cellular trafficking processes(7).

Several bacterial effector proteins manipulate PI metabolism to favor bacterial intracellular replication: *Mycobacterium tuberculosis* secretes the PI(3)P phosphatase SapM(8) and the broad range phosphatase MptpB(9); *Legionella pneumophila* secretes the effector SidP(10) to hydrolyse PI(3)P and PI(3,5)P_2, and effectors SidC, SidM, LidA, LpnE and RidL to use PI(3)P and/or PI(4)P as membrane anchors. Additionally, *Salmonella enterica* serovar Typhimurium increases PI(3)P in infected cells through the activity of the SPI-1 Type 3 secretion system (T3SS) substrate SopB(11, 12), a pleiotropic PI polyphosphatase. Besides promoting *Salmonella* uptake by macropinocytosis(13), SopB also maintains high levels of PI(3)P at the surface of *Salmonella*-containing vacuoles (SCVs) to form large SCVs.(12).

Given the importance of host lipids in *C. burnetii* intracellular development and virulence, we have further investigated the lipid composition of CCVs using lipid-binding sensors and antibodies and screened *C. burnetii* mutants to identify bacterial proteins that could be involved in the manipulation of lipid trafficking during infection. Our results show that PI(3,5)P_2 and PS are passively recruited at CCV membranes, whereas PI(3)P, PI(4)P and lysobisphosphatydic acid (LBPA) are enriched at CCV membranes in a T4SS-dependent manner. We also show that LBPA localization at CCVs depends on the activity of Vice (for Vacuole-inducing *Coxiella* effector, encoded by the gene *cbu2007*), a *C. burnetii* effector protein responsible for the initial CCV expansion and stabilization during infection. Intriguingly, the ectopic expression of Vice in non-phagocytic cells triggers macropinocytosis, leading to the formation of Vice-induced compartments (VICs), large intracellular vacuoles, reminiscent in morphology and composition of early CCVs and bearing multivesicular bodies (MVB) markers. At later time points of expression, Vice perturbs the ESCRT machinery, thereby stabilizing VICs, possibly by perturbing the formation of intraluminal vesicles (ILVs). We propose that Vice is a multifunction *C. burnetii* effector protein essential for the onset of CCVs biogenesis.

Results

PI(3)P, PI(4)P and LBPA are enriched at CCV membranes in a T4SS-dependent manner

To determine the lipid composition of CCVs, a panel of well-established lipid-binding sensors (SI appendix, Table S1) was cloned into mCherry- or RFP-expressing vectors and used to monitor lipid localization by automated confocal live cell imaging of U2OS cells infected with GFP-tagged wt *C. burnetii* for 2, 4 and 6 days. U2OS cells transfected with a plasmid encoding mCherry alone were used as control. Due to the lack of specific sensors, LBPA localization was monitored in U2OS cells infected with *C. burnetii* as above using anti-LBPA antibodies following fixation. The presence of each lipid at CCVs was visually scored from an average of 100 cells per condition (Fig. 1A). mCherry alone was never observed accumulating at CCV membranes (Fig. 1B). At all time points of infection, over 90% of infected cells presented CCVs positive for PS, a typical marker of late endosomal/lysosomal compartments (Fig. 1A, B). Interestingly however, only half of the infected cells presented CCVs that were positive for $PI(3,5)P_2$, another major lipid marker of late endosomes and lysosomes (Fig. 1A, B). This is in line with our previous observation that the *C. burnetii* effector CvpB perturbs PI 3-Kinase PIKFYVE activity, resulting in an accumulation of PI(3)P at CCVs(4). Indeed, 49% (±1.4%) of infected cells presented CCVs that were positive for PI(3)P at 2 days post-infection. This percentage increased to 74.4% (±1.5%) at 4 days post-infection, only to decrease slightly at 61.5% (±0.6%) at 6 days post-infection (Fig. 1A). At all time points of infections, over 90% of infected cells contained CCVs that were also positive for PI(4)P and LBPA (Fig. 1A, B). This latter is a typical marker of MVBs, where it serves an important role in the biogenesis of intraluminal vesicles (ILVs) by anchoring the ESCRT machinery protein ALIX to MVB membranes(14). All the other lipid sensors tested were largely absent from CCVs during the time course of infection (SI appendix, Fig. S1A).

To determine whether *C. burnetii* effector proteins actively control the enrichment or exclusion of lipids at CCVs, we re-assessed the localization of all monitored lipids in cells challenged with the T4SS defective, *dotA*::Tn *C. burnetii* mutant for 2, 4 and 6 days. As expected, PS enrichment at vacuoles containing the *dotA*::Tn mutant remained unchanged as compared to

CCVs harboring wt bacteria (Fig. 1A; SI appendix, Fig. S1B). Conversely, in agreement with our hypothesis, the percentage of PI(3,5)P_2-positive CCVs was increased to 80.2 % (±1.3 %) at 2 days post-infection and further increased to over 90 % at later time points (Fig. 1A). Enrichment of PI(3,5)P_2 correlated with a complete loss of PI(3)P at vacuoles containing the *dotA*::Tn mutant (Fig. 1A; SI appendix, Fig. S1B), as expected from our previous reports on the role of CvpB(4). Similarly, both PI(4)P and LBPA were completely absent from these compartments, indicating that their recruitment to CCV membranes is Dot/Icm-dependent (Fig. 1A). Finally, most of the lipids that were not observed at CCVs remained excluded from vacuoles harboring the *dotA*::Tn mutant, with the exception of diacylglycerol (DAG) and phosphatidic acid (PA), which are both present at the Golgi complex and the plasma membrane (Fig. 1A). Interestingly, PI(4)P (which we found enriched at CCVs but excluded from *dotA*::Tn-containing vacuoles) can be a source of DAG, through hydrolysis by phospholipase C (PLC)(15). In turn, DAG is the source of cellular PA. Thus, the loss of PI(4)P and the enrichment of DAG and PA at vacuoles containing the *dotA*::Tn mutants may be correlated. Together, our observations indicate that *C. burnetii* uses effector proteins to control the lipid composition of its replicative niche.

Screening of C. burnetii effector proteins involved in the subversion of PI(4)P and LBPA trafficking

We previously reported that PI(3)P enrichment at CCVs depends on the translocation of the effector protein CvpB(4). Here, to identify *C. burnetii* effector proteins involved in PI(4)P and LBPA localization at CCVs, we challenged U2OS cells with a library of 60 GFP-tagged *C. burnetii* mutants carrying transposon insertions in genes encoding for candidate and validated effector proteins (Fig. 1C). PI(4)P was monitored by transfecting cells with a plasmid encoding mCherry-tagged OSBP-PH domain, whereas LBPA was monitored using anti-LBPA antibodies. Cells challenged with either wt *C. burnetii* or the *dotA*::Tn mutant (both expressing GFP) were used as positive and negative controls, respectively. At 4 days post-infection, mCherry-OSBP-PH-transfected cells were imaged by automated live confocal microscopy as described above, whereas non-transfected cells were fixed and labeled with anti-LBPA and

anti-LAMP1 antibodies, prior to imaging. PI(4)P or LBPA localization was visually scored as described above to identify mutations that partially or completely impaired their accumulation at CCVs. None of the screened mutants showed a loss of PI(4)P enrichment at CCVs (not shown), suggesting that the manipulation of PI(4)P trafficking may be coordinated by effector proteins not included in our library. Conversely, 25 transposon insertions mildly affected LBPA accumulation at CCVs, and *C. burnetii* carrying a transposon insertion in *cbu2007* (*cbu2007*::Tn) completely failed to accumulate LBPA at CCVs (Fig. 1C, D, E; SI appendix, Fig. S2). Based on LAMP1 labeling, wt CCVs presented a diameter spanning from 5 to 15 µm, while CCVs generated by the *cbu2007*::Tn mutant were 1 to 8 µm in size, revealing a significant reduction in CCVs area (Fig. 1F). The proteolytic activity of CCVs harboring the *cbu2007*::Tn mutant, which is directly correlated with CCV acidification, was indistinguishable from that of CCVs harboring wt *C. burnetii* (Fig. 1G), indicating proper CCV metabolic activation and T4SS secretion of the *cbu2007*::Tn mutant. Electron microscopy revealed that U2OS cells challenged with the *cbu2007*::Tn mutant strain were pleomorphic, with membranes tightly sealed against compact bacterial colonies, while the wt bacterium developed large, spacious CCVs, suggesting a role for CBU2007 in CCV biogenesis (Fig. 1H). We were unable to complement the *cbu2007* mutation by inserting a wt copy of the gene in the mutant strain. Regardless, ectopic expression of HA-tagged CBU2007 in cells challenged with the *cbu2007*::Tn mutant strain restored the shape of CCVs and the localization of LBPA (SI appendix, Fig. S3A, B). To determine the impact of the CCV biogenesis defect associated with the mutation of *cbu2007* on infections, U2OS cells were challenged with either wt *C. burnetii* or the *cbu2007*::Tn mutant strain for 3 and 6 days and intracellular bacterial replication was assessed by colony-forming units (CFU) counts. The mutation in *cbu2007* dramatically reduced *C. burnetii* intracellular replication at both time points of infection (Fig. 1I). Collectively, these observations indicate that CBU2007 is important for infection and is likely involved in the initial expansion of CCVs.

CBU2007 is a T4SS C. burnetii effector important for CCVs expansion

cbu2007 encodes the *C. burnetii* protein with the highest effector prediction score assigned by the S4TE, an algorithm for T4SS effectors prediction(16). Its expression is regulated by a PmrA promoter and it includes a putative C-terminal E-Block secretion signal(17). CBU2007 has been recently validated as a secreted *C. burnetii* effector protein conserved among *C. burnetii* genomes(18), is important for CCV biogenesis(18) and essential for *C. burnetii* survival in primary macrophages(19). Nested PCR followed by sequencing(20) indicated that the transposon insertion occurred 711 bp downstream of the gene starting codon. Southern blot analysis validated the presence of a single transposon insertion in the genome of the *cbu2007*::Tn strain (SI appendix, Fig. S3C). To confirm CBU2007 translocation, *cbu2007* was cloned into the pXDC61K-BLAM vector to generate an N-terminal fusion with β-lactamase, and transformed either into GFP-tagged *C. burnetii* (wt) or the T4SS-defective *dotA*::Tn mutant strain. The expression of β-lactamase-tagged constructs was validated by Western blot using an anti-β-lactamase antibody (SI appendix, Fig. S3D). Protein translocation in U2OS cells was then assessed at 24, 48 and 72 h post-infection by means of a β-lactamase secretion assay. *C. burnetii* expressing β-lactamase alone or β-lactamase-tagged CvpB(4) were used as negative and positive controls, respectively. CBU2007 was efficiently translocated at all time points of infection, whereas no translocation was observed in cells challenged with the T4SS-defective mutant strain (SI appendix, Fig. S3E), indicating that CBU2007 is indeed a T4SS substrate.

CBU2007 interacts with host lipids

As CBU2007 is required to accumulate LBPA at CCVs, we generated Histidine-tagged recombinant CBU2007 to test the lipid-binding properties of the *C. burnetii* effector protein. First, PIP Strips were overlaid with 6xHis-CBU2007 and labeled with an anti-His antibody. This revealed an interaction of 6xHis-CBU2007 with PS and monophosphorylated PIs, with a preferential binding to PI(3)P and PI(5)P (Fig. 2A). No interactions were observed when PIP Strips were incubated with purified 6xHis-GST (SI appendix, Fig. S3F). As commercially available PIP Strips do not include LBPA, an *in vitro* co-sedimentation assay using Large Unilamellar Vesicles (LUVs) was used to assess the binding of CBU2007 to biological membranes containing LBPA. Co-sedimentation of

6xHis-CBU2007 with LUVs containing 80% phosphatidylcholine (PC) in combination with either 20% LBPA or 20% PS (Fig. 2B, C) was not significant. Conversely, 6xHis-CBU2007 efficiently co-sedimented with vesicles containing a mixture of 70% PC, 10% PS and 20% LBPA (Fig. 2B, C), which is compatible with the lipid composition of late endosomes and MVBs. In the absence of LUVs, His-CBU2007 was only detected in the supernatant, indicating that the protein does not precipitate (Fig. 2B, C). Together, these data indicate that CBU2007 can interact with PS and LBPA-enriched membranes.

CBU2007 is a vacuole-inducing C. burnetii effector protein

To assess the role of CBU2007 in manipulating host cell functions leading to CCV expansion, we ectopically expressed the effector protein in U2OS cells. Remarkably, the vast majority of cells expressing CBU2007 presented large, circular vacuoles, whose morphology was reminiscent of early CCVs observed in *C. burnetii*-infected cells (Fig. 2D). Correlative electron microscopy revealed that these compartments are spacious, single-membrane organelles, containing luminal vesicles of a size ranging from 200 nm to 2 µm (Fig. 2E). Organelles reminiscent of lamellar bodies were also observed in the lumen of the compartments (Fig. 2E). Given this remarkable phenotype, we renamed the *C. burnetii* effector Vice (for Vacuole-Inducing *Coxiella* Effector). Co-expression of HA-Vice with lipid-binding sensors, or immunolabeling of HA-Vice-expressing cells with anti-LBPA antibodies, revealed that the membranes of Vice-induced compartments (VICs) contain PS (SI appendix, Fig. S4A) and LBPA (Fig. 2F), but none of the monophosphorylated PIs interacting with Vice indicated above (PI(3)P, PI(4)P and PI(5)P; not shown). Further analysis revealed that VICs are positive for LAMP1 (Fig. 2G), but negative for Lysotracker (SI appendix, Fig. S4B), indicating that they may derive from late endosomes. VICs are also negative for other CCV markers, including LC3, RAB26, RAB24 and ORP1L (not shown), whose recruitment depends on other *C. burnetii* effector proteins. HA-Vice itself was observed decorating VIC membranes in 35% of transfected cells (Fig. 2G). Finally, LAMP1 labeling was used to determine the size of late endosomes and lysosomes in U2OS cells ectopically expressing HA-Vice or the HA tag alone as a control. A population of LAMP1-positive compartments with a

median area of 0.5 μm^2 (corresponding to a diameter of ~0.8 µm) was observed in both conditions (Fig. 2H). In addition, cells overexpressing Vice also presented a population of much larger compartments with an area ranging from 50 to 250 μm^2 (corresponding to a diameter of 8-17 µm; Fig. 2H). We thus defined VICs as intracellular compartments with a diameter ≥ 8 µm.

Vice enhances macropinocytosis

To monitor the biogenesis of Vice-induced compartments (VICs) by live imaging, we generated plasmids encoding either mCherry- or GFP-tagged versions of Vice. Surprisingly, the ectopic expression of either construct led to protein cleavage at multiple sites as observed by Western blot (not shown), and a complete loss-of-function of Vice, which may explain why the formation of VICs was not reported in the recent article by Larson and colleagues(18). We thus opted for an ALFA-tag(21), allowing the imaging of Vice in cells expressing mScarlet- or mNeonGreen-coupled ALFA-targeting nanobodies. Cells were imaged either at early time points after transfection (8h), to observe the initial formation of VICs, or at later time points (24h), to monitor their dynamics and persistence in cells. Early after transfection, HA-ALFA-Vice was mostly cytoplasmic and few large compartments were observed in the cytoplasm of transfected cells (SI appendix, Fig. S5A). Surprisingly, HA-ALFA-Vice transiently accumulated at defined regions of the plasma membrane, which was systematically accompanied by the formation of large vacuoles (Movie S1; Fig. 3A). These remained labeled by HA-ALFA-Vice for a short period of time (1-3 min), after which HA-ALFA-Vice rapidly redistributed to the cytoplasm (Movie S1; Fig. 3A) and the newly formed compartments moved to a perinuclear region, where they sometimes fused with other pre-existing compartments. This phenomenon was never observed in cells expressing the anti-ALFA nanobodies alone (data not shown). Vice accumulation at the plasma membrane and the internalization of large vacuoles were never observed at later time points of transfection. Instead, live cell imaging revealed a remarkable stability of VICs, which persisted unperturbed in cells over 8-10 hours (Movie S2).

Given the remarkable size of VICs, we hypothesized that Vice could enhance macropinocytosis. To explore this possibility, HA-ALFA-Vice was ectopically expressed in cells in

combination with anti-ALFA-mScarlet nanobodies and either the PI(4,5)P_2 sensor 2xPLCδ-GFP, GFP-LifeAct to visualize filamentous actin (F-actin), or GFP-RAB7. Interestingly, Vice accumulation at the plasma membrane was slightly preceded by a strong accumulation of PI(4,5)P_2, which persisted at VICs for a few minutes after the cytoplasmic redistribution of Vice (Movie S3; SI appendix, Fig. S5B). Conversely, Vice and actin accumulated simultaneously at the plasma membrane (Movie S4; SI appendix, Fig. S5C). However, actin persisted at VICs long after Vice dissociation (Movie S4; SI appendix, Fig. S5C). Finally, GFP-RAB7 was observed at VICs rapidly after the closure of the plasma membrane and remained associated with VICs after the dispersion of Vice to the cytoplasm (Movie S5; SI appendix, Fig. S5D). Next, U2OS cells ectopically expressing HA-ALFA-Vice in combination with anti-ALFA-mNeonGreen nanobodies were incubated overnight with 0.5 mg/ml tetramethylrhodamine (TMR)-tagged 70kDa dextran, washed in PBS and imaged over 8 hours to monitor fluid phase macropinocytosis. Live cell imaging indicated that indeed large macropinosomes formed in Vice-expressing cells were positive for TMR-dextran (Movie S6; Fig. 3B). The resulting dextran-positive VICs often fused together to form larger VICs which persisted in cells over the time course of the experiment (Movie S6). Finally, U2OS cells ectopically expressing HA-ALFA-Vice in combination with anti-ALFA-mScarlet nanobodies were incubated overnight with 50 µM of 5-(*N*-ethyl-*N*-isopropyl)amiloride (EIPA), which specifically inhibits macropinocytosis(22). In agreement with our hypothesis, EIPA treatment dramatically reduced the formation of VICs (Fig. 3C, D) and triggered an accumulation of Vice at the plasma membrane (Fig. 3C). Our data indicate that Vice is transiently recruited at the plasma membrane of eukaryotic cells where it triggers macropinocytosis, leading to the formation of large intracellular compartments whose morphology and composition are reminiscent of early CCVs. In the context of infections, this may provide CCVs with a source of membrane required for the initial rapid expansion of the *C. burnetii* replicative niche.

Vice perturbs the ESCRT machinery

As mentioned above, VICs can persist within cells over several hours without significantly altering their morphology and protein/lipid composition. Given that VIC membranes contain LBPA

(Fig. 2F) and RAB7 (SI appendix, Fig. S6A), typical markers of multivesicular bodies (MVBs)(14), we hypothesized that Vice may also interfere with the ESCRT machinery to inhibit membrane invagination and pinching off of ILVs, thus increasing the surface of MVBs and stabilizing VICs. We thus investigated the intracellular localization of ESCRT machinery components in U2OS cells ectopically expressing either HA-Vice or the HA tag alone as a negative control. In cells ectopically expressing the HA tag alone, the ESCRT-I component TSG101 and the ESCRT-III component CHMP4B were observed in spots in the cytoplasm whereas CHMP3 was cytoplasmic (SI appendix, Fig. S6B). Conversely, all three ESCRT markers decorated the contour of approximately 50% of VICs in cells expressing HA-Vice (Fig. 3E, F, G). Moreover, the intracellular localization of GFP-tagged ALIX, one of the few LBPA interactors identified thus far(14), was dramatically affected by ectopic expression of Vice. When co-expressed with the HA-ALFA-tag alone, GFP-ALIX localized at spots in the cytoplasm (Fig. 4A, B), suggesting membrane recruitment at MVBs; conversely, GFP-ALIX was mainly cytoplasmic when co-expressed in combination with HA-ALFA-Vice (Fig. 4A, B), suggesting that Vice may interfere with ALIX membrane anchoring, thereby perturbing the pinching off of ILVs.

Similar phenotypes were recapitulated in U2OS cells infected with wt *C. burnetii*. Infections of U2OS cells by either the wt strain or the *vice*::Tn mutant significantly decreased the number of ALIX dots in the cytoplasm, with a more substantial effect observed in cells infected by the wt strain (Fig. 4C, E). More importantly, when cells were exposed to the *vice*::Tn mutant strain, 78% of CCVs were decorated by ALIX, as opposed to 20% of CCVs in cells challenged with the wt strain (Fig. 4D, E). Finally, we investigated the intracellular localization of CD63, a tetraspanin typically found at MVBs and ILVs(23). CD63 was observed in spots in the cytoplasm of HA-expressing U2OS cells and decorated the contours of VICs in HA-Vice-expressing cells (SI appendix, Fig. S7A). CD63 was also observed within the lumen of VICs (SI appendix, Fig. S7A), in agreement with our CLEM observations reported in Fig. 2E. CD63 decorated the contour of CCVs generated by wt *C. burnetii*, while the protein was observed within the lumen of CCVs generated by the *vice*::Tn mutant strain (Fig. 4F, G). Ectopic expression of Vice in U2OS cells challenged with the *vice*::Tn mutant strain restored CCV morphology and CD63 localization (SI appendix, Fig S7B, C).

It has been previously reported that the ESCRT machinery also regulates HIV release from infected cells(24). Thus, to further investigate the possibility that Vice alters the functionality of the ESCRT machinery, we ectopically expressed the HIV polyprotein Gag in HEK293T cells, in combination with either the HA tag alone or HA-Vice, and monitored the levels of extracellular Gag as a proxy for the release of pseudo-viral particles. HEK293T cells transfected with Gag and siRNA targeting TSG101, an essential component of the ESCRT machinery previously shown to inhibit the release of viral particles(25), were used as control. As expected, cells depleted of TSG101 released significantly less Gag in the supernatant as compared to cells expressing Gag in combination with non-targeting siRNAs (Fig. 4H, I). In agreement with our hypothesis, cells overexpressing HA-Vice also released significantly reduced levels of Gag as compared to cells transfected with Gag in combination with the HA tag alone (Fig. 4H, I). Together, our data indicate that Vice can perturb the functionality of the ESCRT machinery, likely by reducing the membrane targeting of ALIX.

Discussion

Given the importance of PI(3)P in CCV biogenesis and in *C. burnetii* virulence *in vivo*, in this study, we used lipid-binding fluorescent sensors and antibodies to further characterize CCV lipid composition. As expected, lipids that are typically found at late endosomes/lysosomes were also observed at CCVs. Among these, PI(3,5)P_2 and PS were also observed at vacuoles containing the T4SS-defective mutant *dotA::*Tn, suggesting that *C. burnetii* does not alter the trafficking of these lipids. On the other hand, the late-endosome/MVB lipid marker LBPA was specifically enriched at CCVs generated by wt bacteria but absent from vacuoles containing the *dotA*::Tn mutant, indicating that *C. burnetii* actively manipulates LBPA trafficking/metabolism. We also confirmed the active PI(3)P enrichment at CCVs harboring wt bacteria(4). Interestingly, vacuoles harboring the *dotA*::Tn mutant were indeed negative for PI(3)P as expected, but enriched in PI(3,5)P_2, supporting our hypothesis that CvpB interferes with PI(3)P phosphorylation to PI(3,5)P_2. PI(4)P, a membrane lipid primarily observed at the Golgi complex, also localized at CCVs in a T4SS-dependent manner, suggesting that *C. burnetii* effectors may re-route Golgi traffic towards the CCV.

The phenotypic screen of a library of *C. burnetii* mutants carrying transposon insertions in genes encoding predicted and validated effector proteins allowed us to pinpoint a transposon insertion in *cbu2007*, which largely inhibited LBPA localization at CCVs. Of note, CBU2007 is the highest-scoring predicted effector by the S4TE algorithm(16) and has been recently validated as a *C. burnetii* effector protein(18). CBU2007 is required for intracellular replication(18) and, more importantly, is essential for survival in primary macrophages and virulence in mice(19).

Importantly, membranes of CCVs harboring *cbu2007::Tn* mutants are collapsed on bacteria as opposed to the spacious CCVs generated by wt *C. burnetii*. Despite their obvious altered morphology, collapsed CCVs are positive for the late endosomal/lysosomal marker LAMP1 and are acidified, similar to wt CCVs, suggesting that bacterial metabolism and effector translocation are not affected. Indeed, differently from *dotA*::Tn mutants, the *cbu2007*::Tn mutant strain replicates within these compartments, albeit much less than wt bacteria.

Most strikingly, the ectopic expression of CBU2007 in epithelial cells leads to the formation of a very large vacuole, with a diameter ranging from 8 to 17 µm, resembling early CCVs in both morphology and protein and lipid composition. We thus named the protein encoded by *cbu2007* Vice (for Vacuole-inducing *Coxiella* effector). Interestingly, LBPA was also found at the membrane of those compartments; we thus investigated the potential interaction of Vice with several lipids. Recombinant Vice interacts with monophosphorylated phosphoinositides, $PI(3,5)P_2$, $PI(3,4,5)P_3$ and PS, indicating a possible association with the plasma membrane and late endosomal compartments. In particular, Vice co-sedimentation with LUVs enriched in PS and LBPA is suggestive of an interaction with MVBs. Combined with the observation of LBPA at CCVs generated by wt bacteria and the absence of LBPA from CCVs generated by the *cbu2007*::Tn mutant, our data indicate an interaction between MVBs and CCVs.

As the Vice-induced compartment (VIC) membrane is enriched in LBPA and that we observed the presence of a few intraluminal vesicles of a size compatible with ILVs, we believed that these structures could derive from MVBs failing to pinch off intraluminal vesicles, thereby increasing their membrane surface. Moreover, the observation of Vice at VIC membranes in a few percent of cells suggests that Vice is a dynamic protein. Thus, we imaged cells ectopically

expressing Vice over time to explore the biogenesis of VICs formation. To our surprise, VICs are not formed by the expansion of intracellular vesicles, as we expected according to our model of defective ILVs formation, but rather originate from the plasma membrane by macropinocytosis-like events. In agreement with our hypothesis of a dynamic association of Vice with membranes, the *C. burnetii* effector is mainly cytoplasmic, strongly accumulating at the plasma membrane at VIC internalization sites, and dissociating from VIC shortly after internalization (1-2 min). The presence of typical macropinocytic markers and, more importantly, the inhibition of VIC formation by the macropinocytosis inhibitor EIPA, suggest that Vice stimulates macropinocytosis in cells. VIC formation was observed in multiple cell types ectopically expressing Vice but was more prominent in U2OS cells (not shown). As recruitment of Vice at the plasma membrane follows the local accumulation of $PI(4,5)P_2$ at the macropinocytic cup, we hypothesized that Vice recruitment may depend on interactions with specific lipids or proteins. PIP-Strips indicate an interaction between Vice and bi-phosphorylated phosphoinositides; however, the interaction with $PI(4,5)P_2$ appears to be less relevant as compared to other phosphoinositides. Immunoprecipitation assays have thus far failed to inform us on candidate protein interactors for Vice.

Following internalization, VICs move to a perinuclear area where they remain remarkably stable in size and shape over several hours, suggesting that perturbing ILVs formation, which we envisioned as a biogenesis strategy, may in fact be involved in stabilizing these structures. Indeed, besides RAB7, CD63 and LBPA which are typically found at late endosomes and MVBs (26, 27), components of the ESCRT machinery, which normally cycle between late endosomal membranes and the cytoplasm, accumulate at the periphery of VICs, suggesting a perturbation of the machinery itself. In agreement with this hypothesis, the typical ILV/exosomal marker CD63 decorates the contours of CCVs and VICs, whereas it is found within the CCV lumen in cells infected by the *vice*::Tn mutant strain. Moreover, membrane association of the ESCRT-associated protein ALIX, which is involved in pinching off ILVs from MVBs membranes, seems largely impaired in cells expressing Vice. Importantly, a similar phenotype, albeit attenuated, is also observed in cells infected by wt *C. burnetii*, whereas infections by the *vice*::Tn transposon mutant partially restore ALIX association with host cell membranes. The milder phenotype observed during

infection is probably related to the lower amounts of endogenous Vice translocated by bacteria as opposed to the ectopic expression of Vice in non-infected cells. Importantly, the majority of CCVs harboring the *vice::*Tn mutant strain are also positive for ALIX, suggesting an active ESCRT machinery pinching off vesicles from the CCV contours, possibly leading to the convoluted, collapsed morphology of CCVs observed in cells infected with the mutant strain. Conversely, only 20% of CCVs generated by the wt strain are positive for ALIX. In support of a perturbation of the ESCRT machinery, ectopically expressing Vice significantly reduces the release of Gag-containing Viral-like particles, which is also mediated by the activity of the ESCRT machinery at the plasma membrane(24). The recent implication of the ESCRT machinery in the repair of CCV membranes during infections may seem counterintuitive to our findings(28). On the contrary, it has also been reported that in the context of membrane repair, membrane recruitment of ALIX solely relies on ALG-2 and LBPA is never observed at sites of membrane damage(29, 30). Therefore, multiple ESCRT-dependent machineries are involved in membrane repair and MVBs biogenesis, and perturbating the LBPA-dependent pathway allows *C. burnetii* to selectively target the pathway related to ILV biogenesis. Our hypothesis is that Vice association with membranes enriched in PS and LBPA might interfere with ALIX association with membranes, which is similarly mediated by binding to LBPA. During MVB biogenesis, LBPA is also found at ILV membranes within the lumen of MVBs. The perturbation of ILV formation in cells exposed to Vice, either by ectopic expression or by translocation during infections, would lead to the observed accumulation of LBPA at the surface of VICs or CCVs, respectively. This work also adds to our knowledge of the role of MVBs and the ESCRT machinery in infections by intracellular pathogens. Indeed, it has been previously reported that *M. tuberculosis* needs to perturbs the ESCRT machinery notably to escape into the cytoplasm(31, 32). It has also been reported that macrophages infected with *M. avium* or *M. smegmatis* secrete more exosomes as compared to non-infected cells(33). Secreted exosomes contain more Hsp70, which triggers the NF-κB signaling pathway in bystander cells(33). Thus, inhibiting the ESCRT machinery may also be a strategy for stealth pathogens to dampen inflammation. On the other hand, *Anaplasma phagocytophilum*-containing vacuoles (ApVs) are positive for MVB markers including LBPA and CD63, similar to what we have observed here(34).

Indeed, MVB biogenesis is important for *A. phagocytophilum* replication within infected cells. Contrary to *C. burnetii*, however, *A. phagocytophilum* uses exosomes to release infectious progeny to bystander cells(34). Accordingly, ApV membranes are positive for ALIX, suggesting active ESCRT machinery, as opposed to what is observed here with CCVs(34).

In conclusion, here we report how lipid profiling of CCVs led to the identification and characterization of a new multi-functional *C. burnetii* effector protein Vice (CBU2007). Intracellular bacterial pathogens secreting effector proteins with multiple functions during infections have previously been reported, with *Chlamydia* being one of the best examples(35). Regarding *C. burnetii*, the effector protein CaeB was yet the only multi-functional effector described(36–39). Here we propose that early during infection Vice promotes macropinocytosis to deliver membranes and nutrients to support the rapid expansion of early CCVs. At later time points of infection, Vice perturbs the ESCRT machinery by hindering membrane recruitment of ALIX, thereby limiting the formation of ILVs and stabilizing CCVs morphology. Additional work will focus on the precise molecular mechanism regulating Vice functions and will determine whether Vice may be involved in decreasing the release or altering the composition of extracellular vesicles by cells infected with *C. burnetii*.

Materials and methods

Antibodies and reagents

Mouse antibodies used were against Beta-Lactamase (BLAM) (1:2000, MA120370, ThermoFisher Scientific), GAPDH (1:1000, G8795, Sigma), HA (1:1000, 66006-1-Ig, Proteintech), CD63 (WB) (1:50, clone R5G2, MBL), CD63 (IF) (1:200 clone CLB-gran/12, 435, Sanquin), HIS-HRP (1:2000 HIS.H8 ThermoFisher Scientific). Rabbit antibodies used were against ALIX (1:1000, SAB4200476**,** Sigma), HA (1:1000, 51064-2-AP, Proteintech), GFP (1:1000, 50430-2-AP), TSG101 (1:1000, T5701, Sigma), LAMP1 (1:1000, L1418, Sigma). Rabbit anti-*Coxiella* NMII antibodies were generated by Covalab. Hoescht 33258, anti-rabbit and anti-mouse HRP-conjugated antibodies were purchased from Sigma. Mouse and rabbit IgG conjugated to Alexa Fluor 488, 555 or 647 as well as Prolong Gold antifade mounting reagent were purchased from Invitrogen. LysoTracker Red (L7528) was purchased from Life Technologies. Purified L-α-phosphatidylcholine (Egg PC) (Cat# 840051P) , L-α-phosphatidylserine (Brian PS) (Cat#840032C), lysobisphosphatidic acid (LBPA) (cat# 857133C) were purchased from Avanti Polar Lipids, Inc.

Transfections, cell cultures and infections

U2OS (ATCC) cells were routinely maintained in DMEM containing 10% (vol/vol) of foetal bovine serum (FBS) in a humidified atmosphere of 5% CO_2 at 37 °C. For ectopic expression of proteins in mammalian cells, cells were grown to 70% confluence and transfected with JetPEI cationic polymer transfection reagent (Polyplus Transfection) diluted in 150 mM NaCl. SiRNA transfections in cells were performed with calcium phosphate buffer in HEK293T (ATCC) for 24h with siRNA TSG101 (S102664522) and siRNA negative Control (S103650318) from Qiagen. For bacterial infections, U2OS cells were seeded in 24-well plates with coverslip one day prior to infection. Cells were then challenged with different strains at an MOI of 100 followed by 10 minutes of centrifugation at 400 x g for infection synchronization.

Immunofluorescence staining and microscopy

Cells were fixed in 4% (wt/vol) paraformaldehyde in phosphate-buffered saline (PBS) pH 7.4 solution at room temperature for 20 min. Samples were then rinsed with PBS solution and incubated in blocking solution (0.5% bovine serum albumin [BSA], 50 mM NH_4Cl in PBS solution, pH 7.4). Cells were then incubated with the primary antibodies diluted in blocking solution for 1 h at room temperature in a humidified atmosphere, washed five times in PBS solution, and further incubated for 1 h with the secondary antibodies diluted in blocking solution complemented with Hoechst 33258 (Sigma) for DNA staining. Coverslips were then mounted on slides using Fluoromount mounting medium (Sigma). Samples were imaged using an epifluorescence EVOS M5000 (Thermo Fisher Scientific) equipped with 63X or 40X oil immersion objectives. Live cell imaging was performed with a spinning disk Olympus SR microscope equipped with sCMOS Fusion BT Hamamatsu camera. Automated epifluorescence microscopy was performed using an ImageXpress PICO equipped with a CMOS 5Mpx 12bits camera. In this case, 25 fields/well were acquired for image analysis. Image J, ICY and CellProfiler software were used for image analysis and quantifications.

Mutant library screening

U2OS cells were seeded into black 96-well plates with clear bottom (Greiner Bio-One, 1,200 cells / well) 24h prior to infection. Cells were infected with a sub-library of GFP-tagged *C. burnetii* mutants (MOI of 100) and centrifuged at 400 x g for 10 min at room temperature. Following 45 minutes of incubation at 37°C in a humidified atmosphere of 5% CO_2, infected cells were washed 3 times in PBS pH 7.4 and DMEM containing 10% FBS was added. After 4 days of infection, cells were washed 3 times with PBS and fixed with PBS pH 7.4 containing 4% PFA. Immunofluorescence using Hoescht 33258 (Sigma), anti-LBPA (Echelon Biosciences) and anti-LAMP1 (Sigma) was performed as described above. 25 fields/well were imaged with an ImageXpress PICO microscope equipped with a CMOS 5Mpx 12bits camera and analyzed with ICY software.

Beta-Lactamase Translocation Assay

To assess the translocation of CBU2007, U2OS cells were cultured in black 96-well plates with clear bottom (Greiner Bio-One). The cells were then infected with the appropriate *C. burnetii* strain

at a multiplicity of infection (MOI) of 100 and incubated for 24, 48, and 72 hours in a humidified atmosphere of 5% CO_2 at 37 °C. Negative and positive controls were included, consisting of *C. burnetii* expressing BLAM alone or with BLAM-tagged CvpB, respectively. For translocation detection, cells were loaded with the fluorescent substrate CCF4/AM from the LiveBLAzer-FRET B/G loading kit (Invitrogen). The loading solution contained 20 mM HEPES, 15 mM probenecid (Sigma) at pH 7.3, diluted in Hank's balanced salt solution (HBSS). After incubating in the dark at room temperature for 1 hour, cells were visualized using an EVOS inverted fluorescence microscope equipped with DAPI and GFP filter cubes. CellProfiler was used to analyze images as previously described(40).

Transmission Electron Microscopy (TEM)

After 5 days of infection, U2OS cells were immersed in a 2.5% glutaraldehyde solution in PHEM buffer (CliniSciences, pH 7.4) and kept overnight at 4°C. Subsequently, they were rinsed with PHEM buffer and post-fixed with a mixture of 0.5% osmic acid and 0.8% potassium hexacyanoferrate trihydrate in the dark at room temperature for 2 hours. After two additional rinses in PHEM buffer, the cells were dehydrated using a series of ethanol solutions with increasing concentrations (30-100%). The cells were then embedded in EmBed 812 using an Automated Microwave Tissue Processor for Electron Microscopy (Leica EM AMW). Thin sections (70 nm) were obtained from different levels of each block using a Leica-Reichert Ultracut E microtome. These sections were counterstained with 1.5% uranyl acetate in 70% ethanol and 3% lead citrate (Reynolds method - EMS), and observed using a Tecnai F20 transmission electron microscope operating at 120 kV at the Institut des Neurosciences de Montpellier, INSERM U 1298, Université Montpellier, Montpellier, France.

Correlative Light Electron Microscopy (CLEM)

U2OS cells seeded on Gridded Coverslips (MATTEK) were transfected 24h prior to image acquisition using an Olympus SR microscope. The following steps of sample preparation were performed at room temperature: cells were fixed in HEPES buffer (pH 7.4) containing 2.5% Glutaraldehyde for 2 hours and rinsed 3 times for 5 minutes with HEPES buffer (pH 7.4). Samples

were immersed in the Post Fixation solution (HEPES buffer (pH 7.4) containing 1% osmic acid and 1.5% potassium ferrocyanide) for 1h and rinsed 3 times with HEPES buffer (pH 7.4). The enhancement was performed using a solution of 1% tannic acid in HEPES buffer (pH 7.4) for 30 minutes, then washed 3 times with HEPES buffer (pH 7.4). A second post-fixation treatment was done using 1% osmium acid in distilled water for 1h and washed 3 times with distilled water. For dehydration, samples were immersed in a series of ethanol concentrations: 25%, 50%, 75%, and 95% for 10 minutes each and 3 times 15 minutes in 100% ethanol. The first step of embedding was performed using EPON and 2% BDMA (EMS) overnight, and then areas selected by confocal microscopy were specifically encapsulated with the same solution for at least 2 hours. The resin was polymerized for at least 48 hours at 60°C. Images were acquired with a Tecnai F20 transmission electron microscope operating at 120 kV at the Institut des Neurosciences de Montpellier, INSERM U 1298, Université Montpellier, Montpellier, France.

Growth assay using Colony Forming Unit (CFU) assay

U2OS cells were plated in duplicate or triplicate in a 6-well plate at 2×10^5 per well and allowed to adhere overnight. The next day, cells were infected with WT or *vice*::Tn *C. burnetii* in 500 µL 10% DMEM for 2 h, then washed 15 times with PBS to remove extracellular bacteria. Cells were scraped into 2 mL fresh 10% RPMI and replated in a 24-well plate for analysis at day 3 (500 µL cells), and day 6 (125 µL cells + 325 µL 10% RPMI) postinfection. To establish a baseline number of internalized bacteria at day zero, 500 µL of infected cells was centrifuged into a pellet and lysed in sterile water for 5 min. Lysate was serially diluted in ACCM-D and spotted onto ACCM-D agarose plates, with each condition performed in triplicate. ACCM-D agarose plates were incubated for 7 to 10 days at 37°C in 2.5% O_2 and 5% CO_2, and the number of colonies was counted to determine bacterial viability. For each time point, fold change over day zero was determined.

Magic red assay for cathepsin B activity

Active cathepsin B was quantitated in live cells using Magic Red following the manufacturer's protocol. Briefly, $2x10^5$ U2OS cells were infected with WT or *vice*::Tn *C. burnetii* in 6-well plates for 2 h and washed with PBS. At 1dpi, cells were replated onto ibidi slides ($3X10^3$ cells per channel). Magic Red (Cat. 937; ImmunoChemistry Technologies; Bloomington, MN) was reconstituted in 50µl DMSO, vortexed, and stored at -20°C. Immediately before use, the stock was diluted at 1:10 dilution in sterile water, and then further diluted at 1:25 in 10% DMEM. Cells were incubated with 50 µl diluted Magic Red for 30 min at 37°C and 5% CO_2, washed with pre-warmed media, and Z-stack confocal images obtained with identical capture settings with a Nikon spinning disk confocal microscope at 60X. Images were processed identically with ImageJ, and Magic Red fluorescence intensity normalized to the CCV area. At least 15 cells or CCVs were measured per condition in each of three independent experiments.

Protein purification

Codon optimized *vice* was inserted into the pTwist vector and expressed in *Escherichia coli* LEMO21 (New England Biolabs). Bacterial cultures were grown at 37°C to mid-exponential phase (OD600nm = 0.5) and protein expression was induced overnight at 16°C with 1 mM isopropyl-β-D-thiogalactopyranoside (IPTG, Euromedex). Bacteria were harvested by centrifugation, resuspended in lysis buffer (50 mM Tris pH 7.8, 500 mM NaCl, 15 mM imidazole, complete anti-protease (Roche)) and lysed by sonication with 5 rounds of 10 seconds pulsation at 15 watts and 6 rounds at 12 watts with 30 seconds in between each round. Lysates were then cleared by centrifugation (12,000 x g, 30 min, 4°C). Proteins were purified on Econo-Pac Chromatography Columns (Bio-rad) with HIS-Select Nickel Affinity Gel (Sigma). After 5 washes with washing buffer (50 mM Tris pH 7.8, 500 mM NaCl, 50 mM imidazole, complete anti-protease (Roche)) proteins were eluted using elution buffer (50 mM Tris pH 7.8, 500 mM NaCl, 1 M imidazole, complete anti-protease (Roche)).

Protein–Lipid Overlay Assay

Purified 6xHIS-GST or 6xHIS-CBU2007 were incubated with PIP Strips membranes (Echelon Biosciences) according to the manufacturer's instructions. Rapidly, TBS-T/BSA (10 mM Tris-HCl

pH 8, 150 mM NaCl, 0.1% Tween 20, 3% BSA) was used throughout the assay. Membranes were initially blocked with TBS-T/BSA for 1 hour, then incubated with 1 µg/mL of purified protein overnight at 4 °C. After three washes with TBS-T/BSA, membranes were immunoblotted with anti-HIS HRP-conjugated antibodies for 1 hour at room temperature. Following three washes with TBS-T/BSA, membranes were incubated with ECL for signal detection and visualized using a Chemidoc imaging system (Biorad).

In Vitro Cosedimentation Assays with Large Unilamellar Vesicles (LUVs)

To determine the binding of 6xHIS-CBU2007 to LUVs, different mixtures were made using PC, PS and LBPA at different molar ratios: 100/0/0; 90/10/0; 70/10/20 and 80/0/20. The preparation of lipid mixtures and experiment procedures were performed as previously described(4).

Macropinocytosis inhibition assay

U2OS cells were transfected for 8 hours with the appropriate plasmids, then washed 3 times with PBS pH 7.4 and incubated overnight with DMEM containing 50 µM 5-[N-ethyl-N-isopropyl] amiloride (EIPA, MERCK). Cells were then washed 3 times in PBS pH 7.4, fixed in PBS pH 7.4 containing 4% PFA and prepared for fluorescence microscopy as described above.

Dextran internalization assay

U2OS cells were transfected for 8 hours with the appropriate plasmids, then washed 3 times with PBS pH 7.4 and incubated overnight with DMEM containing 0.5 mg/ml 70 kDa TMR Dextran (Thermo Fisher Scientific). Cells were either imaged overnight or directly after being washed 3 times with PBS pH 7.4 24h post-transfection with a spinning disk Olympus SR microscope as described above.

Virion-Like Particles (VLPs) release assay

HEK293T cells were transfected with either scramble or TSG101 targeting siRNA for 24h using the RNAiMAX transfection reagent (Thermo Fisher Scientific) according to the manufacturer's recommendations. Cells were then transfected for 24h with plasmids expressing viral proteins in combination with plasmids expressing either the HA tag alone or HA-Vice. The culture medium of

transfected cells was clarified at 800 × g for 5 minutes at 4°C and VLPs were collected after ultracentrifugation at 100,000 × g for 90 minutes at 4°C in an SW41Ti rotor (Beckman Coulter) through a 25% sucrose cushion in TNE buffer (25 mM Tris-HCl, 4 mM EDTA, and 150 mM NaCl). The resulting pellets were resuspended overnight in TNE buffer at 4°C. To assess the release of Gag-VLPs, an anti-Cap24 immunoblot was performed on both supernatant and cell lysate. The calculation for Gag-VLP release was performed using the blot intensity module on Fiji software and applying the following formula: % of Gag in VLP = Gag released/(Gag released + Gag Intracellular normalized to GAPDH).

Acknowledgements

The authors are grateful to: Raphael Gaudin, Maïka Deffieu (IRIM CNRS UMR9004, Montpellier, France) and Cécile Gauthier-Rouvière (CRBM, CNRS UMR5237) for providing plasmids and for scientific discussions. We acknowledge the imaging facility MRI, member of the national infrastructure France-BioImaging supported by the French National Research Agency (ANR-10-INBS-04, «Investments for the future»). This work was supported by the French National Research Agency (ANR; ANR-17-CE15-0021, project QPiD).

References

1. E. Martinez, F. A. Siadous, M. Bonazzi, Tiny architects: biogenesis of intracellular replicative niches by bacterial pathogens. *Fems Microbiol Rev* 42, 425–447 (2018).
2. E. J. van Schaik, C. Chen, K. Mertens, M. M. Weber, J. E. Samuel, Molecular pathogenesis of the obligate intracellular bacterium Coxiella burnetii. *Nat Rev Microbiol* 11, 561–573 (2013).
3. C. L. Larson, *et al.*, Right on Q: genetics begin to unravel Coxiella burnetii host cell interactions. *Future Microbiol* 11, 919–939 (2016).
4. E. Martinez, et al., Coxiella burnetii effector CvpB modulates phosphoinositide metabolism for optimal vacuole development. *Proc National Acad Sci* 113, E3260–E3269 (2016).
5. E. J. van Schaik, E. D. Case, E. Martinez, M. Bonazzi, J. E. Samuel, The SCID Mouse Model for Identifying Virulence Determinants in Coxiella burnetii. *Frontiers Cell Infect Microbiol* 7, 25 (2017).
6. S. Jean, A. A. Kiger, Coordination between RAB GTPase and phosphoinositide regulation and functions. *Nat Rev Mol Cell Bio* 13, 463–470 (2012).
7. Y. Posor, W. Jang, V. Haucke, Phosphoinositides as membrane organizers. Nat Rev Mol Cell Bio 23, 797–816 (2022).
8. I. Vergne, et al., Mechanism of phagolysosome biogenesis block by viable Mycobacterium tuberculosis. *Proc. Natl. Acad. Sci.* 102, 4033–4038 (2005).
9. N. Beresford, et al., MptpB, a virulence factor from Mycobacterium tuberculosis, exhibits triple-specificity phosphatase activity. *Biochem J* 406, 13–18 (2007).
10. L. Toulabi, X. Wu, Y. Cheng, Y. Mao, Identification and Structural Characterization of a Legionella Phosphoinositide Phosphatase. *J Biol Chem* 288, 24518–24527 (2013).
11. G. V. Mallo, et al., SopB promotes phosphatidylinositol 3-phosphate formation on Salmonella vacuoles by recruiting Rab5 and Vps34. *J Cell Biology* 182, 741–752 (2008).
12. L. D. Hernandez, K. Hueffer, M. R. Wenk, J. E. Galán, Salmonella Modulates Vesicular *Traffic* by Altering Phosphoinositide Metabolism. *Science* 304, 1805–1807 (2004).
13. S. Dai, Y. Zhang, T. Weimbs, M. B. Yaffe, D. Zhou, Bacteria‐generated PtdIns(3)P Recruits VAMP8 to Facilitate Phagocytosis. Traffic 8, 1365–1374 (2007).
14. H. Matsuo, et al., Role of LBPA and Alix in Multivesicular Liposome Formation and Endosome Organization. Science 303, 531–534 (2004).
15. G. Kadamur, E. M. Ross, Mammalian Phospholipase C. *Annu. Rev. Physiol.* 75, 127–154 (2013).
16. C. Noroy, T. Lefrançois, D. F. Meyer, Searching algorithm for Type IV effector proteins (S4TE) 2.0: Improved tools for Type IV effector prediction, analysis and comparison in proteobacteria. *Plos Comput Biol* 15, e1006847 (2019).
17. Z. Lifshitz, et al., Computational modeling and experimental validation of the Legionella and Coxiella virulence-related type-IVB secretion signal. Proc National Acad Sci 110, E707–E715 (2013).
18. C. L. Larson, W. Pullman, P. A. Beare, R. A. Heinzen, Identification of Type 4B Secretion System Substrates That Are Conserved among Coxiella burnetii Genomes and Promote Intracellular Growth. *Microbiol Spectr*, e00696-23 (2023).
19. E. D. R. Case, et al., Primary Murine Macrophages as a Tool for Virulence Factor Discovery in Coxiella burnetii. *Microbiol. Spectr.* 10, e02484-21 (2022).
20. E. Martinez, F. Cantet, L. Fava, I. Norville, M. Bonazzi, Identification of OmpA, a Coxiella burnetii Protein Involved in Host Cell Invasion, by Multi-Phenotypic High-Content Screening. *Plos Pathog* 10, e1004013 (2014).

21. H. Götzke, et al., The ALFA-tag is a highly versatile tool for nanobody-based bioscience applications. *Nat Commun* 10, 4403 (2019).
22. M. Koivusalo, et al., Amiloride inhibits macropinocytosis by lowering submembranous pH and preventing Rac1 and Cdc42 signaling. *J. Cell Biol.* 188, 547–563 (2010).
23. F. J. Verweij, et al., LMP1 association with CD63 in endosomes and secretion via exosomes limits constitutive NF‐κB activation. *EMBO J.* 30, 2115–2129 (2011).
24. J. H. Hurley, A. K. Cada, Inside job: how the ESCRTs release HIV-1 from infected cells. *Biochem. Soc. Trans.* 46, 1029–1036 (2018).
25. J. E. Garrus, et al., Tsg101 and the Vacuolar Protein Sorting Pathway Are Essential for HIV-1 Budding. Cell 107, 55–65 (2001).
26. J. Gruenberg, Life in the lumen: The multivesicular endosome. Traffic 21, 76–93 (2020).
27. P. A. Vanlandingham, B. P. Ceresa, Rab7 Regulates Late Endocytic Trafficking Downstream of Multivesicular Body Biogenesis and Cargo Sequestration*. *J. Biol. Chem.* 284, 12110–12124 (2009).
28. M. Radulovic, et al., ESCRT‐mediated lysosome repair precedes lysophagy and promotes cell survival. *Embo J* 37 (2018).
29. L. L. Scheffer, et al., Mechanism of Ca2+-triggered ESCRT assembly and regulation of cell membrane repair. *Nat. Commun.* 5, 5646 (2014).
30. A. J. Jimenez, et al., ESCRT Machinery Is Required for Plasma Membrane Repair. Science 343, 1247136 (2014).
31. A. Mehra, et al., Mycobacterium tuberculosis Type VII Secreted Effector EsxH Targets Host ESCRT to Impair Trafficking. *PLoS Pathog.* 9, e1003734 (2013).
32. E. Mittal, et al., Mycobacterium tuberculosis Type VII Secretion System Effectors Differentially Impact the ESCRT Endomembrane Damage Response. *mBio* 9, e01765-18 (2018).
33. P. K. Anand, E. Anand, C. K. E. Bleck, E. Anes, G. Griffiths, Exosomal Hsp70 Induces a Pro-Inflammatory Response to Foreign Particles Including Mycobacteria. *Plos One* 5, e10136 (2010).
34. C. B. Read, et al., The Obligate Intracellular Bacterial Pathogen Anaplasma phagocytophilum Exploits Host Cell Multivesicular Body Biogenesis for Proliferation and Dissemination. mBio 13, e02961-22 (2022).
35. R. J. Bastidas, R. H. Valdivia, The emerging complexity of Chlamydia trachomatis interactions with host cells as revealed by molecular genetic approaches. *Curr. Opin. Microbiol.* 74, 102330 (2023).
36. K. L. Carey, H. J. Newton, A. Lührmann, C. R. Roy, The Coxiella burnetii Dot/Icm System Delivers a Unique Repertoire of Type IV Effectors into Host Cells and Is Required for Intracellular Replication. Plos Pathog 7, e1002056 (2011).
37. L. Klingenbeck, R. A. Eckart, C. Berens, A. Lührmann, The Coxiella burnetii type IV secretion system substrate CaeB inhibits intrinsic apoptosis at the mitochondrial level. *Cell Microbiol* 15, 675–687 (2013).
38. M. Rodríguez-Escudero, et al., Studying Coxiella burnetii Type IV Substrates in the Yeast Saccharomyces cerevisiae: Focus on Subcellular Localization and Protein Aggregation. Plos One 11, e0148032 (2016).
39. A. Friedrich, et al., The Coxiella burnetii effector protein CaeB modulates endoplasmatic reticulum (ER) stress signalling and is required for efficient replication in Galleria mellonella. Cell Microbiol 23, e13305 (2021).
40. M. Burette, et al., Modulation of innate immune signaling by a Coxiella burnetii eukaryotic-like effector protein. Proc National Acad Sci 117, 13708–13718 (2020).

Tables

Table S1. List of lipid-binding sensors and markers used in this study

Sensor/marker	Lipid	Source
2xFYVE	**PI(3)P**	pmCherry-2xFYVE was a gift from Harald Stenmark (Addgene plasmid # 140050 ; http://n2t.net/addgene:140050 ; RRID:Addgene_140050)
OSBP-PH	**PI(4)P**	pBGPa-CMV-GFP-OSBP PH was a gift from Tim Levine (Addgene plasmid # 58724 ; http://n2t.net/addgene:58724 ; RRID:Addgene_58724)
2xPHD	**PI(5)P**	GFP-2xPHD was a gift from Bernard Payrastre (Université de Toulouse)
Akt-PH	**PI(3,4)P_2/ PI(3,4,5)P_3**	GFP-C1-AKT-PH was a gift from Tobias Meyer (Addgene plasmid # 21218 ; http://n2t.net/addgene:21218 ; RRID:Addgene_21218)
ML1N-PH	**PI(3,5)P_2**	ML1Nwt_in_pEGFP-C1 was a gift from Rob Parton (Addgene plasmid # 67797 ; http://n2t.net/addgene:67797 ; RRID:Addgene_67797)
2xPLCδ-PH	**PI(4,5)P_2**	2PH-PLCdelta-GFP was a gift from Sergio Grinstein (Addgene plasmid # 35142 ; http://n2t.net/addgene:35142 ; RRID:Addgene_35142)
BTK-PH	**PI(3,4,5)P_3**	PH-Btk-GFP was a gift from Tamas Balla (Addgene plasmid # 51463 ; http://n2t.net/addgene:51463 ; RRID:Addgene_51463)
Gab2-PH	**PI(3,4,5)P_3**	PH-Gab2-GFP was a gift from Sergio Grinstein (Addgene plasmid # 35147 ; http://n2t.net/addgene:35147 ; RRID:Addgene_35147)
Lact-C2	**PS**	mRFP-Lact-C2 was a gift from Sergio Grinstein (Addgene plasmid # 74061 ; http://n2t.net/addgene:74061 ; RRID:Addgene_74061)
PKCɣ-C1A	**DAG**	GFP-C1-PKCgamma-C1A was a gift from Tobias Meyer (Addgene plasmid # 21205 ; http://n2t.net/addgene:21205 ; RRID:Addgene_21205)
Spo1op/Spo2op	**PA**	GFP-Spo1op and GFP-Spo2op were gifts from Nicolas Vitale (University of Strasbourg, FR)
anti-LBPA	**LBPA**	Purified Mouse Anti-LBPA antibodies were purchased from Echelon Biosciences (cat. N. Z-PLBPA)

Table S2. List of strains used in this study

Strain	Description	Origin
WT *C. burnetii*	*C. burnetii* RSA 439 Nine Mile II carrying a transposon insertion between *cbu1847b* and *cbu1849* (*Tn1832*)	Our Laboratory (Martinez *et al.* 2014)
C. burnetii Tn1577	*C. burnetii* RSA 439 Nine Mile II carrying a transposon insertion GFP-CAT in *cbu2007*	Our laboratory
C. burnetii Tn292	*C. burnetii* RSA 439 Nine Mile II carrying a transposon insertion GFP-CAT in *cbu1648* (*dotA*)	Our Laboratory (Martinez *et al.* 2014)
LEMO21(DE3)	*E. coli strain used for T7-driven recombinant protein expression*	New England Biolabs

Table S3. List of primers used in this study

Primer Name	Sequence
BLAM Translocation Assay	
Generation of pXDC61K-BLAM derivatives	
CBU2007-BamHI	AGGGGATCCATGACAGTTTATTCCCGATATGA
CBU2007-XbaI-rev	AGGTCTAGACTAAAGGGTCCGGTATTTGAAG
Ectopic Expression	
Generation of pLVX-mCherry-N2 derivatives	
PH-PLCδ-MluI	aggacgcgtatggactcgggccgg
PH-PLCδ-NotI-rev	agggcggccgctcgcatccatggagcctgagtggtg
PH-Btk-MluI	aggacgcgtatgcagaaagaagaagctatggcc
PH-Btk-NotI-rev	agggcggccgctcgaggttttaagcttccattcctgtt
Generation of pLVX-mCherry-C1 derivatives	
AKT-PH-EcoRI	agggaattcaaacgacgtagccattgtgaag
AKT-PH-BamHI-rev	aggggatccctatgaattccatggtcacacgg
PH-Gab2-EcoRI	agggaattcaatgagcggcggcggc
PH-Gab2-BamHI-rev	aggggatccttagaagccgcagatctggc
Generation of mCherry2-C1 derivatives	
OSBP-PH-HindIII	AAGCTTcatcggctcgagaggg
OSBP-PH-XmaI-rev	CCCGGGtcacgaattcttcttcacagct
ML1N-XhoI	CTCGAGGGtactctgacctgactatggcaacac
ML1N-XmaI-rev	aggtctagattaattatccaggtcaggggggg
PKCg-XhoI	CTCGAGctcacaagttcaccgctcg
PKCgamma-HpaI-rev	GTTAACctagatccggtggatccc
Generation of pRK5-HA derivatives	
CBU2007-BamHI-Fw	CCAGGATCCACAGTTTATTCCCGATATGAATTTC
CBU2007-HindIII-rev	GCTAAGCTTCTAAAGGGTCCGGTATTTGAAG

Generation of pRK5-HA-ALFA	
MluI-ALFA-Fw	CAAACGCGTATGCCATCACGTTTGGAAGAGGAACTGAGACG CCGCTTAACTGAACCTGGATCCCGGGTCGCGAATTC
MluI-pRK5-HA-Rv	CAAACGCGTCGCGCCAGCGTAATCTGGAAC

Generation of pCMV-NbALFA-mScarlet and pCMV-NbALFA-mNeonGreen	
Nanobody-EcoRI-Fw	GTAGAATTCTGGCTCTGGTGATGCATCTG
Nanobody-BamHI-Rv	GTTGGATCCTCAAGAAGTTTGTGGTTTTGGTGTCTTG

Generation of pET28a-GST	
GST-NheI-Fw	GAGTCAGCTAGCATG TCC CCT ATA CTA GGT TAT TGG
GST-BamHI-Rv	CAAGGATCCAACCAGATCCGATTTTGGAG

Table S4. List of plasmids used in this study

Name	Description	Origin
pXDC61K	IPTG-inducible expression vector for N-terminal fusion of Beta-lactamase (BLAM) in *C. burnetii*	(Burette *et al.* 2020)
pXDC61K-CBU0021	IPTG-inducible expression of BLAM-CBU0021 (CvpB)	(Martinez *et al.* 2016)
pXDC61K-CBU2007	IPTG-inducible expression of BLAM-CBU2007	This study
pLVX-mCherry-N2	CMV expression vector expressing a C-terminal mCherry tag	(Martinez *et al.* 2016)
mCherry2-C1	CMV expression vector expressing a N-terminal mCherry tag	Addgene plasmid # 54563 Michael Davidson
pCL-Neo-mCherry-2xFYVE	Encodes mCherry-2xFYVE (PI3P probe)	(Martinez *et al.* 2016)
mCh2-C1-OSBP-PH	Encodes mCherry-OSBP-PH (PI4P probe)	This study
mCherry-PHD2X	Encodes mCherry-2xPHD (PI5P probe)	Bernard Payrastre
pLVX-mCherry-AKT-PH	Encodes mCherry-AKT-PH ($PI3,4P_2$ probe)	This study
mCh2-C1-ML1N-PH	Encodes mCherry-ML1N-PH ($PI3,5P_2$ probe)	This study
pLVX-PLCδ-2xPH-mCherry	Encodes PLCδ-2xPH-mCherry ($PI4,5P_2$ probe)	This study
pLVX-mCherry-Gab2-PH	Encodes mCherry-Gab2-PH ($PI3,4,5P_3$ probe)	This study
pLVX-BTK-PH-mCherry	Encodes mCherry-BTK-PH ($PI3,4,5P_3$ probe)	This study
mRFP-Lactadherin-C2	Encodes RFP-Lactadherin-C2 (PS probe)	Addgene # 74061 Sergio Grinstein
GFP-Lactadherin-C2	Encodes GFP-Lactadherin-C2 (PS probe)	Addgene #22852 Sergio Grinstein
mCh2-C1-PKCɣ-PH	Encodes mCherry-PKCɣ-PH (DAG probe)	This study
Spo2op1-DsRed	Encodes spo2op1-DsRed (PA probe)	Nicolas Vitale
Spo2op2-RFP	Encodes spo2op2-RFP (PA probe)	Nicolas Vitale
pRK5-HA	CMV expression vector for N-terminal fusion of HA tag	(Martinez *et al.* 2016)
pRK5-HA-ALFA	CMV expression vector for N-terminal fusion of HA-ALFA tag	This study
pRK5-HA-Vice	CMV expression vector expressing *cbu2007* with N-terminal fusion of HA tag	This study
pRK5-HA-ALFA-Vice	CMV expression vector expressing *cbu2007* with N-terminal fusion of HA-ALFA tag	This study

pLVX-GFP-N2	CMV expression vector for C-terminal fusion of GFP	(Burette *et al.*, 2020)
peGFP-RAB7	Encodes human *rab7* with N-terminal fusion of GFP tag	Addgene #61803 Gia Voeltz
pTO_CHMP3_LAP_EGFP	Encodes human *chmp3* with N-terminal fusion of GFP tag	Addgene #101849 Daniel Gerlich
pALIX_FLAG_GFP	Encodes human *alix* with N-terminal fusion of GFP tag	Aurélien Roux (Larios *et al.* 2020)
pTWIST_2007	Encodes *6x**HIS-cbu2007* codon optimized for expression in *E. coli*	Renaud Vincentelli
pET28b_GST	Encodes 6x*HIS-gst*	This study
pCMV-NbALFA-mScarlet	Encodes mScarlet-tagged nanobodies targeting ALFA	This study
pCMV-NbALFA-mNeonGreen	Encodes mNeonGreen-tagged nanobodies targeting ALFA	This study
pmCherry-CHMP4B	Encodes human *chmp4b* with C-terminal fusion of mCherry tag	Aurélien Roux (Larios *et al.* 2020)
pCMVGag	Encodes for HIV-1 Gag gene	Delphine Muriaux (Burniston *et al.* 1999)
pLifeact-EGFP	Encodes the GFP-tagged Lifeact peptide.	Delphine Muriaux

Figures legend

Figure 1: Lipid profiling of *Coxiella*-containing vacuoles identifies CBU2007 as an effector required for LBPA localization. (A) U2OS cells were infected with *Coxiella dotA*::Tn (bottom panel) or WT *Coxiella* (upper panel) for 2, 4 and 6 days and transfected with plasmids encoding a mCherry/RFP-tagged catalogue of lipid-binding sensors or labeled with an anti-LBPA antibody. The percentage of cells presenting CCVs positive for the indicated lipids was visually scored. Values are means ± standard deviation of duplicate experiments where 100 cells were scored for each condition, DPI: days post-infection. (B) Representative images of U2OS cells treated as described in (A) (*C. burnetii* is pseudocolored in red, lipid-binding sensors or LBPA labeling are pseudocolored in white). (C) U2OS cells were infected for 4 days either with a library of mutants carrying transposon insertions in validated or predicted effector-coding genes, with wt *C. burnetii* as positive control, or with the *dotA*::Tn mutant as a negative control, fixed and labeled with an anti-LBPA antibody. The presence of LBPA at the CCV was visually scored and ranked as compared to wt *C. burnetii* infected cells: Unaltered LBPA labeling of CCVs (blue), partial loss of LBPA labeling (pink) and complete loss of LBPA labeling (purple). (D) U2OS cells infected for 4 days either with wt *C. burnetii* (upper panel, grey) or the *cbu2007*::Tn mutant (bottom panel, grey) were labeled with Hoechst (blue), anti-LAMP1 (cyan) and anti-LBPA (magenta) antibodies. (E) The fluorescence intensity of LAMP1 (cyan) and LBPA (magenta) was measured along the red dash lines from (D). (F) The area of CCVs harboring either wt *C. burnetii* (WT) or the *cbu2007*::Tn mutant strain (*cbu2007*::Tn) was measured using LAMP1 labeling from U2OS cells infected for 4 days. Values are means ± standard deviation of three independent experiments (****P<0,0002; Unpaired t-test).(G) Proteolysis of cathepsin B-Magic Red was measured for individual CCVs at 4 days post-infection (dpi). Values are means ± standard deviation of three independent experiments (ns: non-significant; Unpaired t-test). (H) Representative electron micrographs of U2OS cells infected with wt *C. burnetii* (left panel) or the *cbu2007*::Tn mutant strain (right panel). The red inset shows an enlarged view of the CCV generated by the *cbu2007*::Tn mutant strain. (I) CFU counts from U2OS cells challenged with the *C. burnetii cbu2007*::Tn mutant strain for 3 and 6 days, normalized by the corresponding cells challenged with wt bacteria. Scale bars: 10 µm

Figure 2: CBU2007/Vice is a lipid-binding effector involved in CCV biogenesis and LBPA enrichment.

(A) Representative protein/lipid overlay assay performed with 6xHIS-CBU2007. (B) Representative Western blot of large unilamellar vesicles (LUVs) co-sedimentation assay using 6xHIS-CBU2007. CBU2007 in the pellet (P; bound to LUVs) or the supernatant (SN; unbound to LUVs) was detected using an anti-Histidine antibody. (C) CBU2007/LUVs binding was determined by measuring CBU2007 signal detected in (B) and using the following formula : ($P_{intensity}$ / ($P_{intensity}$ + $SN_{intensity}$))*100. Values are means ± standard deviation of three independent experiments (***P<0,0001; ns: non-significant. One-way ANOVA, Dunnett's multiple comparisons test). (D) Representative brightfield image of U2OS cells transfected for 24 hours with plasmids encoding HA-Vice (CBU2007, scale bar: 20 µm). (E) Correlative Light-Electron Microscopy (CLEM) of U2OS cells co-transfected for 24h with plasmids encoding HA-ALFA-Vice and NbALFA-mScarlet. Cells were first imaged using confocal microscopy to identify the cell of interest (Vice inset) followed by fixation for electron microscopy ((1) scale bar: 5 µm; (2) scale bar: 2 µm; (3) scale bar: 1 µm). (F) U2OS cells transfected with a plasmid encoding HA-Vice (magenta) and labeled with anti-LBPA antibodies (cyan) present Vice-induced compartments (VICs, white arrows). (G) U2OS cells transfected with a plasmid encoding HA-Vice (magenta) and labeled with anti-LAMP1 antibodies (cyan) indicate that VICs are positive for LAMP1 (white arrows). Hoechst was used to label nuclei (white) in all conditions. Scale bars: 10 µm. (H) The median size of LAMP1-positive compartments in U2OS cells expressing either HA-tag alone or HA-Vice was measured using CellProfiler. Each spot represents a LAMP1-positive compartment from three independent experiments (blue, pink, red; ****P<0,0001, unpaired t-test).

Figure 3: Vice stimulates macropinocytosis and perturbs the localization of ESCRT machinery components.

(A) Representative images from Movie S1 illustrating U2OS cells co-transfected with plasmids encoding HA-ALFA-Vice and NbALFA-mScarlet and imaged after 8 hours in phase contrast (upper

panels) and 555 nm emission (lower panels) channels. Scale bars: 4 µm. (B) Representative images from Movie S6 illustrating U2OS cells co-transfected with plasmids encoding HA-ALFA-Vice and NbALFA-mNeonGreen for 8 hours prior to TMR-Dextran addition. Images were acquired every minute overnight in 555 nm emission (upper panel) and 488 nm emission (lower panel) channels. Scale bars: 4 µm. (C) U2OS cells transfected with a plasmid encoding HA-Vice were incubated overnight with either methanol (Mock, upper panel) or EIPA (lower panel). VIC formation was assessed by using Hoechst to label nuclei (white), anti-HA (magenta) and anti-LAMP1 antibodies (cyan). White arrows point at VICs; scale bars: 20 µm. (D) The percentage of cells described in (C) containing VICs was visually scored. Values are means ± standard deviation of three independent experiments (****P<0,0001, unpaired t-test). U2OS cells were either transfected with plasmids encoding HA-Vice and labeled with Hoechst (white), anti-HA (magenta) and anti-TSG101 (cyan, E) antibodies or co-transfected with plasmids encoding HA-Vice and CHMP3-GFP (cyan, F) or mCherry-CHMP4B (cyan, G). Hoechst was used to label nuclei (white) and anti-HA antibody was used to label Vice-transfected cells (magenta). White arrows point at VICs, scale bars: 10 µm.

Figure 4: Vice inhibits the activity of the ESCRT machinery.

(A) U2OS cells were co-transfected with plasmids encoding GFP-ALIX (cyan), NbALFA-mScarlet (magenta) and either HA-ALFA (left panel)s or HA-ALFA-Vice (right panels). (B) The percentage of cells presenting GFP-ALIX dots in cells treated as in (A), was visually scored. (C) U2OS cells infected for 4 days with either WT *Coxiella* or *vice*::Tn *C. burnetii* mutant were transfected for 24h with a plasmid encoding GFP-ALIX and the number of GFP-ALIX dots in non-infected (NI) and infected cells was visually scored. (D) GFP-ALIX localization at CCVs was visually scored in both infection conditions described in (C). Values are means ± standard deviation of three independent experiments (****P<0,0001, unpaired t-test for B and D, One-way ANOVA, Dunnett's multiple comparisons test for C). (E) Representative images of U2OS cells infected for 4 days with either WT *Coxiella* or *vice*::Tn *C. burnetii* mutant and transfected for 24h with a plasmid encoding GFP-ALIX (magenta). After fixation, cells were labeled with Hoechst (white), anti-*C. burnetii*

(green) anti-LAMP1 antibodies (cyan). Scale bars: 20 µm. (F) U2OS cells infected for 4 days with either WT *Coxiella* or *vice*::Tn *C. burnetii* mutant (green) were labeled with Hoechst (white), anti-LAMP1 (cyan) and anti-CD63 (magenta). (G) Representative distribution of LAMP1 (cyan) and CD63 (magenta) fluorescence intensity was measured along the corresponding red dash lines illustrated in (F). Scale bars: 20 µm. (H) HEK293T were co-transfected with plasmids encoding either HA or HA-Vice and GAG, or transfected with plasmids encoding GAG, 24 hours after transfection with either TSG101-targeting siRNAs (siTSG101) or scrambled siRNA (siCTRL). Virus-like particles (VLP) release was assessed by Western blot using anti-p24 antibodies and the relative percentage of VLPs was measured using ImageJ. Anti-HA, anti-TSG101 and anti-GAPDH were used as controls (WCL: whole cell lysate). (I) p24 signal from triplicates experiments as in (H) was quantified using the following formula: ($VLPs_{p24_intensity}$ / ($VLPs_{p24_intensity}$ + $Cells_{p24_intensity}$)). Values are means ± standard deviation of three independent experiments (**P<0,001, ns: non-significant, One-way ANOVA, Dunnett's multiple comparisons test).

Supplementary Figures legends

Supplementary Figure 1: Lipid composition of wt and *dotA::Tn Coxiella*-Containing Vacuoles. (A) U2OS cells were infected with wt *C. burnetii* (red) and transiently transfected with the indicated mCherry/RFP-tagged lipid-binding sensors (white). (B) U2OS cells were challenged for 4 days with the Dot/Icm defective *dotA::Tn C. burnetii* mutant strain (blue) and transfected with either mCherry/RFP-tagged lipid-binding sensors or labeled with an anti-LBPA antibody (red). Cells were fixed and stained with an anti-LAMP1 antibody (green). White arrows indicate *C. burnetii* colonies. Scale bars: 10 µm.

Supplementary Figure 2: LBPA does not localize to *cbu2007*::Tn mutant strain CCVs.
Representative images of U2OS cells infected for 4 days either with WT *C. burnetii*, the *cbu0635*::Tn, *cbu0505*::Tn or *cbu2007*::Tn mutant strains. Cells were processed for microscopy using Hoechst (white), anti-LBPA (pink), and anti-LAMP1 (cyan).

Supplementary Figure 3: Vice is a T4SS-dependent effector protein required for LBPA recruitment to CCVs.

(A) U2OS cells were infected for 4 days with the *vice*::Tn *C. burnetii* mutant strain (white) and transfected either with HA alone (upper panel) or HA-Vice for 24 hours (lower panel). Cells were fixed and labeled with anti-LBPA (magenta) and anti-HA (cyan) antibodies. Scale bar: 10 µm. (B) The fluorescence intensity of LBPA (magenta) was measured along the red dash lines illustrated in (A) using ImageJ. (C) Southern blot analysis of the *cbu2007*::Tn *C. burnetii* mutant strain *Tn1577* genomic DNA digested with BamHI and probed with a GFP probe. The unique band observed confirms the unique insertion of the transposon in the *cbu2007*::Tn mutant genome. (D) Lysates of wt *C. burnetii* GFP (WT) or the *dotA*::Tn mutant strain transformed with pXDC61K vectors expressing BLAM alone, BLAM-CvpB or BLAM-CBU2007/Vice were probed using anti-BLAM and anti-*C. burnetii* (NMII) antibodies by Western blot. The expected size of BLAM-tagged proteins is indicated below the top blot. (E) U2OS cells were challenged for 24 h, 48 h or 72 h either with wt *C. burnetii* GFP (WT) or the *dotA*::tn *C. burnetii* mutant strain transformed either with vectors expressing BLAM alone (negative control), BLAM-CvpB (positive control) or BLAM-CBU2007/Vice. Effector protein translocation was probed using the □-Lactamase assay. The average percentage of infected cells positive for cleaved CCF-4 was automatically calculated using CellProfiler over the total number of infected cells per each condition. Values are mean ± SD from 3 independent experiments (n.s.: non-significant, ****P<0.0001, one-way ANOVA, Bonferroni's multiple comparison test). (F) Protein-lipid overlay assay performed with 6xHIS-GST as the control for the overlay illustrated in Fig 2A.

Supplementary Figure 4: Vice-induced vacuoles (VICs) are positive for phosphatidylserine but negative for Lysotracker.

(A) U2OS cells transfected with plasmids encoding HA-Vice (magenta) and GFP-Lact-C2 (cyan) indicate that VICs (white arrows) are enriched in phosphatidylserine. (B) U2OS cells transfected with a plasmid encoding HA-Vice were incubated with 1 µM Lysotracker (red) for 1 hour, fixed and

immunolabeled with anti-HA (white) and anti-LAMP1 (cyan) antibodies. Nuclei were labeled using Hoechst (blue). Scale bars, 20 µm.

Supplementary Figure 5: **Vice stimulates macropinocytosis.**

(A) U2OS cells co-transfected with plasmids encoding HA-ALFA-Vice and NbALFA-mScarlet for 8 hours prior to images acquisition in phase contrast (left panel) and 555 nm emission (right panel) channels. (B-D) Representative images from Movies S3 to S5 illustrating U2OS cells co-transfected with plasmids encoding HA-ALFA-Vice, NbALFA-mScarlet and either 2xPLCδ-GFP (B, Movie S3), Lifeact-GFP (C, Movie S4) and GFP-RAB7 (D, Movie S5). After 8 hours post-transfection, images were acquired every minute overnight in 555 nm emission (lower panel) and 488 nm emission (upper panel) channels. Scale bars: 4 µm.

Supplementary Figure 6: **VICs are positive for RAB7**

(A) U2OS cells transfected with plasmids encoding HA-Vice (magenta) and GFP-RAB7 (cyan) indicate that RAB7 localizes to VICS (white arrows). Nuclei were labeled using Hoechst (blue) (B) U2OS cells were either transfected with a plasmid encoding HA and labeled with anti-TSG101 antibodies (upper panels, cyan, scale bar: 20 µm) or co-transfected with plasmids encoding HA and CHMP3-GFP (middle panels, cyan, scale bar: 10 µm) or co-transfected with plasmids encoding HA and mCherry-CHMP4B (bottom panels, cyan, scale bar: 20 µm). In all conditions, Hoechst was used to label nuclei (white) and anti-HA antibody was used to label HA-transfected cells (magenta).

Supplementary Figure 7: Vice is required for recruitment of CD63 at CCVs

(A) U2OS cells were transfected with plasmids encoding either HA or HA-Vice (magenta) and labeled with an anti-CD3 antibody (cyan). CD63 localizes to VICs (white arrows). Hoechst was used to label nuclei (white). (B) U2OS cells were infected with the *vice*::Tn mutant strain (white) for 4 days and transfected with plasmids encoding either the HA tag alone (upper panels) or HA-Vice (lower panels) for 24 hours. Cells were fixed and labeled with anti-CD63 (magenta) and anti-HA

(cyan) antibodies. (C) Representative distribution of CD63 (magenta) fluorescence intensity was measured along the corresponding yellow dashed lines illustrated in (B). Scale bar: 5 µm.

Supplementary movies legends

Movie S1: U2OS cells co-transfected with plasmids encoding HA-ALFA-Vice and NbALFA-mScarlet were imaged after 8 hours in phase contrast (left panel) and 555 nm emission (right panel) channels. Images were acquired every minute for 2h and 20 min.

Movie S2: U2OS cells co-transfected with plasmids encoding HA-ALFA-Vice and NbALFA-mScarlet were imaged after 24 hours in phase contrast channels. Images were acquired every minute for 10h and 33 min.

Movie S3: U2OS cells co-transfected with plasmids encoding the $PI(4,5)P_2$ sensor 2xPLCδ-GFP (left panel, cyan), HA-ALFA-Vice and NbALFA-mScarlet (middle panel, magenta) were imaged after 8 hours. Images were acquired every minute for 26 min.

Movie S4: U2OS cells co-transfected with plasmids encoding Lifeact-GFP (left panel, cyan), HA-ALFA-Vice and NbALFA-mScarlet (middle panel, magenta) were imaged after 8 hours. Images were acquired every minute for 4h and 43 min.

Movie S5: U2OS cells co-transfected with plasmids encoding GFP-RAB7 (left panel, cyan), HA-ALFA-Vice and NbALFA-mScarlet (middle panel, magenta) were imaged after 8 hours. Images were acquired every minute for 1h and 30 min.

Movie S6: U2OS cells co-transfected with plasmids encoding HA-ALFA-Vice and NbALFA-mNeonGreen (middle panel, magenta) for 8 hours were incubated overnight with TMR-Dextran (cyan, left panel). Images were acquired every minute for 2h and 28 min.

Figure 1

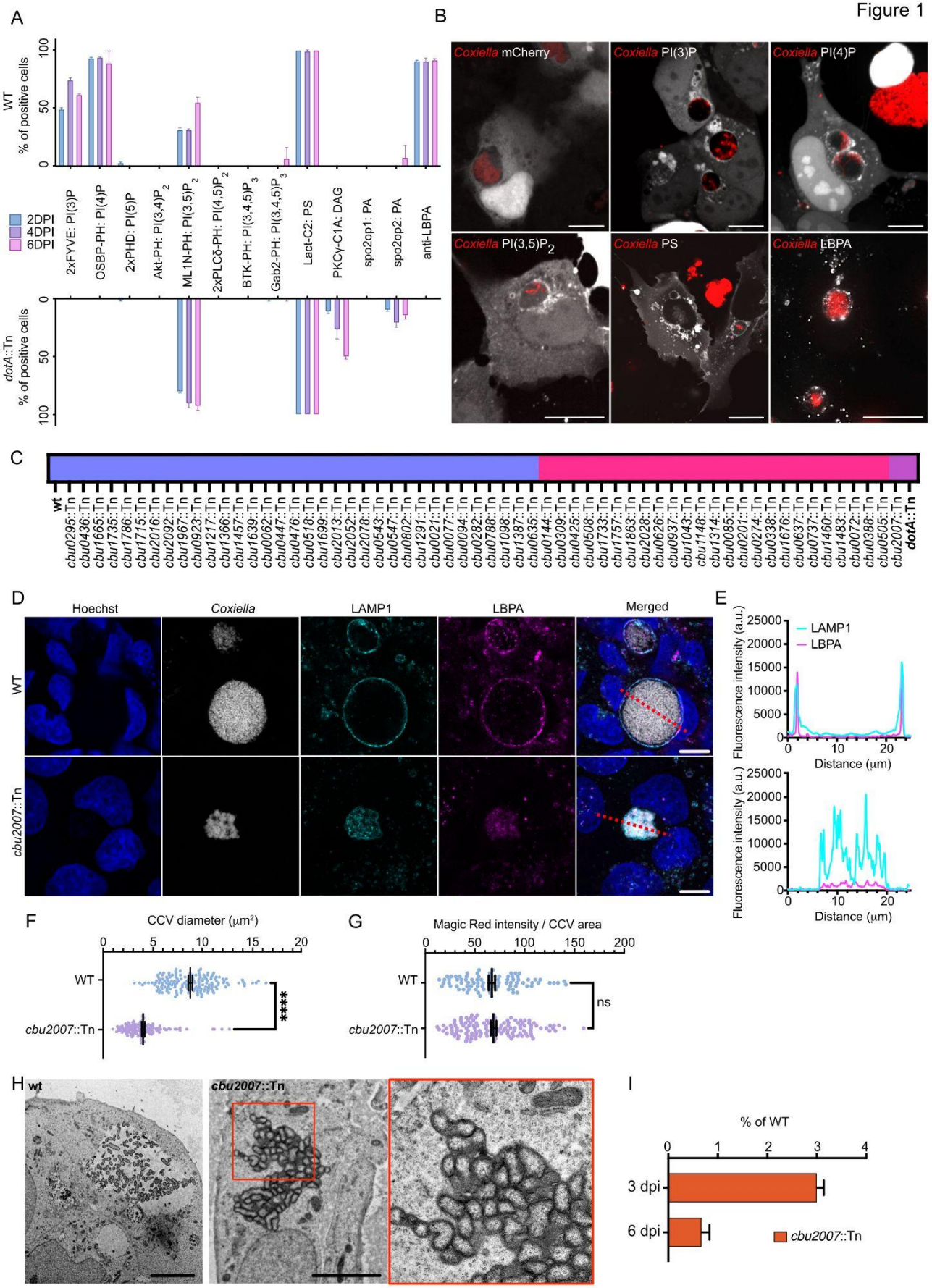

A
B
C
D
E
F
G
H
I
WT
% of positive cells
dotA::Tn
2DPI
4DPI
6DPI
2xFYVE: PI(3)P
OSBP-PH: PI(4)P
2xPHD: PI(5)P
Akt-PH: PI(3,4)P2
ML1N-PH: PI(3,5)P2
2xPLCδ-PH: PI(4,5)P2
BTK-PH: PI(3,4,5)P3
Gab2-PH: PI(3,4,5)P3
Lact-C2: PS
PKCγ-C1A: DAG
spo2op1: PA
spo2op2: PA
anti-LBPA
Coxiella mCherry
Coxiella PI(3)P
Coxiella PI(4)P
Coxiella PI(3,5)P2
Coxiella PS
Coxiella LBPA
wt
dotA::Tn
Hoechst
Coxiella
LAMP1
LBPA
Merged
cbu2007::Tn
Fluorescence intensity (a.u.)
Distance (μm)
CCV diameter (μm²)
Magic Red intensity / CCV area
****
ns
wt
cbu2007::Tn
% of WT
3 dpi
6 dpi

Figure 2

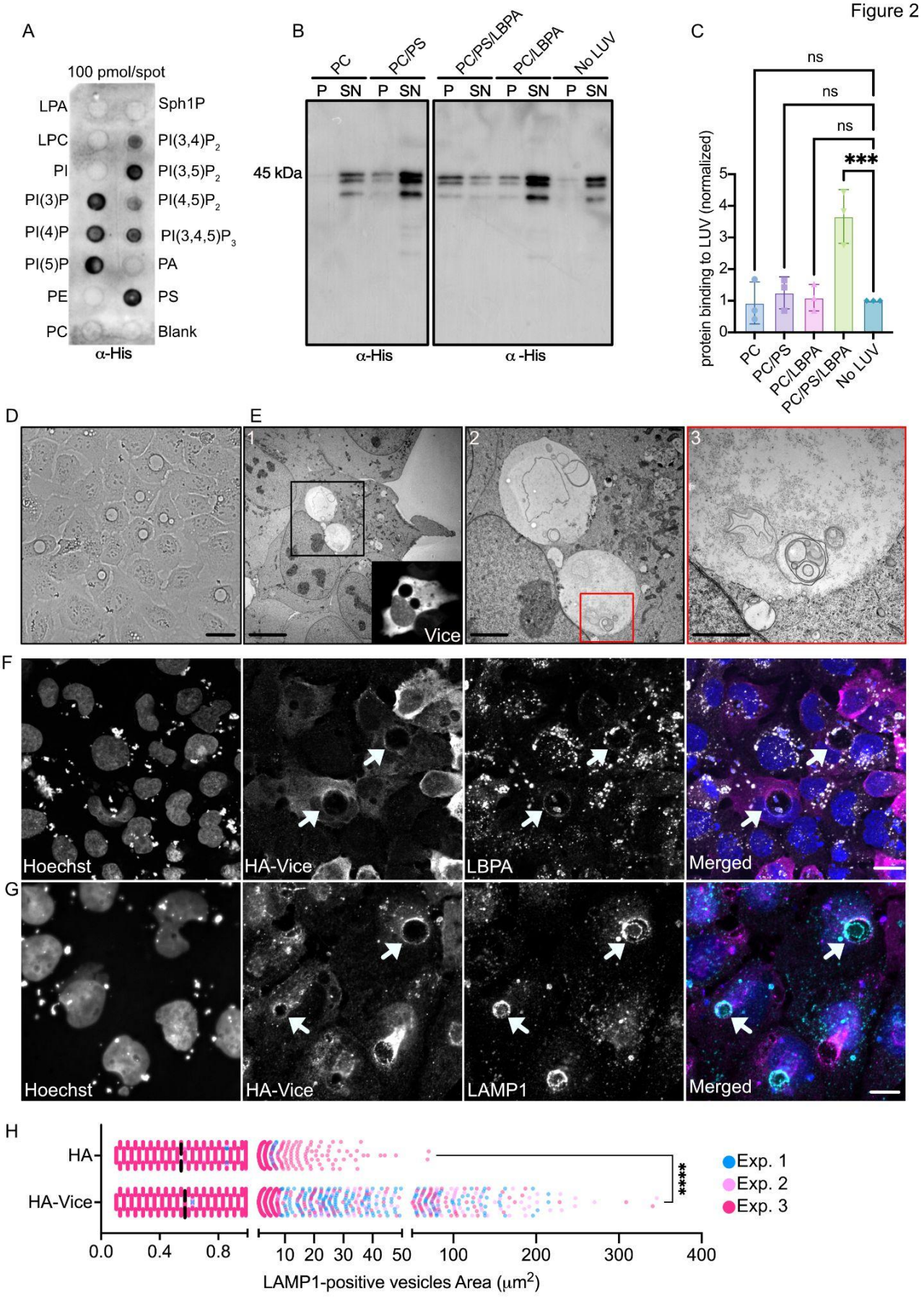

A
100 pmol/spot
LPA
LPC
PI
PI(3)P
PI(4)P
PI(5)P
PE
PC
Sph1P
PI(3,4)P2
PI(3,5)P2
PI(4,5)P2
PI(3,4,5)P3
PA
PS
Blank
α-His
B
PC
PC/PS
PC/PS/LBPA
PC/LBPA
No LUV
P SN P SN P SN P SN P SN
45 kDa
α-His
α -His
C
ns
ns
ns
***
protein binding to LUV (normalized)
0
1
2
3
4
5
PC
PC/PS
PC/LBPA
PC/PS/LBPA
No LUV
D
E
1
2
3
Vice
F
Hoechst
HA-Vice
LBPA
Merged
G
Hoechst
HA-Vice
LAMP1
Merged
H
HA
HA-Vice
****
Exp. 1
Exp. 2
Exp. 3
0.0
0.4
0.8
10
20
30
40
50
100
200
300
400
LAMP1-positive vesicles Area (μm2)

Figure 3

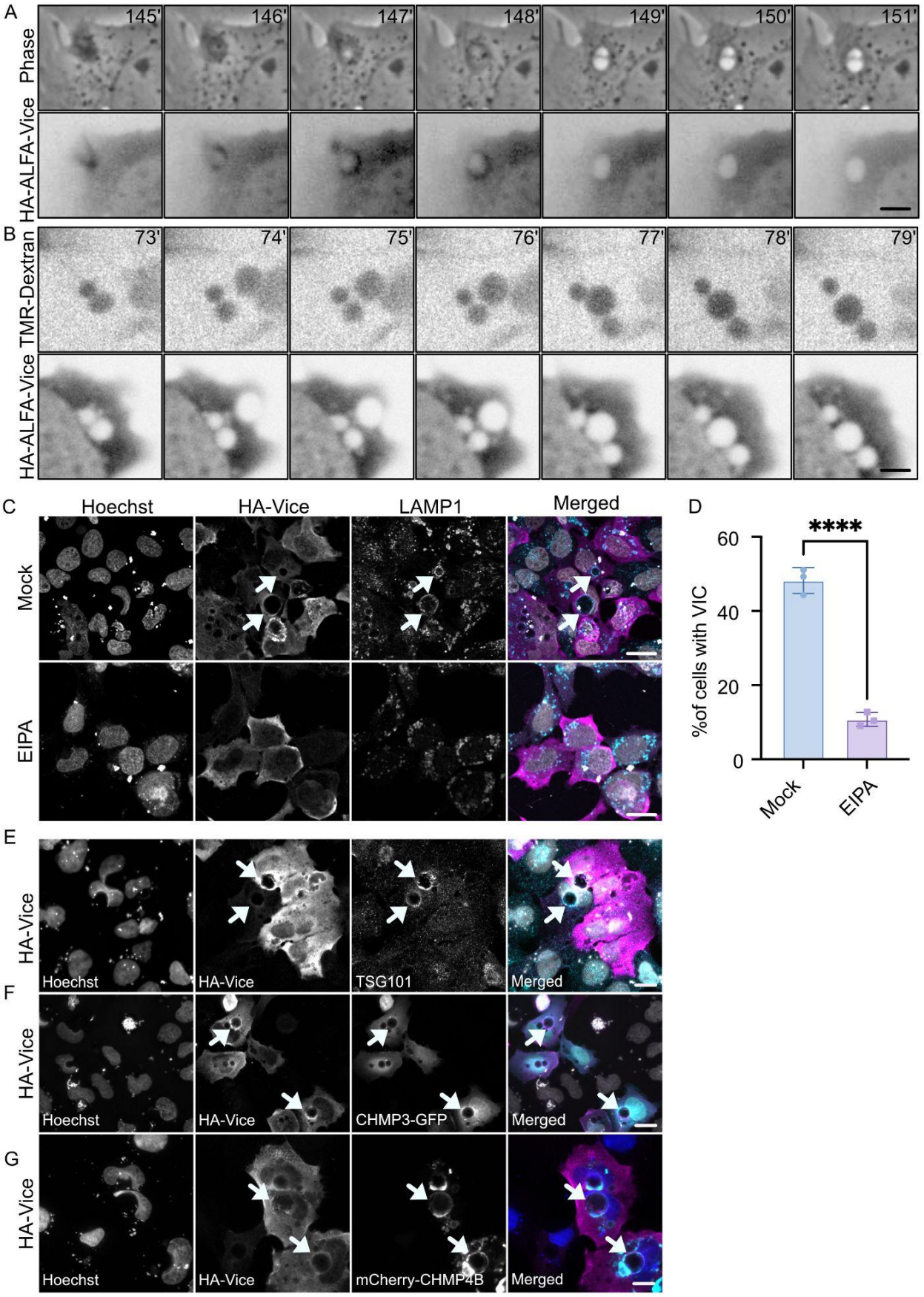
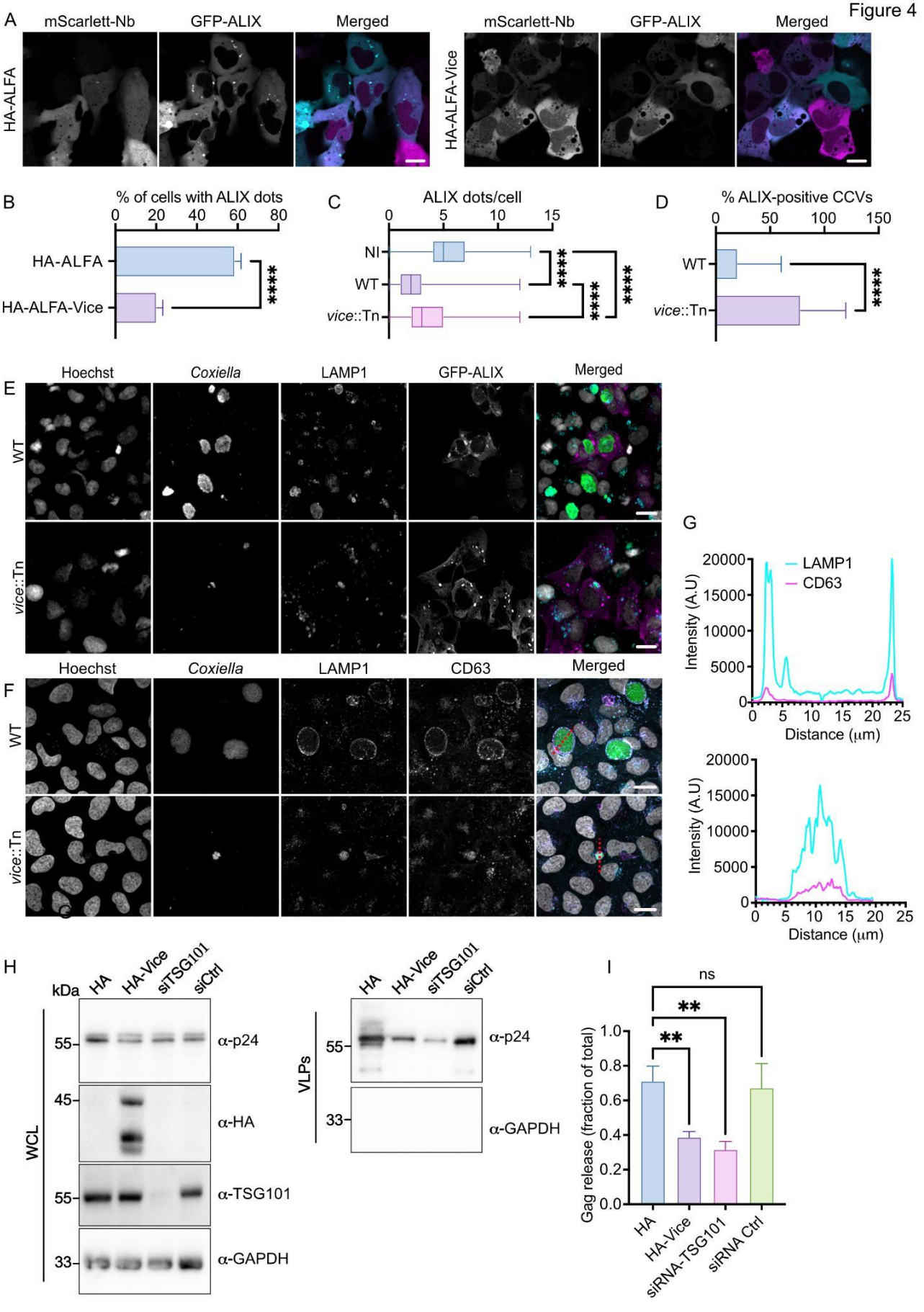
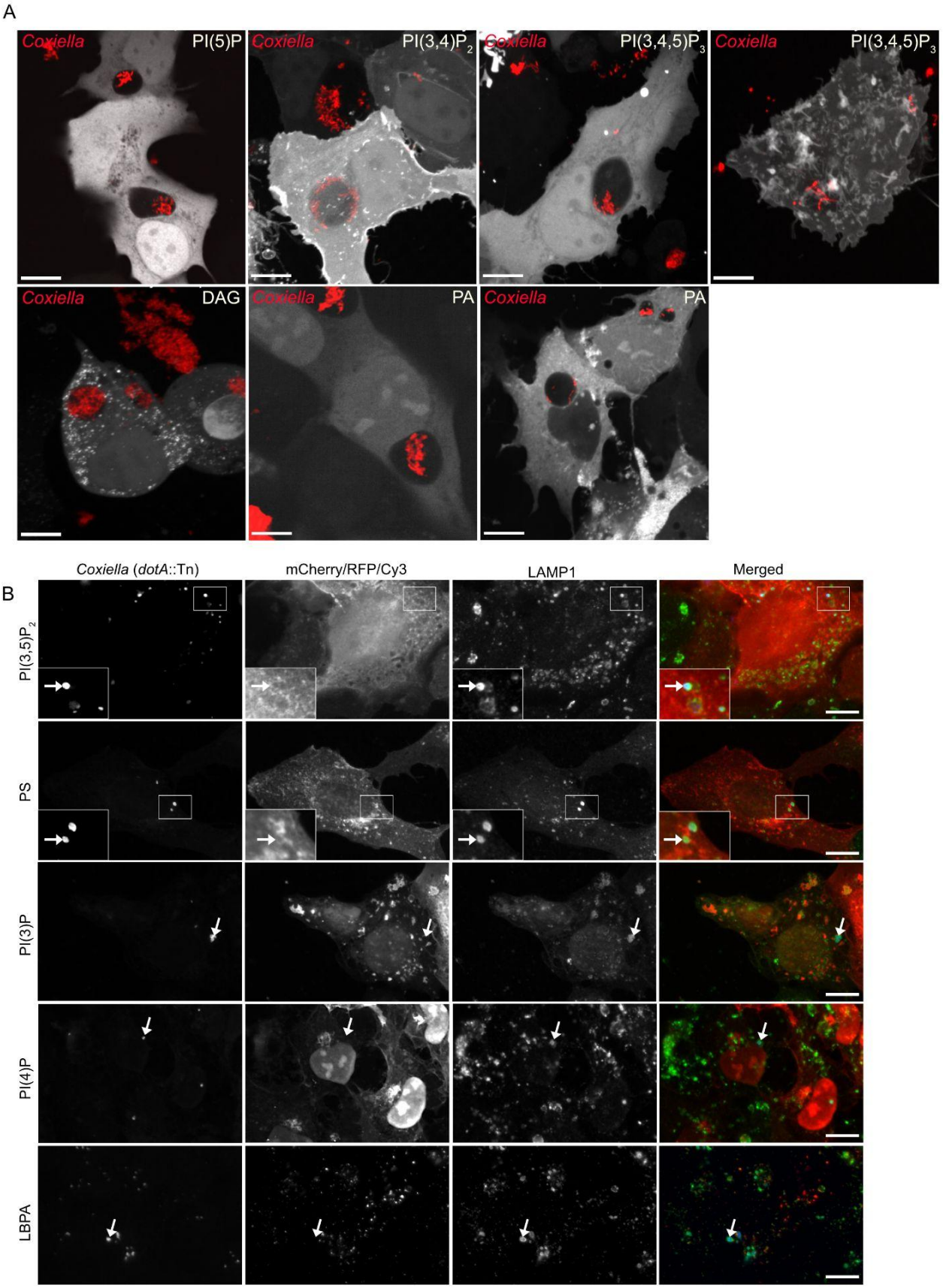

A
Phase
HA-ALFA-Vice
145'
146'
147'
148'
149'
150'
151'
B
TMR-Dextran
HA-ALFA-Vice
73'
74'
75'
76'
77'
78'
79'
C
Hoechst
HA-Vice
LAMP1
Merged
Mock
EIPA
D
%of cells with VIC
60
40
20
0
****
Mock
EIPA
E
HA-Vice
Hoechst
HA-Vice
TSG101
Merged
F
HA-Vice
Hoechst
HA-Vice
CHMP3-GFP
Merged
G
HA-Vice
Hoechst
HA-Vice
mCherry-CHMP4B
Merged

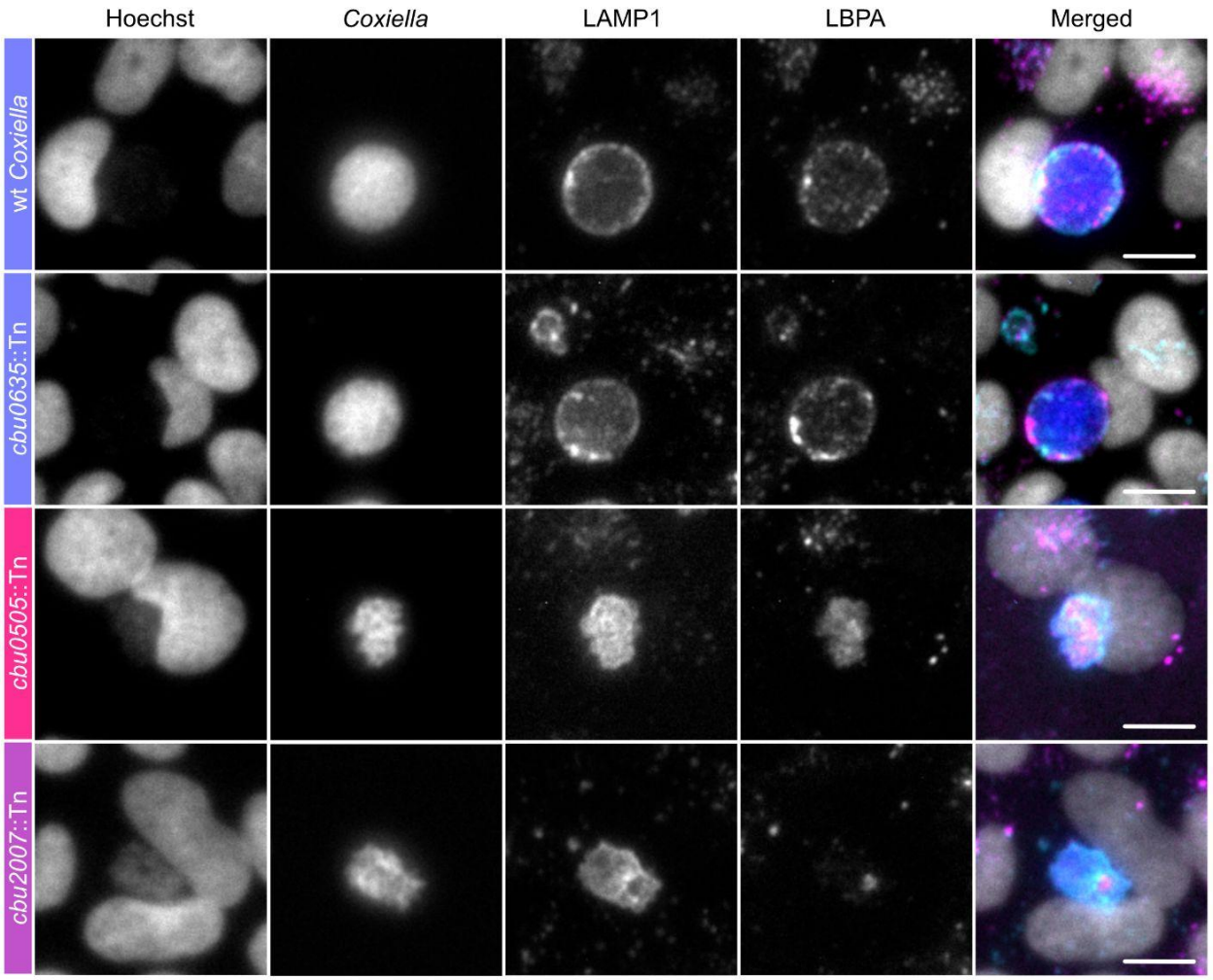
Figure 4


A
mScarlett-Nb
GFP-ALIX
Merged
HA-ALFA
HA-ALFA-Vice
B
% of cells with ALIX dots
HA-ALFA
HA-ALFA-Vice
C
ALIX dots/cell
NI
WT
vice::Tn
D
% ALIX-positive CCVs
WT
vice::Tn
E
Hoechst
Coxiella
LAMP1
GFP-ALIX
Merged
WT
vice::Tn
F
Hoechst
Coxiella
LAMP1
CD63
Merged
G
LAMP1
CD63
Intensity (A.U)
Distance (μm)
H
kDa
HA
HA-Vice
siTSG101
siCtrl
WCL
VLPs
α-p24
α-HA
α-TSG101
α-GAPDH
I
Gag release (fraction of total)
ns
HA
HA-Vice
siRNA-TSG101
siRNA Ctrl

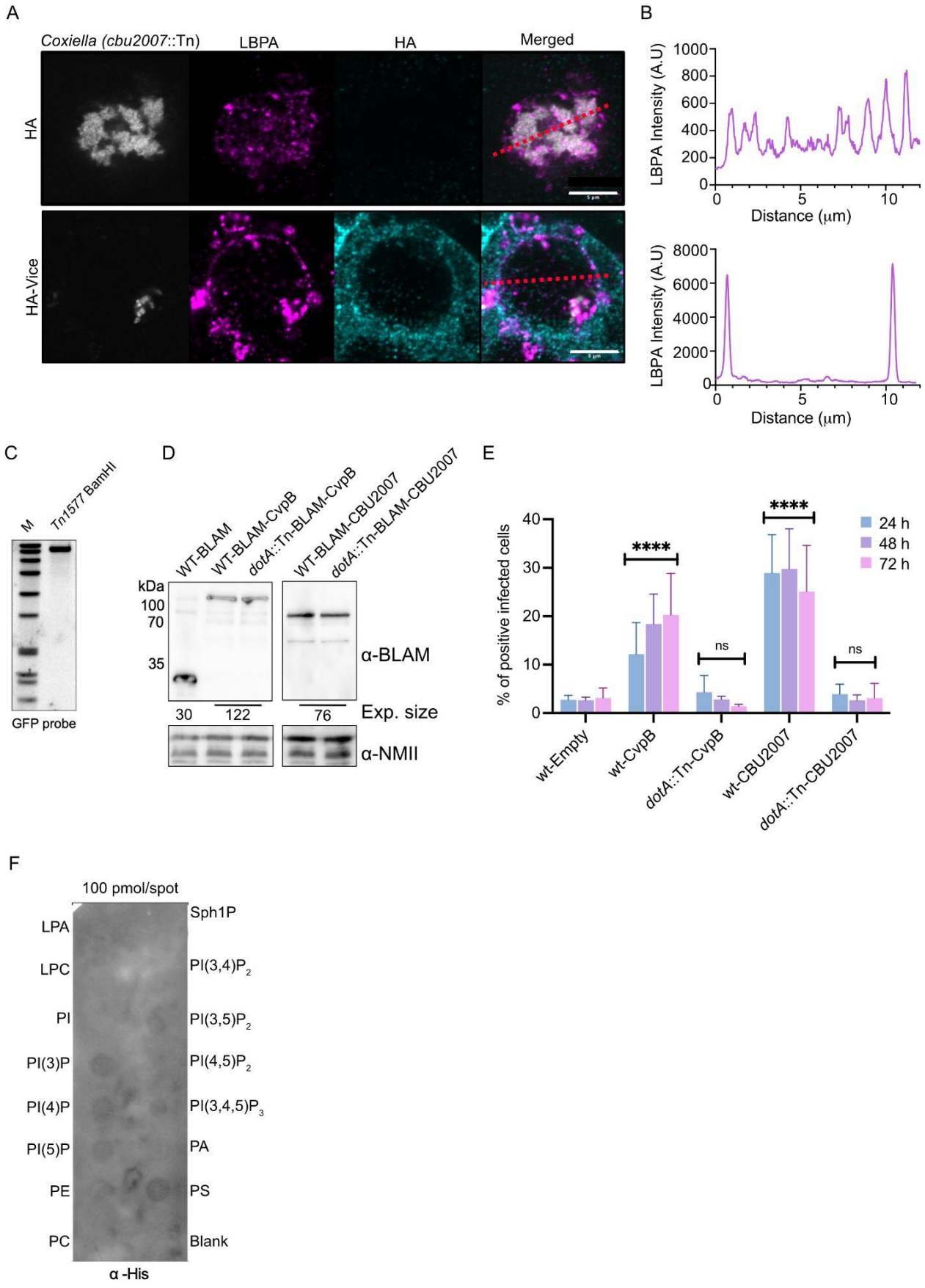
Supplementary Figure 1



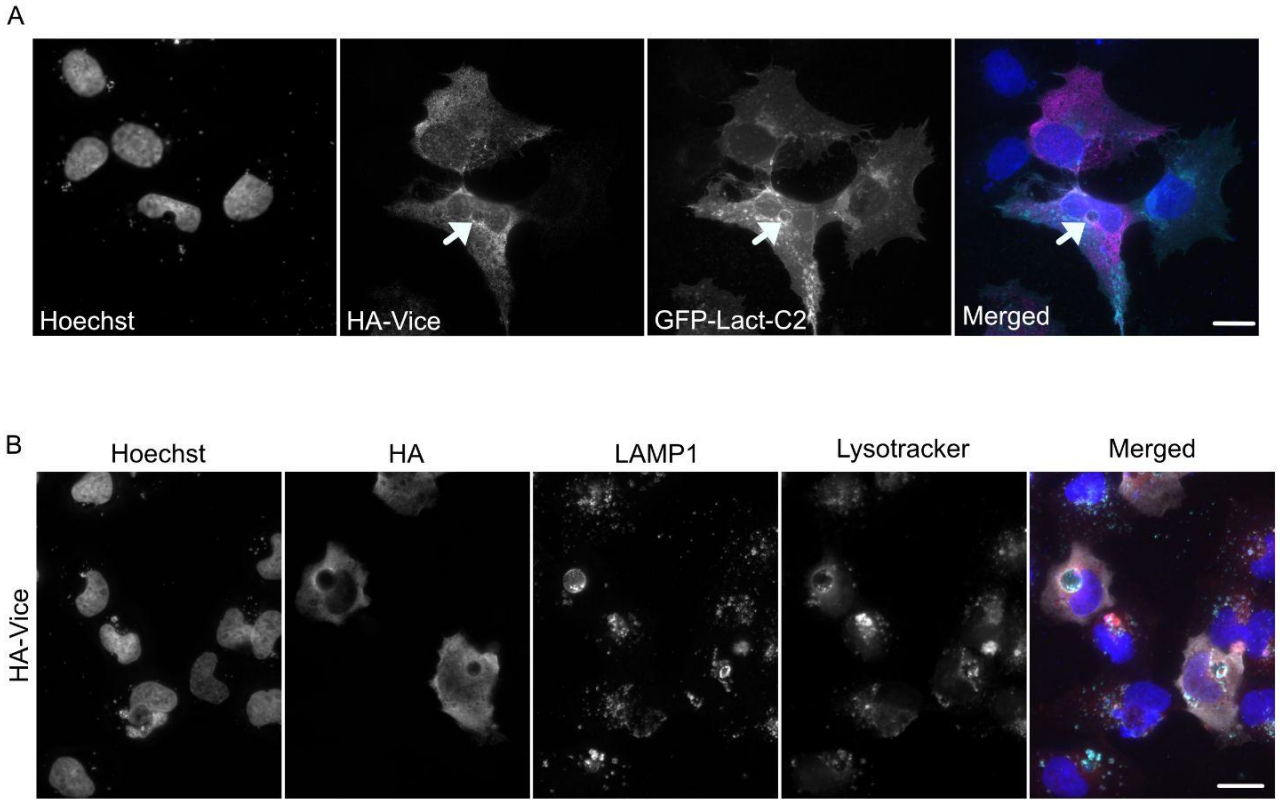
Supplementary Figure 2



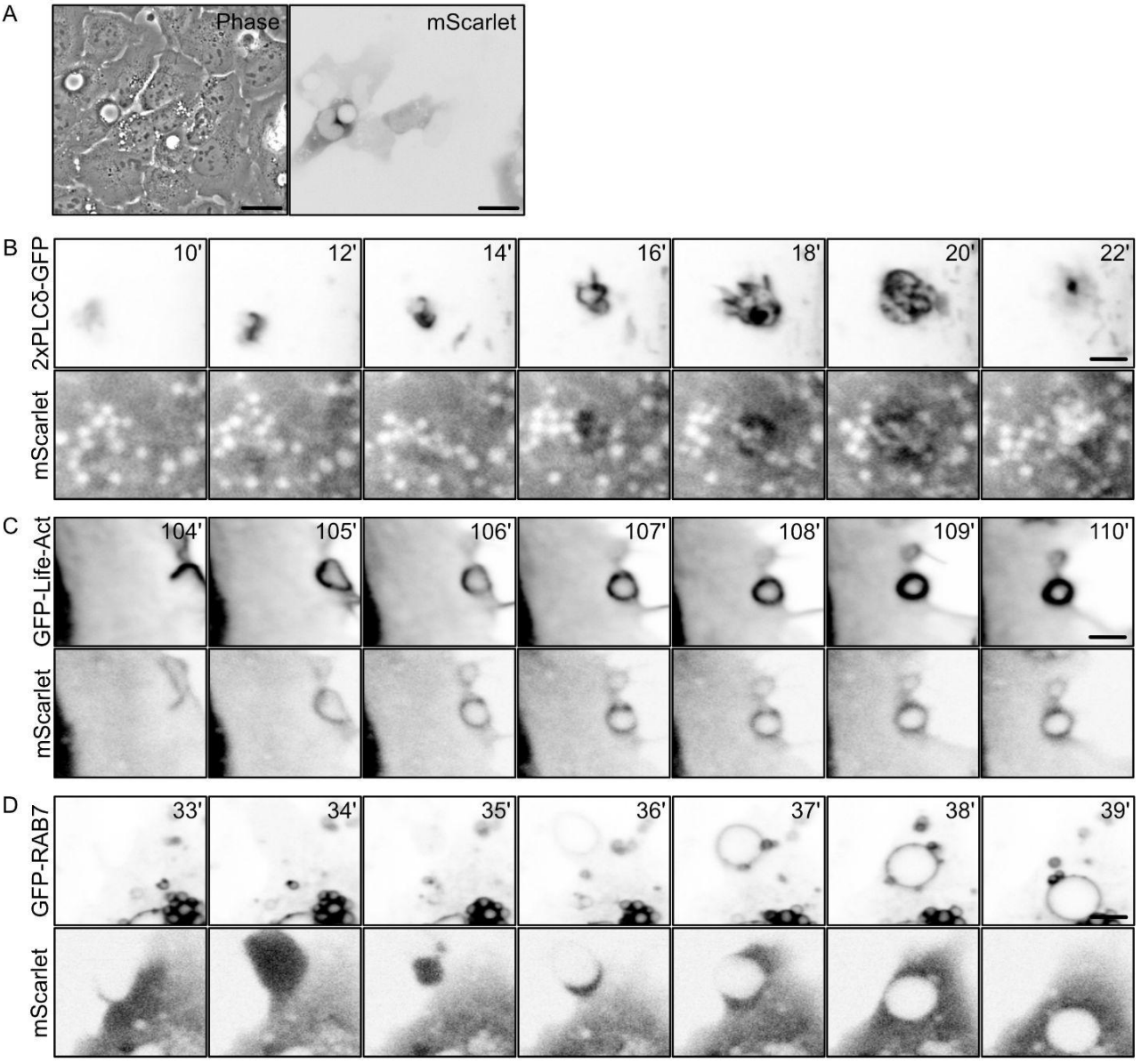
Supplementary Figure 3

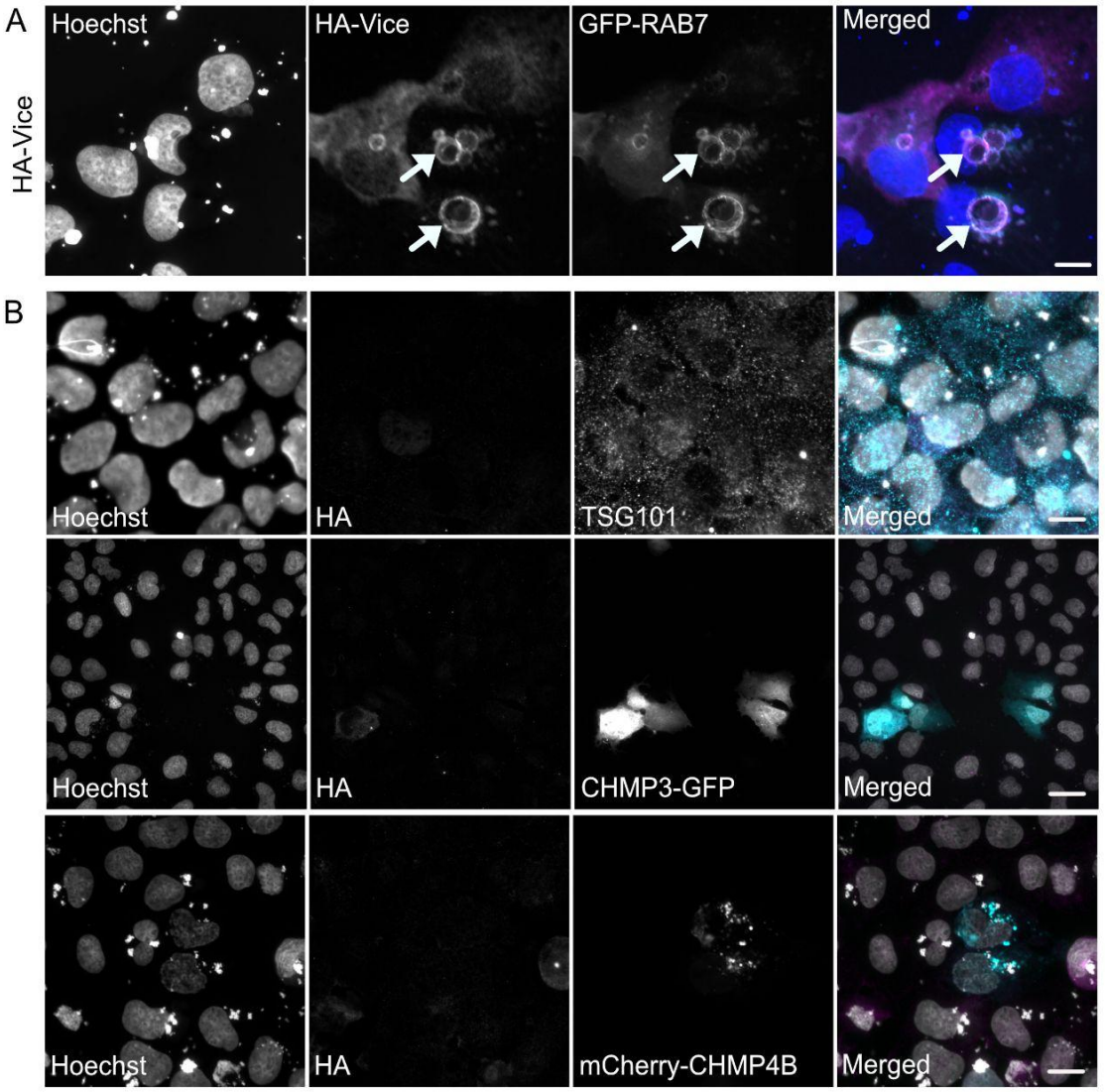


Supplementary Figure 4

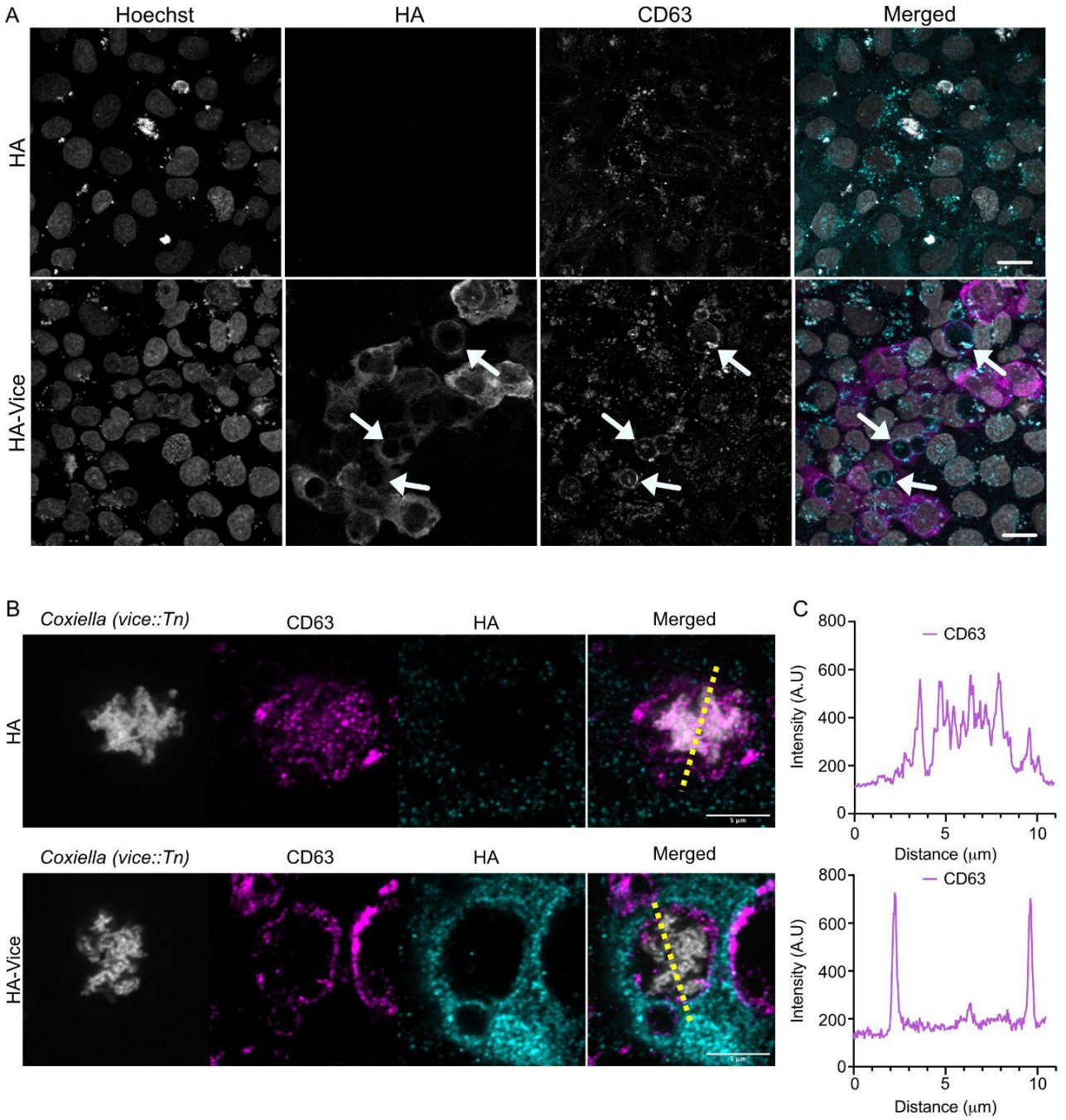


Supplementary Figure 5




A
HA-Vice
Hoechst
HA-Vice
GFP-RAB7
Merged
B
Hoechst
HA
TSG101
Merged
Hoechst
HA
CHMP3-GFP
Merged
Hoechst
HA
mCherry-CHMP4B
Merged

Supplementary Figure 7



2. Vice protein-protein interactions.

Although we succeeded to prove that Vice was interacting with lipids we did not demonstrate any protein-protein interactions. Considering that Vice was involved in different cellular mechanisms, we were wondering if it could directly interact with host cell proteins. To explore this possibility, we had a Yeast double Hybrid screen done by the company Hybrigenics to test the interaction of Vice against a library of Hela cells proteins. We selected Hela cells proteins to be more consistent with the previous generated data in epithelial cells. The assay revealed several putative interacting proteins (**Table 3**) but two only of them were considered as possible candidates. Interestingly, the mu (μ2) subunit of AP2 adaptor complex (AP2M1) was identified as the best candidate. AP2M1 acts as the major heterotetramer (**α**, **β**2, μ2, and **σ**2 subunits) that orchestrates clathrin-mediated endocytosis (Jackson et al., 2010). The YxxØ sorting motifs present in the cytosolic tail of different cargo proteins are recognized by the Mu domain of AP2M1, allowing the targeting within clathrin-coated pits and vesicles (Kadlecova et al., 2017). Interestingly, Y2H assay also indicates that the interaction occurs in a specific region (225-340) of the Mu domain. To validate this result, we tested the interaction between Vice and 3 truncations of AP2M1 (N-Terminal domain, MU domain and AP2M1 domain comprising amino acids 225 to 340) by co-immunoprecipitation (**Figure 19.B**).

Our preliminary results indicate that Vice may specifically interacts with the Mu domain (160-435). Unfortunately, we failed to confirm the interaction between Vice and the specific region of the Mu domain (AA 225-340) identified by Y2H nor with the N-ter domain. Next, we examined the localization of AP2M1 during ectopic expression of Vice in epithelial cells. Indeed, both AP2M1 and Vice were decorating the contour of Vice-induced compartments (**Figure 19.A**).

We observed that the expression of Vice also induces a decrease in the number of AP2M1 spots in cells, which could be due to a direct interaction between Vice and AP2M1 that results in AP2M1 sequestration at Vice-induced vacuoles.

The second putative interactant was CHMP3, discussed in the manuscript; however, we were not able to validate any direct interaction between the two proteins.

Global PBS (for Interactions represented in the Screen)		Nb	%
A	Very high confidence in the interaction	0	0.0%
B	High confidence in the interaction	1	11.1%
C	Good confidence in the interaction	1	11.1%
D	Moderate confidence in the interaction This category is the most difficult to interpret because it mixes two classes of interactions : - False-positive interactions - Interactions hardly detectable by the Y2H technique (low representation of the mRNA in the library, prey folding, prey toxicity in yeast)	7	77.8%
E	Interactions involving highly connected (or relatively highly connected) prey domains, warning of non-specific interaction. The total number of screens performed on each organism is taken into account to set this connectivity threshold: 20 interactions to different bait proteins in our entire database for Human, 10 for Mouse, Drosophila and Arabidopsis and 6 for all other organisms. They can be classified in different categories: - Prey proteins that are known to be highly connected due to their biological function - Proteins with a prey interacting domain that contains a known protein interaction motif or a biochemically promiscuous motif	0	0.0%
F	Experimentally proven technical artifacts	0	0.0%
Non Appliable			
N/A	The PBS is a score that is automatically computed through algorithms and cannot be attributed for the following reasons : - All the fragments of the same reference CDS are antisense - The 5p sequence is missing - All the fragments of the same reference CDS are either all OOF1 or all OOF2 - All the fragments of the same reference CDS lie in the 5' or 3' UTR		

Symbols	Means
✻	The fragment contains the full length ORF
	Fragment is fully in 5' UTR
	Fragment is fully in 3' UTR
x	Fragment contains at least one In Frame STOP codon in 5' UTR
x	Fragment contains at least one In Frame STOP codon in CDS
x	Fragment contains the natural STOP codon
[NR]	Fragment was found to be non relevant (poor quality, high N density)
IF OOF1 OOF2	With regard to the theoretical frame of each corresponding ORF (GenBank),fragments are cloned in frame (IF) if they are in the same frame as Gal4AD.In general, polypeptides synthesized from OOF fragments are not considered of biological interest, unless found together with another frame. However, some of the proteins expressed from an OOF fragment can be translated in the correct frame,due to the existence of natural frame-shift events during translation in yeast. No stop codons are displayed for OOF fragments.
??	Unidentified frame when : - The clone sequence is antisense - The 5p sequence is missing
N	Antisense
Start...Stop	Position of the 5p and 3p prey fragment ends, relative to the position of the ATG start codon (A=0)

Clone Name	Type Seq	Gene Name (Best Match)	Start..Stop (nt)		Frame	Sense	%Id 5p	%Id 3p	PBS
pB27_A-38	5p/3p	Homo sapiens - ALDH1B1	1506..1185		??	N	100.0	93.2	N/A
pB27_A-11	3p	Homo sapiens - AP2M1	..1687		??			89.2	B
pB27_A-33	5p	Homo sapiens - AP2M1	333		IF		99.3		B
pB27_A-22	5p	Homo sapiens - AP2M1	375		IF		99.7		B
pB27_A-5	5p	Homo sapiens - AP2M1	690..1010		IF		98.8		B
pB27_A-8	3p	Homo sapiens - CHMP3	..2425		??			98.3	N/A
pB27_A-14	3p	Homo sapiens - CHMP3	..2425		??			91.5	N/A
pB27_A-26	5p	Homo sapiens - CIRBP	1651..1191		??	N	98.7		N/A
pB27_A-1	5p/3p	Homo sapiens - DOCK6	32..1110		OOF2		100.0	95.2	N/A
pB27_A-32	3p	Homo sapiens - DROSHA	..1740		??			95.6	N/A
pB27_A-40	5p	Homo sapiens - KRT17	1231		OOF1		100.0		N/A
pB27_A-39	5p/3p	Homo sapiens - MRTO4	240..838	x	IF		99.7	98.8	D
pB27_A-7	5p/3p	Homo sapiens - MRTO4	240..838	x	IF		99.7	99.1	D
pB27_A-10	5p/3p	Homo sapiens - MRTO4	240..838	x	IF		99.7	98.2	D
pB27_A-18	5p/3p	Homo sapiens - MRTO4	240..838	x	IF		99.7	99.2	D
pB27_A-12	3p	Homo sapiens - NCL	..503		??	N		97.8	N/A
pB27_A-34	5p/3p	Homo sapiens - NCL	744..458		??	N	100.0	98.6	N/A
pB27_A-6	5p	Homo sapiens - NCL	744..429		??	N	100.0		N/A
pB27_A-17	5p/3p	Homo sapiens - NCL	747..514		??	N	100.0	100.0	N/A
pB27_A-43	5p/3p	Homo sapiens - NCL	792..522		??	N	100.0	89.3	N/A
pB27_A-47	5p/3p	Homo sapiens - NCL	792..486		??	N	100.0	96.1	N/A
pB27_A-41	5p/3p	Homo sapiens - NCL	807..480		??	N	99.4	98.0	N/A
pB27_A-36	3p	Homo sapiens - NCL	1008..721		??	N		94.4	N/A
pB27_A-45	5p/3p	Homo sapiens - OAT	375..851		IF		100.0	93.6	C
pB27_A-3	3p	Homo sapiens - OAT	376..851		OOF1			99.8	C
pB27_A-28	5p	Homo sapiens - PMEPA1	940..1217		OOF1		99.6		N/A
pB27_A-19	5p/3p	Homo sapiens - SLC38A5	464..1075		OOF2		100.0	98.8	N/A
pB27_A-2	5p/3p	Homo sapiens - SUMO3	49..1046		OOF1		99.7	99.0	N/A
pB27_A-25	5p/3p	Homo sapiens - GenMatch	-1		IF		100.0	65.5	D
pB27_A-37	5p/3p	Homo sapiens - GenMatch	-1..483	x	IF		99.8	93.3	D
pB27_A-30	3p	Homo sapiens - GenMatch	..610		??			95.1	N/A
pB27_A-31	3p	Homo sapiens - GenMatch	..610		??			99.8	N/A
pB27_A-27	5p/3p	Homo sapiens - GenMatch	-1..697	x	IF		99.8	97.7	D
pB27_A-29	5p/3p	Homo sapiens - GenMatch	-1..697	x	IF		98.3	98.1	D
pB27_A-23	5p/3p	Homo sapiens - GenMatch	-1..364	x	IF		100.0	100.0	D
pB27_A-13	5p/3p	Homo sapiens - GenMatch	-1..883	x	IF		99.2	99.1	N/A
pB27_A-21	5p	Homo sapiens - GenMatch	-1..562	x	IF		100.0		D
pB27_A-48	5p/3p	Homo sapiens - GenMatch	-1..563	x	IF		100.0	98.1	D
pB27_A-42	5p/3p	Homo sapiens - GenMatch	-1..360	x	IF		100.0	96.7	D

Table 3: Results recap of Yeast Two Hybrid assay provided by the company Hybrigenics.

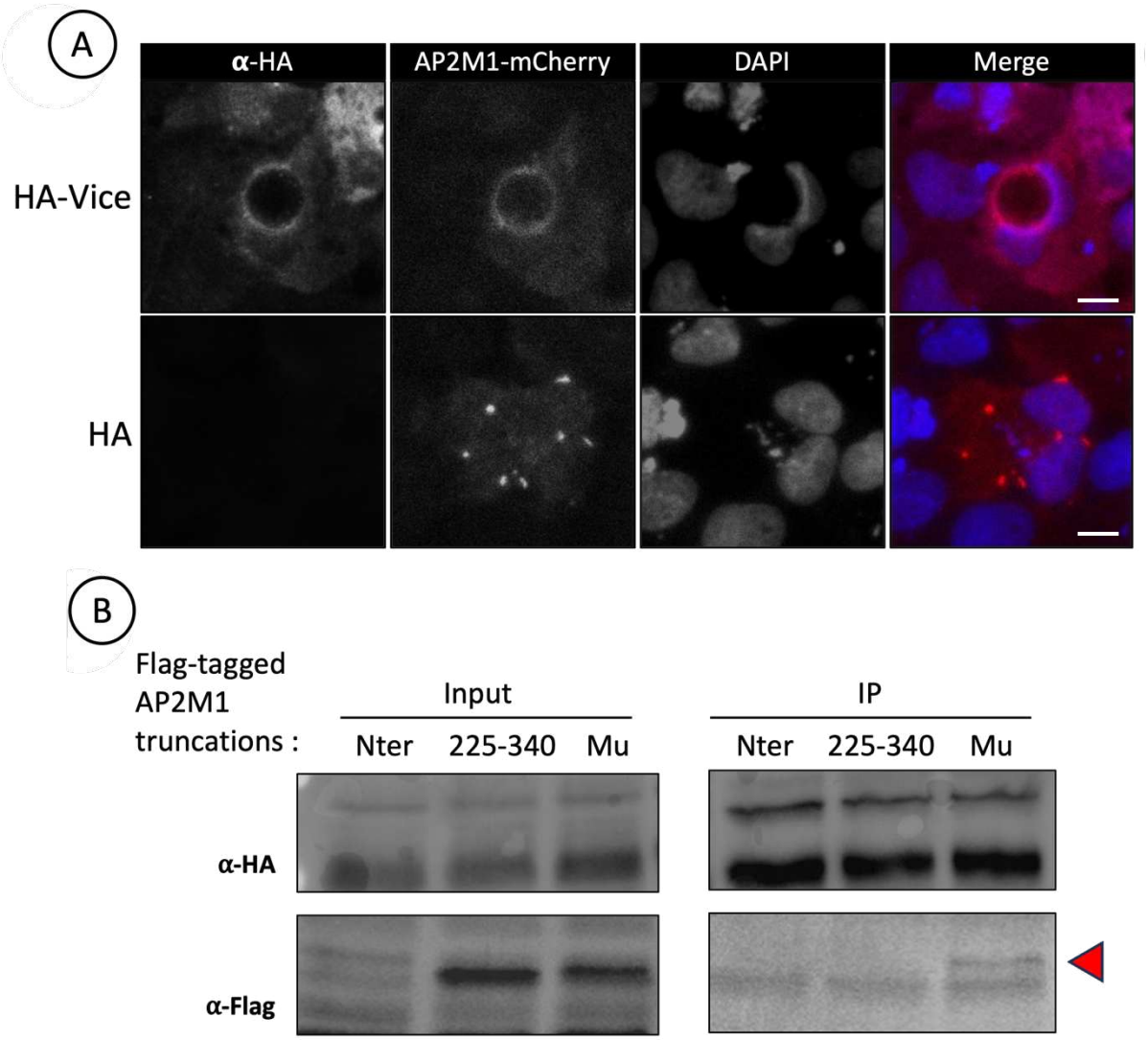


Figure 19: Vice may interact with AP2M1 Mu domain.

(A) Colocalization of AP2M1 and Vice was investigated by fluorescence microscopy in U2OS cells ectopically expressing AP2M1-mCherry in combination with either HA alone or HA-Vice. HA-Vice was detected using anti-HA antibody (scale bar: 10µm). (B) Interaction between AP2M1 and Vice was tested by co-immunoprecipitation. The three truncated versions of AP2M1 (N-Terminal domain, MU domain and the peptide from amino acid 225 to 340) were fused to a Flag tag in a pLVX backbone vector. U2OS cells were co-transfected with PRK5-HA-Vice and pLVX plasmids encoding either of the three truncated versions of AP2M1. Proteins were detected by Western blot using anti-HA and anti-Flag antibodies. Red arrow indicates the Mu domain of AP2M1 that have been co-immunoprecipitated with HA-Vice.

3. Modification of Extracellular Vesicle protein profile.

As mentioned in the introduction, the formation of intracellular vesicles can also be dependent on the ESCRT machinery. Once formed in the lumen of MVBs, ILVs are released in the extracellular media by fusion with the plasma membrane as exosomes, a sub-family of small extracellular vesicles characterized by a size ranging between 30 and 150 nm. We engineered U2OS cells stably expressing NanoLuc luciferase (Nluc) fused to 3 commonly used EV markers CD9, CD63 and HSP70 (**Figure 20.A**). To investigate the effect of Vice on ESCRT machinery, we quantified the EV-content release by measuring the luciferase activity of CD9-Nluc, CD63-Nluc and HSP70-Nluc in cells transfected with either HA alone (as a negative control) or HA-Vice. Interestingly, ectopic expression of HA-Vice decreased the release of CD63-Nluc and HSP70-Nluc while CD9-NLuc release was unchanged (**Figure 20.B**).

Based on those preliminary data, we decided to validate the role of Vice on EV release by implementing an alternative approach due to the lack of consistency given by the Nluc assay. Indeed, EVs were purified from culture supernatant of U2OS cells transfected either with HA or HA-Vice to analyze EVs size, number and markers.. To do so, we isolated EVs by size exclusion chromatography by using columns from which we only analyzed the four first fraction containing EVs. We quantified and measured the size of purified EVs using a Nanoparticle Tracking Analysis machine and observed them by electron microscopy (**Figure 20.C**) to ensure that the purified particles were intact. However, we did not observe any differences in the size and in the number of EVs released from control cells or cells expressing HA-Vice (**Figure 20.D**). Consistently with our first observation, Western-Blot analysis of those purified EVs revealed that some markers are less enriched in EVs released from cells expressing HA-Vice. Of note, we observed that ALIX, CD63, CD9 and more importantly HSP70 are less enriched in EVs from HA-Vice expressing cells compared to cells expressing HA alone (**Figure 20.E)**. These results suggest that Vice induces modulation of ILVs formation leading to a different proteic composition. However, we can assume that compensatory alternative pathways are engaged as we did not observe any difference in the number of total EVs released.

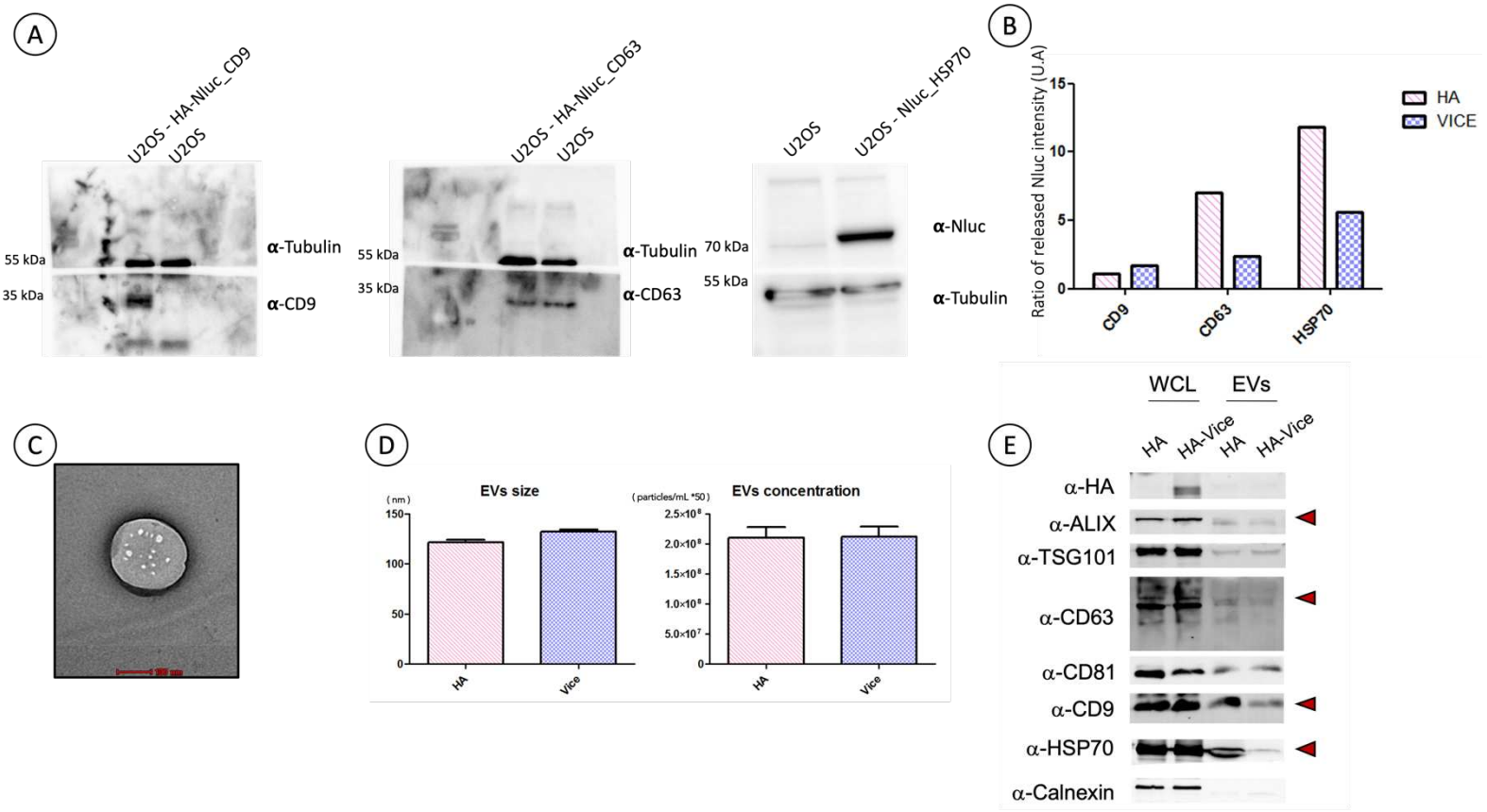


Figure 20: Vice expression leads modifies EVs protein profile.

(A) U2OS cells were transduced using lentivector containing HA-Nluc coupled with either CD9, CD63 and HSP70. Stable cell lines were validated for the expression of EVs marker fused to Nluc by Western-blot. Anti-CD9 and anti-CD63 antibodies were used to detect endogenous and Nluc-coupled proteins. HSP70 coupled to Nluc was detected using an anti-Nluc antibody which only allowed us to detect the Nluc-coupled protein. Anti-Tubulin antibody was used as a loading control. (B) Stable cell lines developed in (A) were transfected with either HA alone (pink) or HA-Vice (purple) to measure EVs release. The Nluc intensity in the supernatant and the cell lysate were measured using Nano-Glo ® luciferase assay. Ratio of Nluc intensity in the supernatant of each condition is shown here following the formula : (Supernatant intensity / (Supernatant intensity + cell lysate intensity))*100. (C) Purified EVs form HA or HA-Vice transfected U2OS were analyzed by electron microscopy. Representative EV is shown. Scale bar : 100nm. (D) Using Nano-cyte® same EVs from (C) were measured and quantified. (E) Presence of different EVs markers was analyzed by Western blot on both purified EVs and on the whole cell lysate (WCL) as an input control. Anti-HA antibody was used to detect HA-Vice transfection in the WCL. Detection of all EVs markers was performed using antibodies against each marker. Anti-Calnexin was used as a control as it is not supposed to be present in EVs. Red arrows indicate markers that are less present in HA-Vice transfected conditions.

4. Vice membrane curvature recognition.

Bioinformatics analysis suggested that Vice possesses a putative F-BAR domain, which plays a role in oligomerization and membrane phospholipid binding (Ahmed et al., 2010). F-BAR domains have also been showed to be implicated in the recognition and the initiation of membrane curvatures (Mahmood et al., 2019). Because we had described that Vice was able to bind to phospholipids and to large Unilamellar vesicles in the manuscript, we wanted to assess if its putative F-BAR domain was functional and able to recognize membrane curvature. To do so, we have collaborated with the team of Dr Laura PICAS at the IRIM institute (Montpellier), who has developed a system of SiO2 nano-pillars on which we can cultivate cells to induce membrane curvature on the basal plasma membrane (**Figure 21.A,B**). Using this system, we investigated if Vice is able to sense membrane curvature by cultivating U2OS cells on nano-pillars followed by transfection with HA-Vice (**Figure 21.C**) (Alaoui et al., 2022). Indeed, HA-Vice appears to accumulate in spots following a consistent pattern with the same distance between spots (**Figure 21.D**). This means that Vice may recognize membrane curvature areas with the same pattern. However, this experiment is very preliminary and needs to be confirmed.

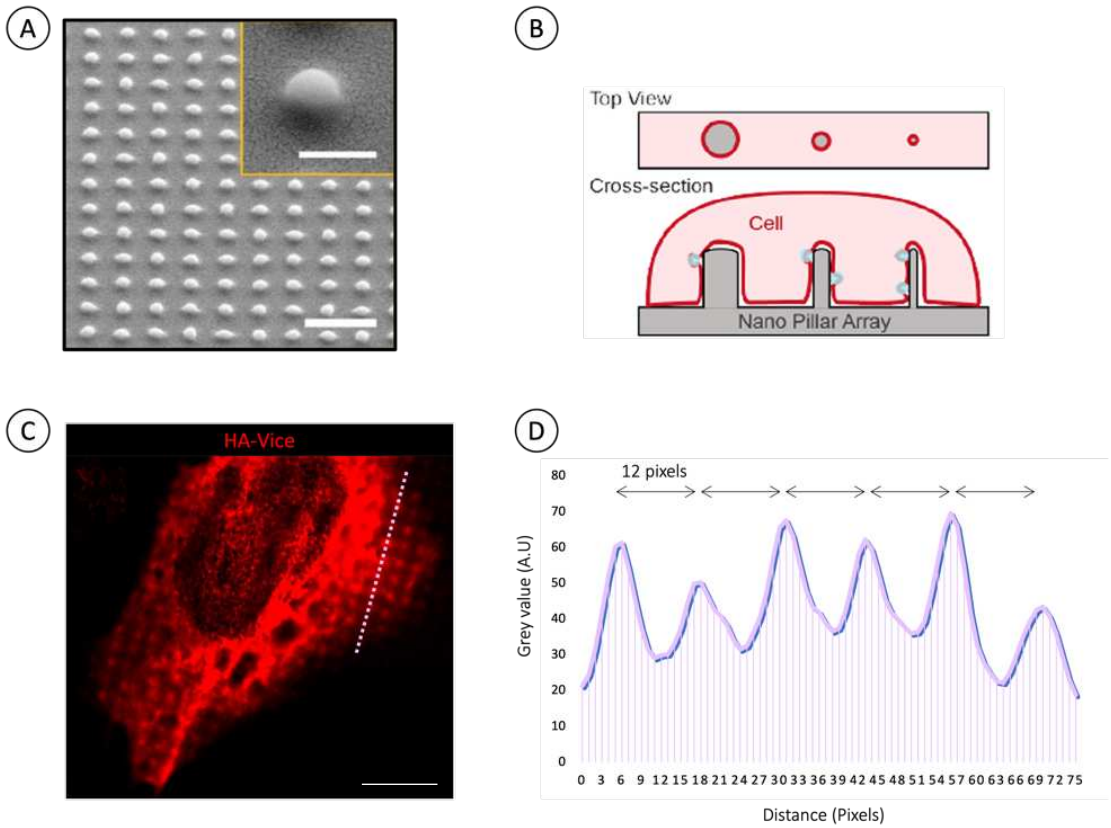


Figure 21: Vice may recognize membrane curvature.

(A) SEM images of SiO2 substrates displaying an array of nano-pillars with a radius, R ~ 150 nm generated by soft-NIL. Scale bar, 2 µm. Inset, scale bar : 500 nm.(from Alaoui et al., 2022) (B) Representative cartoon of different nano-pillars structure from top view and cross section (from Lou et al., 2018). (C) U2OS cells have been cultivated over nano-pillars and transfected with HA-Vice and labelled with an anti-HA antibody. (Scale bare : 10µm). (D) Fluorescence intensity have been measured over the pink line (C) and each double arrow indicate the same distance.

5. Vice-induced compartment RAB profile.

During the characterization of the compartment induced by the ectopic expression of Vice, we investigated which RAB proteins were present on its surface. Indeed, as mentioned earlier the RAB GTPases can define the identity of an organelle. In order to investigate the nature of Vice-induced compartment, U2OS cells were transfected with a GFP-tagged library of RAB GTPases in combination with HA-Vice. We have tested a total of 13 different RABs and have classified their presence at the Vice-induced compartment in 3 phenotypes: a clear localization at VICs, partial localization and absence of localization (Table 4). Only RAB7, RAB9 and RAB33a were clearly enriched at VIC membranes. Unfortunately, the localization of those 3 RABs and the 6 other one with an intermediate phenotype are specific to different compartments making complicated to claim the nature of the compartment based on this RAB screen. However, we can hypothesize that Vice-induced compartment is ,in addition to an abnormal MVB (described in the manuscript), may represent a hybrid organelle resulting from the intersection and fusion of multiple cellular compartments. It is important to note that some VICs are positive for RAB20, which is associated with macropinosomes, thus correlating with the observations reported in the manuscript.

GTP-RABs	Function and localisation	phenotype	Remarks
RAB7	Late endosome to Lysosome (Stenmark, 2009)		Increase the presence of Vice at his own VICs
RAB9	Endosome to Trans-Golgi (Stenmark, 2009)		Over-expression increases the number of VICs
RAB33a	Autophagosome formation (Stenmark, 2009)		
RAB5	Early endosome fusion (Stenmark, 2009)		
RAB20	Early and late macropinosomes (Wandinger-Ness & Zerial, 2014)		Only small compartments are positive
RAB26	Lysosome formation (R. U. Jin & Mills, 2014)		Can cluster around the compartment
RAB32	Mitochondrial fission (Stenmark, 2009)		50% of VICs are positive
RAB33b	Autophagosome formation (Stenmark, 2009)		
RAB37	Secretion and exocytosis (Stenmark, 2009)		
RAB6	Endosome to Golgi (Stenmark, 2009)		Can cluster around but not at the compartment
RAB8	TGN/RE to plasma membrane (Stenmark, 2009)		Very weak signal of GFP-RAB8
RAB11	TGN/RE to plasma membrane (Stenmark, 2009)		Diffused pattern with no clear localization
RAB24	Autophagosome formation (Stenmark, 2009)		

Table 4: Screen of RAB GTPases at the Vice-induced compartments.

U2OS cells were co-transfected with HA-Vice and a panel of GFP tagged RAB GTPases. Anti-HA antibody was used to detect Vice and images were taken. Co-localization of RABs to Vice-induced compartment was visually determined and classified into three phenotypes: clear localization at VICs (bleu), partial localization at VICs (pink) and absence from VICs (purple).

6. *C. burnetii* CCV ultrastructure.

The CCV is a complex replicative niche, that is large and unique. It has been described that the lack of some bacterial effectors leads to a perturbation in the biogenesis of the CCV resulting in different phenotypes. Indeed, the CCV can be multi-vacuolar, smaller than WT CCVs or in the case of CCVs generated by the *Vice*::Tn mutant, the CCV can collapsed with highly convoluted membranes and protrusions extending inside the lumen. However, classical fluorescent and electronic microscopy technics do not allow us to have the degree of resolution necessary to describe in precision the ultrastructure of CCVs generated by the *Vice*::Tn mutant. During my thesis, we have started to develop a protocol in collaboration with the Ultrastructural BioImaging Core Facility at the Pasteur Institut (Paris) to acquire images of *C. burnetii* CCVs in epithelial cells using Focused Ion Beam-Scanning Electron Microscopy (FIB-SEM) which allow us to reconstruct a 3D model of the WT CCV via electron microscopy images showing the ultrastructure of the WT *C. burnetii* CCV (**Figure 22**). This 3D reconstruction is not segmented yet, however in the near future, the idea would be to define the membrane of the CCV to then compare it to CCV generated by *C. burnetii* mutants including *Vice*::Tn mutant.

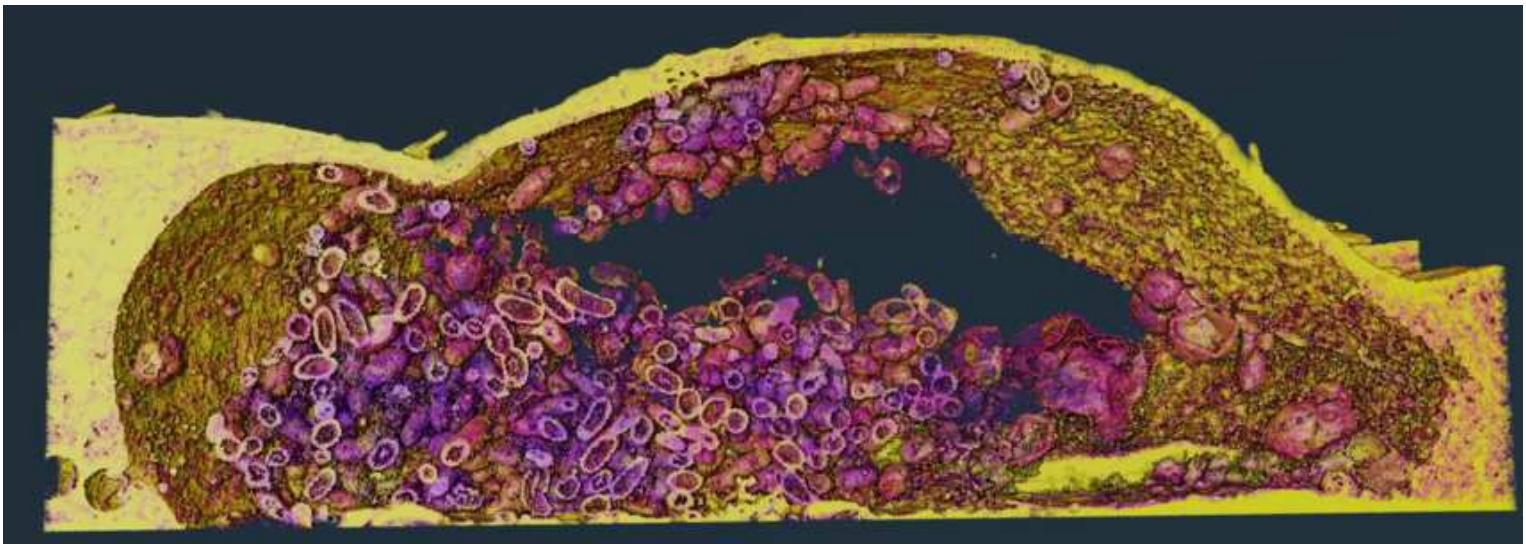


Figure 22: *C. burnetii* CVV ultrastructure.

U2OS cells infected with *wt C. burnetii* for four days were imaged by confocal microscopy to identify infected cells before fixation for electron microscopy. False colored have been applied to the 3D reconstruction to provide more depth. Reconstruction have been performed with images taken every 15 nm.

DISCUSSION & PERSPECTIVES

The establishment of replicative niches is a key step in the infection cycle of many intracellular bacteria. The characterization of the effector CvpB by the team demonstrated that the biogenesis of the CCV is crucial for *C. burnetii* virulence. More importantly, they have shown that the decreased virulence *in vivo* was specifically due to the defect of CCV biogenesis and not related to bacterial replication. Additionally, this work has highlighted the importance of host cell PI(3)P in the establishment of the CCV.

Based on these results, and using lipid binding-probes, the team screened other lipids that could be enriched at the CCV, with the aim to point out the ones that are actively recruited by T4SS effectors. This screen led to the identification of three phospholipids that are recruited at the CCV in the T4SS-dependent manner: PI(4)P, PI(3)P and LBPA. This confirmed the data about CvpB being responsible for PI(3)P enrichment at the CCV. We thus conducted a screening of a *C. burnetii* mutant sub-library containing transposon insertions in genes encoding for predicted or validated effector proteins to identify those involved in the re-routing of LBPA and PI(4)P at CCVs. Surprisingly, none of the mutants tested affected PI(4)P localization at CCVs, suggesting that the manipulation of PI(4)P might be coordinated by an effector protein not present in our mutant library or that its recruitment is dependent on a synergistic effect of multiple effectors. However, we observed that transposon insertions in the *cbu2007* (*vice*) gene significantly inhibited LBPA localization at CCV, indicating that this specific effector may be crucial for LBPA recruitment at the CCV. As mentioned in the thesis manuscript, Vice possesses the highest score for predicted *Coxiella* effectors in the S4TE algorithm (Noroy et al., 2019) and was recently identified as secreted in THP-1 cells (C. L. Larson et al., 2023). Of note, Vice is required for intracellular replication and, more importantly, is essential for survival in primary macrophages and for virulence in the SCID mouse model of infection (Case et al., 2022).

The CCV biogenesis defect observed with the *vice*::Tn mutant strain may correlate with the loss of virulence, as previously observed with *cvpB*::Tn mutants. This defect in CCV biogenesis is defined by a smaller vacuole with the accumulation of internalized membranes. Although *C. burnetii vice*::Tn mutants display an altered CCV morphology, it is important to point out that similar to wild-type CCVs, collapsed CCVs harboring the *vice*::Tn mutant strain are still positive for the late endosomal/lysosomal marker LAMP1 and maintain their acidic pH.

This suggests that bacterial metabolism and effector translocation should not be significantly affected during infections by the *vice*::Tn mutants. In contrast to *dotA*::Tn mutants, which are completely defective in effector translocation and bacterial replication, *vice*::Tn mutants are still able to replicate within these compartments, but the lack of endosomal space might impact their replication.

Unfortunately, we were not able to investigate CCV rupture in the context of *vice*::Tn mutant infections and compare it with *wt* infections as we were not able to transfect infected cells with plasmids expressing galectin-3, a typical endosomal membrane rupture marker (Jia et al., 2020b). To overcome this issue, we used a FIB-SEM protocol to visualize the ultrastructure of CCVs. To date we have only acquired images of *wt* vacuoles, but the objective is to acquire images of CCVs generated by the *vice*::Tn mutant and investigate whether their membranes are ruptured and to further investigate their highly convoluted morphology. In particular FIB-SEM microscopy would allow us to establish whether CCVs harboring the *vice*::Tn mutant strain are indeed a single compartment or multiple smaller CCVs.

To investigate Vice function, we have ectopically expressed the protein coupled to an HA tag in epithelial cells. Interestingly, we observed the formation of a large (8 to 17µm) compartment that resembles an early CCV that we called Vice-Induced compartment (VIC). Typical markers of late endosomes/lysosomes decorate the membranes of VICs whereas, as expected, other proteins and lipids that are actively recruited at CCVs by other *C. burnetii* effectors are excluded. The membrane composition of VICs and the observation of some intraluminal vesicles of a size compatible with typical ILVs led us to believe that these structures could derive from MVBs failing to pinch off intraluminal vesicles, thereby preserving their membrane surface, which would increase upon fusion of new incoming vesicles.

As discussed in the submitted manuscript, to validate this hypothesis, we have fused Vice with GFP or mCherry tags to follow its dynamics by live imaging. Unfortunately, the fusion of Vice with either fluorescent protein provokes the cleavage and the degradation of both proteins and Vice. This result is in agreement with the observation made by Larson and colleagues (C. L. Larson et al., 2023). Indeed, they did not observe any specific localization of Vice or the formation of VICs. To bypass this technical issue, we have used a small Alfa tag which can be recognized by a nanobody fused to either mCherry or mNeongreen. With this tool, we have been able to observe that VICs do not form through endosomal expansion, as we initially

hypothesized. Instead, VICs originate at the plasma membrane through macropinocytosis-like events. Shortly after internalization (within 1-2 minutes), Vice dissociates from VICs to remain cytoplasmic. The presence of typical markers of macropinocytosis and, notably, the inhibition of VICs formation by the macropinocytosis inhibitor EIPA, strongly suggest that Vice induces macropinocytosis in cells. Interestingly, the use of EIPA also accentuated the accumulation of Vice at the plasma membrane.

As we were not able to define a clear localization of Vice, because the protein can either be found cytosolic, at the plasma membrane or to its compartment, we suggested that Vice localization was highly dynamic. One explanation could be the capacity of the protein to bind to various phospholipids, including lipids from the plasma membrane, but also to its ability to bind to vesicles enriched in LBPA and PS at concentrations reminiscent of late endosome/MVBs.

It would be interesting to ectopically express Vice in macrophages and dendritic cells to investigate whether it could increase their macropinocytic capacity as these cell types are specialized in macropinocytosis to capture and degrade pathogens (Lin et al., 2020). Indeed, we have observed VICs formation in several epithelial cell types ectopically expressing Vice. However, U2OS cells presented the most prominent phenotype. U2OS cells have been described to be capable of macropinocytosis under some specific conditions (Xia et al., 2023) while other epithelial cell types show lower levels of basal macropinocytosis.

Interestingly, U2OS cells are also known to enter methuosis when Ras is constitutively active (Maltese & Overmeyer, 2014). Methuosis is a nonapoptotic cell death associated with vacuolization of macropinosomes and endosomal compartments, which resembles what we observe during Vice expression (Figure 23). However, unlike methuosis, Vice expression does not induce cell death and a single compartment is observed in cells ectopically expressing the *C. burnetii* effector protein.

We also observed that VICs persist even during cell division and can be found in daughter cells. It would be interesting to study the effect of Vice during *C. burnetii* infections in the context of methuosis. We can hypothesize that Vice and probably other effectors may promote the fusion of the internalized compartments to avoid cell death. However, it is also possible, although more surprising, that methuosis could be the only cell death pathway that is not inhibited by *C. burnetii* and that Vice could, in contrary, accentuate the phenomenon.

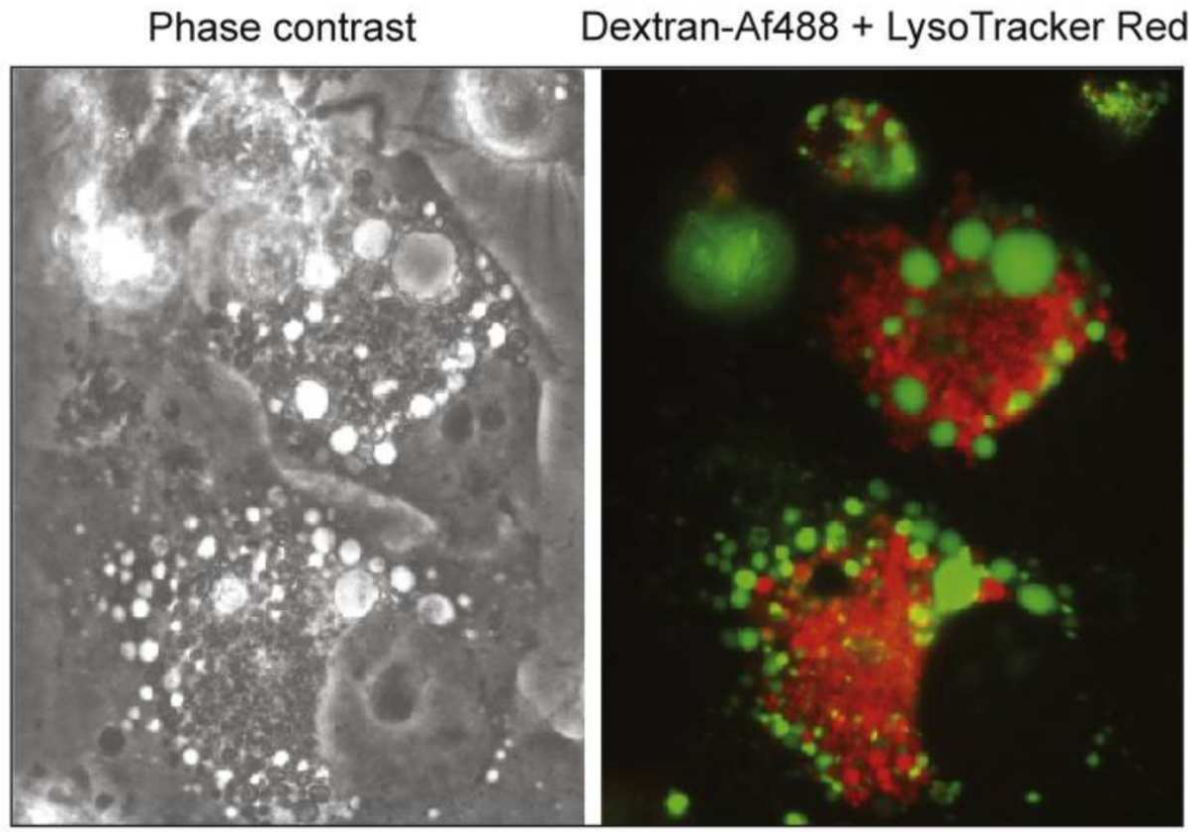


Figure 23: Examples of cell undergoing methuosis. (adapted from Maltese & Overmeyer, 2014)

Examples of U251 human GBM cells undergoing methuosis triggered by ectopic expression of activated Ras. Conditional expression of H-Ras(G12V) was induced by addition of doxycycline to a stable cell line. The macropinosome-derived vacuoles remain separate from lysosomes. Lysosomes were prelabeled for 3 hours with LysoTracker Red. Macropinosome-derived vacuoles were then labeled with dextran–Alexa Fluor 488 (green). The cells were examined 4 hours after addition of the labeled dextran.

Macropinocytosis and actin remodeling are often stimulated by T3SS-equipped pathogen to promote entry (Chang et al., 2021). Interestingly, our findings describe a similar phenomenon, but Vice cannot be implicated in bacterial entry as it is secreted once *C. burnetii* is inside the cell. One possibility is that Vice promotes the entry of extracellular bacteria to increase the bacterial load by inducing macropinocytosis.

In this context, it would be interesting to investigate whether Vice overexpression could still promote, via induced-macropinocytosis, bacterial entry of pathogens with a defective T3SS or with mutations in effectors essential for entry. It would also be interesting to investigate whether *C. burnetii* infections could promote co-infections by other intracellular bacteria.

Our preliminary data suggesting that Vice might interact with the clathrin adaptor AP2M1 is in apparent contrast with our findings on the induction of macropinocytosis. Indeed, the clathrin machinery has never been implicated in macropinocytosis and the size of the clathrin cage is incompatible with that of the vesicles internalized by Vice. However, it has been already observed that during certain bacterial infection, the pathogen could trigger a non-conventional clathrin-mediated endocytosis (Bonazzi et al., 2011). Importantly, AP2M1 has already been described as an interactant of CvpA, another *C. burnetii* effector, highlighting the importance of this host protein in the infectious process. Similarly to what has been observed with bacterial internalization, we can hypothesize that Vice-induced macropinocytosis may be associated with clathrin-mediated mechanisms. This can be further investigated by assessing the dynamics of clathrin associated molecules in cells ectopically expressing Vice. One other possibility is that Vice could use AP2M1 as an anchor to the plasma membrane to then interact with lipids and trigger macropinocytosis. For both hypotheses, AP2M1 localization at the plasma membrane is part of the initiation process, but because we found AP2M1 enriched at VICs, the protein must be part of the transported material from the plasma membrane during internalization of VICs.

Upon internalization, VICs relocate to the perinuclear area where they remain stable in shape and size for hours. This suggests that our initial assumption of a role of Vice in perturbing ILV formation at MVBs, thereby stabilizing VICs, might hold true, as ILV formation would induce loss of membrane at the late endosome surface in favor of ILV accumulation. Intriguingly, in addition to LBPA, VICs feature components of the ESCRT machinery that typically shuttle between late endosomal membranes and the cytoplasm. The accumulation of these markers at VIC membranes suggests a potential disruption of the ESCRT machinery. In support of this hypothesis, membrane targeting of ALIX, an ESCRT-associated protein that is crucial for ILV formation, is strongly decreased in Vice-expressing cells. A similar phenotype is observed in cells infected with *wt C. burnetii*, whereas the membrane association of ALIX is partially restored in cells infected by *vice*::Tn *C. burnetii*. The lesser effect observed on ALIX membrane association during infections may correlate with the translocation of endogenous levels of Vice as opposed to the ectopic expression of the bacterial effector in transfected cells. Notably, most CCVs harboring the *vice*::Tn mutant strain are positive for ALIX, suggesting an active ESCRT machinery pinching off vesicles from CCV membranes. In contrast, only 20% of CCVs harboring

wt C. burnetii are ALIX positive. Accordingly, the typical ILV/exosomal marker CD63 decorates the contours of CCVs and VICs, whereas it is only found within the lumen of CCVs in cells infected by the *vice*::Tn *mutant* strain. Together with the observed reduction of LBPA labelling at CCVs harboring the *vice*::Tn mutant, this supports our hypothesis that Vice perturbs the ESCRT-dependent ILV biogenesis pathway.

As the yeast 2-hybrid screen did not highlight any Vice candidate interactant associated with the ESCRT machinery, our current hypothesis is that Vice's association with PS and LBPA-enriched membranes might obstruct ALIX's membrane association, which also relies on LBPA. In turn, perturbing ALIX membrane association would lead to the observed accumulation of LBPA at VICs and CCVs. As we have mentioned in the introduction, the ESCRT machinery has been reported to repair CCV membranes during infections (Radulovic et al., 2018), implying that C. burnetii infections require an active ESCRT machinery. Importantly however, membrane repair by the ESCRT machinery is independent of LBPA and ALIX, which are specifically required for the biogenesis of MVBs. Thus, by targeting LBPA, Vice might specifically inhibit the ESCRT machinery associated with this latter function.

In support of our model, we have also shown that Vice affect the ESCRT-dependent release of HIV-GAG virus-like particles (VLPs). It would be interesting to go further and use the same system in infection condition. This way, we can expect that *vice*::Tn mutant infections will not affect the release of HIV-GAG.

The inhibition of the ESCRT machinery at MVBs is expected to affect the biogenesis and release of EVs. Indeed, EVs purified from Vice-expressing cells present a different protein profile as compared to those released by control cells. The observation that Vice expression does not alter the overall number of released EVs can be related to the existence of multiple EVs biogenesis pathways that can rescue and balance each other when one of them is downregulated (Stuffers et al., 2009). In this context, it would be interesting to pursue the characterization of EVs released from Vice-expressing cells (or cells infected with *C. burnetii*) to define their complete proteome. Altering the protein profile of EVs released from infected cells may add up to the stealth strategies of *C. burnetii.* Indeed, it has been shown that that macrophages infected either with *Mycobacterium avium* or *Mycobacterium smegmatis* secrete more exosomes as compared to non-infected cells. Interestingly, secreted exosomes from

infected cells are enriched in HSP70, which triggers the NF-κB signaling pathway in bystander, non-infected cells (Anand et al., 2010). In our case, it seems that EVs released by Vice-expressing cells contain less HSP70, suggesting that EVs released from cells infected by *wt C. burnetii* may be less effective in inducing the NF-κB pathway in bystander cells. To test this hypothesis, non-infected cells can be exposed to EVs released from cells infected either by *wt C. burnetii* or by the *vice*::Tn mutant strain to compare the activation of the NF-κB signaling pathway.

As discussed in this manuscript, *C. burnetii* is not the only pathogen with a replicative niche deriving from late endosomes and MVBs through the manipulation of their vesicular trafficking. Indeed, it has been previously reported that *M. tuberculosis* translocated effectors EsxH and EsxG block the ESCRT machinery to perturb endosomal maturation (Mehra et al., 2013) and to prevent the ESCRT machinery to repair endosomal damage (Mittal et al., 2018). In contrast, *Anaplasma phagocytophilum*-occupied vacuole (ApV) or *Brucella* containing vacuole (BCV) are positive for MVB markers like LBPA and CD63, similarly to what we observe with *C. burnetii.* Notably, MVB biogenesis significantly contributes to *A. phagocytophilum* replication within infected cells. However, unlike *C. burnetii*, *A. phagocytophilum* or *Brucella* employs exosomes to release infectious progeny to bystander cells (Spera et al., 2023). Accordingly, ApV membranes are positive for ALIX, suggesting a constitutive active ESCRT machinery, as opposed to what is observed here with CCVs. To conclude, our findings describe a new role of the hijacking of the ESCRT machinery during bacterial infections.

Our study demonstrates how a single *C. burnetii* effector protein is sufficient to trigger the biogenesis of an intracellular compartment that is homologous to an early CCV. It would be interesting to extend this study to the identification of the minimal effector set required to allow *C. burnetii* to successfully infect and multiply in cells. For instance, it has been demonstrated that *Salmonella* only needs 5 of its 30 effectors to successfully infect cells (D. Chen et al., 2021). To do so, the authors have used an effector-less *Salmonella* strain and complemented it with differential combination of effectors. Difficulties in the genetic manipulation of *C. burnetii*, together with the bioinformatics prediction of over 100 effector proteins makes this method unapplicable to our model. Regardless, it could be interesting to

develop stable cell lines expressing a defined set of effector proteins and monitor the replication ot the T4SS-deficient *dotA*::Tn mutant in these cells.

Coxiella burnetii harbours a highly similar T4SS to the Dot/Icm system of L*egionella pneumophila*. It would be then very interesting to express Vice in *Legionella pneumophila* to observe if Vice expression and secretion could trigger the recruitment of LBPA or promote the enlargement of the *Legionella* containing vacuole during infection

Finally, we have observed that VICs and WT CCVs exert pressures leading to nuclear deformations in cells (**Figure.24**), which in turn can trigger DNA damage responses (DDR). Indeed, it has been described that DDR could be induced without DNA damages in a non-canonical pathway, notably following remodeling event of the nuclear envelope or by increasing the phospholipid pool available in the nucleus (Garcia et al., 2022; Ovejero et al., 2022). Based on this observation, we have started a collaboration with Dr Maria Moriel-Carretero at the CRBM institute (Montpellier), who is specialized in DNA damage response activation. This collaboration aims to assess whether *C. burnetii* infections trigger DDR and whether effector proteins can interfere in this pathway. Importantly, the induction of VICs is an interesting tool as we can mimic the presence of WT CCV without the expression of other effectors that could affect DDR. Modulation of DDR pathways could allow *C. burnetii* to remain stealth during the infection as they are linked to cell death pathways. To date, many viral infections have been demonstrated to modulate DDR pathways (Lopez et al., 2022), whereas the interplay between DDR pathways and bacterial infections remain under-investigated.

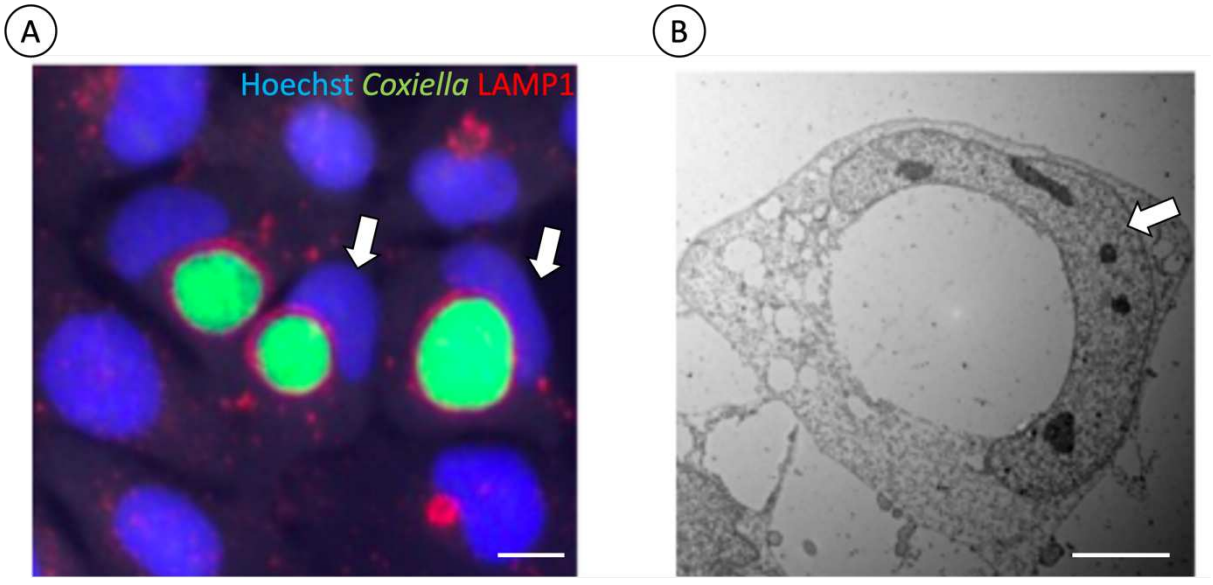


Figure 24: Deformation of nucleus during *C. burnetii* infections and by VICs.

(**A**) U2OS cells infected for 4 days with WT *C. burnetii* (green) were labeled with a LAMP1 antibody to visualize CCVs (red) and nucleus (bleu) were identified using Hoechst. White arrows point at deformed nucleus. Scale bar : 10 µm. (**B**) U2OS cells transfected with HA-Vice for 24h were fixed and prepared for TEM. White arrows point at deformed nucleus. Scale bar : 5 µm.

MATERIAL AND METHODS

Antibodies and reagents

Mouse antibodies used were against Beta-Lactamase (BLAM) (1:2000, MA120370, ThermoFisher Scientific), GAPDH (1:1000, G8795, Sigma), HA (1:1000, 66006-1-Ig, Proteintech), CD63 (WB) (1:50, clone R5G2, MBL), CD63 (IF) (1:200 clone CLB-gran/12, 435, Sanquin), CD9 (WB) (1:2000, 60232-1-Ig, Proteintech), CD81 (1:1000, 66866-1-Ig1, Proteintech) (HIS-HRP (1:2000 HIS.H8 ThermoFisher Scientific), Tubulin (WB) (1:5000, 66031-1-Ig, Proteintech), Nluc (1:1000, N700A, Promega). **Rabbit antibodies** used were against ALIX (WB) (1:1000, 12422-1-AP, Proteintech), HA (1:1000, 51064-2-AP, Proteintech), GFP (1:1000, 50430-2-AP), TSG101 (1:1000, T5701, Sigma), LAMP1 (1:1000, L1418, Sigma), CD63 (WB) (1:1000, 25682-1-AP, Proteintech), Calnexin (WB) (1:2000, 10427-2-AP, Proteintech), HSP70 (WB) (1:2000, 10995-1-AP, Proteintech). Rabbit anti-Coxiella NMII antibodies were generated by Covalab. Hoescht 33258, anti-rabbit and anti-mouse HRP-conjugated antibodies were purchased from Sigma. Mouse and rabbit IgG conjugated to Alexa Fluor 488, 555 or 647 as well as Prolong Gold antifade mounting reagent were purchased from Invitrogen. LysoTracker Red (L7528) was purchased from Life Technologies. Purified L-α-phosphatidylcholine (Egg PC) (Cat# 840051P) , L-α-phosphatidylserine (Brian PS) (Cat#840032C), lysobisphosphatidic acid (LBPA) (cat# 857133C) were purchased from Avanti Polar Lipids, Inc.

Transfections, cell cultures and infections

U2OS (ATCC) cells were routinely maintained in DMEM containing 10% (vol/vol) of foetal bovine serum (FBS) in a humidified atmosphere of 5% CO2 at 37 °C. For ectopic expression of proteins in mammalian cells, cells were grown to 70% confluence and transfected with JetPEI cationic polymer transfection reagent (Polyplus Transfection) diluted in 150 mM NaCl. SiRNA transfections in cells were performed with calcium phosphate buffer in HEK293T (ATCC) for 24h with siRNA TSG101 (S102664522) and siRNA negative Control (S103650318) from Qiagen. For bacterial infections, U2OS cells were seeded in 24-well plates with coverslip one day prior to

infection. Cells were then challenged with different strains at an MOI of 100 followed by 10 minutes of centrifugation at 400 x g for infection synchronization.

E.coli culture

Bacteria were cultured in Luria-Bertani (LB) broth or on LB agar supplemented with ampicillin (100 µg/ml), kanamycin (50 µg/ml) or chloramphenicol (30 µg/ml) as required. Bacterial stocks were made by mixing 500µL of bacterial culture and 500µL of 100% glycerol.

C. burnetii culture

Bacteria were cultured in 1x ACCM-2 (13.4 mM citric acid, 16.1 mM sodium citrate, 3.67 mM potassium phosphate, 1 mM magnesium chloride, 0.02 mM calcium chloride, 0.01 mM iron sulphate, 125.4 mM sodium chloride, 1.5 mM L-cysteine, 0.1 g/L Bacto Neopeptone, 2.5 g/L casamino acids, 1 g/L methyl beta cyclodextrin, 125 ml/L RPMI, pH 4.75) or on 2x ACCM-2 plates supplemented with chloramphenicol (3 µg/ml) and/or kanamycin (375 µg/ml) as required. Bacterial liquid cultures were inoculated into 1x ACCM-2 medium and incubated for 7 days in a humidified atmosphere of 5% CO2 and 2.5% O2 at 37°C. Solid ACCM-2 plates were composed of two layers of agarose in petri dishes by mixing 10ml of pre-warmed 2x ACCM-2 with 10ml of 0.5% of melted Ultra-pure Agarose (Invitrogen). The bacterial inoculum was added to the top agarose solution poured on top of the solidified bottom agarose. Plates were cooled for 20 min, refrigerated at 4°C for 30 min to aid agarose solidification and then placed to air dry in a microbial safety cabinet for 20 min. Plates were incubated for 7 days in a humidified atmosphere of 5% CO2 and 2.5% O2 at 37°C. Colonies were then selected and amplified in liquid culture for 3 weeks. Bacteria were then centrifuged at max speed for 45 minutes and resuspended in 10% DMSO for conservation.

Oligonucleotide primers

Synthetic primers were provided by Sigma-Aldrich GmbH (Germany). Primers used in this study are listed in Table 7. Oligonucleotide primers were used at a final concentration of 10 pmol/µl.

Polymerase Chain Reaction conditions

PCR reactions were performed with 1X Phusion polymerase buffer using 50 ng of template DNA, 1 pmol/µl of each primer, 0.25 mM of each dNTP and 2U/µl of Phusion High-Fidelity DNA polymerase (Thermo Fisher Scientific). PCR was realized in a final volume of 50 µl in 200 µl PCR tubes using the T100 thermal cycler (Bio-RAD) with the following PCR cycle: initial denaturation: 30 seconds at 98°C; 35 denaturation cycles denaturation at 98°C during 30 sec, annealing at X°C for 30 sec, elongation at 72°C for Y min and a final elongation at 72°C for 10 min. X was optimised for each PCR reaction, with a value ranging from 50 to 70°C. X was determined by a Tm calculator software (tmcalculator.neb.com) and Y was calculated according to the estimated size of the DNA fragment to amplify and the polymerisation speed of the DNA polymerase (30 sec per kb on average).

Agarose gel electrophoresis

PCR products were analysed by horizontal electrophoresis. Gels were cast using 1% agarose in 1x TAE buffer (40 mM Tris-acetate, 1 mM EDTA) and a 1:10000 dilution of SYBR Safe DNA gel stain (Invitrogen) to allow DNA visualisation. Prior to gel loading, DNA samples were mixed with 6X loading buffer (2.5% Ficoll®-400, 10 mM EDTA, 3.3 mM Tris-HCl, 0.08% SDS, 0.02% pink/red dye 1, 0.001% blue dye 2). Gels were run in 1x TAE buffer using a constant voltage of 130 V. DNA bands were visualised using a Safe Imager blue light transilluminator (Invitrogen) while fragment size was estimated using a GeneRuler 1 kb Plus DNA ladder (Thermo Fisher Scientific).

Restriction endonuclease digestion and DNA purification

DNA restriction digest was performed overnight at 37°C in a final volume of 50 µl with DNA template, 5 U of each restriction enzyme (NEB), 5 µl of restriction buffer (selected according to the enzyme(s) used, NEB). Digested DNA products were run on agarose gels and purified using a NucleoSpin Gel and PCR clean-up gel extraction kit (Macherey Nagel). Briefly, the agarose plug was melted at 55°C in a high salt-containing buffer and DNA was purified on silica-

membranes columns to remove contaminants. DNA was eluted in 30 µl of sterile deionised water and processed for ligation or stored at -20°C.

Ligation of DNA fragments

Digested PCR fragments were ligated into digested plasmids using T4 DNA ligase and the supplied buffer (NEB). Ligation reactions were performed overnight at room temperature in 20 µl. This comprised 1X ligation buffer (50 mM Tris-HCl pH 7.5, 10 mM MgCl2, 10 mM DTT, 1 mM ATP), 40 U/µl T4 DNA ligase, and digested plasmid and insert DNA used at a vector: insert molar ratio of 1:3.

PCR on colony

PCR on colony was performed in 1X GoTaq® buffer with sample of bacterial colonies, 1 pmol/µl of each primer, 0.25 mM of each dNTP, 1.5mM of MgCl2 and 2U/µl of GoTaq® G2 Flexi DNA polymerase (ProMega). PCR was performed in a final volume of 25 µl using the T100 thermal cycler (Bio-RAD) with the following cycle: initial denaturation for 5 min at 94°C; 35 cycles of denaturation at 94°C for 30 sec, annealing at X°C for 45 sec, elongation at 72°C for Y min; final elongation at 72°C for 10 min. X was optimised for each PCR reaction, with a value ranging from 50 to 70°C. Y was calculated according to the estimated size of the DNA fragment to amplify and the polymerisation speed of the DNA polymerase (1 min per kb on average). PCR-colony amplified was run on agarose gels and successful construct was selected for inoculating overnight liquid culture.

Plasmid DNA purification

Purified plasmid DNA was prepared from 5 ml or 400ml of overnight liquid cultures using GenElute Plasmid Miniprep (Sigma) or NucleoBond Xtra Maxi Pluskit (Macherey Nagel) accordingly, according to the manufacturer's protocols. For conservation and use, plasmid DNA was eluted in sterile water at a concentration of 1 µg/ml when possible.

Immunofluorescence staining and microscopy

Cells were fixed in 4% (wt/vol) paraformaldehyde in phosphate-buffered saline (PBS) pH 7.4 solution at room temperature for 20 min. Samples were then rinsed with PBS solution and incubated in blocking solution (0.5% bovine serum albumin [BSA], 50 mM NHCl in PBS solution, pH 7.4). Cells were then incubated with the primary antibodies diluted in blocking solution for 1 h at room temperature in a humidified atmosphere, washed five times in PBS solution, and further incubated for 1 h with the secondary antibodies diluted in blocking solution complemented with Hoechst 33258 (Sigma) for DNA staining. Coverslips were then mounted on slides using Fluoromount mounting medium (Sigma). Samples were imaged using an epifluorescence EVOS M5000 (Thermo Fisher Scientific) equipped with 63X or 40X oil immersion objectives. Live cell imaging was performed with a spinning disk Olympus SR microscope equipped with sCMOS Fusion BT Hamamatsu camera. Automated epifluorescence microscopy was performed using an ImageXpress PICO equipped with a CMOS 5Mpx 12bits camera. In this case, 25 fields/well were acquired for image analysis. Image J, ICY and CellProfiler software were used for image analysis and quantifications.

Mutant library screening

U2OS cells were seeded into black 96-well plates with clear bottom (Greiner Bio-One, 1,200 cells / well) 24h prior to infection. Cells were infected with a sub-library of GFP-tagged *C. burnetii* mutants (MOI of 100) and centrifuged at 400 x g for 10 min at room temperature. Following 45 minutes of incubation at 37°C in a humidified atmosphere of 5% CO2, infected cells were washed 3 times in PBS pH 7.4 and DMEM containing 10% FBS was added. After 4 days of infection, cells were washed 3 times with PBS and fixed with PBS pH 7.4 containing 4% PFA. Immunofluorescence using Hoescht 33258 (Sigma), anti-LBPA (Echelon Biosciences) and anti-LAMP1 (Sigma) was performed as described above. 25 fields/well were imaged with an ImageXpress PICO microscope equipped with a CMOS 5Mpx 12bits camera and analyzed with ICY software.

Beta-Lactamase Translocation Assay

To assess the translocation of CBU2007, U2OS cells were cultured in black 96-well plates with clear bottom (Greiner Bio-One). The cells were then infected with the appropriate *C. burnetii* strain at a multiplicity of infection (MOI) of 100 and incubated for 24, 48, and 72 hours in a humidified atmosphere of 5% CO2 at 37 °C. Negative and positive controls were included, consisting of *C. burnetii* expressing BLAM alone or with BLAM-tagged CvpB, respectively. For translocation detection, cells were loaded with the fluorescent substrate CCF4/AM from the LiveBLAzer-FRET B/G loading kit (Invitrogen). The loading solution contained 20 mM Hepes, 15 mM probenecid (Sigma) at pH 7.3, diluted in Hank's balanced salt solution (HBSS). After incubating in the dark at room temperature for 1 hour, cells were visualized using an EVOS inverted fluorescence microscope equipped with DAPI and GFP filter cubes. CellProfiler was used to analyze images as previously described(56).

Transmission Electron Microscopy (TEM)

After 5 days of infection, U2OS cells were immersed in a 2.5% glutaraldehyde solution in PHEM buffer (CliniSciences, pH 7.4) and kept overnight at 4°C. Subsequently, they were rinsed with PHEM buffer and post-fixed with a mixture of 0.5% osmic acid and 0.8% potassium hexacyanoferrate trihydrate in the dark at room temperature for 2 hours. After two additional rinses in PHEM buffer, the cells were dehydrated using a series of ethanol solutions with increasing concentrations (30-100%). The cells were then embedded in using an Automated Microwave Tissue Processor for Electron Microscopy (Leica EM AMW). Thin sections (70 nm) were obtained from different levels of each block using a Leica-Reichert Ultracut E microtome. These sections were counterstained with 1.5% uranyl acetate in 70% ethanol and 3% lead citrate (Reynolds method – EMS) and observed using a Tecnai F20 transmission electron microscope operating at 120 kV at the Institut des Neurosciences de Montpellier, INSERM U 1298, Université Montpellier, Montpellier, France.

Correlative Light Electron Microscopy (CLEM)

U2OS cells seeded on Gridded Coverslips (MATTEK) were transfected 24h prior to image acquisition using an Olympus SR microscope. The following steps of sample preparation were performed at room temperature: cells were fixed in HEPES buffer (pH 7.4) containing 2.5% Glutaraldehyde for 2 hours and rinsed 3 times for 5 minutes with HEPES buffer (pH 7.4). Samples were immersed in the Post Fixation solution (HEPES buffer (pH 7.4) containing 1% osmic acid and 1.5% potassium ferrocyanide) for 1h and rinsed 3 times with HEPES buffer (pH 7.4). The enhancement was performed using a solution of 1% tannic acid in HEPES buffer (pH 7.4) for 30 minutes, then washed 3 times with HEPES buffer (pH 7.4). A second post-fixation treatment was done using 1% osmium acid in distilled water for 1h and washed 3 times with distilled water. For dehydration, samples were immersed in a series of ethanol concentrations: 25%, 50%, 75%, and 95% for 10 minutes each and 3 times 15 minutes in 100% ethanol. The first step of embedding was performed using EPON and 2% BDMA (EMS) overnight, and then areas selected by confocal microscopy were specifically encapsulated with the same solution for at least 2 hours. The resin was polymerized for at least 48 hours at 60°C. Images were acquired with a Tecnai F20 transmission electron microscope operating at 120 kV at the Institut des Neurosciences de Montpellier, INSERM U 1298, Université Montpellier, Montpellier, France.

Focused Ion Beam Scanning Electron Microscopy (FIB-SEM)

After the same preparation sample as it has been done for CLEM, with the exception that no encapsulation step has been done, resins were embedded with both infected cells and mounted on aluminum stubs. Crossbeam Auriga (Carl Zeiss, Iena, Germany) workstation microscope chamber. 500 pA milling current was applied for the slice series to remove a 15 nm layer from the specimen block surface. Scanning EM images were recorded with an aperture of 60 µm in the high-current mode at 2 kV of the in-lens EsB detector with the EsB grid set to −300 to −500 V. The voxel size was 15 nm in x, y, and z. The contrast of back-scattered electron images was inverted and acquired using ATLAS 5 software (Carl Zeiss).

Growth assay using Colony Forming Unit (CFU) assay

U2OS cells were plated in duplicate or triplicate in a 6-well plate at 2×105 per well and allowed to adhere overnight. The next day, cells were infected with *wt* or vice::Tn *C. burnetii* in 500µL 10% DMEM for 2 h, then washed 15 times with PBS to remove extracellular bacteria. Cells were scraped into 2mL fresh 10% RPMI and replated in a 24-well plate for analysis at day 3 (500µL cells), and day 6 (125µL cells+325µL 10% RPMI) post infection. To establish a baseline number of internalized bacteria at day zero, 500µL of infected cells was centrifuged into a pellet and lysed in sterile water for 5 min. Lysate was serially diluted in ACCM-D and spotted onto ACCM-D agarose plates, with each condition performed in triplicate. ACCM-D agarose plates were incubated for 7 to 10days at 37°C in 2.5% O2 and 5% CO2, and the number of colonies was counted to determine bacterial viability. For each time point, fold change over day zero was determined.

Magic red assay for cathepsin B activity

Active cathepsin B was quantitated in live cells using Magic Red following the manufacturer's protocol. Briefly, 2x105 U2OS cells were infected with *wt* or vice::Tn *C. burnetii* in 6-well plates for 2 h and washed with PBS. At 1dpi, cells were replated onto Ibidi slides (3X103 cells per channel). Magic Red (Cat. 937; ImmunoChemistry Technologies; Bloomington, MN) was reconstituted in 50µl DMSO, vortexed, and stored at -20°C. Immediately before use, the stock was diluted at 1:10 dilution in sterile water, and then further diluted at 1:25 in 10% DMEM. Cells were incubated with 50 µl diluted Magic Red for 30 min at 37°C and 5% CO2, washed with pre-warmed media, and Z-stack confocal images obtained with identical capture settings with a Nikon spinning disk confocal microscope at 60X. Images were processed identically with ImageJ, and Magic Red fluorescence intensity normalized to the CCV area. At least 15 cells or CCVs were measured per condition in each of three independent experiments.

Protein purification

Codon optimized vice was inserted into the pTwist vector and expressed in Escherichia coli LEMO21 (New England Biolabs). Bacterial cultures were grown at 37°C to mid-exponential phase (OD600nm = 0.5) and protein expression was induced overnight at 16°C with 1 mM isopropyl-β-D-thiogalactopyranoside (IPTG, Euromedex). Bacteria were harvested by centrifugation, resuspended in lysis buffer (50 mM Tris pH 7.8, 500 mM NaCl, 15 mM imidazole, complete anti-protease (Roche)) and lysed by sonication with 5 rounds of 10 seconds pulsation at 15 watts and 6 rounds at 12 watts with 30 seconds in between each round. Lysates were then cleared by centrifugation (12,000 x g, 30 min, 4°C). Proteins were purified on Econo-Pac Chromatography Columns (Bio-rad) with HIS-Select Nickel Affinity Gel (Sigma). After 5 washes with washing buffer (50 mM Tris pH 7.8, 500 mM NaCl, 50 mM imidazole, complete anti-protease (Roche)) proteins were eluted using elution buffer (50 mM Tris pH 7.8, 500 mM NaCl, 1 M imidazole, complete anti-protease (Roche)).

Protein–Lipid Overlay Assay

Purified 6xHIS-GST or 6xHIS-CBU2007 were incubated with PIP Strips membranes (Echelon Biosciences) according to the manufacturer's instructions. Rapidly, TBS-T/BSA (10 mM Tris-HCl pH 8, 150 mM NaCl, 0.1% Tween 20, 3% BSA) was used throughout the assay. Membranes were initially blocked with TBS-T/BSA for 1 hour, then incubated with 1 µg/mL of purified protein overnight at 4 °C. After three washes with TBS-T/BSA, membranes were immunoblotted with anti-HIS HRP-conjugated antibodies for 1 hour at room temperature. Following three washes with TBS-T/BSA, membranes were incubated with ECL for signal detection and visualized using a Chemidoc imaging system (Biorad).

In Vitro Co-sedimentation Assays with Large Unilamellar Vesicles (LUVs)

L-α-phosphatidylcholine, L-α-phosphatidylserine (Brian PS), lysobisphosphatidic acid; LBPA lipids were utilized in this investigation. These lipids were provided by Avanti Polar Lipids. A lipid mix with the proper ratio compositions was made using chloroform, and lipid mixture solutions were dried to make lipid films using a vacuum pump connected rotavapor. Each experiment

compensated for the addition of additional lipid by reducing Egg-PC by an equal mol%. Following a room-temperature incubation, lipid films were hydrated in Tris-buffer (150 mM NaCl, 10 mM Tris-HCl, pH 7.4) via freeze-thaw cycles and extruded through a 200-nm Whatman polycarbonate filter (GE Healthcare). Different molar ratios of lipids were used : 100/0/0; 90/10/0; 70/10/20 and 80/0/20.

At room temperature, a required amount of desired protein was incubated with LUVs of 200 nm (1 mg/mL) in a final volume of 100 µL for 30 minutes. The samples were then centrifuged at 220,000xg for 30 minutes in a Beckman TLA 100 rotor at 4°C. Each sample was then separated into supernatant (S = 90 µL) and pellet (P = 10 µL) containing LUV-bound protein. To maintain the equivalency of the S and P volumes, P was diluted in 80 µL of Tris-NaCl buffer (150 mM NaCl, 10 mM Tris-HCl, pH 7.4). The lipid bound and unbound protein were detected by using western blot. The protein intensities (Intensity of supernatant: Is, intensity of pellet: Ip) were quantified using the Image J software.

Macropinocytosis inhibition assay

U2OS cells were transfected for 8 hours with the appropriate plasmids, then washed 3 times with PBS pH 7.4 and incubated overnight with DMEM containing 50 µM 5-[N-ethyl-N-isopropyl] amiloride (EIPA, MERCK). Cells were then washed 3 times in PBS pH 7.4, fixed in PBS pH 7.4 containing 4% PFA and prepared for fluorescence microscopy as described above.

Dextran internalization assay

U2OS cells were transfected for 8 hours with the appropriate plasmids, then washed 3 times with PBS pH 7.4 and incubated overnight with DMEM containing 0.5 mg/ml 70 kDa TMR Dextran (Thermo Fisher Scientific). Cells were either imaged overnight or directly after being washed 3 times with PBS pH 7.4 24h post-transfection with a spinning disk Olympus SR microscope as described above.

Virion-Like Particles (VLPs) release assay

HEK293T cells were transfected with either scramble or TSG101 targeting siRNA for 24h using the RNAiMAX transfection reagent (Thermo Fisher Scientific) according to the manufacturer's recommendations. Cells were then transfected for 24h with plasmids expressing viral proteins in combination with plasmids expressing either the HA tag alone or HA-Vice. The culture medium of transfected cells was clarified at 800 × g for 5 minutes at 4°C and VLPs were collected after ultracentrifugation at 100,000 × g for 90 minutes at 4°C in an SW41Ti rotor (Beckman Coulter) through a 25% sucrose cushion in TNE buffer (25 mM Tris-HCl, 4 mM EDTA, and 150 mM NaCl). The resulting pellets were resuspended overnight in TNE buffer at 4°C. To assess the release of Gag-VLPs, an anti-Cap24 immunoblot was performed on both supernatant and cell lysate. The calculation for Gag-VLP release was performed using the blot intensity module on Fiji software and applying the following formula: % of Gag in VLP = Gag released/(Gag released + Gag Intracellular normalized to GAPDH).

Lentivirus production and stable cell line engineering

To produce lentiviral particles, HEK293T cells were seeded in a a 100mm dish and co-transfected with **pLENTI** pCMV-dR8.91 and pMD.G at a ratio of 1:1:0.5, respectively. The medium was replaced after 12h, and viral particles were harvested 42 h later, filtered on 0.45-µm filters (Clearline, 146561), and directly used to transduce U2OS target cells. After 4 to 6 h, the transduction medium was replaced with fresh DMEM containing 10% FCS, and puromycin was added 48 h later to select transduced U2OS.

Nanoluc release assay

U2OS cells stably expressing Nluc were plated in a 24well/plate and transfected with HA or HA-Vice. Cells were washed with PBS 8 hours post-transfection, and media was changed for 48 hours before collection. Supernatant was centrifuged at 2,000 x g for 5 minutes at 4°C and 100 µL of clear supernatant of each condition was conserved on ice. Cells were trypsinized and pellet at 500 x g for 5 minutes. NanoLuc (Nano-Glo – Promega) solution assay was prepared following the ration of 1 : 50 (Reagent : Buffer). 100 µL of solution assay was added to the 100

µL of supernatant and the mixture was then split in 3 technical replicates in a 96-well plate (flat white). Cells pellets were resuspended with 200 µL of solution assay and split for technical replicates. Luminescence was measured using TECAN with 0.1s of integration time, no settle time and automatic attenuation.

EVs production, purification and analysis

To produce EVs, U2OS expressing Nluc constructs cells were seeded in 4 150mm dishes and transfected with control HA or with HA-Vice. 24h hours after transfections media was replaced with DMEM + 10% EXO-FREE FBS for 24 hours, to only collect EVs from transfected cells.
The culture media was collected and transferred into a 50 mL Falcon tube placed on ice before cells of both conditions were counted to adjust media volume. Cell lysate was prepared with 1 x 10^7 cells of each condition, centrifuged at 1000 rpm for 5 minutes, followed by removal of the supernatant. The cell pellet was then resuspended in 1 mL of cold PBS centrifuged again at 1000 rpm for 5 minutes. The pellet was finally resuspended in 1 mL of Lysis buffer (RIPA buffer : 25mM Tris pH 7,6; 100mM NaCl; 1% Deoxycholate sodium; 1% NP40; 0,1% SDS; protease inhibitor (ROCHE)) . This mixture is incubated for 30 minutes at 4°C on a rotating wheel. Following incubation, lysates were centrifuged at 12,000 x g for 10 minutes at 4°C and the resulting supernatant (whole cell lysate, WCL) is frozen at -20°C for subsequent Western blot analysis.
For the isolation of extracellular vesicles (EVs), the collected media was centrifuged at 300 x g for 10 minutes at 4°C to remove any floating cells. The media was then a centrifuged at 2,000 x g for 30 minutes at 4°C to eliminate larger EVs, and supernatant was collected again. Amicon-15 Ultra 10KD (Millipore) was used to concentrate media by centrifugation at 4000 x g for 30 minutes at 4°C, resulting in a final volume of 500 µL. Samples were loaded into IZON size exclusion chromatography qEV columns (70nm) and EVs concentrate fraction 1 to 4 were collected. Finally, EVs were concentrate again to a volume of 250 µL using an Amicon-4 Ultra 10KD (Millipore) at 4 000 x g for 25 minutes at 4°C. Samples were then diluted in PBS to NTA (NanoSight300) analysis and TEM. NTA quantification of EVs allowed to us to analyze an equal amount of EVs in between conditions by Western-Blot.

IMMUNOPRECIPITATION ASSAY

U2OS cells were co-transfected at 60% of confluency in a 100mm dish with HA-Vice and AP2M1 constructions for 24h. Cells were washed 2 times with ice-cold PBS and resuspended in 500 µL of PBS at before centrifugation at 4°C at 1,200 x g during 10 minutes. Pellet was resuspended with 200 µL of either RIPA LYSIS buffer or IP LYSIS buffer (25mM Tris; 150mM NaCl; 1mM EDTA; 1% NP40; 5%Glycerol; protease inhibitor) and let 30 minutes on ice. Supernatant of cell lysis was taken after a centrifugation at max speed for 30 minutes at 4°C. For each condition, 40 µL of Anti-HA magnetic beads (PIERCE-ThermoFisher) were washed with 500 µL of IP WASHING buffer (150mmM NaCl; 0,05% TWEEN20; 20mM TRIS-HCL pH 7,6; protease inhibitor). Cell lysate was split, 50 µL LB4X was added to 50 µL of cell lysate and the rest of cell lysate was added to the magnetic beads. Beads and cell lysate were incubated at 4°C on a rotating wheel for at least 2h. Beads were then washed 3 times with IP WASHING buffer and finally resuspended in 50 µL of LB4X prior to Western Blot analysis.

Membrane curvature recognition assay

U2OS cells were seeded in a 6 well-plate and transfected for 24 hours with HA-Vice. SiO2 nano-pillars were treated with 0,1 mg/ml poly-D-lysine (ThermoFisher) for 30 minutes and washed 2 times with DMEM+10% FBS. Transfected cells were trypsinized and resuspended in DMEM, 50,000 cells were seeded in SiO2 nano-pillars containing wells for 24 hours prior to fixation and imaging.

Table 5: List of lipid-binding sensors and markers used in this study.

Sensor/marker	Lipid	Source
2xFYVE	**PI(3)P**	pmCherry-2xFYVE was a gift from Harald Stenmark (Addgene plasmid # 140050 ; http://n2t.net/addgene:140050 ; RRID:Addgene_140050)
OSBP-PH	**PI(4)P**	pBGPa-CMV-GFP-OSBP PH was a gift from Tim Levine (Addgene plasmid # 58724 ; http://n2t.net/addgene:58724 ; RRID:Addgene_58724)
2xPHD	**PI(5)P**	GFP-2xPHD was a gift from Bernard Payrastre (Université de Toulouse)
Akt-PH	**$PI(3,4)P_2$/ $PI(3,4,5)P_3$**	GFP-C1-AKT-PH was a gift from Tobias Meyer (Addgene plasmid # 21218 ; http://n2t.net/addgene:21218 ; RRID:Addgene_21218)

ML1N-PH	**PI(3,5)P_2**	ML1Nwt_in_pEGFP-C1 was a gift from Rob Parton (Addgene plasmid # 67797 ; http://n2t.net/addgene:67797 ; RRID:Addgene_67797)
2xPLCδ-PH	**PI(4,5)P_2**	2PH-PLCdelta-GFP was a gift from Sergio Grinstein (Addgene plasmid # 35142 ; http://n2t.net/addgene:35142 ; RRID:Addgene_35142)
BTK-PH	**PI(3,4,5)P_3**	PH-Btk-GFP was a gift from Tamas Balla (Addgene plasmid # 51463 ; http://n2t.net/addgene:51463 ; RRID:Addgene_51463)
Gab2-PH	**PI(3,4,5)P_3**	PH-Gab2-GFP was a gift from Sergio Grinstein (Addgene plasmid # 35147 ; http://n2t.net/addgene:35147 ; RRID:Addgene_35147)
Lact-C2	**PS**	mRFP-Lact-C2 was a gift from Sergio Grinstein (Addgene plasmid # 74061 ; http://n2t.net/addgene:74061 ; RRID:Addgene_74061)
PKCɣ-C1A	**DAG**	GFP-C1-PKCgamma-C1A was a gift from Tobias Meyer (Addgene plasmid # 21205 ; http://n2t.net/addgene:21205 ; RRID:Addgene_21205)
Spo1op/Spo2op	**PA**	GFP-Spo1op and GFP-Spo2op were gifts from Nicolas Vitale (University of Strasbourg, FR)
anti-LBPA	**LBPA**	Purified Mouse Anti-LBPA antibodies were purchased from Echelon Biosciences (cat. N. Z-PLBPA)

Table 6: List of strains used in this study.

Strain	Description	Origin
WT *C. burnetii*	*C. burnetii* RSA 439 Nine Mile II carrying a transposon insertion between *cbu1847b* and *cbu1849* (*Tn1832*)	Our Laboratory (Martinez *et al.* 2014)
C. burnetii Tn1577	*C. burnetii* RSA 439 Nine Mile II carrying a transposon insertion GFP-CAT in *cbu2007*	Our laboratory
C. burnetii Tn292	*C. burnetii* RSA 439 Nine Mile II carrying a transposon insertion GFP-CAT in *cbu1648* (*dotA*)	Our Laboratory (Martinez *et al.* 2014)
LEMO21(DE3)	*E. coli strain used for T7-driven recombinant protein expression*	New England Biolabs

Table 7: List of primers used in this study.

Primer Name	Sequence
<u>BLAM Translocation Assay</u>	
Generation of pXDC61K-BLAM derivatives	
CBU2007-BamHI	AGGGGATCCATGACAGTTTATTCCCGATATGA
CBU2007-XbaI-rev	AGGTCTAGACTAAAGGGTCCGGTATTTGAAG

Ectopic Expression	
Generation of pLVX-mCherry-N2 derivatives	
PH-PLCδ-MluI	aggacgcgtatggactcgggccgg
PH-PLCδ-NotI-rev	agggcggccgctcgcatccatggagcctgagtggtg
PH-Btk-MluI	aggacgcgtatgcagaaagaagaagctatggcc
PH-Btk-NotI-rev	agggcggccgctcgaggttttaagcttccattcctgtt
Generation of pLVX-mCherry-C1 derivatives	
AKT-PH-EcoRI	agggaattcaaacgacgtagccattgtgaag
AKT-PH-BamHI-rev	aggggatccctatgaattccatggtcacacgg
PH-Gab2-EcoRI	agggaattcaatgagcggcggcggc
PH-Gab2-BamHI-rev	aggggatccttagaagccgcagatctggc
Generation of mCherry2-C1 derivatives	
OSBP-PH-HindIII	AAGCTTcatcggctcgagaggg
OSBP-PH-XmaI-rev	CCCGGGtcacgaattcttcttcacagct
ML1N-XhoI	CTCGAGGGtactctgacctgactatggcaacac
ML1N-XmaI-rev	aggtctagattaattatccaggtcaggggg
PKCg-XhoI	CTCGAGctcacaagttcaccgctcg
PKCgamma-HpaI-rev	GTTAACctagatccggtggatccc
Generation of pRK5-HA derivatives	
CBU2007-BamHI-Fw	CCAGGATCCACAGTTTATTCCCGATATGAATTTC
CBU2007-HindIII-rev	GCTAAGCTTCTAAAGGGTCCGGTATTTGAAG
Generation of pRK5-HA-ALFA	
MluI-ALFA-Fw	CAAACGCGTATGCCATCACGTTTGGAAGAGGAACTGGACGCCGCTTAA CTGAACCTGGATCCCGGGTCGCGAATTC
MluI-pRK5-HA-Rv	CAAACGCGTCGCGCCAGCGTAATCTGGAAC

Generation of pCMV-NbALFA-mScarlet and pCMV-NbALFA-mNeonGreen	
Nanobody-EcoRI-Fw	GTAGAATTCTGGCTCTGGTGATGCATCTG
Nanobody-BamHI-Rv	GTTGGATCCTCAAGAAGTTTGTGGTTTTGGTGTCTTG

Generation of pET28a-GST	
GST-NheI-Fw	GAGTCAGCTAGCATG TCC CCT ATA CTA GGT TAT TGG
GST-BamHI-Rv	CAAGGATCCAACCAGATCCGATTTTGGAG

Generation pLVX-AP2M1 constructs	
225-340 AP2M1 Fw Xho1	GCTCTCGAGGTAcagggcaaaggcacagc
225-340 AP2M1 Rev XmaI	AGCCCCGGGCTAccccttcatgcagatcacc
AP2M1 MU Domain Fw Xho1	GCTCTCGAGGTAtggcggcgagagggtatc
AP2M1 MU Domain Rev XmaI	AGCCCCGGGCTAgcagcgagtttcataaatgccac
AP2M1 N-Ter Fw Xho1	GCTCTCGAGGTAGCTattggaggcttattcatctataatcac
AP2M1 N-Ter Rev XmaI	AGCCCCGGGCTAggtaactgggcagattggc

Table 8: List of plasmids used in this study.

Name	Description	Origin
pXDC61K	IPTG-inducible expression vector for N-terminal fusion of Beta-lactamase (BLAM) in *C. burnetii*	(Burette *et al.* 2020)
pXDC61K-CBU0021	IPTG-inducible expression of BLAM-CBU0021 (CvpB)	(Martinez *et al.* 2016)
pXDC61K-CBU2007	IPTG-inducible expression of BLAM-CBU2007	This study
pLVX-mCherry-N2	CMV expression vector expressing a C-terminal mCherry tag	(Martinez *et al.* 2016)
mCherry2-C1	CMV expression vector expressing a N-terminal mCherry tag	Addgene plasmid # 54563 Michael Davidson
pCL-Neo-mCherry-2xFYVE	Encodes mCherry-2xFYVE (PI3P probe)	(Martinez *et al.* 2016)
mCh2-C1-OSBP-PH	Encodes mCherry-OSBP-PH (PI4P probe)	This study
mCherry-PHD2X	Encodes mCherry-2xPHD (PI5P probe)	Bernard Payrastre
pLVX-mCherry-AKT-PH	Encodes mCherry-AKT-PH ($PI3,4P_2$ probe)	This study
mCh2-C1-ML1N-PH	Encodes mCherry-ML1N-PH ($PI3,5P_2$ probe)	This study
pLVX-PLCδ-2xPH-mCherry	Encodes PLCδ-2xPH-mCherry ($PI4,5P_2$ probe)	This study
pLVX-mCherry-Gab2-PH	Encodes mCherry-Gab2-PH ($PI3,4,5P_3$ probe)	This study
pLVX-BTK-PH-mCherry	Encodes mCherry-BTK-PH ($PI3,4,5P_3$ probe)	This study
mRFP-Lactadherin-C2	Encodes RFP-Lactadherin-C2 (PS probe)	Addgene # 74061 Sergio Grinstein
GFP-Lactadherin-C2	Encodes GFP-Lactadherin-C2 (PS probe)	Addgene #22852 Sergio Grinstein
mCh2-C1-PKCɣ-PH	Encodes mCherry-PKCɣ-PH (DAG probe)	This study
Spo2op1-DsRed	Encodes spo2op1-DsRed (PA probe)	Nicolas Vitale
Spo2op2-RFP	Encodes spo2op2-RFP (PA probe)	Nicolas Vitale
pRK5-HA	CMV expression vector for N-terminal fusion of HA tag	(Martinez *et al.* 2016)
pRK5-HA-ALFA	CMV expression vector for N-terminal fusion of HA-ALFA tag	This study
pRK5-HA-Vice	CMV expression vector expressing *cbu2007* with N-terminal fusion of HA tag	This study
pRK5-HA-ALFA-Vice	CMV expression vector expressing *cbu2007* with N-terminal fusion of HA-ALFA tag	This study
pLVX-GFP-N2	CMV expression vector for C-terminal fusion of GFP	(Burette *et al.*, 2020)
peGFP-RAB7	Encodes human *rab7* with N-terminal fusion of GFP tag	Addgene #61803 Gia Voeltz

pTO_CHMP3_LAP_EGFP	Encodes human *chmp3* with C - terminal fusion of GFP tag	Addgene #101849 Daniel Gerlich
pALIX_FLAG_GFP	Encodes human *alix* with N-terminal fusion of GFP tag	Aurélien Roux (Larios *et al.* 2020)
pTWIST_2007	Encodes *6x**HIS-cbu2007* codon optimised for expression in *E. coli*	Renaud Vincentelli
pET28b_GST	Encodes 6x*HIS-gst*	This study
pCMV-NbALFA-mScarlet	Encodes mScarlet-tagged nanobodies targeting ALFA	This study
pCMV-NbALFA-mNeonGreen	Encodes mNeonGreen-tagged nanobodies targeting ALFA	This study
pmCherry-CHMP4B	Encodes human *chmp4b* with N-terminal fusion of mCherry tag	Aurélien Roux (Larios *et al.* 2020)
pCMVGag	Encodes for HIV-1 *gag* gene	Delphine Muriaux (Burniston *et al.* 1999)
pLifeact-EGFP	Encodes the GFP-tagged Lifeact peptide.	Delphine Muriaux
pCMV-dR8.91	Encodes HIV-1 *gagpol*	Antoine Gross
pMD.G	Encodes *vsv-g*	Antoine Gross
pLenti-4V5 Nanoluc-HSP70	Encodes *hsp-70* with N-terminal fusion of NanoLuc	Cécile Gauthier-Rouvière
pLenti-4V5 Nanoluc-HA-CD63	Encodes *cd63* with N-terminal fusion of NanoLuc	Cécile Gauthier-Rouvière
pLenti-4V5 Nanoluc-HA-CD9	Encodes *cd9* with N-terminal fusion of NanoLuc	Cécile Gauthier-Rouvière
pLVX-FLAG-AP2M1-N-ter	Encodes *ap2m1* N-ter domain with N-terminal fusion of FLAG-tag	This study
pLVX-FLAG-AP2M1-MU	Encodes *ap2m1* mu domain with N-terminal fusion of FLAG-tag	This study
pLVX-FLAG-AP2M1-225-340	Encodes *ap2m1* 225-340 region with N-terminal fusion of FLAG-tag	This study
pmCherry-AP2M1	Encodes *ap2m1* with N-terminal fusion of mCherry-tag	This study
pLVX-GFP-RAB5	Encodes *rab5* with N-terminal fusion of GFP tag	Éric Martinez
pLVX-GFP-RAB6	Encodes *rab6* with N-terminal fusion of GFP tag	Éric Martinez
pLVX-GFP-RAB8	Encodes *rab8* with N-terminal fusion of GFP tag	Éric Martinez
pLVX-GFP-RAB9	Encodes *rab9* with N-terminal fusion of GFP tag	Éric Martinez
pLVX-GFP-RAB11	Encodes *rab11* with N-terminal fusion of GFP tag	Éric Martinez
pLVX-GFP-RAB20	Encodes *rab20* with N-terminal fusion of GFP tag	Éric Martinez
pLVX-GFP-RAB24	Encodes *rab24* with N-terminal fusion of GFP tag	Éric Martinez
pLVX-GFP-RAB26	Encodes *rab26* with N-terminal fusion of GFP tag	Éric Martinez
pLVX-GFP-RAB32	Encodes *rab32* with N-terminal fusion of GFP tag	Éric Martinez

pLVX-GFP-RAB33a	Encodes *rab33a* with N-terminal fusion of GFP tag	Éric Martinez
pLVX-GFP-RAB33b	Encodes *rab33b* with N-terminal fusion of GFP tag	Éric Martinez
pLVX-GFP-RAB37	Encodes *rab37* with N-terminal fusion of GFP tag	Éric Martinez

BIBLIOGRAPHY

Abnave, P., Muracciole, X., & Ghigo, E. (2017). Coxiella burnetii Lipopolysaccharide: What Do We Know? *International Journal of Molecular Sciences*, *18*(12). https://doi.org/10.3390/IJMS18122509

Abou Abdallah, R., Million, M., Delerce, J., Anani, H., Diop, A., Caputo, A., Zgheib, R., Rousset, E., Sidi Boumedine, K., Raoult, D., & Fournier, P. E. (2022). Pangenomic analysis of Coxiella burnetii unveils new traits in genome architecture. *Frontiers in Microbiology*, *13*, 4258. https://doi.org/10.3389/FMICB.2022.1022356/BIBTEX

Ahmadinezhad, M., mounesan, leila, Doostiirani, A., & Yousefi Behzadi, M. (2022). The prevalence of Q fever in the Eastern Mediterranean region: a systematic review and meta-analysis. *Epidemiology and Health*, *44*, e2022097. https://doi.org/10.4178/EPIH.E2022097

Ahmed, S., Bu, W., Lee, R. T. C., Maurer-Stroh, S., & Goh, W. I. (2010). F-BAR domain proteins: Families and function. *Communicative & Integrative Biology*, *3*(2), 116. https://doi.org/10.4161/CIB.3.2.10808

Aistleitner, K., Jeske, R., Wölfel, R., Wießner, A., Kikhney, J., Moter, A., & Stoecker, K. (2018). Detection of Coxiella burnetii in heart valve sections by fluorescence in situ hybridization. *Journal of Medical Microbiology*, *67*(4), 537–542. https://doi.org/10.1099/JMM.0.000704

Akamine, C. M., Perez, M. L., Lee, J. H., & Ing, M. B. (2019). Q Fever in Southern California: a Case Series of 20 Patients from a VA Medical Center. *The American Journal of Tropical Medicine and Hygiene*, *101*(1), 33. https://doi.org/10.4269/AJTMH.18-0283

Alaoui, F. El, Casuso, I., Sanchez-Fuentes, D., Arpin-Andre, C., Rathar, R., Baecker, V., Castro, A., Lorca, T., Viaud, J., Vassilopoulos, S., Carretero-Genevrier, A., & Picas, L. (2022). Structural organization and dynamics of FCHo2 docking on membranes. *ELife*, *11*. https://doi.org/10.7554/ELIFE.73156

Alessandri, C., Bombardieri, M., Di Prospero, L., Conigliaro, P., Conti, F., Labbadia, G., Misasi, R., Sorice, M., & Valesini, G. (2005). Anti-lysobisphosphatidic acid antibodies in patients with antiphospholipid syndrome and systemic lupus erythematosus. *Clinical and Experimental Immunology*, *140*(1), 173. https://doi.org/10.1111/J.1365-2249.2005.02727.X

Allen, P. E., & Martinez, J. J. (2020). Modulation of Host Lipid Pathways by Pathogenic Intracellular Bacteria. *Pathogens 2020, Vol. 9, Page 614*, *9*(8), 614. https://doi.org/10.3390/PATHOGENS9080614

Amano, K. I., & Williams, J. C. (1984). Chemical and immunological characterization of lipopolysaccharides from phase I and phase II Coxiella burnetii. *Journal of Bacteriology*, *160*(3), 994–1002. https://doi.org/10.1128/JB.160.3.994-1002.1984

Amidon, B., Brown, A., & Waite, M. (1996). Transacylase and phospholipases in the synthesis of bis(monoacylglycero)phosphate. *Biochemistry*, *35*(44), 13995–14002. https://doi.org/10.1021/BI961164O

Amidon, B., Schmitt, J. D., King, L., Thuren, T., & Waite, M. (1995). Biosynthetic conversion of phosphatidylglycerol to sn-1:sn-1' bis(monoacylglycerol) phosphate in a macrophage-like cell line. *Biochemistry*, *34*(16), 5554–5560. https://doi.org/10.1021/BI00016A029

Anand, P. K., Anand, E., Bleck, C. K. E., Anes, E., & Griffiths, G. (2010). Exosomal Hsp70 Induces a Pro-Inflammatory Response to Foreign Particles Including Mycobacteria. *PLOS ONE*, *5*(4), e10136. https://doi.org/10.1371/JOURNAL.PONE.0010136

Anderson, A. D., Smoak, B., Shuping, E., Ockenhouse, C., & Petruccelli, B. (2005). Q fever and the US military. *Emerging Infectious Diseases*, *11*(8), 1320–1322. https://doi.org/10.3201/EID1108.050314

Angelakis, E., & Raoult, D. (2010). Q Fever. *Veterinary Microbiology*, *140*(3–4), 297–309. https://doi.org/10.1016/J.VETMIC.2009.07.016

Aronson, N. E., Sanders, J. W., & Moran, K. A. (2006). In harm's way: infections in deployed American military forces. *Clinical Infectious Diseases : An Official Publication of the Infectious Diseases Society of America*, *43*(8), 1045–1051. https://doi.org/10.1086/507539

Aylan, B., Bernard, E. M., Pellegrino, E., Botella, L., Fearns, A., Athanasiadi, N., Bussi, C., Santucci, P., & Gutierrez, M. G. (2023). ATG7 and ATG14 restrict cytosolic and phagosomal Mycobacterium tuberculosis replication in human macrophages. *Nature Microbiology*, *8*(5), 803. https://doi.org/10.1038/S41564-023-01335-9

Babudieri, B., & Moscovici, C. (1952). Experimental and natural infection of birds by Coxiella burneti. *Nature*, *169*(4292), 195–196. https://doi.org/10.1038/169195A0

Baca, O. G., Li, Y. P., & Kumar, H. (1994). Survival of the Q fever agent Coxiella burnetii in the phagolysosome. *Trends in Microbiology*, *2*(12), 476–480. https://doi.org/10.1016/0966-842X(94)90651-3

Balla, T. (2013). Phosphoinositides: Tiny Lipids With Giant Impact on Cell Regulation. *Physiological Reviews*, *93*(3), 1019. https://doi.org/10.1152/PHYSREV.00028.2012

Beare, P. A., Gilk, S. D., Larson, C. L., Hill, J., Stead, C. M., Omsland, A., Cockrell, D. C., Howe, D., Voth, D. E., & Heinzen, R. A. (2011). Dot/Icm type IVB secretion system requirements for Coxiella burnetii growth in human macrophages. *MBio*, *2*(4). https://doi.org/10.1128/MBIO.00175-11

Beare, P. A., Howe, D., Cockrell, D. C., Omsland, A., Hansen, B., & Heinzen, R. A. (2009). Characterization of a Coxiella burnetii ftsZ Mutant Generated by Himar1 Transposon Mutagenesis. *Journal of Bacteriology*, *191*(5), 1369. https://doi.org/10.1128/JB.01580-08

Beare, P. A., Jeffrey, B. M., Long, C. M., Martens, C. M., & Heinzen, R. A. (2018). Genetic mechanisms of Coxiella burnetii lipopolysaccharide phase variation. *PLOS Pathogens*, *14*(3), e1006922. https://doi.org/10.1371/JOURNAL.PPAT.1006922

Beare, P. A., Jeffrey, B. M., Martens, C. A., & Heinzen, R. A. (2017). Draft Genome Sequences of the Avirulent Coxiella burnetii Dugway 7D77-80 and Dugway 7E65-68 Strains Isolated from Rodents in Dugway, Utah. *Genome Announcements*, *5*(39). https://doi.org/10.1128/GENOMEA.00984-17

Beare, P. A., Samuel, J. E., Howe, D., Virtaneva, K., Porcella, S. F., & Heinzen, R. A. (2006a). Genetic diversity of the Q fever agent, Coxiella burnetii, assessed by microarray-based whole-genome comparisons. *Journal of Bacteriology*, *188*(7), 2309–2324. https://doi.org/10.1128/JB.188.7.2309-2324.2006

Beare, P. A., Samuel, J. E., Howe, D., Virtaneva, K., Porcella, S. F., & Heinzen, R. A. (2006b). Genetic diversity of the Q fever agent, Coxiella burnetii, assessed by microarray-based whole-genome comparisons. *Journal of Bacteriology*, *188*(7), 2309–2324. https://doi.org/10.1128/JB.188.7.2309-2324.2006

Beare, P. A., Samuel, J. E., Howe, D., Virtaneva, K., Porcella, S. F., & Heinzen, R. A. (2006c). Genetic diversity of the Q fever agent, Coxiella burnetii, assessed by microarray-based whole-genome comparisons. *Journal of Bacteriology*, *188*(7), 2309–2324. https://doi.org/10.1128/JB.188.7.2309-2324.2006

Beare, P. A., Sandoz, K. M., Larson, C. L., Howe, D., Kronmiller, B., & Heinzen, R. A. (2014). Essential Role for the Response Regulator PmrA in Coxiella burnetii Type 4B Secretion and Colonization of Mammalian Host Cells. *Journal of Bacteriology*, *196*(11), 1925. https://doi.org/10.1128/JB.01532-14

Beare, P. A., Unsworth, N., Andoh, M., Voth, D. E., Omsland, A., Gilk, S. D., Williams, K. P., Sobral, B. W., John J. Kupko, I., Porcella, S. F., Samuel, J. E., & Heinzen, R. A. (2009). Comparative Genomics Reveal Extensive Transposon-Mediated Genomic Plasticity and Diversity among Potential Effector Proteins within the Genus Coxiella. *Infection and Immunity*, *77*(2), 642. https://doi.org/10.1128/IAI.01141-08

Beare, P. A., Unsworth, N., Andoh, M., Voth, D. E., Omsland, A., Gilk, S. D., Williams, K. P., Sobral, B. W., Kupko, J. J., Porcella, S. F., Samuel, J. E., & Heinzen, R. A. (2009). Comparative genomics reveal extensive transposon-mediated genomic plasticity and diversity among potential effector proteins within the genus coxiella. *Infection and Immunity*, *77*(2), 642–656. https://doi.org/10.1128/IAI.01141-08/SUPPL_FILE/SUPPLEMENTAL_TABLES_S1_S13.ZIP

Behnia, R., & Munro, S. (2005). Organelle identity and the signposts for membrane traffic. *Nature 2005 438:7068*, *438*(7068), 597–604. https://doi.org/10.1038/nature04397

Bergelson, L. D., Dyatlovitskaya, E. V., Sorokina, I. B., & Gorkova, N. P. (1974). Phospholipid composition of mitochondria and microsomes from regenerating rat liver and hepatomas of different growth rate. *Biochimica et Biophysica Acta (BBA)/Lipids and Lipid Metabolism*, *360*(3), 361–365. https://doi.org/10.1016/0005-2760(74)90067-8

Berón, W., Gutierrez, M. G., Rabinovitch, M., & Colombo, M. I. (2002). Coxiella burnetii localizes in a Rab7-labeled compartment with autophagic characteristics. *Infection and Immunity*, *70*(10), 5816–5821. https://doi.org/10.1128/IAI.70.10.5816-5821.2002

Bhatty, M., Laverde Gomez, J. A., & Christie, P. J. (2013). The Expanding Bacterial Type IV Secretion Lexicon. *Research in Microbiology*, *164*(6), 620–639. https://doi.org/10.1016/J.RESMIC.2013.03.012

Bienvenu, A., Martinez, E., & Bonazzi, M. (2021). Undercover Agents of Infection: The Stealth Strategies of T4SS-Equipped Bacterial Pathogens. *Toxins*, *13*(10). https://doi.org/10.3390/TOXINS13100713

Birmingham, C. L., Smith, A. C., Bakowski, M. A., Yoshimori, T., & Brumell, J. H. (2006). Autophagy controls Salmonella infection in response to damage to the Salmonella-

containing vacuole. *The Journal of Biological Chemistry*, *281*(16), 11374–11383. https://doi.org/10.1074/JBC.M509157200

Bissig, C., Lenoir, M., Velluz, M. C., Kufareva, I., Abagyan, R., Overduin, M., & Gruenberg, J. (2013). Viral Infection Controlled by a Calcium-Dependent Lipid-Binding Module in ALIX. *Developmental Cell*, *25*(4), 364–373. https://doi.org/10.1016/J.DEVCEL.2013.04.003

Bloomfield, G., & Kay, R. R. (2016). Uses and abuses of macropinocytosis. *Journal of Cell Science*, *129*(14), 2697–2705. https://doi.org/10.1242/JCS.176149

Boarbi, S., Fretin, D., & Mori, M. (2015). Coxiella burnetii, Q fever microbe. *Canadian Journal of Microbiology*, *62*(2), 102–122. https://doi.org/10.1139/CJM-2015-0551/ASSET/IMAGES/CJM-2015-0551TAB2.GIF

Bonazzi, M., Vasudevan, L., Mallet, A., Sachse, M., Sartori, A., Prevost, M. C., Roberts, A., Taner, S. B., Wilbur, J. D., Brodsky, F. M., & Cossart, P. (2011). Clathrin phosphorylation is required for actin recruitment at sites of bacterial adhesion and internalization. *The Journal of Cell Biology*, *195*(3), 525–536. https://doi.org/10.1083/JCB.201105152

Brankatschk, B., Pons, V., Parton, R. G., & Gruenberg, J. (2011). Role of SNX16 in the dynamics of tubulo-cisternal membrane domains of late endosomes. *PloS One*, *6*(7). https://doi.org/10.1371/JOURNAL.PONE.0021771

Breiden, B., & Sandhoff, K. (2019). Lysosomal Glycosphingolipid Storage Diseases. *Annual Review of Biochemistry*, *88*, 461–485. https://doi.org/10.1146/ANNUREV-BIOCHEM-013118-111518

Brooke, R. J., Kretzschmar, M. E. E., Mutters, N. T., & Teunis, P. F. (2013). Human dose response relation for airborne exposure to Coxiella burnetii. *BMC Infectious Diseases*, *13*(1), 1–8. https://doi.org/10.1186/1471-2334-13-488/FIGURES/5

Burette, M., Allombert, J., Lambou, K., Maarifi, G., Nisole, S., Di Russo Case, E., Blanchet, F., Hassen-Khodja, C., Cabantous, S., Samuel, J., Martinez, E., & Bonazzi, M. (2020). Modulation of innate immune signaling by a Coxiella burnetii eukaryotic-like effector protein. *Proceedings of the National Academy of Sciences of the United States of America*, *117*(24), 13708–13718. https://doi.org/10.1073/PNAS.1914892117

Burnet, F. M., & Freeman, M. (1937). EXPERIMENTAL STUDIES ON THE VIRUS OF "Q" FEVER. *Medical Journal of Australia*, *2*(8), 299–305. https://doi.org/10.5694/J.1326-5377.1937.TB43744.X

Buysse, M., Duhayon, M., Cantet, F., Bonazzi, M., & Duron, O. (2021). Vector competence of the African argasid tick Ornithodoros moubata for the Q fever agent Coxiella burnetii. *PLoS Neglected Tropical Diseases*, *15*(1), 1–14. https://doi.org/10.1371/JOURNAL.PNTD.0009008

Campoy, E. M., Martín Zoppino, F. C., & Colombo, M. I. (2011). The early secretory pathway contributes to the growth of the coxiella-replicative niche. *Infection and Immunity*, *79*(1), 402–413. https://doi.org/10.1128/IAI.00688-10

Canton, J., Schlam, D., Breuer, C., Gütschow, M., Glogauer, M., & Grinstein, S. (2016). Calcium-sensing receptors signal constitutive macropinocytosis and facilitate the uptake of NOD2 ligands in macrophages. *Nature Communications*, *7*. https://doi.org/10.1038/NCOMMS11284

Capo, C., Lindberg, F. P., Meconi, S., Zaffran, Y., Tardei, G., Brown, E. J., Raoult, D., & Mege, J.-L. (1999). Subversion of Monocyte Functions by Coxiella burnetii: Impairment of the Cross-Talk Between v 3 Integrin and CR3 1. *The Journal of Immunology*, *163*, 6078–6085. http://journals.aai.org/jimmunol/article-pdf/163/11/6078/1105470/im239906078p.pdf

Carey, K. L., Newton, H. J., Lührmann, A., & Roy, C. R. (2011). The Coxiella burnetii Dot/Icm System Delivers a Unique Repertoire of Type IV Effectors into Host Cells and Is Required for Intracellular Replication. *PLOS Pathogens*, *7*(5), e1002056. https://doi.org/10.1371/JOURNAL.PPAT.1002056

Case, E. D. R., Mahapatra, S., Hoffpauir, C. T., Konganti, K., Hillhouse, A. E., Samuel, J. E., & Van Schaik, E. J. (2022). Primary Murine Macrophages as a Tool for Virulence Factor Discovery in Coxiella burnetii. *Microbiology Spectrum*, *10*(4). https://doi.org/10.1128/SPECTRUM.02484-21

Celina, S. S., & Cerný, J. (2022). Coxiella burnetii in ticks, livestock, pets and wildlife: A mini-review. *Frontiers in Veterinary Science*, *9*. https://doi.org/10.3389/FVETS.2022.1068129

Chandran Darbari, V., & Waksman, G. (2015). Structural Biology of Bacterial Type IV Secretion Systems. *Annual Review of Biochemistry*, *84*, 603–629. https://doi.org/10.1146/ANNUREV-BIOCHEM-062911-102821

Chang, Y.-Y., Enninga, J., Stévenin, V., Yuen-Yan Chang, C., & Pasteur, I. (2021). New methods to decrypt emerging macropinosome functions during the host–pathogen crosstalk. *Cellular Microbiology*, *23*(7), e13342. https://doi.org/10.1111/CMI.13342

Chen, C., Banga, S., Mertens, K., Weber, M. M., Gorbaslieva, I., Tan, Y., Luo, Z. Q., & Samuel, J. E. (2010). Large-scale identification and translocation of type IV secretion substrates by Coxiella burnetii. *Proceedings of the National Academy of Sciences of the United States of America*, *107*(50), 21755–21760. https://doi.org/10.1073/PNAS.1010485107/SUPPL_FILE/ST07.DOC

Chen, D., Burford, W. B., Pham, G., Zhang, L., Alto, L. T., Ertelt, J. M., Winter, M. G., Winter, S. E., Way, S. S., & Alto, N. M. (2021). Systematic Reconstruction of an Effector Gene Network Reveals Determinants of Salmonella Cellular and Tissue Tropism. *Cell Host & Microbe*, *29*(10), 1531. https://doi.org/10.1016/J.CHOM.2021.08.012

Chetrit, D., Hu, B., Christie, P. J., Roy, C. R., & Liu, J. (2018). A unique cytoplasmic ATPase complex defines the Legionella pneumophila type IV secretion channel. *Nature Microbiology*, *3*(6), 678–686. https://doi.org/10.1038/S41564-018-0165-Z

Chevallier, J., Sakai, N., Robert, F., Kobayashi, T., Gruenberg, J., & Matile, S. (2000). Rapid access to synthetic lysobisphosphatidic acids using P(III) chemistry. *Organic Letters*, *2*(13), 1859–1861. https://doi.org/10.1021/OL0059246

Christie, P. J. (2016). The Mosaic Type IV Secretion Systems. *EcoSal Plus*, *7*(1). https://doi.org/10.1128/ECOSALPLUS.ESP-0020-2015

Christie, P. J., Whitaker, N., & González-Rivera, C. (2014). BBA Review Revised Mechanism and Structure of the Bacterial Type IV Secretion Systems. *Biochimica et Biophysica Acta*, *1843*(8), 1578. https://doi.org/10.1016/J.BBAMCR.2013.12.019

Cianciotto, N. P. (2005). Type II secretion: A protein secretion system for all seasons. *Trends in Microbiology*, *13*(12), 581–588. https://doi.org/10.1016/j.tim.2005.09.005

Cooper, K. F. (2018). Till Death Do Us Part: The Marriage of Autophagy and Apoptosis. *Oxidative Medicine and Cellular Longevity*, *2018*. https://doi.org/10.1155/2018/4701275

Crabill, E., Schofield, W. B., Newton, H. J., Goodman, A. L., & Roy, C. R. (2018). Dot/Icm-Translocated Proteins Important for Biogenesis of the Coxiella burnetii-Containing Vacuole Identified by Screening of an Effector Mutant Sublibrary. *Infection and Immunity*, *86*(4). https://doi.org/10.1128/IAI.00758-17

D'Amato, F., Eldin, C., & Raoult, D. (2016). The contribution of genomics to the study of Q fever. *Future Microbiology*, *11*(2), 253–272. https://doi.org/10.2217/FMB.15.137

Davis, G. E., & Cox, H. R. (1938). A FILTER-PASSING INFECTIOUS AGENT ISOLATED FROM TICKS I 1. ISOLATION FROM DERMACENTOR ANDERSONI, REACTIONS IN ANIMALS, AND FILTRATION EXPERIMENTS. *PUBLIC HEALTH REPORTS*.

De Felipe, K. S., Pampou, S., Jovanovic, O. S., Pericone, C. D., Ye, S. F., Kalachikov, S., & Shuman, H. A. (2005). Evidence for acquisition of Legionella type IV secretion substrates via interdomain horizontal gene transfer. *Journal of Bacteriology*, *187*(22), 7716–7726. https://doi.org/10.1128/JB.187.22.7716-7726.2005

de Lange, M. M. A., Scheepmaker, A., van der Hoek, W., Leclercq, M., & Schneeberger, P. M. (2019). Risk of chronic Q fever in patients with cardiac valvulopathy, seven years after a large epidemic in the Netherlands. *PLoS ONE*, *14*(8). https://doi.org/10.1371/JOURNAL.PONE.0221247

Delepelaire, P. (2004). Type I secretion in gram-negative bacteria. *Biochimica et Biophysica Acta (BBA) - Molecular Cell Research*, *1694*(1–3), 149–161. https://doi.org/10.1016/J.BBAMCR.2004.05.001

Derrick, E. H. (1939). Rickettsia burneti: the Cause of "Q" Fever. *Medical Journal of Australia*, *1*.

Di Paolo, G., & De Camilli, P. (2006). Phosphoinositides in cell regulation and membrane dynamics. *Nature*, *443*(7112), 651–657. https://doi.org/10.1038/NATURE05185

Dickson, E. J., & Hille, B. (2019). Understanding phosphoinositides: rare, dynamic, and essential membrane phospholipids. *The Biochemical Journal*, *476*(1), 1. https://doi.org/10.1042/BCJ20180022

Dimik, M., Abeysinghe, P., Logan, J., & Mitchell, M. (2022). The exosome: a review of current therapeutic roles and capabilities in human reproduction. *Drug Delivery and Translational Research 2022 13:2*, *13*(2), 473–502. https://doi.org/10.1007/S13346-022-01225-3

Doherty, G. J., & McMahon, H. T. (2009). Mechanisms of endocytosis. *Annual Review of Biochemistry*, *78*, 857–902. https://doi.org/10.1146/ANNUREV.BIOCHEM.78.081307.110540

Dold, C., Zhu, H., Silva-Reyes, L., Blackwell, L., Linder, A., Bewley, K., Godwin, K., Fotheringham, S., Charlton, S., Kim, Y. C., Pollard, A. J., & Rollier, C. S. (2023). Immunisation with purified Coxiella burnetii phase I lipopolysaccharide confers partial protection in mice independently of co-administered adenovirus vectored vaccines. *Vaccine*, *41*(19). https://doi.org/10.1016/J.VACCINE.2023.04.012

Duden, R. (2003). ER-to-Golgi transport: COP I and COP II function (Review). *Molecular Membrane Biology*, *20*(3), 197–207. https://doi.org/10.1080/0968768031000122548

Dupuis, G., Peter, O., Peacock, M., Burgdorfer, W., & Haller, E. (1985). Immunoglobulin responses in acute Q fever. *Journal of Clinical Microbiology*, *22*(4), 484–487. https://doi.org/10.1128/JCM.22.4.484-487.1985

Durie, C. L., Sheedlo, M. J., Chung, J. M., Byrne, B. G., Su, M., Knight, T., Swanson, M., Lacy, D. B., & Ohi, M. D. (2020). Structural analysis of the Legionella pneumophila Dot/Icm type IV secretion system core complex. *ELife*, *9*, 1–23. https://doi.org/10.7554/ELIFE.59530

Duron, O., Noël, V., McCoy, K. D., Bonazzi, M., Sidi-Boumedine, K., Morel, O., Vavre, F., Zenner, L., Jourdain, E., Durand, P., Arnathau, C., Renaud, F., Trape, J. F., Biguezoton, A. S., Cremaschi, J., Dietrich, M., Léger, E., Appelgren, A., Dupraz, M., … Chevillon, C. (2015). The Recent Evolution of a Maternally-Inherited Endosymbiont of Ticks Led to the Emergence of the Q Fever Pathogen, Coxiella burnetii. *PLoS Pathogens*, *11*(5). https://doi.org/10.1371/JOURNAL.PPAT.1004892

Duron, O., Sidi-Boumedine, K., Rousset, E., Moutailler, S., & Jourdain, E. (2015). The Importance of Ticks in Q Fever Transmission: What Has (and Has Not) Been Demonstrated? *Trends in Parasitology*, *31*(11), 536–552. https://doi.org/10.1016/J.PT.2015.06.014

Edouard, S., & Raoult, D. (2016). Lyophilization to improve the sensitivity of qPCR for bacterial DNA detection in serum: the Q fever paradigm. *Journal of Medical Microbiology*, *65*(6), 462–467. https://doi.org/10.1099/JMM.0.000253

Egami, Y., & Araki, N. (2009). Dynamic Changes in the Spatiotemporal Localization of Rab21 in Live RAW264 Cells during Macropinocytosis. *PLoS ONE*, *4*(8), 6689. https://doi.org/10.1371/JOURNAL.PONE.0006689

Eldin, C., Mélenotte, C., Mediannikov, O., Ghigo, E., Million, M., Edouard, S., Mege, J. L., Maurin, M., & Raoult, D. (2017). From Q Fever to Coxiella burnetii Infection: a Paradigm Change. *Clinical Microbiology Reviews*, *30*(1), 115. https://doi.org/10.1128/CMR.00045-16

Elwell, C. A., & Engel, J. N. (2012). Lipid Acquisition by Intracellular Chlamydiae. *Cellular Microbiology*, *14*(7), 1010. https://doi.org/10.1111/J.1462-5822.2012.01794.X

Eskelinen, E. L. (2006). Roles of LAMP-1 and LAMP-2 in lysosome biogenesis and autophagy. *Molecular Aspects of Medicine*, *27*(5–6), 495–502. https://doi.org/10.1016/J.MAM.2006.08.005

Farge, E., & Devaux, P. F. (1992). Shape changes of giant liposomes induced by an asymmetric transmembrane distribution of phospholipids. *Biophysical Journal*, *61*(2), 347. https://doi.org/10.1016/S0006-3495(92)81841-6

Fernandes, T. D., Cunha, L. D., Ribeiro, J. M., Massis, L. M., Lima-Junior, D. S., Newton, H. J., & Zamboni, D. S. (2016). Murine Alveolar Macrophages Are Highly Susceptible to Replication of Coxiella burnetii Phase II In Vitro. *Infection and Immunity*, *84*(9), 2439–2448. https://doi.org/10.1128/IAI.00411-16

Fernandez, P., López, A. P., & Olmos, Y. (2022). The ESCRT Machinery: Remodeling, Repairing, and Sealing Membranes. *Membranes 2022, Vol. 12, Page 633*, *12*(6), 633. https://doi.org/10.3390/MEMBRANES12060633

Fournier, P. E., Marrie, T. J., & Raoult, D. (1998). Diagnosis of Q fever. *Journal of Clinical Microbiology*, *36*(7), 1823–1834. https://doi.org/10.1128/JCM.36.7.1823-1834.1998/ASSET/6F66806A-9D49-4FCA-9D93-13B69FA12C05/ASSETS/GRAPHIC/JM0781200003.JPEG

Frankel, D., Richet, H., Renvoisé, A., & Raoult, D. (2011). Q fever in France, 1985-2009. *Emerging Infectious Diseases*, *17*(3), 350–356. https://doi.org/10.3201/EID1703.100882

Freed, E. O. (2015). HIV-1 assembly, release and maturation. *Nature Reviews Microbiology 2015 13:8*, *13*(8), 484–496. https://doi.org/10.1038/nrmicro3490

Fu, M., Zhang, J., Zhao, M., Zhang, S., Dai, L., Ouyang, X., Yu, Y., Wen, B., Zhou, D., Sun, Y., Jiao, J., & Xiong, X. (2022). Coxiella burnetii Plasmid Effector B Promotes LC3-II Accumulation and Contributes To Bacterial Virulence in a SCID Mouse Model. *Infection and Immunity*, *90*(6). https://doi.org/10.1128/IAI.00016-22

Füllgrabe, J., Ghislat, G., Cho, D. H., & Rubinsztein, D. C. (2016). Transcriptional regulation of mammalian autophagy at a glance. *Journal of Cell Science*, *129*(16), 3059–3066. https://doi.org/10.1242/JCS.188920

Funato, K., Riezman, H., & Muñiz, M. (2020). Vesicular and non-vesicular lipid export from the ER to the secretory pathway. *Biochimica et Biophysica Acta (BBA) - Molecular and Cell Biology of Lipids*, *1865*(1), 158453. https://doi.org/10.1016/J.BBALIP.2019.04.013

Galve-de Rochemonteix, B., Kobayashi, T., Rosnoblet, C., Lindsay, M., Parton, R. G., Reber, G., De Maistre, E., Wahl, D., Kruithof, E. K. O., Gruenberg, J., & De Moerloose, P. (2000). Interaction of anti-phospholipid antibodies with late endosomes of human endothelial

cells. *Arteriosclerosis, Thrombosis, and Vascular Biology*, *20*(2), 563–574. https://doi.org/10.1161/01.atv.20.2.563

Garcia, M., Kumanski, S., Elías-Villalobos, A., Cazevieille, C., Soulet, C., & Moriel-Carretero, M. (2022). Nuclear ingression of cytoplasmic bodies accompanies a boost in autophagy. *Life Science Alliance*, *5*(9). https://doi.org/10.26508/LSA.202101160

Gaspard, G. J., & McMaster, C. R. (2015). Cardiolipin metabolism and its causal role in the etiology of the inherited cardiomyopathy Barth syndrome. *Chemistry and Physics of Lipids*, *193*, 1–10. https://doi.org/10.1016/J.CHEMPHYSLIP.2015.09.005

Gefenaite, G., Munster, J. M., van Houdt, R., & Hak, E. (2011). Effectiveness of the Q fever vaccine: A meta-analysis. *Vaccine*, *29*(3), 395–398. https://doi.org/10.1016/J.VACCINE.2010.11.008

Gilk, S. D., Cockrell, D. C., Luterbach, C., Hansen, B., Knodler, L. A., Ibarra, J. A., Steele-Mortimer, O., & Heinzen, R. A. (2013). Bacterial colonization of host cells in the absence of cholesterol. *PLoS Pathogens*, *9*(1). https://doi.org/10.1371/JOURNAL.PPAT.1003107

Gillooly, D. J., Morrow, I. C., Lindsay, M., Gould, R., Bryant, N. J., Gaullier, J. M., Parton, R. G., & Stenmark, H. (2000). Localization of phosphatidylinositol 3-phosphate in yeast and mammalian cells. *The EMBO Journal*, *19*(17), 4577–4588. https://doi.org/10.1093/EMBOJ/19.17.4577

Goessweiner-Mohr, N., Arends, K., Keller, W., & Grohmann, E. (2013). Conjugative type IV secretion systems in Gram-positive bacteria. *Plasmid*, *70*(3), 289. https://doi.org/10.1016/J.PLASMID.2013.09.005

Gomez-Navarro, N., & Miller, E. (2016). Protein sorting at the ER-Golgi interface. *The Journal of Cell Biology*, *215*(6), 769–778. https://doi.org/10.1083/JCB.201610031

González-Barrio, D., & Ruiz-Fons, F. (2019). Coxiella burnetii in wild mammals: A systematic review. *Transboundary and Emerging Diseases*, *66*(2), 662–671. https://doi.org/10.1111/TBED.13085

Gonzalez-Rivera, C., Bhatty, M., & Christie, P. J. (2016). Mechanism and function of type IV secretion during infection of the human host. *Microbiology Spectrum*, *4*(3). https://doi.org/10.1128/MICROBIOLSPEC.VMBF-0024-2015

Goursot, A., Mineva, T., Bissig, C., Gruenberg, J., & Salahub, D. R. (2010). Structure, dynamics, and energetics of lysobisphosphatidic acid (LBPA) isomers. *The Journal of Physical Chemistry. B*, *114*(47), 15712–15720. https://doi.org/10.1021/JP108361D

Gozzelino, L., De Santis, M. C., Gulluni, F., Hirsch, E., & Martini, M. (2020). PI(3,4)P2 Signaling in Cancer and Metabolism. *Frontiers in Oncology*, *10*, 360. https://doi.org/10.3389/FONC.2020.00360

Graham, J. G., Winchell, C. G., Sharma, U. M., & Voth, D. E. (2015). Identification of ElpA, a Coxiella burnetii pathotype-specific Dot/Icm type IV secretion system substrate. *Infection and Immunity*, *83*(3), 1190–1198. https://doi.org/10.1128/IAI.02855-14

Gruenberg, J. (2020). Life in the lumen: The multivesicular endosome. *Traffic*, *21*(1), 76–93. https://doi.org/10.1111/TRA.12715/

Gutierrez, M. G., Vázquez, C. L., Munafó, D. B., Zoppino, F. C. M., Berón, W., Rabinovitch, M., & Colombo, M. I. (2005). Autophagy induction favours the generation and maturation of the Coxiella-replicative vacuoles. *Cellular Microbiology*, *7*(7), 981–993. https://doi.org/10.1111/J.1462-5822.2005.00527.X

Hackstadt, T. (1990). The role of lipopolysaccharides in the virulence of Coxiella burnetii. *Annals of the New York Academy of Sciences*, *590*(1), 27–32. https://doi.org/10.1111/J.1749-6632.1990.TB42203.X

Hackstadt, T. (1996). Biosafety concerns and Coxiella burnetii. *Trends in Microbiology*, *4*(9), 341–342. https://doi.org/10.1016/0966-842x(96)81555-1

Hackstadt, T., & Williams, J. C. (1981). Biochemical stratagem for obligate parasitism of eukaryotic cells by Coxiella burnetii. *Proceedings of the National Academy of Sciences of the United States of America*, *78*(5), 3240–3244. https://doi.org/10.1073/PNAS.78.5.3240

Harayama, T., & Riezman, H. (2018). Understanding the diversity of membrane lipid composition. *Nature Reviews. Molecular Cell Biology*, *19*(5), 281–296. https://doi.org/10.1038/NRM.2017.138

Hartzell, J. D., Peng, S. W., Wood-Morris, R. N., Sarmiento, D. M., Collen, J. F., Robben, P. M., & Moran, K. A. (2007). Atypical Q Fever in US Soldiers. *Emerging Infectious Diseases*, *13*(8), 1247. https://doi.org/10.3201/EID1308.070218

Heinzen, R. A., Scidmore, M. A., Rockey, D. D., & Hackstadt, T. (1996). Differential interaction with endocytic and exocytic pathways distinguish parasitophorous vacuoles of Coxiella burnetii and Chlamydia trachomatis. *Infection and Immunity*, *64*(3), 796. https://doi.org/10.1128/IAI.64.3.796-809.1996

Hemsley, C. M., Essex-lopresti, A., Norville, I. H., & Titball, R. W. (2021). Correlating genotyping data of coxiella burnetii with genomic groups. *Pathogens*, *10*(5). https://doi.org/10.3390/PATHOGENS10050604/S1

Hemsley, C. M., O'Neill, P. A., Essex-Lopresti, A., Norville, I. H., Atkins, T. P., & Titball, R. W. (2019). Extensive genome analysis of Coxiella burnetii reveals limited evolution within genomic groups. *BMC Genomics*, *20*(1). https://doi.org/10.1186/S12864-019-5833-8

Heymann, J. A. W., & Hinshaw, J. E. (2009). Dynamins at a glance. *Journal of Cell Science*, *122*(19), 3427. https://doi.org/10.1242/JCS.051714

Hilbink, F., Penrose, M., Ko Vacova, E., & Kazar, J. (1993). Q fever is absent from New Zealand. *International Journal of Epidemiology*, *22*(5), 945–949. https://doi.org/10.1093/IJE/22.5.945

Holmback, J., Karlsson, A., & Arnoldsson, K. C. (2001). Characterization of N-acylphosphatidylethanolamine and acylphosphatidylglycerol in oats. *Lipids*, *36*(2), 153–165. https://doi.org/10.1007/S11745-001-0702-Z

Hoover, T. A., Culp, D. W., Vodkin, M. H., Williams, J. C., & Thompson, H. A. (2002). Chromosomal DNA deletions explain phenotypic characteristics of two antigenic variants, phase II and RSA 514 (crazy), of the Coxiella burnetii nine mile strain. *Infection and Immunity*, *70*(12), 6726–6733. https://doi.org/10.1128/IAI.70.12.6726-2733.2002

Howe, D., & Heinzen, R. A. (2006). Coxiella burnetii inhabits a cholesterol-rich vacuole and influences cellular cholesterol metabolism. *Cellular Microbiology*, *8*(3), 496–507. https://doi.org/10.1111/J.1462-5822.2005.00641.X

Howe, D., Shannon, J. G., Winfree, S., Dorward, D. W., & Heinzen, R. A. (2010). Coxiella burnetii phase I and II variants replicate with similar kinetics in degradative phagolysosome-like compartments of human macrophages. *Infection and Immunity*, *78*(8), 3465–3474. https://doi.org/10.1128/IAI.00406-10

Howe, V., Melnicáková, J., Barák, I., Heinzen, R. A., Howe, D., Melnicáková, J., Barák, I., & Heinzen, R. A. (2003). Maturation of the Coxiella burnetii parasitophorous vacuole requires bacterial protein synthesis but not replication. *Cellular Microbiology*, *5*(7), 469–480. https://doi.org/10.1046/J.1462-5822.2003.00293.X

Huang, B., Ojogun, N., Ragland, S. A., & Carlyon, J. A. (2012). Monoubiquitinated proteins decorate the Anaplasma phagocytophilum-occupied vacuolar membrane. *FEMS*

Immunology and Medical Microbiology, *64*(1), 32–41. https://doi.org/10.1111/J.1574-695X.2011.00873.X

Huang, L., Boyd, D., Amyot, W. M., Hempstead, A. D., Luo, Z. Q., O'Connor, T. J., Chen, C., Machner, M., Montminy, T., & Isberg, R. R. (2011). The E Block motif is associated with Legionella pneumophila translocated substrates. *Cellular Microbiology*, *13*(2), 227–245. https://doi.org/10.1111/J.1462-5822.2010.01531.X

Hudait, A., Hurley, J. H., & Voth, G. A. (2023). Dynamics of upstream ESCRT organization at the HIV-1 budding site. *Biophysical Journal*. https://doi.org/10.1016/J.BPJ.2023.05.020

Hullin-Matsuda, F., Kawasaki, K., Delton-Vandenbroucke, I., Xu, Y., Nishijima, M., Lagarde, M., Schlame, M., & Kobayashi, T. (2007). De novo biosynthesis of the late endosome lipid, bis(monoacylglycero)phosphate. *Journal of Lipid Research*, *48*(9), 1997–2008. https://doi.org/10.1194/JLR.M700154-JLR200

Huotari, J., & Helenius, A. (2011). Endosome maturation. *The EMBO Journal*, *30*(17), 3481. https://doi.org/10.1038/EMBOJ.2011.286

Hurley, J. H. (2015). ESCRTs are everywhere. *The EMBO Journal*, *34*(19), 2398–2407. https://doi.org/10.15252/EMBJ.201592484

Ikonen, E. (2008). Cellular cholesterol trafficking and compartmentalization. *Nature Reviews. Molecular Cell Biology*, *9*(2), 125–138. https://doi.org/10.1038/NRM2336

Jackson, L. P., Kelly, B. T., McCoy, A. J., Gaffry, T., James, L. C., Collins, B. M., Höning, S., Evans, P. R., & Owen, D. J. (2010). A large-scale conformational change couples membrane recruitment to cargo binding in the AP2 clathrin adaptor complex. *Cell*, *141*(7), 1220–1229. https://doi.org/10.1016/J.CELL.2010.05.006

Jacquemyn, J., Cascalho, A., & Goodchild, R. E. (2017). The ins and outs of endoplasmic reticulum-controlled lipid biosynthesis. *EMBO Reports*, *18*(11), 1905–1921. https://doi.org/10.15252/EMBR.201643426

Jäger, C., Lautenschläger, S., Willems, H., & Baljer, G. (2002). Coxiella burnetii plasmid types QpDG and QpH1 are closely related and likely identical. *Veterinary Microbiology*, *89*(2–3), 161–166. https://doi.org/10.1016/S0378-1135(02)00155-4

Jain, A., & Holthuis, J. C. M. (2017). Membrane contact sites, ancient and central hubs of cellular lipid logistics. *Biochimica et Biophysica Acta. Molecular Cell Research*, *1864*(9), 1450–1458. https://doi.org/10.1016/J.BBAMCR.2017.05.017

Jia, J., Claude-Taupin, A., Gu, Y., Choi, S. W., Peters, R., Bissa, B., Mudd, M. H., Allers, L., Pallikkuth, S., Lidke, K. A., Salemi, M., Phinney, B., Mari, M., Reggiori, F., & Deretic, V. (2020a). Galectin-3 Coordinates a Cellular System for Lysosomal Repair and Removal. *Developmental Cell*, *52*(1), 69-87.e8. https://doi.org/10.1016/J.DEVCEL.2019.10.025

Jia, J., Claude-Taupin, A., Gu, Y., Choi, S. W., Peters, R., Bissa, B., Mudd, M. H., Allers, L., Pallikkuth, S., Lidke, K. A., Salemi, M., Phinney, B., Mari, M., Reggiori, F., & Deretic, V. (2020b). Galectin-3 Coordinates a Cellular System for Lysosomal Repair and Removal. *Developmental Cell*, *52*(1), 69-87.e8. https://doi.org/10.1016/J.DEVCEL.2019.10.025

Jin, N., Lang, M. J., & Weisman, L. S. (2016). Phosphatidylinositol 3,5-bisphosphate: Regulation of cellular events in space and time. *Biochemical Society Transactions*, *44*(1), 177. https://doi.org/10.1042/BST20150174

Jin, R. U., & Mills, J. C. (2014). RAB26 coordinates lysosome traffic and mitochondrial localization. *Journal of Cell Science*, *127*(5), 1018–1032. https://doi.org/10.1242/JCS.138776/-/DC1

Justis, A. V., Hansen, B., Beare, P. A., King, K. B., Heinzen, R. A., & Gilk, S. D. (2017). Interactions between the Coxiella burnetii parasitophorous vacuole and the endoplasmic reticulum involve the host protein ORP1L. *Cellular Microbiology*, *19*(1). https://doi.org/10.1111/CMI.12637

Kadlecova, Z., Spielman, S. J., Loerke, D., Mohanakrishnan, A., Reed, D. K., & Schmid, S. L. (2017). Regulation of clathrin-mediated endocytosis by hierarchical allosteric activation of AP2. *The Journal of Cell Biology*, *216*(1), 167–179. https://doi.org/10.1083/JCB.201608071

Kagawa, F. T., Wehner, J. H., & Mohindra, V. (2003). Q fever as a biological weapon. *Seminars in Respiratory Infections*, *18*(3), 183–195. https://europepmc.org/article/med/14505280

Kampschreur, L. M., Dekker, S., Hagenaars, J. C. J. P., Lestrade, P. J., Renders, N. H. M., de Jager-Leclercq, M. G. L., Hermans, M. H. A., Groot, C. A. R., Groenwold, R. H. H., Hoepelman, A. I. M., Wever, P. C., & Oosterheert, J. J. (2012). Identification of Risk Factors for Chronic Q Fever, the Netherlands - Volume 18, Number 4—April 2012 - Emerging Infectious Diseases journal - CDC. *Emerging Infectious Diseases*, *18*(4), 563–570. https://doi.org/10.3201/EID1804.111478

Kampschreur, L. M., Delsing, C. E., Groenwold, R. H. H., Wegdam-Blans, M. C. A., Bleeker-Rovers, C. P., De Jager-Leclercq, M. G. L., Hoepelman, A. I. M., Van Kasteren, M. E., Buijs, J., Renders, N. H. M., Nabuurs-Franssen, M. H., Oosterheert, J. J., & Wever, P. C. (2014).

Chronic Q fever in the Netherlands 5 years after the start of the Q fever epidemic: Results from the dutch chronic Q fever database. *Journal of Clinical Microbiology*, *52*(5), 1637–1643. https://doi.org/10.1128/JCM.03221-13/ASSET/EE93016A-D4E8-416D-8B9D-3A057FFCD76F/ASSETS/GRAPHIC/ZJM9990933660002.JPEG

Keijmel, S. P., Krijger, E., Delsing, C. E., Sprong, T., Nabuurs-Franssen, M. H., & Bleeker-Rovers, C. P. (2015). Differentiation of Acute Q Fever from Other Infections in Patients Presenting to Hospitals, the Netherlands. *Emerging Infectious Diseases*, *21*(8), 1348. https://doi.org/10.3201/EID2108.140196

Kersh, G. J. (2013). Antimicrobial therapies for Q fever. *Expert Review of Anti-Infective Therapy*, *11*(11), 1207. https://doi.org/10.1586/14787210.2013.840534

Kersh, G. J., Oliver, L. D., Self, J. S., Fitzpatrick, K. A., & Massung, R. F. (2011). Virulence of pathogenic Coxiella burnetii strains after growth in the absence of host cells. *Vector Borne and Zoonotic Diseases (Larchmont, N.Y.)*, *11*(11), 1433–1438. https://doi.org/10.1089/VBZ.2011.0670

Khandia, R., Dadar, M., Munjal, A., Dhama, K., Karthik, K., Tiwari, R., Yatoo, M. I., Iqbal, H. M. N., Singh, K. P., Joshi, S. K., & Chaicumpa, W. (2019). A Comprehensive Review of Autophagy and Its Various Roles in Infectious, Non-Infectious, and Lifestyle Diseases: Current Knowledge and Prospects for Disease Prevention, Novel Drug Design, and Therapy. *Cells 2019, Vol. 8, Page 674*, *8*(7), 674. https://doi.org/10.3390/CELLS8070674

Kim, S. G., Kim, E. H., Lafferty, C. J., & Dubovi, E. (2005). Coxiella burnetii in Bulk Tank Milk Samples, United States. *Emerging Infectious Diseases*, *11*(4), 619. https://doi.org/10.3201/EID1104.041036

KITO, M., ISHINAGA, M., NISHIHARA, M., KATO, M., HATA, T., & SAWADA, S. (1975). Metabolism of the Phosphatidylglycerol Molecular Species in Escherichia coli. *European Journal of Biochemistry*, *54*(1), 55–63. https://doi.org/10.1111/j.1432-1033.1975.tb04113.x

Klee, S. R., Tyczka, J., Ellerbrok, H., Franz, T., Linke, S., Baljer, G., & Appel, B. (2006). Highly sensitive real-time PCR for specific detection and quantification of Coxiella burnetii. *BMC Microbiology*, *6*(1), 1–8. https://doi.org/10.1186/1471-2180-6-2/TABLES/4

Knobel, D. L., Maina, A. N., Cutler, S. J., Ogola, E., Feikin, D. R., Junghae, M., Halliday, J. E. B., Richards, A. L., Breiman, R. F., Cleaveland, S., & Njenga, M. K. (2013). Coxiella burnetii in Humans, Domestic Ruminants, and Ticks in Rural Western Kenya. *The American Journal of Tropical Medicine and Hygiene*, *88*(3), 513. https://doi.org/10.4269/AJTMH.12-0169

Kobayashi, T., Beuchat, M. H., Chevallier, J., Makino, A., Mayran, N., Escola, J. M., Lebrand, C., Cosson, P., Kobayashi, T., & Gruenberg, J. (2002). Separation and characterization of late endosomal membrane domains. *The Journal of Biological Chemistry*, *277*(35), 32157–32164. https://doi.org/10.1074/JBC.M202838200

Kobayashi, T., Stang, E., Fang, K. S., De Moerloose, P., Parton, R. G., & Gruenberg, J. (1998a). A lipid associated with the antiphospholipid syndrome regulates endosome structure and function. *Nature*, *392*(6672), 193–197. https://doi.org/10.1038/32440

Kobayashi, T., Stang, E., Fang, K. S., De Moerloose, P., Parton, R. G., & Gruenberg, J. (1998b). A lipid associated with the antiphospholipid syndrome regulates endosome structure and function. *Nature*, *392*(6672), 193–197. https://doi.org/10.1038/32440

Kohler, L. J., Reed, S. R., Sarraf, S. A., Arteaga, D. D., Newton, H. J., & Roy, C. R. (2016). Effector Protein Cig2 Decreases Host Tolerance of Infection by Directing Constitutive Fusion of Autophagosomes with the Coxiella-Containing Vacuole. *MBio*, *7*(4). https://doi.org/10.1128/MBIO.01127-16

Koivusalo, M., Welch, C., Hayashi, H., Scott, C. C., Kim, M., Alexander, T., Touret, N., Hahn, K. M., & Grinstein, S. (2010). Amiloride inhibits macropinocytosis by lowering submembranous pH and preventing Rac1 and Cdc42 signaling. *The Journal of Cell Biology*, *188*(4), 547. https://doi.org/10.1083/JCB.200908086

Kuba, M., Neha, N., Newton, P., Lee, Y. W., Bennett-Wood, V., Hachani, A., De Souza, D. P., Nijagal, B., Dayalan, S., Tull, D., McConville, M. J., Sansom, F. M., & Newton, H. J. (2020). EirA Is a Novel Protein Essential for Intracellular Replication of Coxiella burnetii. *Infection and Immunity*, *88*(6). https://doi.org/10.1128/IAI.00913-19

Landais, C., Fenollar, F., Thuny, F., & Raoult, D. (2007). From acute Q fever to endocarditis: serological follow-up strategy. *Clinical Infectious Diseases : An Official Publication of the Infectious Diseases Society of America*, *44*(10), 1337–1340. https://doi.org/10.1086/515401

Larson, C., Beare, P., Voth, D., Howe, D., Cockrell, D., Bastidas, R., Valdivia, R., & Heinzen, R. (2015). Coxiella burnetii effector proteins that localize to the parasitophorous vacuole membrane promote intracellular replication. *Infection and Immunity*, *83*(2), 661–670. https://doi.org/10.1128/IAI.02763-14

Larson, C. L., Beare, P. A., Howe, D., & Heinzen, R. A. (2013). Coxiella burnetii effector protein subverts clathrin-mediated vesicular trafficking for pathogen vacuole biogenesis.

Proceedings of the National Academy of Sciences of the United States of America, *110*(49). https://doi.org/10.1073/PNAS.1309195110

Larson, C. L., Pullman, W., Beare, P. A., & Heinzen, R. A. (2023). Identification of Type 4B Secretion System Substrates That Are Conserved among Coxiella burnetii Genomes and Promote Intracellular Growth. *Microbiology Spectrum*, *11*(3). https://doi.org/10.1128/SPECTRUM.00696-23

Larson, C. L., Sandoz, K. M., Cockrell, D. C., & Heinzen, R. A. (2019). Noncanonical Inhibition of mTORC1 by Coxiella burnetii Promotes Replication within a Phagolysosome-Like Vacuole. *MBio*, *10*(1). https://doi.org/10.1128/MBIO.02816-18

Latomanski, E. A., & Newton, H. J. (2018). Interaction between autophagic vesicles and the Coxiella-containing vacuole requires CLTC (clathrin heavy chain). *Autophagy*, *14*. https://doi.org/10.1080/15548627.2018.1483806

Latomanski, E. A., Newton, P., Khoo, C. A., & Newton, H. J. (2016). The Effector Cig57 Hijacks FCHO-Mediated Vesicular Trafficking to Facilitate Intracellular Replication of Coxiella burnetii. *PLoS Pathogens*, *12*(12). https://doi.org/10.1371/JOURNAL.PPAT.1006101

Lautenschläger, S., Willems, H., Jäger, C., & Baljer, G. (2000). Sequencing and characterization of the cryptic plasmid QpRS from Coxiella burnetii. *Plasmid*, *44*(1), 85–88. https://doi.org/10.1006/PLAS.2000.1470

Ledda, S., Santucciu, C., Chisu, V., & Masala, G. (2020). Validation of a Novel Commercial ELISA Test for the Detection of Antibodies against Coxiella burnetii. *Pathogens*, *9*(12), 1–14. https://doi.org/10.3390/PATHOGENS9121075

Lee, M. S. (2018). Overview of the Minireviews on Autophagy. *Molecules and Cells*, *41*(1), 1–2. https://doi.org/10.14348/MOLCELLS.2018.0400

Lee, Y. A., Noon, L. A., Akat, K. M., Ybanez, M. D., Lee, T. F., Berres, M. L., Fujiwara, N., Goossens, N., Chou, H. I., Parvin-Nejad, F. P., Khambu, B., Kramer, E. G. M., Gordon, R., Pfleger, C., Germain, D., John, G. R., Campbell, K. N., Yue, Z., Yin, X. M., … Friedman, S. L. (2018). Autophagy is a gatekeeper of hepatic differentiation and carcinogenesis by controlling the degradation of Yap. *Nature Communications*, *9*(1). https://doi.org/10.1038/S41467-018-07338-Z

Lepidi, H., Gouriet, F., & Raoult, D. (2009). Immunohistochemical detection of Coxiella burnetii in chronic Q fever hepatitis. *Clinical Microbiology and Infection : The Official Publication of*

the European Society of Clinical Microbiology and Infectious Diseases, *15 Suppl 2*(SUPPL. 2), 169–170. https://doi.org/10.1111/J.1469-0691.2008.02212.X

Leung-Shea, C., & Danaher, P. J. (2006). Q fever in members of the United States armed forces returning from Iraq. *Clinical Infectious Diseases : An Official Publication of the Infectious Diseases Society of America*, *43*(8). https://doi.org/10.1086/507639

Levental, I., Levental, K. R., & Heberle, F. A. (2020). Lipid Rafts: Controversies Resolved, Mysteries Remain. *Trends in Cell Biology*, *30*(5), 341–353. https://doi.org/10.1016/J.TCB.2020.01.009

Li, G., Liu, H., Luo, Z., & Qiu, J. (2021). Modulation of phagosome phosphoinositide dynamics by a Legionella phosphoinositide 3-kinase. *EMBO Reports*, *22*(3). https://doi.org/10.15252/EMBR.202051163

Liang, X. H., Jackson, S., Seaman, M., Brown, K., Kempkes, B., Hibshoosh, H., & Levine, B. (1999). Induction of autophagy and inhibition of tumorigenesis by beclin 1. *Nature*, *402*(6762), 672–676. https://doi.org/10.1038/45257

Liang, X. H., Kleeman, L. K., Jiang, H. H., Gordon, G., Goldman, J. E., Berry, G., Herman, B., & Levine, B. (1998). Protection against fatal Sindbis virus encephalitis by beclin, a novel Bcl-2-interacting protein. *Journal of Virology*, *72*(11), 8586–8596. https://doi.org/10.1128/JVI.72.11.8586-8596.1998

Lifshitz, Z., Burstein, D., Peeri, M., Zusman, T., Schwartz, K., Shuman, H. A., Pupko, T., & Segal, G. (2013). Computational modeling and experimental validation of the Legionella and Coxiella virulence-related type-IVB secretion signal. *Proceedings of the National Academy of Sciences of the United States of America*, *110*(8), E707. https://doi.org/10.1073/PNAS.1215278110/-/DCSUPPLEMENTAL

Lifshitz, Z., Burstein, D., Schwartz, K., Shuman, H. A., Pupko, T., & Segal, G. (2014). Identification of novel Coxiella burnetii Icm/Dot effectors and genetic analysis of their involvement in modulating a mitogen-activated protein kinase pathway. *Infection and Immunity*, *82*(9), 3740–3752. https://doi.org/10.1128/IAI.01729-14

Lin, X. P., Mintern, J. D., & Gleeson, P. A. (2020). Macropinocytosis in Different Cell Types: Similarities and Differences. *Membranes*, *10*(8), 1–21. https://doi.org/10.3390/MEMBRANES10080177

Liscum, L. (2000). Niemann-Pick type C mutations cause lipid traffic jam. *Traffic (Copenhagen, Denmark)*, *1*(3), 218–225. https://doi.org/10.1034/J.1600-0854.2000.010304.X

Liu, F. T., & Stowell, S. R. (2023). The role of galectins in immunity and infection. *Nature Reviews. Immunology*, 1. https://doi.org/10.1038/S41577-022-00829-7

Long, C. M. (2021). Q fever vaccine development: Current strategies and future considerations. *Pathogens*, *10*(10). https://doi.org/10.3390/PATHOGENS10101223

Lopez, A., Nichols Doyle, R., Sandoval, C., Nisson, K., Yang, V., & Fregoso, O. I. (2022). Viral Modulation of the DNA Damage Response and Innate Immunity: Two Sides of the Same Coin. *Journal of Molecular Biology*, *434*(6), 167327. https://doi.org/10.1016/J.JMB.2021.167327

Lorente-Rodríguez, A., & Barlowe, C. (2011). A Highlights from MBoC Selection: Requirement for Golgi-localized PI(4)P in fusion of COPII vesicles with Golgi compartments. *Molecular Biology of the Cell*, *22*(2), 216. https://doi.org/10.1091/MBC.E10-04-0317

Lou, H. Y., Zhao, W., Zeng, Y., & Cui, B. (2018). The Role of Membrane Curvature in Nanoscale Topography-Induced Intracellular Signaling. *Accounts of Chemical Research*, *51*(5), 1046–1053. https://doi.org/10.1021/ACS.ACCOUNTS.7B00594

Luedtke, B. E., Mahapatra, S., Lutter, E. I., & Shaw, E. I. (2017). The Coxiella Burnetii type IVB secretion system (T4BSS) component DotA is released/secreted during infection of host cells and during in vitro growth in a T4BSS-dependent manner. *Pathogens and Disease*, *75*(4). https://doi.org/10.1093/FEMSPD/FTX047

Luo, S., Lu, S., Fan, H., Chen, Z., Sun, Z., Hu, Y., Li, R., An, X., Uversky, V. N., Tong, Y., & Song, L. (2021). The Coxiella burnetii QpH1 Plasmid Is a Virulence Factor for Colonizing Bone Marrow-Derived Murine Macrophages. *Journal of Bacteriology*, *203*(9). https://doi.org/10.1128/JB.00588-20

Madariaga, M. G., Rezai, K., Trenholme, G. M., & Weinstein, R. A. (2003). Q fever: A biological weapon in your backyard. In *Lancet Infectious Diseases* (Vol. 3, Issue 11, pp. 709–721). Lancet Publishing Group. https://doi.org/10.1016/S1473-3099(03)00804-1

Mahmood, M. I., Noguchi, H., & Okazaki, K. ichi. (2019). Curvature induction and sensing of the F-BAR protein Pacsin1 on lipid membranes via molecular dynamics simulations. *Scientific Reports 2019 9:1*, *9*(1), 1–11. https://doi.org/10.1038/s41598-019-51202-z

Maltese, W. A., & Overmeyer, J. H. (2014). Methuosis: nonapoptotic cell death associated with vacuolization of macropinosome and endosome compartments. *The American Journal of Pathology*, *184*(6), 1630–1642. https://doi.org/10.1016/J.AJPATH.2014.02.028

Margiotta, A., & Bucci, C. (2016). Role of Intermediate Filaments in Vesicular Traffic. *Cells*, *5*(2). https://doi.org/10.3390/CELLS5020020

Marrie, T. J., & Raoult, D. (1997). Q fever--a review and issues for the next century. *International Journal of Antimicrobial Agents*, *8*(3), 145–161. https://doi.org/10.1016/S0924-8579(96)00369-X

Martin, T. F. J. (2012). Role of PI(4,5)P2 in Vesicle Exocytosis and Membrane Fusion. *Sub-Cellular Biochemistry*, *59*, 111. https://doi.org/10.1007/978-94-007-3015-1_4

Martinez, E., Allombert, J., Cantet, F., Lakhani, A., Yandrapalli, N., Neyret, A., Norville, I. H., Favard, C., Muriaux, D., & Bonazzi, M. (2016). Coxiella burnetii effector CvpB modulates phosphoinositide metabolism for optimal vacuole development. *Proceedings of the National Academy of Sciences of the United States of America*, *113*(23), E3260–E3269. https://doi.org/10.1073/pnas.1522811113

Martinez, E., Cantet, F., Fava, L., Norville, I., & Bonazzi, M. (2014). Identification of OmpA, a Coxiella burnetii protein involved in host cell invasion, by multi-phenotypic high-content screening. *PLoS Pathogens*, *10*(3), e1004013. https://doi.org/10.1371/journal.ppat.1004013

Martinez, E., Huc-Brandt, S., Brelle, S., Allombert, J., Cantet, F., Gannoun-Zaki, L., Burette, M., Martin, M., Letourneur, F., Bonazzi, M., & Molle, V. (2020). The secreted protein kinase CstK from Coxiella burnetii influences vacuole development and interacts with the GTPase-activating host protein TBC1D5. *The Journal of Biological Chemistry*, *295*(21), 7391. https://doi.org/10.1074/JBC.RA119.010112

Mason, D., Mallo, G. V., Terebiznik, M. R., Payrastre, B., Finlay, B. B., Brumell, J. H., Rameh, L., & Grinstein, S. (2007a). Alteration of Epithelial Structure and Function Associated with PtdIns(4,5)P2 Degradation by a Bacterial Phosphatase. *Journal of General Physiology*, *129*(4), 267–283. https://doi.org/10.1085/JGP.200609656

Mason, D., Mallo, G. V., Terebiznik, M. R., Payrastre, B., Finlay, B. B., Brumell, J. H., Rameh, L., & Grinstein, S. (2007b). Alteration of Epithelial Structure and Function Associated with PtdIns(4,5)P2 Degradation by a Bacterial Phosphatase. *The Journal of General Physiology*, *129*(4), 267. https://doi.org/10.1085/JGP.200609656

Matos, P. M., Marin, M., Ahn, B., Lam, W., Santos, N. C., & Melikyan, G. B. (2013). Anionic Lipids Are Required for Vesicular Stomatitis Virus G Protein-mediated Single Particle Fusion with

Supported Lipid Bilayers. *The Journal of Biological Chemistry*, *288*(18), 12416. https://doi.org/10.1074/JBC.M113.462028

Matsuo, H., Chevallier, J., Mayran, N., Le Blanc, I., Ferguson, C., Fauré, J., Blanc, N. S., Matile, S., Dubochet, J., Sadoul, R., Parton, R. G., Vilbois, F., & Gruenberg, J. (2004). Role of LBPA and Alix in multivesicular liposome formation and endosome organization. *Science (New York, N.Y.)*, *303*(5657), 531–534. https://doi.org/10.1126/SCIENCE.1092425

Maurin, M., Benoliel, A. M., Bongrand, P., & Raoult, D. (1992). Phagolysosomal alkalinization and the bactericidal effect of antibiotics: the Coxiella burnetii paradigm. *The Journal of Infectious Diseases*, *166*(5), 1097–1102. https://doi.org/10.1093/INFDIS/166.5.1097

Maurin, M., & Raoult, D. (1999). Q Fever. *Clinical Microbiology Reviews*, *12*(4), 518–553. https://doi.org/10.1128/CMR.12.4.518

Mayor, S., Parton, R. G., & Donaldson, J. G. (2014). Clathrin-Independent Pathways of Endocytosis. *Cold Spring Harbor Perspectives in Biology*, *6*(6). https://doi.org/10.1101/CSHPERSPECT.A016758

Mayr, J. A. (2015). Lipid metabolism in mitochondrial membranes. *Journal of Inherited Metabolic Disease*, *38*(1), 137–144. https://doi.org/10.1007/S10545-014-9748-X

McDonough, J. A., Newton, H. J., Klum, S., Swiss, R., Agaisse, H., & Roy, C. R. (2013a). Host pathways important for Coxiella burnetii infection revealed by genome-wide RNA interference screening. *MBio*, *4*(1). https://doi.org/10.1128/MBIO.00606-12/SUPPL_FILE/MBO001131430ST2.XLSX

McDonough, J. A., Newton, H. J., Klum, S., Swiss, R., Agaisse, H., & Roy, C. R. (2013b). Host pathways important for Coxiella burnetii infection revealed by genome-wide RNA interference screening. *MBio*, *4*(1). https://doi.org/10.1128/mBio.00606-12

Meconi, S., Jacomo, V., Boquet, P., Raoult, D., Mege, J. L., & Capo, C. (1998). Coxiella burnetii Induces Reorganization of the Actin Cytoskeleton in Human Monocytes. *Infection and Immunity*, *66*(11), 5527. https://doi.org/10.1128/IAI.66.11.5527-5533.1998

Mehra, A., Zahra, A., Thompson, V., Sirisaengtaksin, N., Wells, A., Porto, M., Köster, S., Penberthy, K., Kubota, Y., Dricot, A., Rogan, D., Vidal, M., Hill, D. E., Bean, A. J., & Philips, J. A. (2013). Mycobacterium tuberculosis Type VII Secreted Effector EsxH Targets Host ESCRT to Impair Trafficking. *PLOS Pathogens*, *9*(10), e1003734. https://doi.org/10.1371/JOURNAL.PPAT.1003734

Melenotte, C., Epelboin, L., Million, M., Hubert, S., Monsec, T., Djossou, F., Mège, J. L., Habib, G., & Raoult, D. (2019). Acute Q Fever Endocarditis: A Paradigm Shift Following the Systematic Use of Transthoracic Echocardiography During Acute Q Fever. *Clinical Infectious Diseases : An Official Publication of the Infectious Diseases Society of America*, *69*(11), 1987–1995. https://doi.org/10.1093/CID/CIZ120

Melenotte, C., Million, M., & Raoult, D. (2019). New insights in Coxiella burnetii infection: diagnosis and therapeutic update. *Https://Doi.Org/10.1080/14787210.2020.1699055*, *18*(1), 75–86. https://doi.org/10.1080/14787210.2020.1699055

Mercer, J., & Helenius, A. (2009). Virus entry by macropinocytosis. *Nature Cell Biology*, *11*(5), 510–520. https://doi.org/10.1038/NCB0509-510

Metters, G., Hemsley, C., Norville, I., & Titball, R. (2023). *Identification of essential genes in Coxiella burnetii*. https://doi.org/10.1099/mgen.0.000944

Metters, G., Norville, I. H., Titball, R. W., & Hemsley, C. M. (2019). From cell culture to cynomolgus macaque: infection models show lineage-specific virulence potential of Coxiella burnetii. *Journal of Medical Microbiology*, *68*(10), 1419–1430. https://doi.org/10.1099/JMM.0.001064

Meusser, B., Purfuerst, B., & Luft, F. C. (2020). *HIV-1 Gag release from yeast reveals ESCRT interaction with the Gag N-terminal protein region*. https://doi.org/10.1074/jbc.RA120.014710

Meyer, D. F., Noroy, C., Moumène, A., Raffaele, S., Albina, E., & Vachiéry, N. (2013). Searching algorithm for type IV secretion system effectors 1.0: a tool for predicting type IV effectors and exploring their genomic context. *Nucleic Acids Research*, *41*(20), 9218. https://doi.org/10.1093/NAR/GKT718

Mijaljica, D., Prescott, M., & Devenish, R. J. (2007). Different fates of mitochondria: alternative ways for degradation? *Autophagy*, *3*(1), 4–9. https://doi.org/10.4161/AUTO.3011

Miller, H. K., Binder, A. M., Peterson, A., Theel, E. S., Volpe, J. M., Couturier, M. R., Cherry, C. C., & Kersh, G. J. (2018). Trends in Q fever serologic testing by immunofluorescence from four large reference laboratories in the United States, 2012-2016. *Scientific Reports*, *8*(1). https://doi.org/10.1038/S41598-018-34702-2

Million, M., Lepidi, H., & Raoult, D. (2009). [Q fever: current diagnosis and treatment options]. *Medecine et Maladies Infectieuses*, *39*(2), 82–94. https://doi.org/10.1016/J.MEDMAL.2008.07.008

Million, M., Roblot, F., Carles, D., D'Amato, F., Protopopescu, C., Carrieri, M. P., & Raoult, D. (2014). Reevaluation of the Risk of Fetal Death and Malformation After Q Fever. *Clinical Infectious Diseases*, *59*(2), 256–260. https://doi.org/10.1093/CID/CIU259

Mittal, E., Skowyra, M. L., Uwase, G., Tinaztepe, E., Mehra, A., Köster, S., Hanson, P. I., & Philips, J. A. (2018). Mycobacterium tuberculosis Type VII Secretion System Effectors Differentially Impact the ESCRT Endomembrane Damage Response. *MBio*, *9*(6). https://doi.org/10.1128/MBIO.01765-18

Mizushima, N. (2007). Autophagy: process and function. *Genes & Development*, *21*(22), 2861–2873. https://doi.org/10.1101/GAD.1599207

Moffatt, J. H., Newton, P., & Newton, H. J. (2015). Coxiella burnetii: turning hostility into a home. *Cellular Microbiology*, *17*(5), 621–631. https://doi.org/10.1111/CMI.12432

Moos, A., & Hackstadt, T. (1987). Comparative virulence of intra- and interstrain lipopolysaccharide variants of Coxiella burnetii in the guinea pig model. *Infection and Immunity*, *55*(5), 1144–1150. https://doi.org/10.1128/IAI.55.5.1144-1150.1987

Moreau, D., Vacca, F., Vossio, S., Scott, C., Colaco, A., Montoya, J. P., Ferguson, C., Damme, M., Moniatte, M., Parton, R. G., Platt, F. M., & Gruenberg, J. (2019). Drug-induced increase in lysobisphosphatidic acid reduces the cholesterol overload in Niemann–Pick type C cells and mice. *EMBO Reports*, *20*(7). https://doi.org/10.15252/EMBR.201847055

Mujalli, A., Viaud, J., Severin, S., Gratacap, M. P., Chicanne, G., Hnia, K., Payrastre, B., & Terrisse, A. D. (2023). Exploring the Role of PI3P in Platelets: Insights from a Novel External PI3P Pool. *Biomolecules*, *13*(4), 583. https://doi.org/10.3390/BIOM13040583/S1

Mulye, M., Samanta, D., Winfree, S., Heinzen, R. A., & Gilk, S. D. (2017). Elevated Cholesterol in the Coxiella burnetii Intracellular Niche Is Bacteriolytic. *MBio*, *8*(1). https://doi.org/10.1128/MBIO.02313-16

Mulye, M., Zapata, B., & Gilk, S. D. (2018). Altering lipid droplet homeostasis affects Coxiella burnetii intracellular growth. *PLOS ONE*, *13*(2), e0192215. https://doi.org/10.1371/JOURNAL.PONE.0192215

Murphy, A. M., & Field, P. R. (1970). The persistence of complement-fixing antibodies to Q-fever (Coxiella burneti) after infection. *The Medical Journal of Australia*, *1*(23), 1148–1150. https://doi.org/10.5694/J.1326-5377.1970.TB84481.X

Nagai, H., & Kubori, T. (2011). Type IVB Secretion Systems of Legionella and Other Gram-Negative Bacteria. *Frontiers in Microbiology*, *2*(JUNE). https://doi.org/10.3389/FMICB.2011.00136

Nagashima, Y., Ma, Z., Liu, X., Qian, X., Zhang, X., von Schaewen, A., & Koiwa, H. (2020). Multiple Quality Control Mechanisms in the ER and TGN Determine Subcellular Dynamics and Salt-Stress Tolerance Function of KORRIGAN1. *The Plant Cell*, *32*(2), 470–485. https://doi.org/10.1105/TPC.19.00714

Newton, H. J., Kohler, L. J., McDonough, J. A., Temoche-Diaz, M., Crabill, E., Hartland, E. L., & Roy, C. R. (2014). A screen of Coxiella burnetii mutants reveals important roles for Dot/Icm effectors and host autophagy in vacuole biogenesis. *PLoS Pathogens*, *10*(7). https://doi.org/10.1371/JOURNAL.PPAT.1004286

Newton, H. J., McDonough, J. A., & Roy, C. R. (2013). Effector protein translocation by the Coxiella burnetii Dot/Icm type IV secretion system requires endocytic maturation of the pathogen-occupied vacuole. *PloS One*, *8*(1), e54566. https://doi.org/10.1371/journal.pone.0054566

Niebuhr, K., Giuriato, S., Pedron, T., Philpott, D. J., Gaits, F., Sable, J., Sheetz, M. P., Parsot, C., Sansonetti, P. J., & Payrastre, B. (2002a). Conversion of PtdIns(4,5)P2 into PtdIns(5)P by the S.flexneri effector IpgD reorganizes host cell morphology. *The EMBO Journal*, *21*(19), 5069–5078. https://doi.org/10.1093/EMBOJ/CDF522

Niebuhr, K., Giuriato, S., Pedron, T., Philpott, D. J., Gaits, F., Sable, J., Sheetz, M. P., Parsot, C., Sansonetti, P. J., & Payrastre, B. (2002b). Conversion of PtdIns(4,5)P2 into PtdIns(5)P by the S.flexneri effector IpgD reorganizes host cell morphology. *The EMBO Journal*, *21*(19), 5069. https://doi.org/10.1093/EMBOJ/CDF522

Nielsen, S. Y., Mølbak, K., Henriksen, T. B., Krogfelt, K. A., Larsen, C. S., & Villumsen, S. (2014). Adverse Pregnancy Outcomes and Coxiella burnetii Antibodies in Pregnant Women, Denmark - Volume 20, Number 6—June 2014 - Emerging Infectious Diseases journal - CDC. *Emerging Infectious Diseases*, *20*(6), 925–931. https://doi.org/10.3201/EID2006.130584

Noah, D. L., Noah, D. L., & Crowder, H. R. (2002). Biological terrorism against animals and humans: a brief review and primer for action. *Journal of the American Veterinary Medical Association*, *221*(1), 40–43. https://doi.org/10.2460/JAVMA.2002.221.40

Nolta, K. V., Rodriguez-Paris, J. M., & Steck, T. L. (1994). Analysis of successive endocytic compartments isolated from Dictyostelium discoideum by magnetic fractionation. *BBA* -

Molecular Cell Research, *1224*(2), 237–246. https://doi.org/10.1016/0167-4889(94)90196-1

Noroy, C., Lefrançois, T., & Meyer, D. F. (2019). Searching algorithm for Type IV effector proteins (S4TE) 2.0: Improved tools for Type IV effector prediction, analysis and comparison in proteobacteria. *PLOS Computational Biology*, *15*(3), e1006847. https://doi.org/10.1371/JOURNAL.PCBI.1006847

Nunès, J. A., & Guittard, G. (2013). An emerging role for PI5P in T cell biology. *Frontiers in Immunology*, *4*(APR), 45995. https://doi.org/10.3389/FIMMU.2013.00080/BIBTEX

Ogawa, M., Yoshimori, T., Suzuki, T., Sagara, H., Mizushima, N., & Sasakawa, C. (2005). Escape of intracellular Shigella from autophagy. *Science (New York, N.Y.)*, *307*(5710), 727–731. https://doi.org/10.1126/SCIENCE.1106036

Omsland, A., Cockrell, D. C., Howe, D., Fischer, E. R., Virtaneva, K., Sturdevant, D. E., Porcella, S. F., & Heinzen, R. A. (2009). Host cell-free growth of the Q fever bacterium Coxiella burnetii. *Proceedings of the National Academy of Sciences of the United States of America*, *106*(11), 4430. https://doi.org/10.1073/PNAS.0812074106

Ovejero, S., Soulet, C., Kumanski, S., & Moriel-Carretero, M. (2022). Coordination between phospholipid pools and DNA damage sensing. *Biology of the Cell*, *114*(8), 211–219. https://doi.org/10.1111/BOC.202200007

Oyston, P. C. F., & Davies, C. (2011). Q fever: The neglected biothreat agent. *Journal of Medical Microbiology*, *60*(1), 9–21. https://doi.org/10.1099/JMM.0.024778-0/CITE/REFWORKS

Padmanabhan, B., Fielden, L. F., Hachani, A., Newton, P., Thomas, D. R., Cho, H.-J., Khoo, C. A., Stojanovski, D., Roy, C. R., Scott, N. E., & Newton, H. J. (2020). *Biogenesis of the Spacious Coxiella-Containing Vacuole Depends on Host Transcription Factors TFEB and TFE3*. https://doi.org/10.1128/IAI.00534-19

Palm, W., & Thompson, C. B. (2017). Nutrient Acquisition Strategies of Mammalian Cells. *Nature*, *546*(7657), 234. https://doi.org/10.1038/NATURE22379

Pan, X., Lührmann, A., Satoh, A., Laskowski-Arce, M. A., & Roy, C. R. (2008). Ankyrin repeat proteins comprise a diverse family of bacterial type IV effectors. *Science*, *320*(5883), 1651–1654. https://doi.org/10.1126/science.1158160

Pareja, M. E. M., Bongiovanni, A., Lafont, F., & Colombo, M. I. (2017). Alterations of the Coxiella burnetii Replicative Vacuole Membrane Integrity and Interplay with the Autophagy

Pathway. *Frontiers in Cellular and Infection Microbiology*, *7*(APR). https://doi.org/10.3389/FCIMB.2017.00112

Park, D., Steiner, S., Shao, M., Roy, C. R., & Liu, J. (2022). Developmental Transitions Coordinate Assembly of the Coxiella burnetii Dot/Icm Type IV Secretion System. *Infection and Immunity*, *90*(10). https://doi.org/10.1128/IAI.00410-22

Parker, N. R., Barralet, J. H., & Bell, A. M. (2006). Q fever. *The Lancet*, *367*(9511), 679–688. https://doi.org/10.1016/S0140-6736(06)68266-4

Patil, S. M., & Regunath, H. (2022). Q Fever. *StatPearls*. https://www.ncbi.nlm.nih.gov/books/NBK556095/

Pattingre, S., Tassa, A., Qu, X., Garuti, R., Xiao, H. L., Mizushima, N., Packer, M., Schneider, M. D., & Levine, B. (2005). Bcl-2 antiapoptotic proteins inhibit Beclin 1-dependent autophagy. *Cell*, *122*(6), 927–939. https://doi.org/10.1016/J.CELL.2005.07.002

Paz, I., Sachse, M., Dupont, N., Mounier, J., Cederfur, C., Enninga, J., Leffler, H., Poirier, F., Prevost, M. C., Lafont, F., & Sansonetti, P. (2010). Galectin-3, a marker for vacuole lysis by invasive pathogens. *Cellular Microbiology*, *12*(4), 530–544. https://doi.org/10.1111/J.1462-5822.2009.01415.X

Peabody, C. R., Chung, Y. J., Yen, M. R., Vidal-Ingigliardi, D., Pugsley, A. P., & Saier, M. H. (2003). Type II protein secretion and its relationship to bacterial type IV pili and archaeal flagella. *Microbiology*, *149*(11), 3051–3072. https://doi.org/10.1099/MIC.0.26364-0/CITE/REFWORKS

Pearson, T., Hornstra, H. M., Hilsabeck, R., Gates, L. T., Olivas, S. M., Birdsell, D. M., Hall, C. M., German, S., Cook, J. M., Seymour, M. L., Priestley, R. A., Kondas, A. V., Clark Friedman, C. L., Price, E. P., Schupp, J. M., Liu, C. M., Price, L. B., Massung, R. F., Kersh, G. J., & Keim, P. (2014). High prevalence and two dominant host-specific genotypes of Coxiella burnetii in U.S. milk. *BMC Microbiology*, *14*(1), 41. https://doi.org/10.1186/1471-2180-14-41

Pechstein, J., Schulze-Luehrmann, J., Bisle, S., Cantet, F., Beare, P. A., Ölke, M., Bonazzi, M., Berens, C., & Lührmann, A. (2020). The Coxiella burnetii T4SS Effector AnkF Is Important for Intracellular Replication. *Frontiers in Cellular and Infection Microbiology*, *10*. https://doi.org/10.3389/FCIMB.2020.559915

Philip, C. B. (1948). Comments on the Name of the Q Fever Organism. *Public Health Reports*, *63*(2), 58. https://doi.org/10.2307/4586402

Pizarro-Cerdá, J., Moreno, E., Sanguedolce, V., Mege, J. L., & Gorvel, J. P. (1998). Virulent Brucella abortus Prevents Lysosome Fusion and Is Distributed within Autophagosome-Like Compartments. *Infection and Immunity*, *66*(5), 2387. https://doi.org/10.1128/IAI.66.5.2387-2392.1998

Poli, A., Zaurito, A. E., Abdul-Hamid, S., Fiume, R., Faenza, I., & Divecha, N. (2019). Phosphatidylinositol 5 Phosphate (PI5P): From Behind the Scenes to the Front (Nuclear) Stage. *International Journal of Molecular Sciences*, *20*(9). https://doi.org/10.3390/IJMS20092080

Posor, Y., Jang, W., & Haucke, V. (2022). Phosphoinositides as membrane organizers. *Nature Reviews Molecular Cell Biology 2022 23:12*, *23*(12), 797–816. https://doi.org/10.1038/s41580-022-00490-x

Pouquet, M., Bareille, N., Guatteo, R., Moret, L., & Beaudeau, F. (2020). Coxiella burnetii infection in humans: to what extent do cattle in infected areas free from small ruminants play a role? *Epidemiology and Infection*, *148*. https://doi.org/10.1017/S0950268820001880

Prudent, E., Lepidi, H., Angelakis, E., & Raoult, D. (2018). Fluorescence In Situ Hybridization (FISH) and Peptide Nucleic Acid Probe-Based FISH for Diagnosis of Q Fever Endocarditis and Vascular Infections. *Journal of Clinical Microbiology*, *56*(9). https://doi.org/10.1128/JCM.00542-18

Rabanal-Ruiz, Y., Otten, E. G., & Korolchuk, V. I. (2017). mTORC1 as the main gateway to autophagy. *Essays in Biochemistry*, *61*(6), 565–584. https://doi.org/10.1042/EBC20170027

Radulovic, M., Schink, K. O., Wenzel, E. M., Nähse, V., Bongiovanni, A., Lafont, F., & Stenmark, H. (2018). ESCRT-mediated lysosome repair precedes lysophagy and promotes cell survival. *The EMBO Journal*, *37*(21). https://doi.org/10.15252/EMBJ.201899753

Raposo, G., & Stoorvogel, W. (2013). Extracellular vesicles: Exosomes, microvesicles, and friends. *The Journal of Cell Biology*, *200*(4), 373. https://doi.org/10.1083/JCB.201211138

Read, C. B., Lind, M. C. H., Chiarelli, T. J., Izac, J. R., Adcox, H. E., Marconi, R. T., & Carlyon, J. A. (2022). The Obligate Intracellular Bacterial Pathogen Anaplasma phagocytophilum Exploits Host Cell Multivesicular Body Biogenesis for Proliferation and Dissemination. *MBio*, *13*(6). https://doi.org/10.1128/MBIO.02961-22

Recouvreux, M. V., & Commisso, C. (2017). Macropinocytosis: A Metabolic Adaptation to Nutrient Stress in Cancer. *Frontiers in Endocrinology*, *8*(SEP), 261. https://doi.org/10.3389/FENDO.2017.00261

Rennick, J. J., Johnston, A. P. R., & Parton, R. G. (2021a). Key principles and methods for studying the endocytosis of biological and nanoparticle therapeutics. *Nature Nanotechnology 2021 16:3*, *16*(3), 266–276. https://doi.org/10.1038/s41565-021-00858-8

Rennick, J. J., Johnston, A. P. R., & Parton, R. G. (2021b). Key principles and methods for studying the endocytosis of biological and nanoparticle therapeutics. *Nature Nanotechnology 2021 16:3*, *16*(3), 266–276. https://doi.org/10.1038/s41565-021-00858-8

Reukers, D. F. M., van Jaarsveld, C. H. M., Akkermans, R. P., Keijmel, S. P., Morroy, G., van Dam, A. S. G., Wever, P. C., Wielders, C. C. H., van der Velden, K., van Loenhout, J. A. F., & Hautvast, J. L. A. (2022). Impact of Q-fever on physical and psychosocial functioning until 8 years after Coxiella burnetii infection: An integrative data analysis. *PLoS ONE*, *17*(2). https://doi.org/10.1371/JOURNAL.PONE.0263239

Rivera-Cuevas, Y., & Carruthers, V. B. (2023). The multifaceted interactions between pathogens and host ESCRT machinery. *PLOS Pathogens*, *19*(5), e1011344. https://doi.org/10.1371/JOURNAL.PPAT.1011344

ROBBINS, F. C., GAULD, R. L., & WARNER, F. B. (1946). Q fever in the Mediterranean area; report of its occurrence in Allied troops; epidemiology. *American Journal of Hygiene*, *44*(1), 23–50. https://doi.org/10.1093/OXFORDJOURNALS.AJE.A119082

Roest, H. I. J., Ruuls, R. C., Tilburg, J. J. H. C., Nabuurs-Franssen, M. H., Klaassen, C. H. W., Vellema, P., van den Brom, R., Dercksen, D., Wouda, W., Spierenburg, M. A. H., van der Spek, A. N., Buijs, R., de Boer, A. G., Willemsen, P. T. J., & van Zijderveld, F. G. (2011). Molecular Epidemiology of Coxiella burnetii from Ruminants in Q Fever Outbreak, the Netherlands. *Emerging Infectious Diseases*, *17*(4), 668. https://doi.org/10.3201/EID1704.101562

Rolain, J. M., Lambert, F., & Raoult, D. (2005). Activity of Telithromycin against Thirteen New Isolates of C. burnetii Including Three Resistant to Doxycycline. *Annals of the New York Academy of Sciences*, *1063*(1), 252–256. https://doi.org/10.1196/ANNALS.1355.039

Rosales, E. M., Aguilera, M. O., Salinas, R. P., Carminati, S. A., Colombo, M. I., Martinez-Quiles, N., & Berón, W. (2012). Cortactin Is Involved in the Entry of Coxiella burnetii into Non-Phagocytic Cells. *PLoS ONE*, *7*(6). https://doi.org/10.1371/JOURNAL.PONE.0039348

Roy, C. R., & Kagan, J. C. (2013). *Evasion of Phagosome Lysosome Fusion and Establishment of a Replicative Organelle by the Intracellular Pathogen Legionella pneumophila*. https://www.ncbi.nlm.nih.gov/books/NBK6111/

Ruiz, S., & Wolfe, D. N. (2014). Vaccination against Q fever for biodefense and public health indications. *Frontiers in Microbiology*, *5*(DEC), 726. https://doi.org/10.3389/FMICB.2014.00726/BIBTEX

Salamon, R. S., & Backer, J. M. (2013). Phosphatidylinositol-3,4,5-trisphosphate: tool of choice for class I PI 3-kinases. *BioEssays : News and Reviews in Molecular, Cellular and Developmental Biology*, *35*(7), 602–611. https://doi.org/10.1002/BIES.201200176

Salinas, R. P., Flores, R. M. O., Distel, J. S., Aguilera, M. O., Colombo, M. I., & Berón, W. (2015). Coxiella burnetii Phagocytosis Is Regulated by GTPases of the Rho Family and the RhoA Effectors mDia1 and ROCK. *PLoS ONE*, *10*(12). https://doi.org/10.1371/JOURNAL.PONE.0145211

Sallusto, F., Cella, M., Danieli, C., & Lanzavecchia, A. (1995). Dendritic cells use macropinocytosis and the mannose receptor to concentrate macromolecules in the major histocompatibility complex class II compartment: downregulation by cytokines and bacterial products. *The Journal of Experimental Medicine*, *182*(2), 389. https://doi.org/10.1084/JEM.182.2.389

Samanta, D., Clemente, T. M., Schuler, B. E., & Gilk, S. D. (2019). Coxiella burnetii Type 4B Secretion System-dependent manipulation of endolysosomal maturation is required for bacterial growth. *PLOS Pathogens*, *15*(12), e1007855. https://doi.org/10.1371/JOURNAL.PPAT.1007855

Sanchez, S. E., Vallejo-Esquerra, E., & Omsland, A. (2018). Use of Axenic Culture Tools to Study Coxiella burnetii. *Current Protocols in Microbiology*, *50*(1). https://doi.org/10.1002/CPMC.52

Sander, W. E., King, R., Graser, W., Kapfer, J. M., Engel, A. I., Adamovicz, L., & Allender, M. C. (2021). Coxiella burnetii in 3 Species of Turtles in the Upper Midwest, United States. *Emerging Infectious Diseases*, *27*(12), 3199. https://doi.org/10.3201/EID2712.211278

Sarkes, D., & Rameh, L. E. (2010). A novel HPLC-based approach makes possible the spatial characterization of cellular PtdIns5P and other phosphoinositides. *The Biochemical Journal*, *428*(3), 375–384. https://doi.org/10.1042/BJ20100129

Schink, K. O., Tan, K. W., & Stenmark, H. (2016). Phosphoinositides in Control of Membrane Dynamics. *Annual Review of Cell and Developmental Biology*, *32*, 143–171. https://doi.org/10.1146/ANNUREV-CELLBIO-111315-125349

Schuler, B., Sladek, M., & Gilk, S. D. (2023). Host Lipid Transport Protein ORP1 Is Necessary for Coxiella burnetii Growth and Vacuole Expansion in Macrophages. *MSphere*, *8*(3). https://doi.org/10.1128/MSPHERE.00104-23/ASSET/B48648A8-EDCB-4906-8124-5E272F3603B6/ASSETS/IMAGES/MEDIUM/MSPHERE.00104-23-F005.GIF

Schulze-Luehrmann, J., Eckart, R. A., Ölke, M., Saftig, P., Liebler-Tenorio, E., & Lührmann, A. (2016). LAMP proteins account for the maturation delay during the establishment of the Coxiella burnetii-containing vacuole. *Cellular Microbiology*, *18*(2), 181–194. https://doi.org/10.1111/CMI.12494

Scott, C. C., & Gruenberg, J. (2011). Ion flux and the function of endosomes and lysosomes: pH is just the start: the flux of ions across endosomal membranes influences endosome function not only through regulation of the luminal pH. *BioEssays : News and Reviews in Molecular, Cellular and Developmental Biology*, *33*(2), 103–110. https://doi.org/10.1002/BIES.201000108

Seshadri, R., Paulsen, I. T., Eisen, J. A., Read, T. D., Nelson, K. E., Nelson, W. C., Ward, N. L., Tettelin, H., Davidsen, T. M., Beanan, M. J., Deboy, R. T., Daugherty, S. C., Brinkac, L. M., Madupu, R., Dodson, R. J., Khouri, H. M., Lee, K. H., Carty, H. A., Scanlan, D., … Heidelberg, J. F. (2003a). Complete genome sequence of the Q-fever pathogen Coxiella burnetii. *Proceedings of the National Academy of Sciences of the United States of America*, *100*(9), 5455–5460. https://doi.org/10.1073/PNAS.0931379100

Seshadri, R., Paulsen, I. T., Eisen, J. A., Read, T. D., Nelson, K. E., Nelson, W. C., Ward, N. L., Tettelin, H., Davidsen, T. M., Beanan, M. J., Deboy, R. T., Daugherty, S. C., Brinkac, L. M., Madupu, R., Dodson, R. J., Khouri, H. M., Lee, K. H., Carty, H. A., Scanlan, D., … Heidelberg, J. F. (2003b). Complete genome sequence of the Q-fever pathogen Coxiella burnetii. *Proceedings of the National Academy of Sciences of the United States of America*, *100*(9), 5455–5460. https://doi.org/10.1073/PNAS.0931379100/SUPPL_FILE/1379FIG5.JPG

Shannon, J. G., Howe, D., & Heinzen, R. A. (2005). Virulent Coxiella burnetii does not activate human dendritic cells: role of lipopolysaccharide as a shielding molecule. *Proceedings of the National Academy of Sciences of the United States of America*, *102*(24), 8722–8727. https://doi.org/10.1073/PNAS.0501863102

Sheedlo, M. J., Durie, C. L., Chung, J. M., Chang, L., Roberts, J., Swanson, M., Lacy, D. B., & Ohi, M. D. (2021). Cryo-EM reveals new species-specific proteins and symmetry elements in the Legionella pneumophila Dot/Icm T4SS. *ELife*, *10*. https://doi.org/10.7554/ELIFE.70427

Shepard, C. C. (1947). An outbreak of q fever in a Chicago packing house. *American Journal of Epidemiology*, *46*(2), 185–192. https://doi.org/10.1093/OXFORDJOURNALS.AJE.A119162/2/46-2-185.PDF.GIF

Siadous, F. A., Cantet, F., Van Schaik, E., Burette, M., Allombert, J., Lakhani, A., Bonaventure, B., Goujon, C., Samuel, J., Bonazzi, M., & Martinez, E. (2020). Coxiella effector protein CvpF subverts RAB26-dependent autophagy to promote vacuole biogenesis and virulence. *Autophagy*, 1–17. https://doi.org/10.1080/15548627.2020.1728098

Signs, K. A., Stobierski, M. G., & Gandhi, T. N. (2012). Q fever cluster among raw milk drinkers in Michigan, 2011. *Clinical Infectious Diseases : An Official Publication of the Infectious Diseases Society of America*, *55*(10), 1387–1389. https://doi.org/10.1093/CID/CIS690

Simons, K., & Gruenberg, J. (2000). Jamming the endosomal system: lipid rafts and lysosomal storage diseases. *Trends in Cell Biology*, *10*(11), 459–462. https://doi.org/10.1016/S0962-8924(00)01847-X

Skotland, T., Hessvik, N. P., Sandvig, K., & Llorente, A. (2019). Thematic Review Series: Exosomes and Microvesicles: Lipids as Key Components of their Biogenesis and Functions: Exosomal lipid composition and the role of ether lipids and phosphoinositides in exosome biology. *Journal of Lipid Research*, *60*(1), 9. https://doi.org/10.1194/JLR.R084343

Skowyra, M. L., Schlesinger, P. H., Naismith, T. V., & Hanson, P. I. (2018). Triggered recruitment of ESCRT machinery promotes endolysosomal repair. *Science (New York, N.Y.)*, *360*(6384). https://doi.org/10.1126/SCIENCE.AAR5078

Slotte, J. P. (2013). Biological functions of sphingomyelins. *Progress in Lipid Research*, *52*(4), 424–437. https://doi.org/10.1016/J.PLIPRES.2013.05.001

Smith, C. B., Evavold, C., & Kersh, G. J. (2019). The Effect of pH on Antibiotic Efficacy against Coxiella burnetii in Axenic Media. *Scientific Reports 2019 9:1*, *9*(1), 1–9. https://doi.org/10.1038/s41598-019-54556-6

Sobotta, K., Bonkowski, K., Liebler-Tenorio, E., Germon, P., Rainard, P., Hambruch, N., Pfarrer, C., Jacobsen, I. D., & Menge, C. (2017). Permissiveness of bovine epithelial cells from lung, intestine, placenta and udder for infection with Coxiella burnetii. *Veterinary Research*, *48*(1). https://doi.org/10.1186/S13567-017-0430-9

Sobotta, K., Hillarius, K., Mager, M., Kerner, K., Heydel, C., & Menge, C. (2016). Coxiella burnetii Infects Primary Bovine Macrophages and Limits Their Host Cell Response. *Infection and Immunity*, *84*(6), 1722–1734. https://doi.org/10.1128/IAI.01208-15

Somerharju, P. (1979). Subcellular localization of three degeneration-associated phospholipids in cultured hamster fibroblasts (BHK21 cells). *Biochimica et Biophysica Acta (BBA)/Lipids and Lipid Metabolism*, *574*(3), 461–470. https://doi.org/10.1016/0005-2760(79)90242-X

Spera, J. M., Guaimas, F., Czibener, C., & Ugalde, J. E. (2023). Brucella Egresses from Host Cells Exploiting Multivesicular Bodies. *MBio*, *14*(1). https://doi.org/10.1128/MBIO.03338-22

Stead, C. M., Omsland, A., Beare, P. A., Sandoz, K. M., & Heinzen, R. A. (2013). Sec-mediated secretion by Coxiella burnetii. *BMC Microbiology*, *13*(1), 1–10. https://doi.org/10.1186/1471-2180-13-222/FIGURES/6

Stenmark, H. (2009). Rab GTPases as coordinators of vesicle traffic. *Nature Reviews Molecular Cell Biology 2009 10:8*, *10*(8), 513–525. https://doi.org/10.1038/nrm2728

Strauss, B., Löschau, M., Seidel, T., Stallmach, A., & Thomas, A. (2012). Are fatigue symptoms and chronic fatigue syndrome following Q fever infection related to psychosocial variables? *Journal of Psychosomatic Research*, *72*(4), 300–304. https://doi.org/10.1016/J.JPSYCHORES.2012.01.010

Stuffers, S., Sem Wegner, C., Stenmark, H., & Brech, A. (2009). Multivesicular Endosome Biogenesis in the Absence of ESCRTs. *Traffic*, *10*(7), 925–937. https://doi.org/10.1111/J.1600-0854.2009.00920.X

Suhan, M. L., Chen, S. Y., & Thompson, H. A. (1996). Transformation of Coxiella burnetii to ampicillin resistance. *Journal of Bacteriology*, *178*(9), 2701–2708. https://doi.org/10.1128/JB.178.9.2701-2708.1996

Sun, Y., Thapa, N., Hedman, A. C., & Anderson, R. A. (2013). Phosphatidylinositol 4,5-bisphosphate: targeted production and signaling. *BioEssays : News and Reviews in Molecular, Cellular and Developmental Biology*, *35*(6), 513–522. https://doi.org/10.1002/BIES.201200171

Szymańska-Czerwińska, M., Galińska, E. M., Niemczuk, K., & Knap, J. P. (2015). Prevalence of Coxiella burnetii Infection in Humans Occupationally Exposed to Animals in Poland. *Vector Borne and Zoonotic Diseases*, *15*(4), 261. https://doi.org/10.1089/VBZ.2014.1716

Tan, H. H., Makino, A., Sudesh, K., Greimel, P., & Kobayashi, T. (2012). Spectroscopic evidence for the unusual stereochemical configuration of an endosome-specific lipid. *Angewandte*

Chemie (International Ed. in English), *51*(2), 533–535. https://doi.org/10.1002/ANIE.201106470

Tan, X., Thapa, N., Choi, S., & Anderson, R. A. (2015). Emerging roles of PtdIns(4,5)P2 – beyond the plasma membrane. *Journal of Cell Science*, *128*(22), 4047. https://doi.org/10.1242/JCS.175208

Tanida, I., Ueno, T., & Kominami, E. (2008). LC3 and Autophagy. *Methods in Molecular Biology (Clifton, N.J.)*, *445*, 77–88. https://doi.org/10.1007/978-1-59745-157-4_4

Tatsumi, N., Baumgartner, A., Qiao, Y., Yamamoto, I., & Yamaguchi, K. (2006). Detection of Coxiella burnetii in market chicken eggs and mayonnaise. *Annals of the New York Academy of Sciences*, *1078*, 502–505. https://doi.org/10.1196/ANNALS.1374.096

Thiele, D., Willems, H., Haas, M., & Krauss, H. (1994). Analysis of the entire nucleotide sequence of the cryptic plasmid QpH1 from Coxiella burnetti. *European Journal of Epidemiology*, *10*(4), 413–420. https://doi.org/10.1007/BF01719665

Thomas, D. R., Newton, P., Lau, N., & Newton, H. J. (2020). Interfering with Autophagy: The Opposing Strategies Deployed by Legionella pneumophila and Coxiella burnetii Effector Proteins. *Frontiers in Cellular and Infection Microbiology*, *10*, 599762. https://doi.org/10.3389/FCIMB.2020.599762/BIBTEX

Tilburg, J. J. H. C., Roest, H. J. I. J., Buffet, S., Nabuurs-Franssen, M. H., Horrevorts, A. M., Raoult, D., & Klaassen, C. H. W. (2012a). Epidemic Genotype of Coxiella burnetii among Goats, Sheep, and Humans in the Netherlands. *Emerging Infectious Diseases*, *18*(5), 887. https://doi.org/10.3201/EID1805.111907

Tilburg, J. J. H. C., Roest, H. J. I. J., Buffet, S., Nabuurs-Franssen, M. H., Horrevorts, A. M., Raoult, D., & Klaassen, C. H. W. (2012b). Epidemic genotype of Coxiella burnetii among goats, sheep, and humans in the Netherlands. *Emerging Infectious Diseases*, *18*(5), 887–889. https://doi.org/10.3201/EID1805.111907

Tissot-Dupont, H., Amadei, M. A., Nezri, M., & Raoult, D. (2004). Wind in November, Q fever in December - Volume 10, Number 7—July 2004 - Emerging Infectious Diseases journal - CDC. *Emerging Infectious Diseases*, *10*(7), 1264–1269. https://doi.org/10.3201/EID1007.030724

Topping, N. H., Shepard, C. C., & Irons, J. V. (1947). Q FEVER IN THE UNITED STATES: Epidemiologic Studies of an Outbreak Among Stock Handlers and Slaughterhouse

Workers. *Journal of the American Medical Association*, *133*(12), 813–815. https://doi.org/10.1001/JAMA.1947.02880120001001

Tudela, J. G., Capmany, A., Romao, M., Quintero, C., Miserey-Lenkei, S., Raposo, G., Goud, B., & Damiani, M. T. (2015). The late endocytic Rab39a GTPase regulates the interaction between multivesicular bodies and chlamydial inclusions. *Journal of Cell Science*, *128*(16), 3068–3081. https://doi.org/10.1242/JCS.170092

Upadhyay, S., & Philips, J. A. (2019). *LC3-associated phagocytosis: host defense and microbial response*. https://doi.org/10.1016/j.coi.2019.04.012

Vacca, F., Scott, C., & Gruenberg, J. (2016). *The Late Endosome*. https://doi.org/10.1016/B978-0-12-394447-4.20017-5

Valkova, D., & Kazar, J. (1995). A new plasmid (QpDV) common to Coxiella burnetii isolates associated with acute and chronic Q fever. *FEMS Microbiology Letters*, *125*(2–3), 275–280. https://doi.org/10.1111/J.1574-6968.1995.TB07368.X

Van Meer, G., & De Kroon, A. I. P. M. (2011). Lipid map of the mammalian cell. *Journal of Cell Science*, *124*(Pt 1), 5–8. https://doi.org/10.1242/JCS.071233

Van Meer, G., Voelker, D. R., & Feigenson, G. W. (2008a). Membrane lipids: where they are and how they behave. *Nature Reviews. Molecular Cell Biology*, *9*(2), 112–124. https://doi.org/10.1038/NRM2330

Van Meer, G., Voelker, D. R., & Feigenson, G. W. (2008b). Membrane lipids: where they are and how they behave. *Nature Reviews. Molecular Cell Biology*, *9*(2), 112. https://doi.org/10.1038/NRM2330

Van Niel, G., D'Angelo, G., & Raposo, G. (2018). Shedding light on the cell biology of extracellular vesicles. *Nature Reviews. Molecular Cell Biology*, *19*(4), 213–228. https://doi.org/10.1038/NRM.2017.125

van Roeden, S. E., Wever, P. C., & Oosterheert, J. J. (2019). 'Chronic Q fever-related complications and mortality: data from a nationwide cohort' – Author's reply. *Clinical Microbiology and Infection*, *25*(11), 1436–1437. https://doi.org/10.1016/j.cmi.2019.03.004

van Schaik, E. J., Case, E. D., Martinez, E., Bonazzi, M., & Samuel, J. E. (2017). The SCID mouse model for identifying virulence determinants in Coxiella burnetii. *Frontiers in Cellular and Infection Microbiology*, *7*(FEB). https://doi.org/10.3389/fcimb.2017.00025

Van Schaik, E. J., Chen, C., Mertens, K., Weber, M. M., & Samuel, J. E. (2013). Molecular pathogenesis of the obligate intracellular bacterium Coxiella burnetii. *Nature Reviews. Microbiology*, *11*(8), 561. https://doi.org/10.1038/NRMICRO3049

Vanderburg, S., Rubach, M. P., Halliday, J. E. B., Cleaveland, S., Reddy, E. A., & Crump, J. A. (2014). Epidemiology of Coxiella burnetii infection in Africa: a OneHealth systematic review. *PLoS Neglected Tropical Diseases*, *8*(4). https://doi.org/10.1371/JOURNAL.PNTD.0002787

Vázquez, C. L., & Colombo, M. I. (2010). Coxiella burnetii modulates Beclin 1 and Bcl-2, preventing host cell apoptosis to generate a persistent bacterial infection. *Cell Death and Differentiation*, *17*(3), 421–438. https://doi.org/10.1038/CDD.2009.129

Verweij, F. J., Bebelman, M. P., George, A. E., Couty, M., Bécot, A., Palmulli, R., Heiligenstein, X., Sirés-Campos, J., Raposo, G., Pegtel, D. M., & van Niel, G. (2022). ER membrane contact sites support endosomal small GTPase conversion for exosome secretion. *Journal of Cell Biology*, *221*(12). https://doi.org/10.1083/JCB.202112032/VIDEO-4

Verzella, D., Pescatore, A., Capece, D., Vecchiotti, D., Ursini, M. V., Franzoso, G., Alesse, E., & Zazzeroni, F. (2020). Life, death, and autophagy in cancer: NF-κB turns up everywhere. *Cell Death & Disease*, *11*(3). https://doi.org/10.1038/S41419-020-2399-Y

Viaud, J., & Payrastre, B. (2015). Les phosphoinositides Ces lipides qui coordonnent la dynamique cellulaire. *Médecine/Science*, *31 : 996-1005*. https://doi.org/10.1051/medsci/20153111014

Vincent, G. (2014). Molecular characterisation of Australian Coxiella burnetii isolates. In *Murdoch University*. https://researchportal.murdoch.edu.au/esploro/outputs/doctoral/Molecular-characterisation-of-Australian-Coxiella-burnetii/991005542398607891

Vishwanath, S., & Hackstadt, T. (1988). Lipopolysaccharide phase variation determines the complement-mediated serum susceptibility of Coxiella burnetii. *Infection and Immunity*, *56*(1), 40–44. https://doi.org/10.1128/IAI.56.1.40-44.1988

Vogel, J. P. (2004). Turning a tiger into a house cat: Using Legionella pneumophila to study Coxiella burnetii. *Trends in Microbiology*, *12*(3), 103–105. https://doi.org/10.1016/j.tim.2004.01.008

Vogel, J. P., Andrews, H. L., Wong, S. K., & Isberg, R. R. (1998). Conjugative transfer by the virulence system of Legionella pneumophila. *Science (New York, N.Y.)*, *279*(5352), 873–876. https://doi.org/10.1126/SCIENCE.279.5352.873

Voth, D. E., Broederdorf, L. J., & Graham, J. G. (2012). Bacterial Type IV Secretion Systems: Versatile Virulence Machines. *Future Microbiology*, *7*(2), 241. https://doi.org/10.2217/FMB.11.150

Voth, D. E., & Heinzen, R. A. (2007). Lounging in a lysosome: the intracellular lifestyle of Coxiella burnetii. *Cellular Microbiology*, *9*(4), 829–840. https://doi.org/10.1111/J.1462-5822.2007.00901.X

Voth, D. E., Howe, D., Beare, P. A., Vogel, J. P., Unsworth, N., Samuel, J. E., & Heinzen, R. A. (2009). The Coxiella burnetii ankyrin repeat domain-containing protein family is heterogeneous, with C-terminal truncations that influence Dot/Icm-mediated secretion. *Journal of Bacteriology*, *191*(13), 4232–4242. https://doi.org/10.1128/JB.01656-08

Wachter, S., Bonazzi, M., Shifflett, K., Moses, A. S., Raghavan, R., & Minnick, M. F. (2019). A CsrA-Binding, trans-Acting sRNA of Coxiella burnetii Is Necessary for Optimal Intracellular Growth and Vacuole Formation during Early Infection of Host Cells. *Journal of Bacteriology*, *201*(22). https://doi.org/10.1128/JB.00524-19

Wandinger-Ness, A., & Zerial, M. (2014). Rab Proteins and the Compartmentalization of the Endosomal System. *Cold Spring Harbor Perspectives in Biology*, *6*(11), a022616. https://doi.org/10.1101/CSHPERSPECT.A022616

Watt, S. A., Kular, G., Fleming, I. N., Downes, C. P., & Lucocq, J. M. (2002). Subcellular localization of phosphatidylinositol 4,5-bisphosphate using the pleckstrin homology domain of phospholipase C delta1. *The Biochemical Journal*, *363*(Pt 3), 657–666. https://doi.org/10.1042/0264-6021:3630657

Weber, M. M., Chen, C., Rowin, K., Mertens, K., Galvan, G., Zhi, H., Dealing, C. M., Roman, V. A., Banga, S., Tan, Y., Luo, Z. Q., & Samuel, J. E. (2013). Identification of Coxiella burnetii type IV secretion substrates required for intracellular replication and Coxiella-containing vacuole formation. *Journal of Bacteriology*, *195*(17), 3914–3924. https://doi.org/10.1128/JB.00071-13

Weber, M. M., Faris, R., Van Schaik, E. J., McLachlan, J. T., Wright, W. U., Tellez, A., Roman, V. A., Rowin, K., Case, E. D. R., Luo, Z. Q., & Samuel, J. E. (2016). The Type IV Secretion System Effector Protein CirA Stimulates the GTPase Activity of RhoA and Is Required for Virulence

in a Mouse Model of Coxiella burnetii Infection. *Infection and Immunity*, *84*(9), 2524. https://doi.org/10.1128/IAI.01554-15

Weisburg, W. G., Dobson, M. E., Samuel, J. E., Dasch, G. A., Mallavia, L. P., Baca, O., Mandelco, L., Sechrest, J. E., Weiss, E., & Woese, C. R. (1989). Phylogenetic diversity of the Rickettsiae. *Journal of Bacteriology*, *171*(8), 4202. https://doi.org/10.1128/JB.171.8.4202-4206.1989

Wiener-Well, Y., Fink, D., Schlesinger, Y., Raveh, D., Rudensky, B., & Yinnon, A. M. (2010). Q fever endocarditis; not always expected. *Clinical Microbiology and Infection*, *16*(4), 359–362. https://doi.org/10.1111/J.1469-0691.2009.02805.X

Willems, H., Ritter, M., Jäger, C., & Thiele, D. (1997). Plasmid-homologous sequences in the chromosome of plasmidless Coxiella burnetii Scurry Q217. *Journal of Bacteriology*, *179*(10), 3293–3297. https://doi.org/10.1128/JB.179.10.3293-3297.1997

Winchell, C. G., Dragan, A. L., Brann, K. R., Onyilagha, F. I., Kurten, R. C., & Voth, D. E. (2018). Coxiella burnetii Subverts p62/Sequestosome 1 and Activates Nrf2 Signaling in Human Macrophages. *Infection and Immunity*, *86*(5). https://doi.org/10.1128/IAI.00608-17

Winchell, C. G., Graham, J. G., Kurten, R. C., & Voth, D. E. (2014). Coxiella burnetii Type IV Secretion-Dependent Recruitment of Macrophage Autophagosomes. *Infection and Immunity*, *82*(6), 2229. https://doi.org/10.1128/IAI.01236-13

Woldeyohannes, S. M., Gilks, C. F., Baker, P., Perkins, N. R., & Reid, S. A. (2018). Seroprevlance of Coxiella burnetii among abattoir and slaughterhouse workers: A meta-analysis. *One Health*, *6*, 23. https://doi.org/10.1016/J.ONEHLT.2018.09.002

Wu, Y. W., & Li, F. (2019). Bacterial interaction with host autophagy. *Virulence*, *10*(1), 352. https://doi.org/10.1080/21505594.2019.1602020

Xia, H., Huang, Y., Zhang, L., Luo, L., Wang, X., Lu, Q., Xu, J., Yang, C., Jiwa, H., Liang, S., Xie, L., Luo, X., & Luo, J. (2023). Inhibition of Macropinocytosis Enhances the Sensitivity of Osteosarcoma Cells to Benzethonium Chloride. *Cancers*, *15*(3). https://doi.org/10.3390/CANCERS15030961

Xiong, Q., Yang, M., Li, P., & Wu, C. (2019). Bacteria Exploit Autophagy For Their Own Benefit. *Infection and Drug Resistance*, *12*, 3205. https://doi.org/10.2147/IDR.S220376

Yamaji, T., & Hanada, K. (2015). Sphingolipid metabolism and interorganellar transport: localization of sphingolipid enzymes and lipid transfer proteins. *Traffic (Copenhagen, Denmark)*, *16*(2), 101–122. https://doi.org/10.1111/TRA.12239

Yang, Z., & Klionsky, D. J. (2010). Mammalian autophagy: core molecular machinery and signaling regulation. *Current Opinion in Cell Biology*, *22*(2), 124–131. https://doi.org/10.1016/J.CEB.2009.11.014

Yoshikawa, Y., Ogawa, M., Hain, T., Yoshida, M., Fukumatsu, M., Kim, M., Mimuro, H., Nakagawa, I., Yanagawa, T., Ishii, T., Kakizuka, A., Sztul, E., Chakraborty, T., & Sasakawa, C. (2009). Listeria monocytogenes ActA-mediated escape from autophagic recognition. *Nature Cell Biology*, *11*(10), 1233–1240. https://doi.org/10.1038/NCB1967

Young, F. W. (1948). Q FEVER IN ARTESIA, CALIFORNIA. *California Medicine*, *69*(2), 89. https://www.ncbi.nlm.nih.gov/pmc/articles/PMC1643471/

Yun, C. W., & Lee, S. H. (2018). The Roles of Autophagy in Cancer. *International Journal of Molecular Sciences*, *19*(11). https://doi.org/10.3390/IJMS19113466

Zhang, G., Russell-Lodrigue, K. E., Andoh, M., Zhang, Y., Hendrix, L. R., & Samuel, J. E. (2007). Mechanisms of Vaccine-Induced Protective Immunity against Coxiella burnetii Infection in BALB/c Mice. *The Journal of Immunology*, *179*(12), 8372–8380. https://doi.org/10.4049/JIMMUNOL.179.12.8372

Zhang, Y., Fu, J., Liu, S., Wang, L., Qiu, J., van Schaik, E. J., Samuel, J. E., Song, L., & Luo, Z. Q. (2022). Coxiella burnetii inhibits host immunity by a protein phosphatase adapted from glycolysis. *Proceedings of the National Academy of Sciences of the United States of America*, *119*(1), e2110877119. https://doi.org/10.1073/PNAS.2110877119/SUPPL_FILE/PNAS.2110877119.SAPP.PDF

Zhao, K., & Ridgway, N. D. (2017). Oxysterol-Binding Protein-Related Protein 1L Regulates Cholesterol Egress from the Endo-Lysosomal System. *Cell Reports*, *19*(9), 1807–1818. https://doi.org/10.1016/J.CELREP.2017.05.028